UNIVERSITÀ
DEGLI STUDI
DI PADOVA

Sede Amministrativa: Università degli Studi di Padova

Dipartimento di Scienze del Farmaco

SCUOLA DI DOTTORATO DI RICERCA IN: Scienze Molecolari

INDIRIZZO: Scienze Farmaceutiche

CICLO XXVII

DESIGN, SYNTHESIS AND BIOCHEMICAL EVALUATION OF NOVEL CK2 AND CDK2 INHIBITORS

Direttore della Scuola: Ch.mo Prof. Antonino Polimeno

Coordinatore d'indirizzo: Ch.mo Prof. Stefano Moro

Supervisore: Ch.mo Prof. Giuseppe Zagotto

Co-supervisori: Ch.mi Prof. Roger J. Griffin e Prof. Bernard T. Golding

Dottoranda: Elena Costa

UNIVERSITÀ DEGLI STUDI DI PADOVA

Sede Amministrativa: Università degli Studi di Padova

Dipartimento di Scienze del Farmaco

SCUOLA DI DOTTORATO DI RICERCA IN: Scienze Molecolari

INDIRIZZO: Scienze Farmaceutiche

CICLO XXVII

DESIGN, SYNTHESIS AND BIOCHEMICAL EVALUATION OF NOVEL CK2 AND CDK2 INHIBITORS

Direttore della Scuola: Ch.mo Prof. Antonino Polimeno

Coordinatore d'indirizzo: Ch.mo Prof. Stefano Moro

Supervisore: Ch.mo Prof. Giuseppe Zagotto

Co-supervisori: Ch.mi Prof. Roger J. Griffin e Prof. Bernard T. Golding

Dottoranda: Elena Costa

… Ai miei genitori

The following thesis presents the research carried out since January 2012 for the doctoral studies by Elena Costa at Scuola di Dottorato in Scienze Molecolari, Università degli Studi di Padova, Padova, under the supervision of Prof. Giuseppe Zagotto (Jan 2012-Jan 2013, Nov 2013-Dec 2014) and at Newcastle University, Northern Institute for Cancer Research, Newcastle University, Newcastle Upon Tyne, under the supervision of Prof. Roger J. Griffin† and Prof. Bernard T. Golding (Jan-Nov 2013, Sep-Oct 2014).

These studies are focused on the design, synthesis and biochemical evaluation of novel CK2 and CDK2 inhibitors. What follows provides a literature summary, an overview on the precedent results, followed by the synthesis program carried out since January 2012, the biological results and the docking studies. Finally, the future work will be proposed.

† Deceased 24 September 2014

ACKNOWLEDGEMENTS

I would like to thank Prof. Giuseppe Zagotto for the opportunity to do an internship at Newcastle University under the supervision of Prof. Roger J. Griffin† and Prof. Bernard T. Golding. I would like to thank them for their invaluable and continued support and helpfulness during the PhD and the writing up of this thesis. I would like to thank Prof. Moro and all the lab colleagues for their helpfulness and friendship during my placement in the Molecular Modeling Section (MMS) at the University of Padua. I would like to thank Prof. Manlio Palumbo for his support and the Head of the Doctoral School Prof. Antonino Polimeno at the University of Padua. I would also like to thank Dr Karen Haggerty and Carlo Bawn for their technical expertise and assistance during my internship in the Chemical School at Newcastle University.

I would like to thank the lab colleagues in Padua and all the members of the Newcastle ADDI group for making my time in Newcastle an unforgettable experience: Santosh, Bian, Andrew, Nick, James, Honorine, Tristan, Annalisa, Suzannah, Benoit, Duncan, Sarah, Denise, Stephanie, Stephen, Ruth and Daniela. I would also like to acknowledge all of the collaborators of the CDK2 project for their helpfulness during my placement in structural biology at Newcastle University: Dr Jane Endicott, Dr Martin Noble, Dr Lan-Zhen Wang, Dr William Stanley and Dr Martyna Pastok.

Last but not least, I would like to thank my parents Patrizia and Ottaviano for their continued support and encouragement throughout my studies, my boyfriend Claudio and all my friends: Francesca, Pietro, Marica, Nicola, Martina, Fabio, Elena, Enrico, Claudio and Eva for their true friendship.

RIASSUNTO

Le chinasi sono una classe di enzimi in grado di catalizzare il trasferimento di un gruppo fosfato terminale di una molecola di ATP, o più raramente di GTP, ad una proteina che agisce da substrato. Questo processo è reversibile, ed è mantenuto tale dalla presenza di altri enzimi, le fosfatasi, che catalizzano la reazione inversa. Uno squilibrio tra questi enzimi gioca un ruolo rilevante nell'incidenza di diverse patologie, le quali sono attribuibili ad elevati livelli di fosforilazione.

Questo lavoro di ricerca ha avuto lo scopo di progettare e sviluppare nuovi potenti e selettivi inibitori di casein chinasi 2 (CK2) a struttura benzimidazolica, e progettare e sviluppare nuovi inibitori a struttura pirimidinica di chinasi ciclina dipendente 2 (CDK2). La ricerca è stata svolta presso l'Università degli Studi di Padova (IT) in collaborazione con l'Università di Newcastle (UK).

CK2 è una Ser/Thr chinasi ubiquitaria, altamente pleiotropica e coinvolta in ogni fase della progressione del ciclo cellulare. DRB è stato il primo inibitore di CK2 ATP-mimetico ad essere identificato (IC_{50} = 23 μM), e anche punto di partenza per la sintesi di una nuova classe di inibitori poli-alogenati a struttura benzimidazolica.

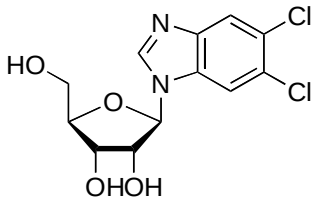

DRB

E' stata proposta la sintesi di inibitori bifunzionali di CK2, i quali si pensa vadano ad interagire simultaneamente con la tasca catalitica dell'ATP e con il sito di legame del substrato. Come punto di partenza è stato scelto uno scaffold benzimidazolico poli-alogenato, il quale è stato poi legato ad una serie di sequenze peptidiche.

CDK2 appartiene anch'essa ad una famiglia di chinasi Ser/Thr-dipendenti. CDK2, complessandosi con subunità regolatorie (ciclina A o E), è coinvolta nella progressione del ciclo cellulare. Una caratteristica ricorrente nei tumori sono la sovraespressione di CDK2 e la deregolazione delle cicline ad essa associate. NU6300, un inibitore a scaffold purinico di CDK2 (IC_{50} = 63 nM), è considerato il primo inibitore di CDK2 irreversibile, questo grazie all'interazione covalente tra il gruppo vinilsulfonico e un residuo di lisina (Lys89), presente all'interno della tasca catalitica dell'enzima CDK2.

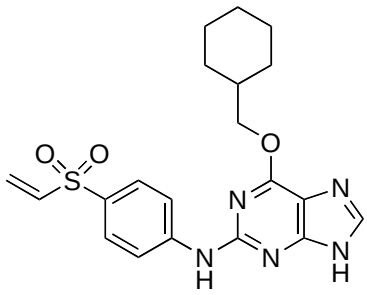

NU6300

Studi di relazione struttura-attività (SAR) riguardanti una serie di O^6-alchilguanine hanno rivelato che il farmacoforo di tipo purinico non è un requisito essenziale per l'attività inibitoria su CDK2. Per questo è stata sviluppata una serie di inibitori CDK2 di tipo pirimidinico. Sono state quindi considerate alcune modifiche strutturali allo scaffold pirimidinico, in modo da esaminare l'affinità di binding, la potenza e la selettività dei nuovi inibitori di CDK2.

I nuovi inibitori sono stati valutati per la loro attività inibitoria su CK2 e CDK2 rispettivamente. Gli inibitori più promettenti sono stati poi sottoposti ad ulteriori studi biologici. Per quanto riguarda gli inibitori di CDK2 sono stati effettuati studi di docking molecolare e di co-cristallizzazione per razionalizzare i risultati ottenuti e pianificare nuove vie di sintesi.

ABSTRACT

Kinases are a class of enzymes, which catalyse the transfer of the terminal phosphate of a molecule of ATP, or more rarely of GTP, to a protein that acts as a substrate. This process is reversible and is maintained by the presence of other enzymes, namely the phosphatases, which catalyse the reverse reaction. An imbalance between these enzymes plays a crucial role in the occurrence of diseases, which is attributable to abnormal levels of phosphorylation.

The aim of this research was the design and synthesis of novel potent and selective benzimidazole-based inhibitors of Casein Kinase 2 (CK2) and the design and synthesis of pyrimidine-based inhibitors of Cyclin-dependent Kinase 2 (CDK2). This research was carried out at the University of Padua in collaboration with Newcastle University.

CK2 is a ubiquitous, highly pleiotropic Ser/Thr protein kinase, which has been implicated in every stage of cell cycle progression. DRB was the first CK2 ATP-mimetic inhibitor identified (IC_{50} = 23 μM) and was also the starting point for a new fruitful class of polyhalogenated benzimidazole-based compounds.

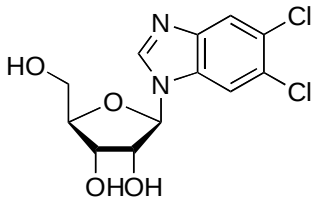

DRB

The synthesis of CK2 bifunctional inhibitors, which could simultaneously interact with the ATP pocket and the substrate-binding domain, was proposed. A polyhalogenated benzimidazole scaffold was used as starting point and was then coupled to different peptidic chains.

CDK2, belongs to a family of Ser/Thr kinases. In complex with regulatory subunits, cyclin E or A, CDK2 is involved in driving the cell cycle. The overexpression of CDK2 and the deregulation of cyclins associated with CDK2 are often observed in cancer. NU6300 (**2**), a purine-based CDK2 inhibitor (IC_{50} = 63 nM), can be considered the first CDK2 irreversible inhibitor due to a covalent interaction between the vinyl sulfone moiety and Lys89 within the ATP-binding domain of CDK2.

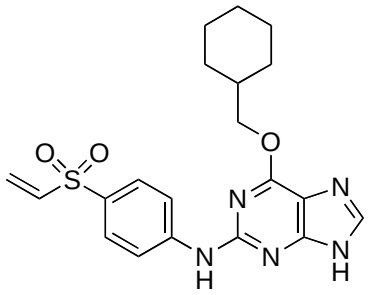

NU6300

Structure-activity relationship (SAR) studies on the O^6-alkylguanine series revealed that the purine pharmacophore is not a prerequisite for CDK2-inhibitory activity. Hence, a series of pyrimidine-based CDK2 inhibitors was synthesised. Structural modifications at the pyrimidine scaffold were then considered in order to investigate the binding affinity, potency and selectivity of the novel CDK2 inhibitors.

All new compounds were evaluated for CK2- and CDK2-inhibitory activity, with promising inhibitors being subjected to more comprehensive biological studies.
Concerning CDK2 inhibitors, docking and co-crystallisation studies were also performed in order to rationalise the results and propose new compounds to be synthesised.

TABLE OF CONTENTS

ABBREVIATIONS

A	AcOH	Acetic acid
	Aq	Aqueous
	ATP	Adenosine triphosphate
B	BOP	(Benzotriazol-1-yloxy)tris(dimethylamino) phosphonium hexafluorophosphate
	Br_2	Bromine
C	°C	Celsius degrees
	cAMP	Cyclic Adenosine Monophosphate
	CDK	Cyclin-dependent Kinase
	cGMP	Cyclic Guanosine Monophosphate
	CK	Casein Kinase
	CML	Chronic Myeloid Leukaemia
D	d	Doublet
	δ	Delta, ppm
	DABCO	1,4-Diazabicyclo[2.2.2]octane
	DBU	1,8-Diazabicyclo[5.4.0]undec-7-ene
	DCM	Dichloromethane
	dd	Doublet of doublets
	DIAD	Diisopropyl azodicarboxylate
	DIPEA/DIEA	Diisopropylethylamine (Hünig's base)
	DMA	Dimethylacetamide
	DMEM	Dulbecco's Modified Eagle Medium
	DMF	Dimethylformamide
	DMSO	Dimethylsulfoxide
	DNA	Deoxyribonucleic Acid
	DTT	Dithiothreitol

E	Equiv.	Equivalent/s
	EtOAc	Ethyl acetate
	Et_2O	Ether
	EtOH	Ethanol
	Et_3N	Triethylamine
F	FCS	Fetal Calf Serum
	FDA	Food and Drug Administration
	Fmoc	Fluorenylmethyloxycarbonyl chloride
G	GTP	Guanosine triphosphate
	G-CK	Golgi Casein Kinase
H	h	Hour/s
	HBr	Hydrobromic acid
	HBTU	O-(Benzotriazol-1-yl)-N,N,N',N'-tetramethyluronium hexafluorophosphate
	HMPA	Hexamethylphosphoramide
	H_2NOH HCl	Hydroxylamine hydrochloride
	H_2O	Water
	HOBt	Hydroxybenzotriazole
	HPLC	High-performance liquid chromatography
	HRMS	High resolution mass spectrometry
I	IC_{50}	Half maximal inhibitory concentration
	IR	Infrared
J	J	Coupling constant
K	K_i	Inhibition constant
	KOH	Potassium hydroxide

L	LCMS	Liquid chromatography mass spectrometry
	LIE	Linear Interaction Energy
M	M	Molarity
	m	Multiplet
	µ	Micro
	mCPBA	Meta-chloroperbenzoic acid
	MeCN	Acetonitrile
	MeOH	Methanol
	mg	Milligram/s
	$MgCl_2$	Magnesium chloride
	$MgSO_4$	Magnesium sulfate
	MHz	Megahertz
	mL	Millilitre/s
	min	Minute/s
	miRNA	MicroRNA
	mmol	Millimolar
	MMS	Molecular Modeling Section
	MOE	Molecular Operating Environment
	Mp	Melting point
	mRNA	MessengerRNA
	MTT	3-(4,5-dimethylthiazol-2-yl)-2,5-diphenyltetrazolium bromide
	MW	Microwave
N	NaCl	Sodium chloride
	Na_2CO_3	Sodium carbonate
	NaH	Sodium hydride
	$NaHCO_3$	Sodium bicarbonate
	NH_3	Ammonia
	NMP	N-methyl-1-pyrrolidone

	NMR	Nuclear Magnetic Resonance
	NaOH	Sodium hydroxide
O	On	Overnight
	OtBu	Tert-butyl ester
P	PBS	Phosphate-Buffered Saline
	PDB	Protein Data Bank
	Pe	Petroleum ether
	Phe	Phenylalanine
	PK	Protein Kinases
	$POCl_3$	Phosphorus oxychloride
	POG	Paul O'Gorman
	ppm	Parts per million
	PyBOP	Benzotriazol-1-yl-oxytripyrrolidinophosphonium hexafluorophosphate
R	Rf	Retention factor
	RNA	Ribonucleic Acid
	RPMI	Roswell Park Memorial medium
	rRNA	Ribosomal RNA
	Rt	Room temperature
S	s	Singlet
	SAR	Structure-Activity Relationship
	SDS	Sodium Dodecyl Sulphate
	S_NAr	Nucleophilic Aromatic substitution
	snRNA	Small nuclear RNA
	SPPS	Solid Phase Peptide Synthesis

T	t	Triplet
	TFA	Trifluoroacetic acid
	TFE	Trifluoroethanol
	TIS	Triisopropylsilane
	TLC	Thin Layer Chromatography
	THF	Tetrahydrofuran
	TMS	Tetramethylsilane
U	UV	Ultraviolet
Z	Zn	Zinc

Amino acids abbreviations

Three letter code	Name	One letter code
Ala	Alanine	A
Arg	Arginine	R
Asn	Asparagine	N
Asp	Aspartic acid	D
Cys	Cysteine	C
Glu	Glutamic acid	E
Gln	Glutamine	Q
Gly	Glycine	G
His	Histidine	H
Ile	Isoleucine	I
Leu	Leucine	L
Lys	Lysine	K
Met	Methionine	M
Phe	Phenylalanine	F
Pro	Proline	P
Ser	Serine	S
Thr	Threonine	T
Trp	Tryptophan	W
Tyr	Tyrosine	Y
Val	Valine	V

1. BACKGROUND

1.1. Protein Kinases (PK)

Kinases are a class of enzymes, which catalyse the transfer of the terminal phosphate of a molecule of ATP, or more rarely of GTP, to a protein that acts as a substrate (Fig. 1). [1, 2] Phosphorylation induces structural changes in the protein, which are translated into activation or inhibition signals of the protein. [3] This process is reversible and this condition is guaranteed by the presence of other enzymes, namely the phosphatases, which catalyse the reverse reaction (Fig. 1). [4] An imbalance between these enzymes plays a crucial role in the occurrence of diseases, which is attributable to abnormal levels of phosphorylation. [3-5]

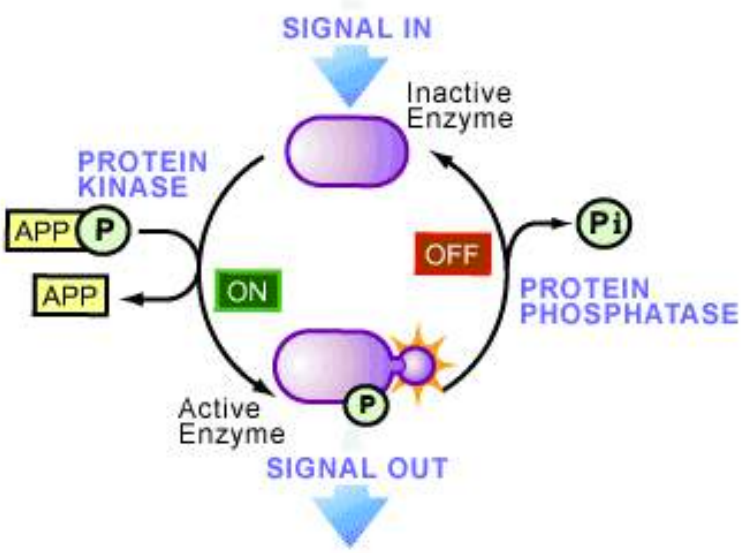

Fig. 1 The phosphorylation process [4]

Reversible protein phosphorylation plays an essential role in the regulation of most eukaryotic cellular processes, such as cell survival, growth, proliferation, angiogenesis, metabolism, intracellular protein transfer and migration. [5]

Phosphorylation within the cell is generally controlled by extracellular signals such as hormones, growth factors, neurotransmitters and antigens that bind to specific receptors in the cell membrane. In the evolution, protein kinases developed two characteristics, which are essential for their functionality: sensitive mean of regulation and high specificity for substrates. [6]

About 518 kinases are encoded in the human genome, divided into more than 57 families and corresponding to 2% of the entire genome. [7] However, only a small part of the complex set concerning the functional interactions of these proteins has been discovered so far. [7]

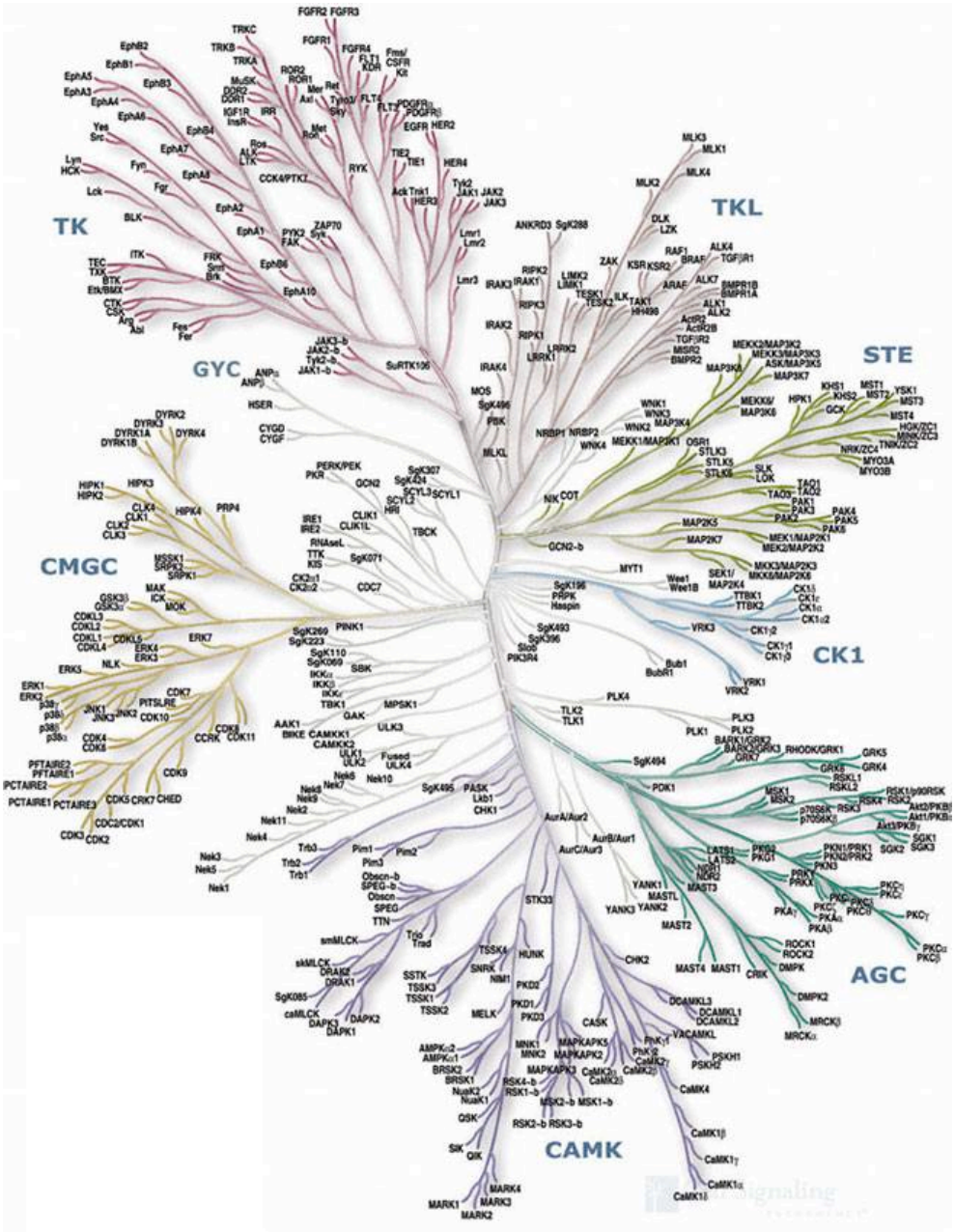

Fig. 2 The human kinome [8]

There are different classifications of protein kinases, which represent the set of the human kinome (Fig. 2). They can be grouped on the basis of the amino acid sequence within the catalytic domain, on the basis of substrate specificity or on their mechanism of action. [9-11]

Concerning the first classification the human kinome is divided into seven main families, which are then divided into subfamilies: [9-11]

- AGC kinases (protein kinases A, G, C, βARK, ribosomal S6 family) consist in core intracellular signalling kinases, which are regulated by second messengers, such as cyclic nucleotides and calcium. AGC kinases preferably phosphorylate Ser/Thr residues.

- CAMK kinases (Ca^{2+}/Calmodulin dependent protein kinases) are mainly characterised by Ca^{2+}/Calmodulin regulation, as their activation is often induced by bind with calcium or calmodulin.

- CMGC kinases (CDK, MAPK, GSK3, CLKs protein kinases) are directly involved in cell cycle progression and its regulation. They can be found in all eukaryotes.

- TK kinases (Tyrosine Kinase family) specifically phosphorylate tyrosine residues. They play an essential role in inter- and intracellular signal transduction. Abnormalities in tyrosine phosphorylation are closely related to oncogenic transformation and to the development of diseases, including diabetes and cancer.

- TKL kinases (Tyrosine-like Kinase family) are similar to tyrosine kinases, but they phosphorylate Ser/Thr residues. TKLs are well represented in metazoans, but they are also present in protists and in photosynthetic organisms. They are the largest group of kinases found in land plants, representing about 80% of the plant kinome. In animals these kinases are involved in crucial cellular pathways.

- STE kinases (homologues to yeast sterile 7, 11, 20 kinases) include protein kinases, involved in MAP kinase cascades, such as transduction of various extra- and intracellular signals. Abnormalities in MAP kinase cascades are tightly linked to oncogenic transformation.

- CK1, known as Casein Kinase 1, phosphorylates many different substrates involved in cell differentiation control, proliferation, chromosome segregation and circadian rhythms. CK1 kinase activity is regulated by extracellular signals and its deregulation is implicated in the occurrence of several diseases.

The second classification implies kinases division on the basis of the amino acid residue that is phosphorylated: Ser/Thr-specific kinases, Tyr-specific kinases, dual-specificity kinases (Ser/Thr- and Tyr-specific) and besides these three main groups there are also His-, Cys-, Glu- and Asp-specific kinases. [9-11]

The third classification consists in: protein kinases regulated by cAMP or cGMP, protein kinases regulated by diacylglycerol, S6 kinase family, protein kinases regulated by cyclins (CDK) and independent protein kinases, which are constitutively active. [9-11]

Among protein kinases there are some conserved structural motifs (Fig. 3). [12, 13]

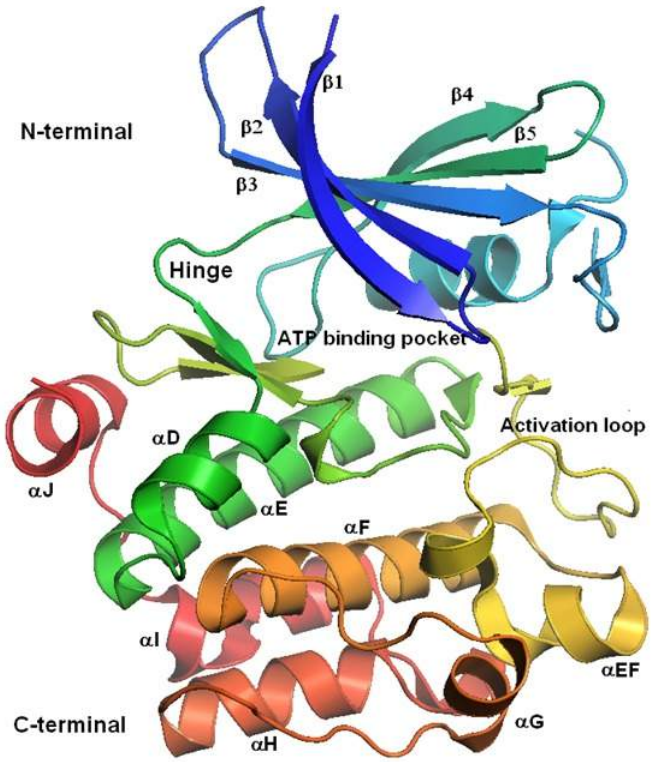

Fig. 3 Structural domains of protein kinases [14]

The main components of protein kinases are two structural subdomains: the N-lobe, which is formed of β-sheets and the C-lobe, which is formed of α-helices. The catalytic domain in protein kinases consists in approximately 200-250 amino acids and accommodates the ATP-binding site. This is localised at the interface between the N-lobe and the C-lobe, in the so-called "hinge" region. Although most of kinases display a similar structure in the ATP-binding site, there are few differences among them, which allow drugs to target a specific subfamily without affecting the others. Five regions can be distinguished in the ATP-binding site: adenine region, sugar region, hydrophobic pocket and channel and phosphate binding region. The hydrophobic pocket is not used by ATP, but is exploited by most of kinase inhibitors and plays a crucial role for the selectivity. [12, 13]

As mentioned before, several studies highlighted the importance of the balance between the activity of kinases and phosphatases in order to have a proper cellular functionality. [15] Over 400 human diseases, including diabetes, neurodegenerative diseases, rheumatoid arthritis, many malignancies and viral diseases are attributable to abnormal levels of phosphorylation and because of the potential consequences, phosphorylation requires a strict control. [15-16] To date, protein kinases have become the second largest class of drug targets after G-protein-coupled receptors and they account for 20-30% of the drug discovery programs of many pharmaceutical companies. [16]

Kinase inhibitors can be divided into four main groups: [17, 18]

- Most of kinase inhibitors are ATP-mimetics (Type I) they compete with ATP interacting with residues within the active site, preventing ATP from transferring the phosphate group to the substrate protein. ATP-competitive inhibitors recognise the active conformation of kinases and commonly present heterocycles in their structures. [19]

- Type 2 inhibitors recognise the inactive conformation of kinases. The first protein kinase inhibitor being commercialised was Gleevec (Imatinib, Novartis, Fig. 4), a tyrosine-kinase inhibitor, approved by FDA in 2001 for the treatment of CML, bone marrow disorders, skin cancer, or certain tumours of the stomach and digestive system. [16] In particular, its discover pointed out that full kinase selectivity was not necessarily crucial for the clinical success of protein kinase inhibitors.

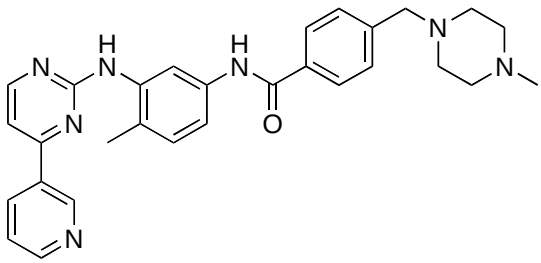

Fig. 4 Gleevec (Imatinib, Novartis 2001)

- A third group of inhibitors includes the allosteric inhibitors, which bind an allosteric site outside the kinase catalytic domain. These inhibitors are characterised by high selectivity, as they exploit binding sites and regulatory mechanisms that are unique to a particular kinase. [20]

- Another group of kinase inhibitors is represented by the covalent inhibitors, designed with an electrophile group, which undergoes a Michael addition reaction with a nucleophile species within the catalytic domain. The formation of a covalent bond irreversibly blocks ATP from binding the kinase. Despite the great interest in developing this kind of inhibitors, many researchers are concerned about the potential toxicity for their potential off-target activity. [21] This issue will be discussed later on (see Par. 1.3.3.2.2.).

This work focused on the development of kinase inhibitors targeting CK2 (Casein Kinase 2) and CDK2 (Cyclin-dependent Kinase 2), both part of the CMGC kinase group.

1.2. Casein Kinases (CK)

The first casein kinase activity was identified in the mid-twentieth century, performing experiments on rat liver using casein as phosphorylatable substrate. [22]

In particular, two classes of enzymes belong to the casein kinase family:

- Mammary gland casein kinase or Golgi Casein Kinase (G-CK), which is tissue-specific and able to phosphorylate the proteic fraction of milk, including casein, its natural substrate. Proteins are synthesised in the Golgi apparatus of the mammary secreting cells. [22-24]

- Ubiquitous protein kinases, which include Casein Kinase 1 and 2 (CK1, CK2). Their physiological substrates are represented by a number of enzymes and proteins involved in several biological functions. [22-24]

The CK1 protein kinases are Ser/Thr-selective enzymes found in most eukaryotic cell types from yeast to humans, involved in different cellular processes including circadian rhythm, cell cycle progression, chromosome segregation, apoptosis, cellular proliferation and differentiation. The CK1 family in mammals consists of seven different isoforms: α, β, γ_1, γ_2, γ_3, δ and ε. [25] While CK1 and G-CK are only able to use ATP as phosphate donor, CK2 is able to use both ATP and GTP, because it provides enough space for the nucleotide within the binding site. [26] Another aspect that differentiates CK2 from CK1 and G-CK involves its heterotetrameric structure, rather rare among protein kinase. [27]

CK2, which for about twenty years since its discovery was orphaned of its physiological substrates, is now considered the most pleiotropic protein kinase in eukaryotes. To date, more than 300 CK2 substrates are known and the number is still growing. [24] Despite many efforts and the great amount of knowledge gained in this field, the mechanism of protein kinases still remains unclear, although it is possible to assume their role in signal transduction pathways, gene expression, proliferation and, more generally, in cell regulation. [24]

1.2.1. Casein Kinase 2 (CK2)

Casein kinase 2 (CK2) is a constitutively active kinase, which mainly phosphorylates Ser/Thr residues and effectively uses both ATP and GTP as phosphate donors. [26] It is highly pleiotropic, ubiquitously distributed in eukaryotes and able to phosphorylate hundreds of substrates. It has been detected within the nucleus, the cytoplasm, on the outer surface of the cell membrane and it has been associated with specific organelles, including Golgi apparatus, endoplasmic reticulum and ribosomes. [24, 28] Therefore, it is not surprising that its abnormal high constitutive activity has been implicated in several human diseases, as it plays a crucial role in several physiological and pathological pathways.

1.2.1.1. CK2 structural motifs

Protein kinase CK2 is a tetrameric enzyme composed of two catalytic (αα or αα′) and two regulatory subunits (ββ), which is rare among kinases. [27-29]

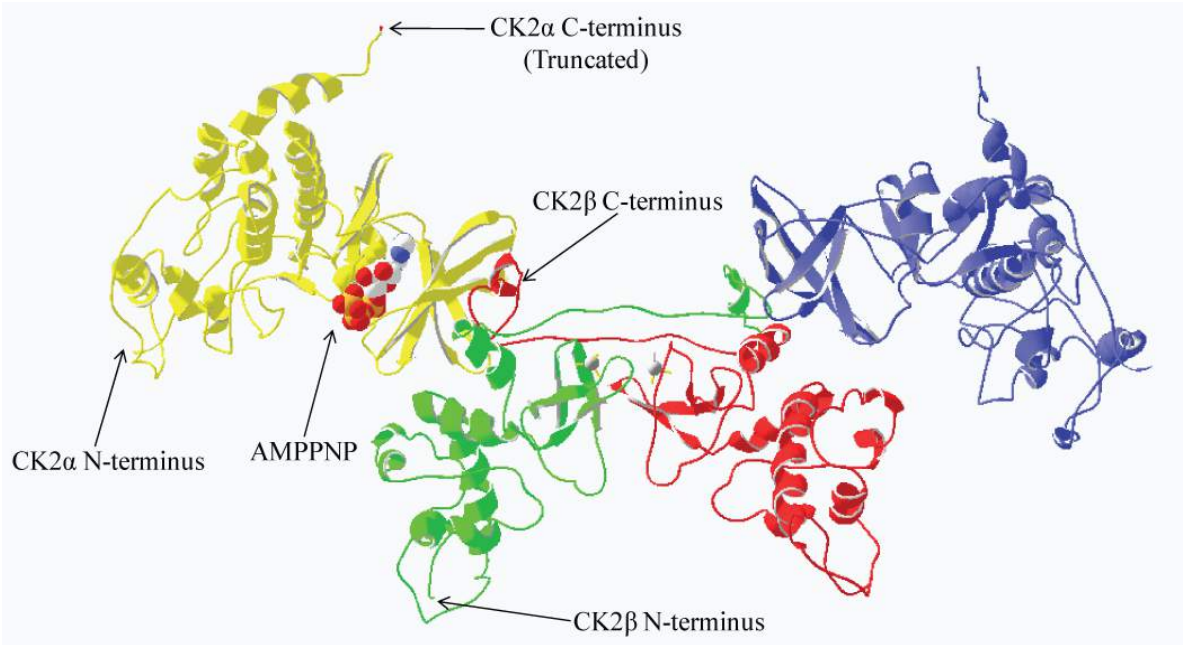

Fig. 5 Representation of CK2 tetramer [30]

In humans, two different isoforms of the catalytic subunits (α and α') were initially discovered, while only one form of the regulatory subunit (β) was identified. [31] The two isoforms of the catalytic subunits, with the exception of their unrelated C-terminal domains, are very similar, exhibiting approximately 90% of identity within their catalytic domains and maintaining the main structural motifs of all other protein kinases: [27-31]

- The Phosphate-binding loop (or P-loop), which is associated with the phosphate-binding domain and can be found in many ATP or GTP-associated proteins.

- The substrate-binding site, which just in CK2 is characterised by the presence of several consecutive basic amino acids, useful for the binding of acidic substrates.

- The catalytic loop, a polypeptide region supposed to play a role in catalysis, transition to and stabilisation of the active conformation of the kinase domain.

- The activation loop (or T-loop), which lies outside the active-site cleft.

The structure of CK2α subunit consists in a small lobe including the β-strands and the helix-αC and a large lobe dominated by α-helixes. The ATP pocket is located between these two lobes, linked together through a short loop, namely the "hinge region" (Fig. 6). [31, 32]

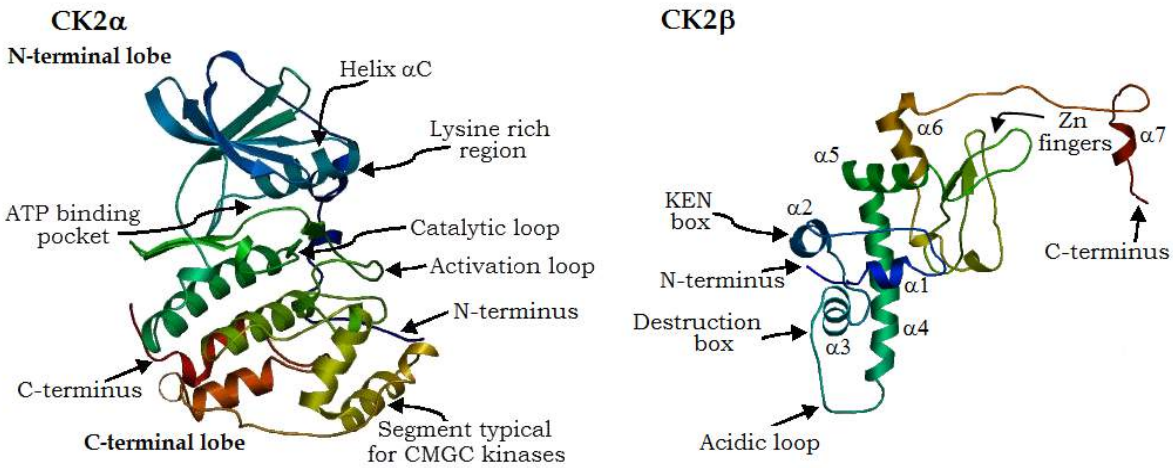

Fig. 6 Representation of the CK2 subunits and its domains [32]

CK2β subunit has no sequence similarity with other protein regulatory subunits, but is remarkably conserved among species. The primary sequence consists in a distribution of basic and acidic residues at the C-terminal and N-terminal respectively. [31, 32]

The C-terminal is responsible for the positive regulation of the α-subunit, for the β-β dimerisation, for the association with the α-subunit and for its preservation against unfolding and proteolysis. [29] Conversely, the N-terminal seems involved in the negative regulation of the enzyme. A group of four cysteines are involved in the Zn^{2+}-binding motif. The so-called "Zn-finger" is responsible for the β-β dimerisation. Furthermore, as the regulatory subunit of CK2 is associated with cell cycle progression, CK2β is reminiscent of cyclins, the regulatory subunits of CDKs. It is also particularly interesting that CK2β presents structural motifs previously characterised as regulators of cyclin degradation. For example, CK2 presents a sequence similar to the so-called "destruction box", which plays a key role in the degradation of cyclin B at the end of mitosis. Several proteins, including CK2, also contain one or more KEN boxes (Lys-Glu-Asn), which seem to mediate cell cycle dependent protein degradation. Anyway, the functional relevance of the putative destruction and KEN boxes of CK2β have not been characterised yet. [27-32]

Despite CK2 presents structural motifs common to all other kinases, it also displays some peculiar characteristics, which differentiate it from them and could also be exploited by novel inhibitors: [33]

- The N-terminal region seems to have a key role in the CK2 constitutively active conformation. Activation of all other kinases is given by a phosphorylation event in Ser/Thr or Tyr residues, in the T-loop. Concerning CK2, a phosphorylation event in this region has never been reported, conversely it is accepted that the CK2 N-terminal domain is able to constraint the activation loop in its open and consequently always active conformation. [34]

- The P-loop (or glycine-rich loop), which just in CK2 is composed only by two glycine residues. The third glycine residue is replaced with a serine (Ser51), Lys49 seems to have a role in the substrate recognition and Tyr50 is the homolog of Tyr15 of CDKs, a key residue in the CDKs activity regulation. [35]

- Both CK2 α- and α'-subunits present 6 out of 7 consecutive basic residues nearby the substrate recognition site, which are exploited by acidic substrates. No other kinase displays such a large number of basic residues in the same region. [36]

- CK2 possesses a particular stretch of four histidines, two of which (His160, His166) are unique among all the other kinases. The role of these histidines still remains unclear but may contribute to the recognition of the substrate upstream the phosphorylated residue. [35]

- The ATP-binding domain also displays some specific characteristics. As previously mentioned, CK2 is able to use both ATP and GTP as phosphate donors. Furthermore, residues like Met163 are responsible for the more hydrophobicity of the ATP cavity and this explains the particular susceptibility of CK2 to hydrophobic and bulky molecules. [35]

1.2.1.2. Regulation of CK2

Since the discovery of CK2, several studies have been conducted in order to understand its physiological role and the mechanism by which it is regulated. [37] Still 60 years after its discovery, neither the way in which CK2 regulates cell processes, nor the way in which the enzyme is regulated is fully understood. It seems reasonable to assume the existence of different regulatory mechanisms depending on the cell type, the subcellular compartment, but also depending on the cell cycle phase. [38] Some of the mechanisms that may contribute to the regulation of CK2 in cells include: [27]

- Regulated expression and assembly. There is some evidence that CK2β is able to modulate the catalytic subunit activity and substrate specificity, as well as assembly of CK2 tetramer. Furthermore, the existence of a destruction box within CK2β subunit would further emphasise its potential similarities with cyclins. [39]

- Phosphorylation. Despite phosphorylation is a required process for the activation of most of the kinases, for CK2 is not the case. [40] Auto-phosphorylation processes can be considered important to indirectly regulate CK2 activity. [40, 41]

- Regulatory interactions with protein molecules. Considered a major mechanism for CK2 regulation. Several proteins have been shown to interact with CK2 and regulate its activity. [42]

- Regulation interactions. Considered a second-messenger-independent protein kinase, CK2 can be regulated by small molecules: inhibited by negatively charged compounds and activated by positively charged compounds, such as polyamines. [43]

To date, at least three different groups of CK2-regulatory molecules have emerged:

- CK2-activity modulators. They interfere with the recognition of the protein substrate. The activators are positively charged compounds, such as polyamines, histones, protamines and basic polypeptides. The inhibitors include negatively charged compounds, such as polyanions, oligo-glutamic and oligo-aspartic peptides. [38, 44]

- CK2 inhibitors. They compete with the nucleotide within the catalytic domain. [45] Structurally different from ATP, the efficiency of these inhibitors is due to some structural elements that allow them to interact with specific residues localised in the active site, thus interfering with the proper CK2-ATP interaction.

- CK2 allosteric modulators. Considered an emerging class of compounds capable of binding to the ATP pocket, but also to an allosteric site, at the interface with the CK2β regulatory subunit. [46] This hydrophobic pocket on the outer surface of the N-terminal portion of the β-subunit might represent a new target to induce a selective disassembly of CK2 subunits, with simultaneous inhibition of the activity of the α-subunit.

A particular attention was then given to proteins able to interact with the holoenzyme or the individual subunits, without being necessarily substrates for CK2. This situation presupposes the existence of disassembled catalytic and/or regulatory subunits within the cell.

1.2.1.3. Biological implication of CK2

As previously mentioned, CK2 can be detected in a variety of cellular compartments, both in the cytoplasm and in the nucleus. [47] More recently the enzyme was also detected in the cell membrane. Thus, because of the potential consequences, its activity requires strict control. [48-50] Both the catalytic and the regulatory subunits of CK2 are essential for cell survival and it is evident the potential relationship between CK2, antiapoptotic activity and abnormal cellular proliferation. [29]

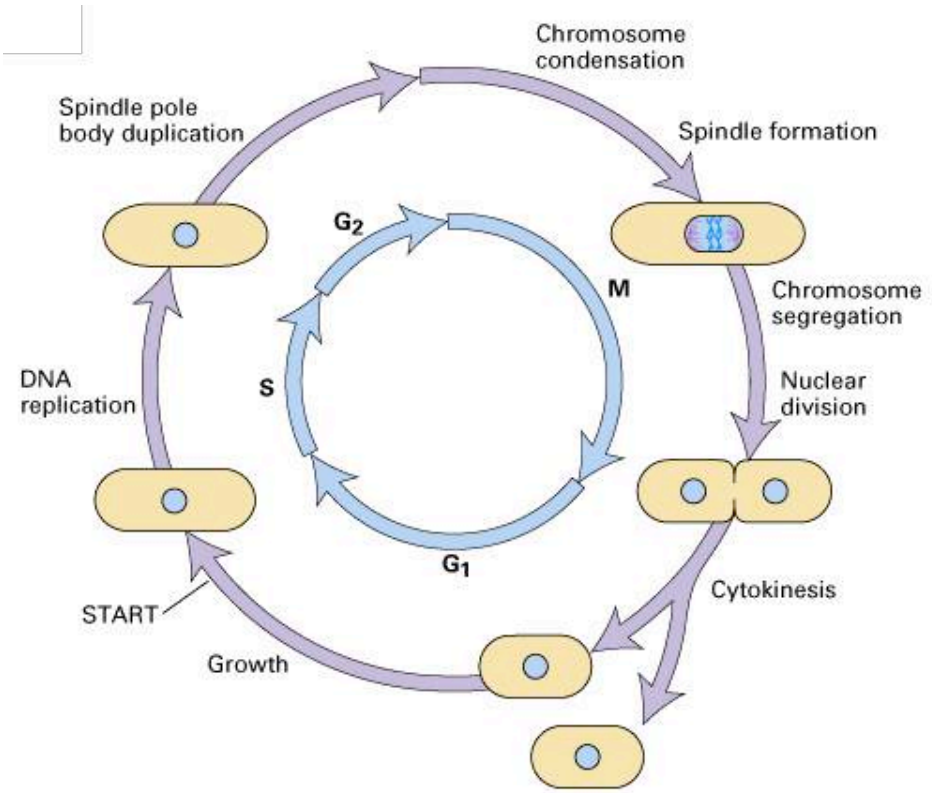

Fig. 7 The cell cycle [51]

CK2 has been shown essential for progression through the G1/S and G2/M transitions in yeast and necessary for G0/G1, G1/S and G2/M transitions in mammals. [52, 53] CK2 has then been connected to the regulation of the CDK activating kinase (CAK), which activates the cyclin-CDK complex by phosphorylating Thr160 in the CDK-activation loop. [54] CAK itself is a member of the CDK family and functions as a positive regulator of CDK1, CDK2, CDK4 and CDK6. [54]

CK2 has then been shown involved in the physiological response to cell damage, playing a crucial role in cell "adaptation" processes against DNA damage. In particular, CK2 is fundamental for RNA-polymerase III activity, which is involved in DNA transcription to synthesise small RNAs, such as tRNA (transfer RNA) and also for the regulation of the RNA-polymerase I (Pol I) and II (Pol II) activities. [55] RNA-polymerase I transcribes rRNA (ribosomal RNA), which account for over 50% of the total RNA synthesised within the cell, while RNA-polymerase II catalyses the transcription of DNA to synthesise precursors of mRNA (messenger RNA), snRNA (small nuclear RNA) and miRNA (micro RNA). [55, 56]

Furthermore, as previously mentioned in this paragraph, CK2 is mostly present in the cytoplasm and in the nucleus within the cells, but it was also recently detected in cell membrane of rat liver. [28] In particular, it was established that the regulatory subunit of CK2 is responsible for the enzyme association to cell membrane and for controlling several ion channels. In accordance to its pleiotropism, CK2 requires strict control in fact its down-regulation has been implicated in neurodegenerative, inflammatory, vascular, skeletal muscle and bone tissue diseases as well as viral diseases, parasitosis and several types of cancers. [57]

CK2 overexpression in neurodegenerative disorders such as Alzheimer and Parkinson has been reported. [58-62] In particular, CK2 phosphorylate proteins, such as tau-protein and α-synuclein, directly involved in the progression of these pathologies. The former stabilises microtubules and cytoskeleton components and is abundant in the neurons of the central nervous system. Dementia pathologies can occur when tau-proteins become defective and no longer stabilise the microtubule system.

The latter is abundant in the central nervous system, mainly localised in the presynaptic terminals, which release neurotransmitters and it aggregates to form insoluble fibrils in pathological conditions. [58-62]

The overexpression of CK2 has been shown in several inflammatory diseases, as many CK2 substrates are involved in signalling pathways implicated in inflammation processes. CK2 has also been reported in atherosclerosis, laminar shear stress, hypoxia, angiogenesis and angiogenesis related diseases. [63, 64]

Phosphorylation of viral proteins has then been reported in several recent studies. CK2 is involved in replication and transcription processes of the viral genome and it is also able to regulate the viral enzyme activity. For example, CK2 activity has been shown overexpressed in herpes virus type 1 and Epstein-Barr virus. Moreover, HIV-1 reverse transcriptase is also phosphorylated by CK2. [65-68]

Finally, CK2 activity is associated with carcinogenesis. CK2 hyperactivity was demonstrated in several cancers, such as colorectal, breast, prostate tumours and leukaemia. CK2 has been implicated in every stage of cell cycle progression. One of the most well-established roles of CK2 in G1/S phase is the regulation of protein p53, a tumour suppressor involved in DNA damage signalling, which can elicit both cell cycle arrest and induction of apoptosis. This transcription factor is phosphorylated by CK2 in response to DNA damage, resulting in an increased DNA transcriptional activation. [69-71]

CK2 can be considered a valuable drug target, in particular for cancer therapy because it is present at abnormal levels in cancer, it strongly promotes cell survival and it strengthens the multidrug-resistance phenotypes, thus establishing favourable conditions for carcinogenesis.

1.2.1.4. CK2 inhibitors

Kinase inhibitors can be divided into five different groups: [28]

- Type I, classical ATP-competitive inhibitors.
- Type II, inhibitors that partially bind to an allosteric pocket.
- Type III, inhibitors that specifically bind to an allosteric pocket close to the ATP-binding region.
- Type IV, inhibitors that directly compete with the protein kinase substrate.
- Type V, allosteric inhibitors that bind to a pocket unrelated to the substrate or ATP binding regions. [72]

The majority of CK2 inhibitors belongs to the Type I group. ATP competitive inhibitors have been developed by the combination of SAR studies based on in silico models, organic and peptide synthesis, biological assays and structural biology studies. X-ray crystal structures of CK2 in complex with ATP-competitive inhibitors are reported in the Protein Data Bank (PDB).

Only very recently, the oral compound CX-4945 (**1**, IC_{50} = 0.38 nM, K_i = 1 nM), a potent and selective ATP-competitive CK2 inhibitor developed by Cylene Pharmaceutical, has entered the Phase I clinical study in patients with advanced solid tumours, Castelman's disease and multiple myeloma, thus giving a new impulse in the research and identification of novel type I CK2 inhibitors. [73]

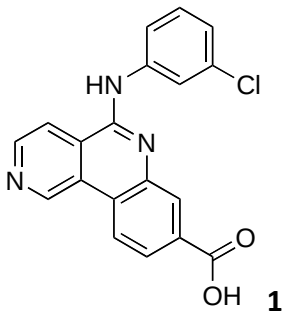

1

Fig. 8 CX-4945

The X-ray crystal structure of human CK2α in complex with CX-4945 (**1**, Fig. 9) firstly discloses two hydrogen bond interactions: the pyridine group of CX-4945 (**1**) interacts with Val116 within the hinge region and the carboxylate substituent of CX-4945 (**1**) interacts with Lys68. Furthermore, two water molecules (W1 and W2) mediate additional protein-inhibitor interactions. [73]

The combination of these interactions and the planar three-ring structure of CX-4945 within CK2-catalytic domain establish the structural basis for the high-affinity binding of this inhibitor. [73]

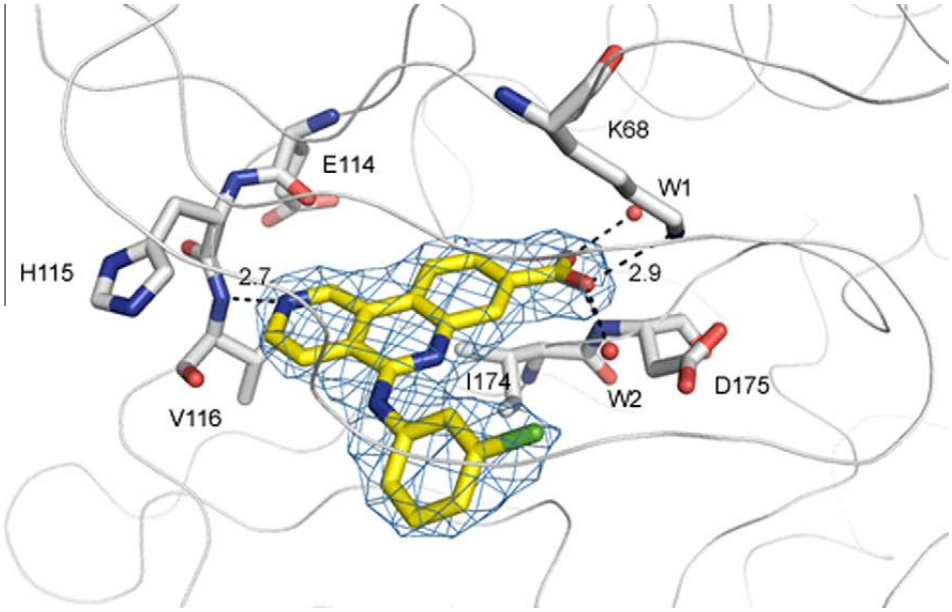

Fig. 9 CK2 in complex with CX-4945 (**1**, PDB code: 3NGA) [73]

Type I inhibitors

The most representative classes of CK2 inhibitors belonging to Type I group are: [28, 31]

- Benzimidazole derivatives.
- Natural derivatives: ellagic acid, flavonoids and coumarins.
- Anthraquinones and xanthenones.
- Pyrazolo-triazine derivatives.
- Carboxyl acid derivatives.

Benzimidazole derivatives

DRB (**2**, 5,6-dichloro-1-(β-D-ribofuranosyl)benzimidazol) was the first CK2 ATP-mimetic inhibitor (K_i = 23 μM) identified and was the starting point for a new fruitful class of polyhalogenated benzimidazole compounds. [74]

Among them TBB (**3**, 4,5,6,7-tetrabromobenzotriazole) showed a K_i value of 0.4 μM and to be selective on a panel of 30 protein kinases. Moreover, TBB (**3**) also showed to be efficiently active on endo-CK2. [75]

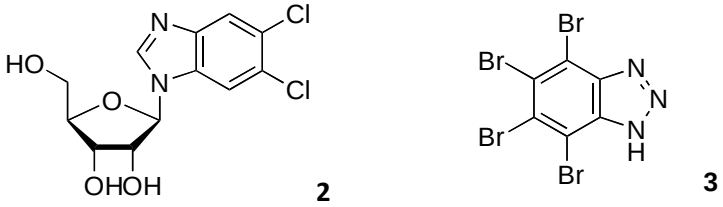

Fig. 10 DRB (**2**) and TBB (**3**)

The presence of four bromine atoms on the benzene ring seems to play a critical role, assuring the optimal hydrophobic interactions, in particular with Val66 and Ile174 residues within the catalytic pocket (Fig. 11). [76] Reduction of the number of the bromine atoms or their replacement by less bulky halogen atoms severely impairs CK2-inhibitory activity.

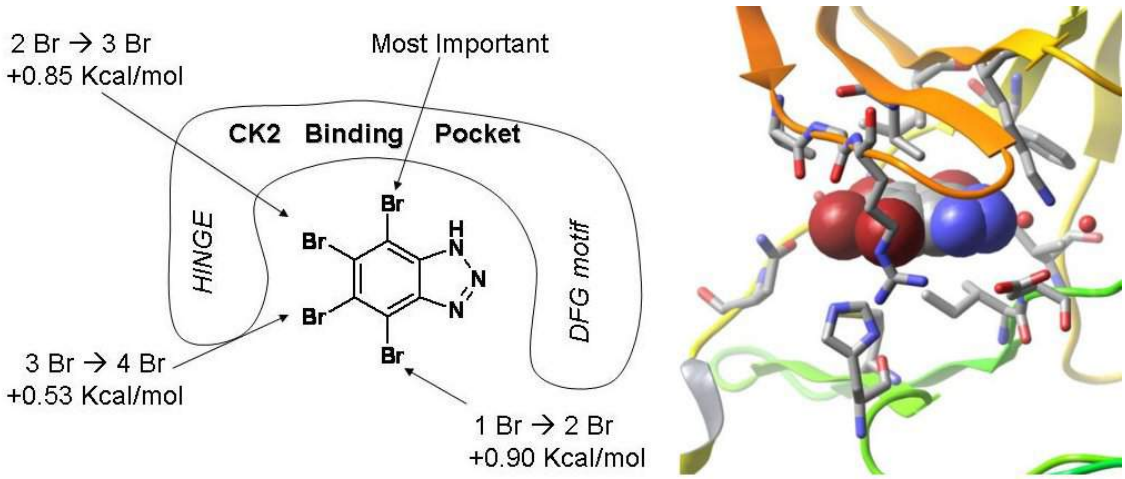

Fig. 11 Role of the bromine functionalities (left) and CK2 in complex with TBB (**3**, right) [76]

CK2-catalytic pocket presents a hydrophobic character and this characteristic plays a key role for inhibitors binding. An estimation of each bromine functionality importance was reported using a linear interaction energy (LIE) model. This approach was used to evaluate the binding free energy of this class of inhibitors. In particular, the bromine group in 4-position, localised deep inside the ATP pocket, is the most important, followed by bromine groups at the benzimidazole 7-, 5- and 6-position respectively, as they are more exposed to the solvent. [76]

Since then, several other benzimidazole-based inhibitors were designed and synthesised (Fig. 12). [31]

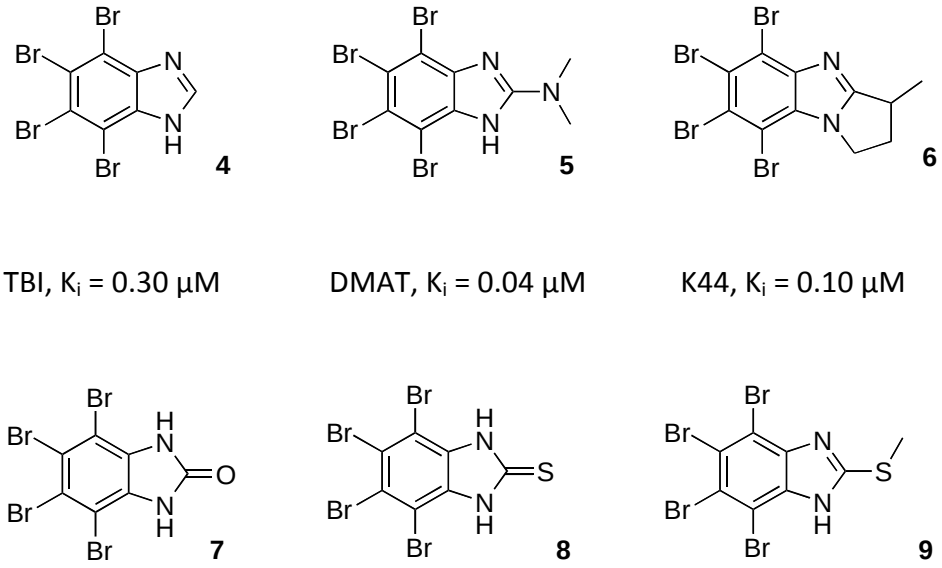

Fig. 12 Polyhalogenated benzimidazole-based CK2 inhibitors

DMAT (**5**, K_i = 0.04 µM) can be considered one of the best polyhalogenated benzimidazole-based CK2 inhibitors. DMAT showed good pharmacokinetics, cell permeation and pharmacodynamics characteristics. K32 (**7**) and K22 (**8**), with DMAT (**5**), have a similar CK2-binding mode to TBI (**4**). [77]

In the case of TBI, the bromine groups at the benzimidazole 5- and 6-position interact with the backbone carbonyls of Glu114 and Val116 (Fig. 13). [78] K44 (**6**) was shown about 60° rotated compared to the previous CK2 inhibitors, in fact the bromine groups at the benzimidazole 4- and 5-position of compound K44 (**6**) interact with the hinge region. [79, 80]

Finally, K37 (**9**) displayed two different orientations: one similar to K44 (**6**) and the other one similar to the other inhibitors. Both the hydrophobic and polar moieties of these inhibitors are fundamental in the interaction with the enzyme, one responsible for the potency and the other responsible in orienting the molecules in the ATP-binding site. [31]

Comparison between TBB (**3**) and TBI (**4**) binding modes disclosed a different orientation of the two inhibitors within the active site (Fig. 13). [31]

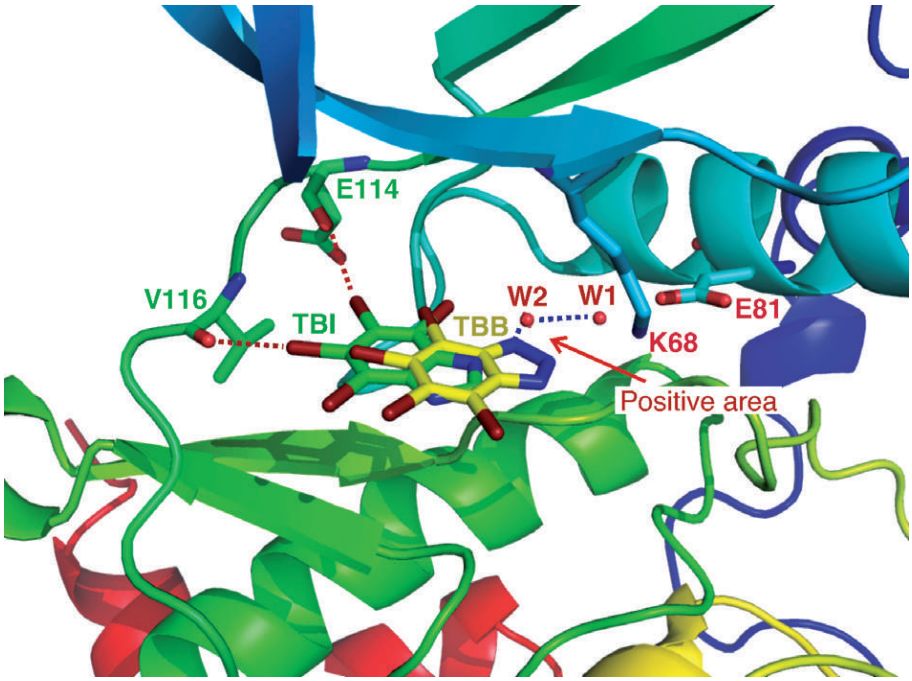

Fig. 13 CK2 in complex with TBB (**3**) and TBI (**4**) [31]

The acidic nature of TBB (**3**, pKa = 8.9), ionised on the imidazole ring at physiological pH, ensure an interaction with Glu 81 residue. This does not occur with TBI (**4,** pKa = 5), which presents a triazole ring instead of the imidazole ring. [81]

Using the benzimidazole scaffold as starting point, in order to reach the substrate-binding region, a series of new inhibitors were synthesised. The aim of this strategy was to design inhibitors able to interact simultaneously with the ATP pocket and the substrate-binding domain.

Bi-substrate inhibitors are composed of two different fragments, one that fits inside the ATP-pocket and the other that reaches the substrate-binding domain, with phospho-donor and phospho-acceptor characteristics respectively. [82] Recently, Enkvist *et al*. reported the design and synthesis of bi-substrate inhibitors. [83] In particular, ARC-1154 (**10**, Fig. 14), a CK2 bifunctional inhibitor composed of a tetrabromobenzimidazole moiety and a peptidic chain linked through an aliphatic spacer, showed an IC_{50} value of 83 nM on CK2. [83]

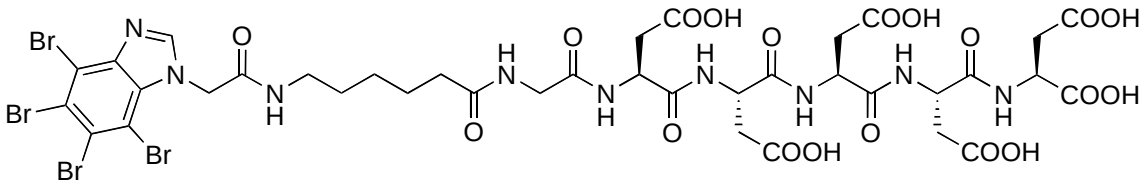

Fig. 14 ARC-1154 (**10**) [82]

The co-crystal structure of the CK2/ARC-1154 complex disclosed that the inhibitor occupies the catalytic pocket with the polyhalogenated benzimidazole moiety, while it was not possible to determine the orientation of the side-chain because its electron-density was not visible.

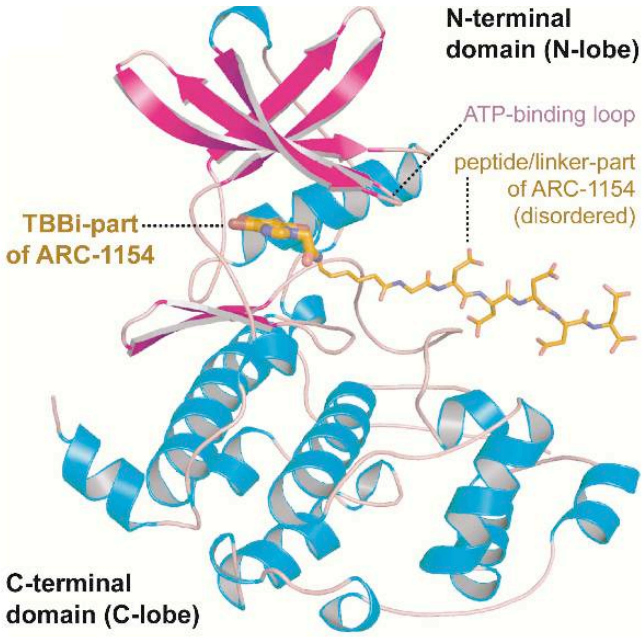

Fig. 15 CK2 in complex with ARC-1154 (**10**, PDB code: 4FBX) [82]

Several polyhalogenated benzimidazole-based molecules, useful as starting point for the synthesis of bi-substrate inhibitors, have been synthesised and explored, so far. In particular, compound K134 (**11**, IC_{50} = 0.12 μM) and compound K137 (**12**, IC_{50} = 0.28 μM) showed good CK2-inhibitory activities and can be easely derivatised for this purpose. [84]

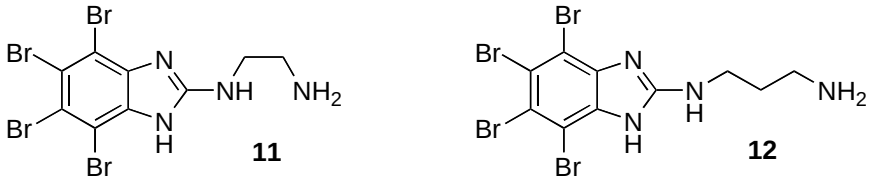

Fig. 16 K134 (**11**) and K137 (**12**)

The bi-substrate approach should serve to improve both selectivity and specificity, which is considered a major problem for the development of novel protein kinase inhibitors due to the conserved domains of these enzymes.

Natural derivatives: flavonoids, ellagic acid and coumarins

Other potent inhibitors of CK2 are related to natural compounds such as flavonoids, ellagic acid and its derivatives and coumarins. Flavonoids represent a class of plant metabolites that can be found in fruit, vegetables, grains, bark, roots, stems, flowers, tea and wine. [85] They are characterised by a relatively low toxicity and thanks to their chemical properties they are active as antiallergic, antimicrobial, anticancer and anti-inflammatory agents, besides they play a fundamental role as scavengers of oxygen-derived free radicals. [85, 86]

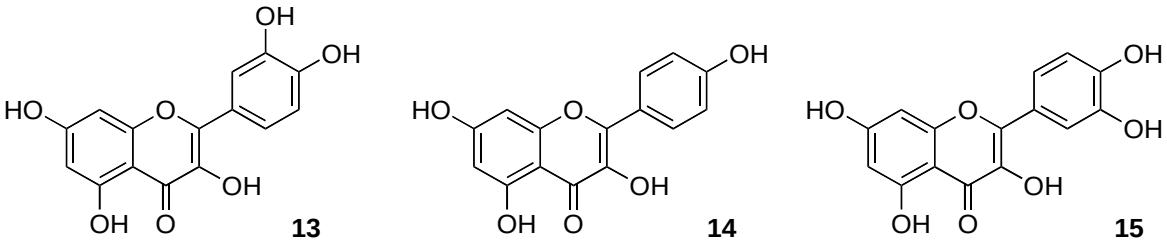

Fig. 17 Quercetin (**13**), Apigenin (**14**), Fisetin (**15**)

Several flavonoids such as quercetin (**13**, 3,3',4',5,7-penta-hydroxy-flavone), apigenin (**14**, 4',5,7-tri-hydroxy-flavone) and fisetin (**15**, 3,3',4',7-tetrahydroxy-flavone) displayed CK2-inhibitory activity with an IC_{50} values of 0.92, 0.55 and 0.80 µM respectively (Fig. 17). [85, 86]

Ellagic acid (**16**) is an ATP-mimetic inhibitor and occupies the ATP active site in a way similar to TBB and other polyphenolic compounds (Fig. 18). [87]

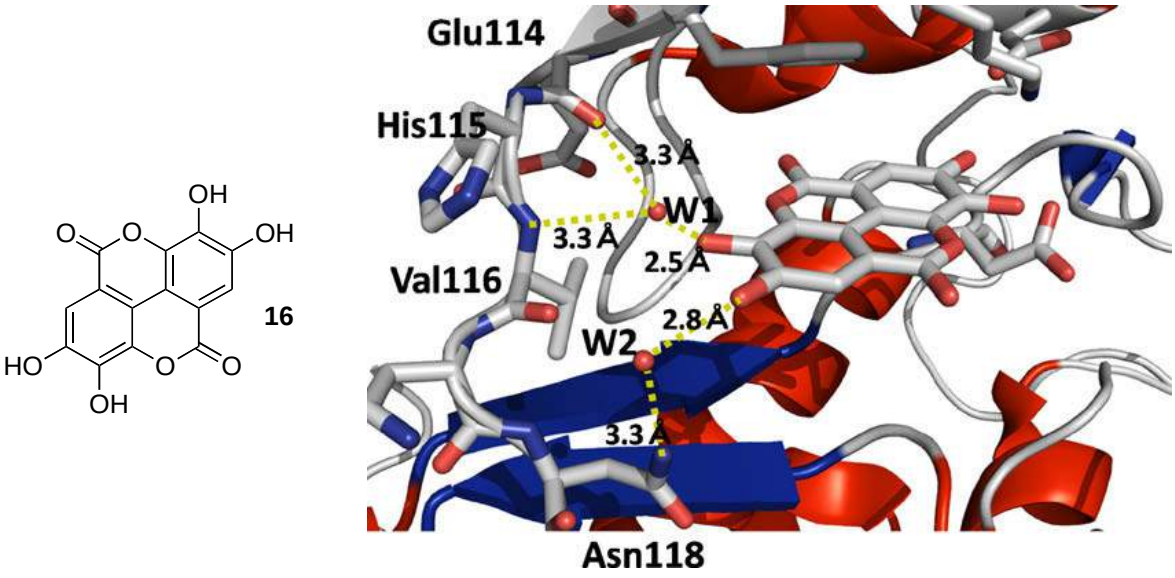

Fig. 18 Ellagic acid (**16**, right) and CK2 in complex with ellagic acid (**16**, left) [87]

Ellagic acid (**16**, K_i = 20 nM) is a very potent and quite specific CK2 inhibitor and presents a planar structure, which can be described as two fused coumarins. Ellagic acid (**16**) can be found in strawberries, raspberries and pomegranates and several studies confirmed its antineoplastic, antioxidant and antimutagenic properties. [87, 88] The X-ray crystal structure of CK2 in complex with ellagic acid (**16**) showed the ability of this inhibitor to simultaneously interact with the hinge region and the phosphate-binding region. In particular, the hydroxyl group at the ellagic acid (**16**) 3-position interacts with Glu114 through a water bridge, while the hydroxyl groups at ellagic acid 7- and 8-position interact with Asp175 through a hydrogen bond. Moreover, the hydrophobic interactions with Val53, Val66, Phe113, Met163 and Ile174 stabilise the CK2-ellagic acid complex. [87]

Coumarins are also largely distributed in plants. Polyhydroxylated coumarins are well known as anticancer compounds for several tumours, such as prostate cancer, melanoma and metastatic kidney carcinoma. A broad series of coumarins, such as DBC (**17**, K_i = 0.06 µM), has been synthesised and tested as CK2 inhibitors. [89]

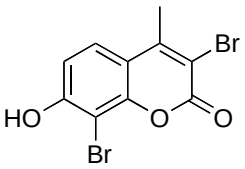

17

Fig. 19 DBC

Anthraquinones and xanthenones

Most of anthraquinone derivatives originate from the natural compound emodin (**18**, K_i = 1.9 µM). [90, 91] Emodin (**18**), is a natural anthraquinones, which can be found in the roots and barks of several plants, molds and lichens and displays anti-inflammatory and antineoplastic properties. Emodin (**18**) was the first anthraquinone-based compound identified as CK2 inhibitor. [90, 91]

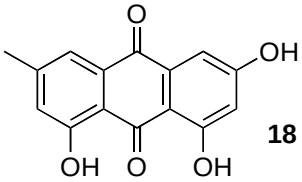

18

Fig. 20 Emodin

X-ray crystal structure of the CK2-emodin complex suggested that the anthraquinone-scaffold performs excellent apolar interactions thanks to its shape and size. [90] Emodin (**18**) encouraged an intensive structure-based inhibitors screening, which brought to the development of CK2 inhibitors, such as MNX (**19**, 1,8-dihydroxy-4-nitro-xanthen-9-one), MNA (**20**, 1,8-dihydroxy-4-nitro anthraquinone) and DAA (**21**, 1,4-diamino-5,8-dihydroxy anthraquinone). [92-94]

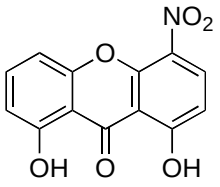

19

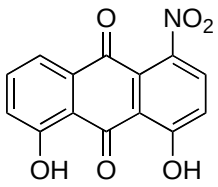

20

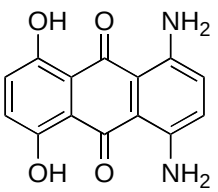

21

Fig. 21 MNX (**19**), MNA (**20**), DAA (**21**)

Recently, quinalizarin (**22**, 1,2,5,8-tetrahydroxy-anthraquinone), a novel CK2 inhibitor, was identified and showed to be a potent ATP-competitive CK2 inhibitor with a K_i value of 60 nM. [95]

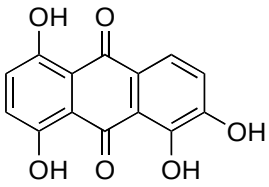

22

Fig. 22 Quinalizarin

Pyrazolo-triazine derivatives

Pyrazolo-triazine-based derivatives represent another family of ATP-mimetic CK2 inhibitors. These inhibitors were designed by Polaris Pharmaceuticals and can be considered the most potent CK2 inhibitors known so far. [96, 97] The pyrazolo-triazine moiety occupies the adenine region and interacts with Val116 in the hinge region via two hydrogen bonds. [31]

A series of macrocyclic pyrazolo-triazines were also designed and synthesised in order to obtain drug-like candidates. In particular, compound **23** (K_i = 24 nM) was obtained and the co-crystal structure within CK2 active site was determined. [31] An alkyl linker, which fits into the hydrophobic region I, was introduced and enabled important hydrophobic interactions with the enzyme. The amide group interacts with Asp175 and Lys68 *via* two hydrogen bonds. [31]

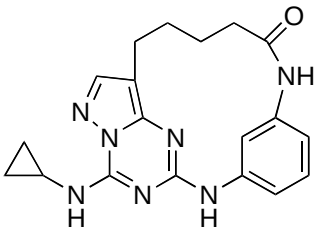

23

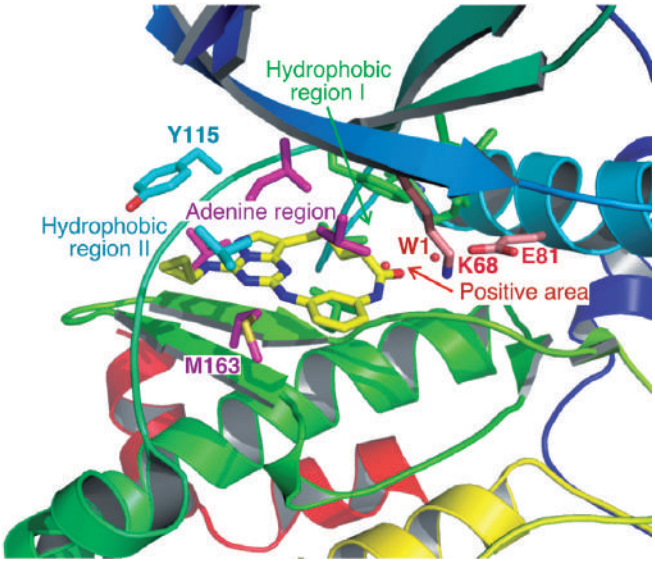

Fig. 23 CK2 in complex with compound **23** [31]

Compounds of this family, with potent CK2-inhibitory activity, are currently under investigation for their antineoplastic properties.

Carboxyl acid derivatives

This is another interesting class of inhibitors. Indoloquinazoline IQA (**24**, 5- oxo-5,6-dihydroindolo-(1,2-a)quinazolin-7-yl acetic acid) was one of the first compounds identified by Novartis, with a K_i value of 0.40 μM. [98, 99]

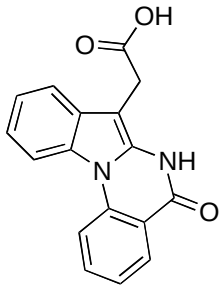

24

Fig. 24 Indoloquinazoline IQA (**24**)

Other CK2 inhibitors

Type II and III CK2 inhibitors display a double mode of binding: one, which partially recognises the ATP-binding domain, the other, which recognises a hydrophobic binding region in its proximity. The development of Type II or Type III CK2 inhibitors is complicated because of CK2 constitutively active characteristic. [100] No type IV or V CK2 inhibitors, able to compete with the substrate and to interact at the interface region between CK2α and CK2β subunits, have been identified so far. [28]

1.3. Cyclin-dependent Kinases (CDKs)

CDKs are a family of conserved Ser/Thr protein kinases, which are grouped in the CMGC kinase family with other 39 kinases and can be divided into two main groups: those involved in cell cycle and others. [101] CDKs are relatively small proteins, with molecular weights in a range of 34-40 kDa and are activated by binding to regulatory subunits, known as cyclins, which were discovered in 1982 by Hunt T. [102] Cyclins are synthesised and degraded at specific times during the cell cycle (Fig. 25), thus regulating kinase activity. To date thirteen CDKs have been identified in humans and only a certain subset of CDK-cyclin complexes is directly involved in driving the cell cycle. In particular, they include three interphase CDKs (CDK2, CDK4 and CDK6), a mitotic CDK (CDK1) and ten cyclins belonging to four different classes (A-, B-, D- and E-type cyclins). CDKs are inactive in their monomeric conformation, while they are activated by binding to cyclins, thus forming an active heterodimer. [103-105]

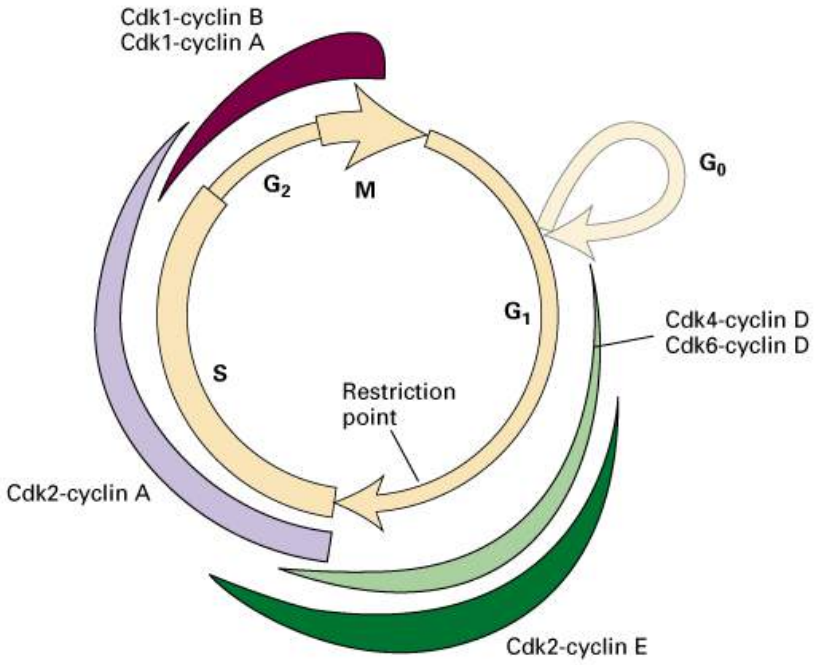

Fig. 25 CDK/Cyclin complexes involved in cell cycle progression [106]

The progression from G0 to S phase involves three CDKs: CDK4, CDK6 and CDK2. Mitogen signals stimulate the synthesis of cyclin D, while CDK4 and CDK6 are carried to the nucleus.

CDK4/Cyclin D and CDK6/Cyclin D complexes accumulate in G1 phase and phosphorylate members of the retinoblastoma (Rb) protein family. Phosphorylation of pRb activates the synthesis of cyclin E, which binds to CDK2. CDK2 activity is restricted to the G1-S phase and is essential for the G1/S transition. CDK2 associates either with cyclin E or cyclin A. In particular, cyclin E binds to CDK2 during G1 phase, while binding with cyclin A is required to progress through S phase. In this phase, DNA replication starts to ensure only one replication and CDK2/Cyclin E complex is silenced by degradation of cyclin E. Once CDK2/Cyclin E complex has been dissociated, CDK2 binds cyclin A1 and cyclin A2. These complexes are responsible for phosphorylation of several proteins essential for S phase exit. At the end of S phase, cyclin A binds preferably to CDK1 and CDK2. During G2 phase, cyclin A is degraded, while cyclin B is synthesised. With degradation of cyclin A, CDK1 binds to cyclin B, forming a complex essential for mitosis trigger and responsible for the phosphorylation of more than 70 proteins involved in G2/M transition and M phase. Finally, to exit mitosis, cyclin B is degraded by ubiquitination. Of the four main CDKs involved in the cell cycle (CDK1, 2, 4 and 6), only the crystal structures of CDK2 and 6 have been reported so far, even if the amino acid sequences of the other members have been determined. CDK2/Cyclin A and CDK4/Cyclin D complexes are often used as prototypes for the major classes of regulatory pathways that control CDK activity. [107-109] Moreover, to be activated, CDK/Cyclin complexes need to be phosphorylated in the conserved T-loop. This phosphorylation is catalysed by the presence of CDK Activating Kinase (CAK) complex, formed by CDK7, Cyclin-H and Mat1, which is responsible for transcription.[110-112] CDK5 is activated by non-cyclin p35 factor, which is expressed only in neurons, whereas CDK8 and CDK9, activated by cyclins C, T and K respectively, have key roles in the control of transcription by RNA polymerase II. [113, 114] Finally, the activation mechanism of CDK10 still remains unclear and CDK11-CDK13 seem to be activated by L-type cyclins. [115]

Hence, besides binding to cyclins, CDKs are also regulated by other processes such as phosphorylation, tight-binding inhibitors, regulated assembly of holoenzymes, ubiquitin-mediated proteolysis of cyclins and CDK inhibitors. All processes implicated in CDK regulation induce extensive conformational changes, in particular in the shape of the active site. [116]

1.3.1. CDKs as drug targets

Mutated and overexpressed genes, within the human genome, are peculiar in the development and progression of pathological processes (Fig. 26), in particular of cancer.

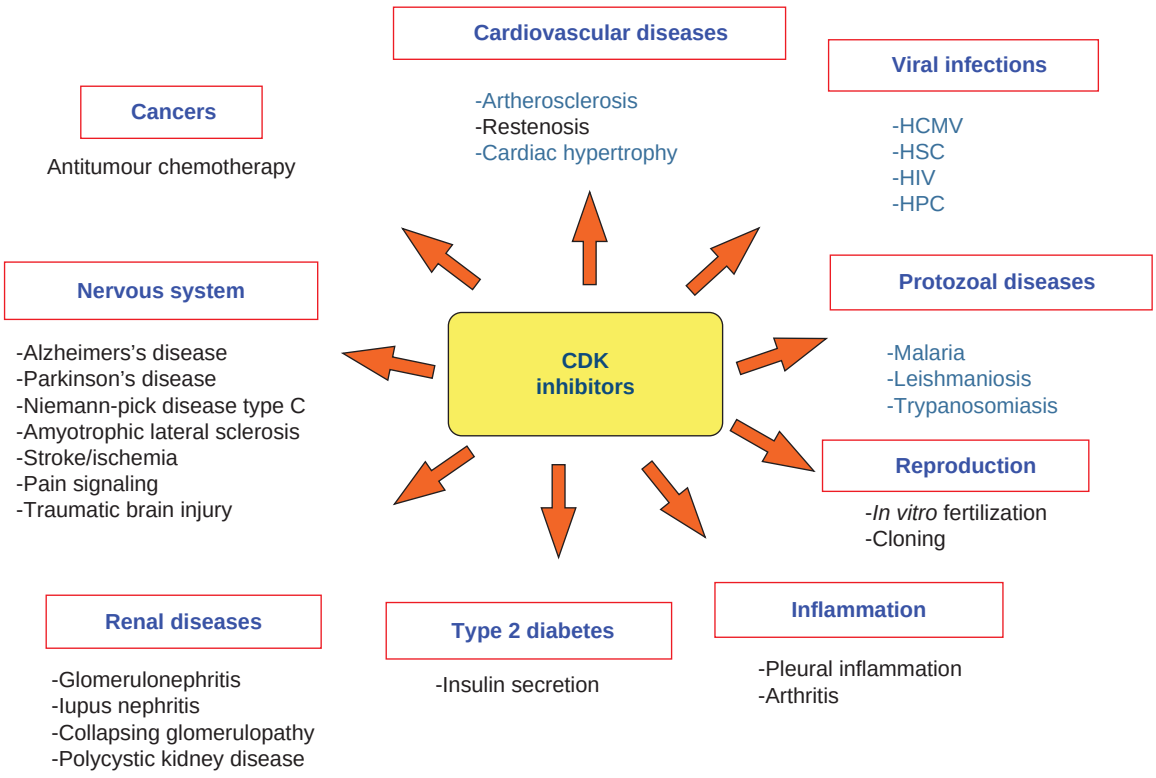

Fig. 26 CDKs implication in diseases [117]

Such modifications are involved in the down-regulation of cell cycle kinases, which is often associated with aberrant division and uncontrolled proliferation of cancer cells. Between the 1970s and 1980s the studies carried out by Hartwell, Nurse and Hunt clarified the mechanisms of mammalian cell division. Furthermore, gene products playing key roles in regulating the cell cycle machinery were investigated as cancer drug targets. [118] At that time, CDKs were also included in these studies, as they could be considered master regulators of cell proliferation. In particular, phosphorylation and subsequent inactivation of pRb by CDKs is a crucial step in the regulation of cell cycle progression, promoting or inhibiting protein biosynthesis (e.g. G1/S transition). [119] CDKs also play an important role in the control of cell cycle checkpoints (e.g. G2/M *via* p53), effectively protecting the integrity of the genome. [120, 121]

A direct link between the molecular pathology of cancer and a number of CDK-related cellular abnormalities was established, such as cyclin overexpression, amplification and mutation of CDKs, loss of endogenous CDK inhibition and altered levels of CDK-specific substrates. The rationale for the design of novel CDK inhibitors relies on restoring the proliferative controls and cell cycle checkpoints in mutated cells. [122] To date, several structurally diverse CDK inhibitors have been reported. The search for novel CDK inhibitors not only intends their use as anticancer agents but also for the treatment of several other diseases, such as Alzheimer, atherosclerosis, HIV and malaria. [123-125]

1.3.2. CDKs inhibition strategies

As previously mentioned, CDKs have been shown overexpressed in several diseases due to several genetic and epigenetic events that affect their regulatory pathways. Despite the intensive search for novel small molecules able to target CDKs, no CDK inhibitors have been approved for commercial use so far. First-generation compounds, which include pan-CDK inhibitors such as flavopiridol (**25**), olomoucine (**26**) and (R)-roscovitine (**27**), generally showed low activity and/or high toxicity in the clinical trials. [105, 126-128]

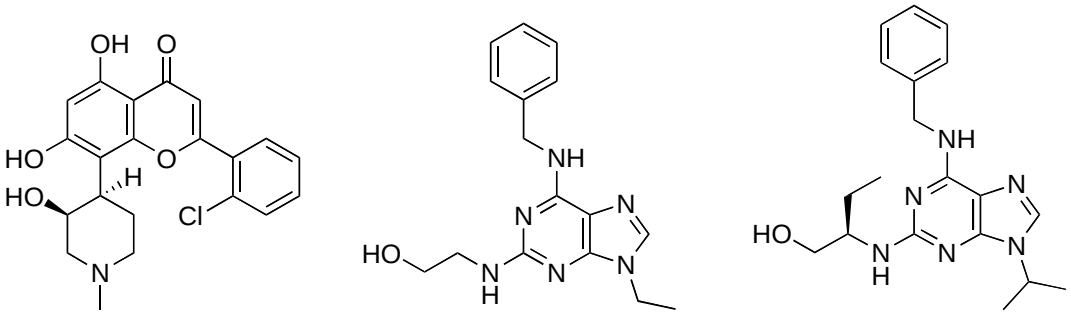

25 **26** **27**

Fig. 27 Flavopiridol (**25**), olomoucine (**26**) and (R)-roscovitine (**27**)

ATP-competitive CDK inhibitors have also been developed and few of them are currently undergoing clinical trials. For example, the pyrazole-3-carboxamide AT-7519 (Fig. 30), a pan-CDK inhibitor, recently entered Phase I clinical trials in patients with advanced solid tumours or refractory non-Hodgkin's lymphoma. [105, 129]

The 2,6,9-trisubstituted purine family, which also includes (R)-roscovitine and the second-generation CDK inhibitors such as NU6140 (**28**), has also been intensively explored for CDK-inhibitory activity in order to identify novel analogues with enhanced potency and selectivity. [130]

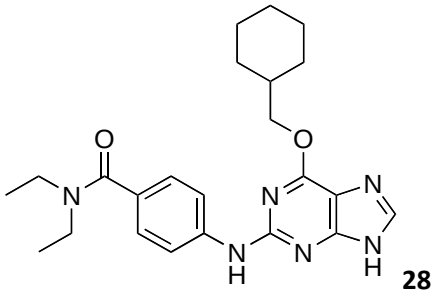

28

Fig. 28 NU6140 (**28**)

Second-generation CDK inhibitors can be grouped into three different classes:

- Compounds with a broad CDK activity spectrum, such as SNS-032 (**29**) and R547 (**30**). [131-133]

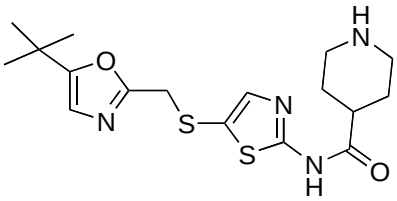

29

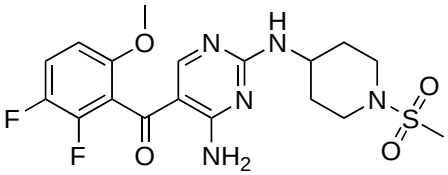

30

Fig. 29 SNS-032 (**29**) and R547 (**30**)

- Compounds with preferential CDK4/CDK6- or CDK2-inhibitory activity, such as AT-7519 (**31**, CDK2) and P276-00 (**32**, CDK4/CDK6). [105, 129, 134, 135]

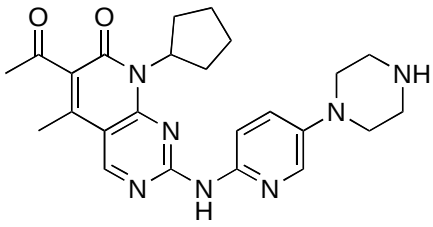

31

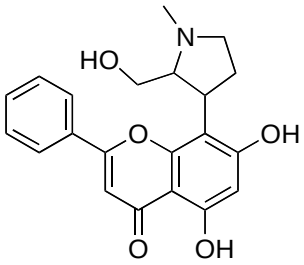

32

Fig. 30 AT-7519 (**31**) and P276-00 (**32**).

- Compounds with CDK-inhibitory activity and off-kinase targets, which can be exploited to enhance their anticancer activity. This class includes ZK-304709 (**33**, CDK/VEGFR activity) and JNJ-7706621 (**34**, CDK/Aurora A and B activity). [136-138]

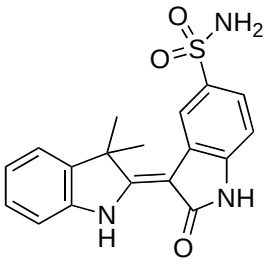

33

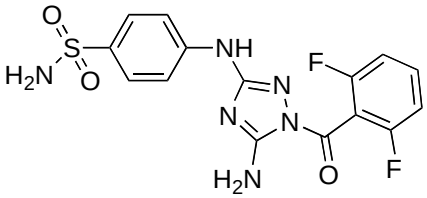

34

Fig. 31 ZK-304709 (**33**) and JNJ-7706621 (**34**).

A crucial question that remains unanswered for CDK inhibitors is which CDK or spectrum of CDKs should be targeted. Selectivity is still a key issue in the development of CDK inhibitors.

1.3.3. Cyclin-dependent Kinase 2 (CDK2)

CDK2 has been shown overexpressed in several tumours, such as lung carcinoma, melanoma, osteosarcoma, ovarian carcinoma, pancreatic cancer and sarcomas. Furthermore, deregulation of cyclin A and cyclin E is also often noticed in cancer. [139] For years, CDK2 has been regarded as a controversial target. CDK2 activity has been studied in several tumour cell lines and inhibition of CDK2 was showed not to cause growth arrest in some of them. CDK2 activity was found to be dispensable for G2/S transition in colon carcinoma but no cell accumulation was noticed in G0/G1 transition. From these observations, CDK2 did not appear essential in cell cycle progression and CDK1 and CDK4 were suggested to substitute CDK2 during the phosphorylation process. Anyway, recent results have re-positioned CDK2 as crucial regulator of the cell cycle. With genetic loss, cyclin E binds to CDK1, as its CDK2 partner does not exist, but when CDK2 is inhibited cyclin E does not switch partner and as a result does not bind to CDK1. [140-142]

Moreover, CDK2 was found overexpressed in MYCN-amplified neuroblastoma, causing bad prognosis and suppression of CDK2 led to apoptosis of mutated cells. [141, 143]

Hence, CDK2 still appears as a good candidate target for novel valid therapeutic approaches. Phosphorylation of pRb by CDK2 is the penultimate step in the G1/S transition before release of the transcription factor E2F and entry into S phase (Fig. 32). Inhibition of this step may result in inhibition of proliferation and apoptosis of transformed cells. [105]

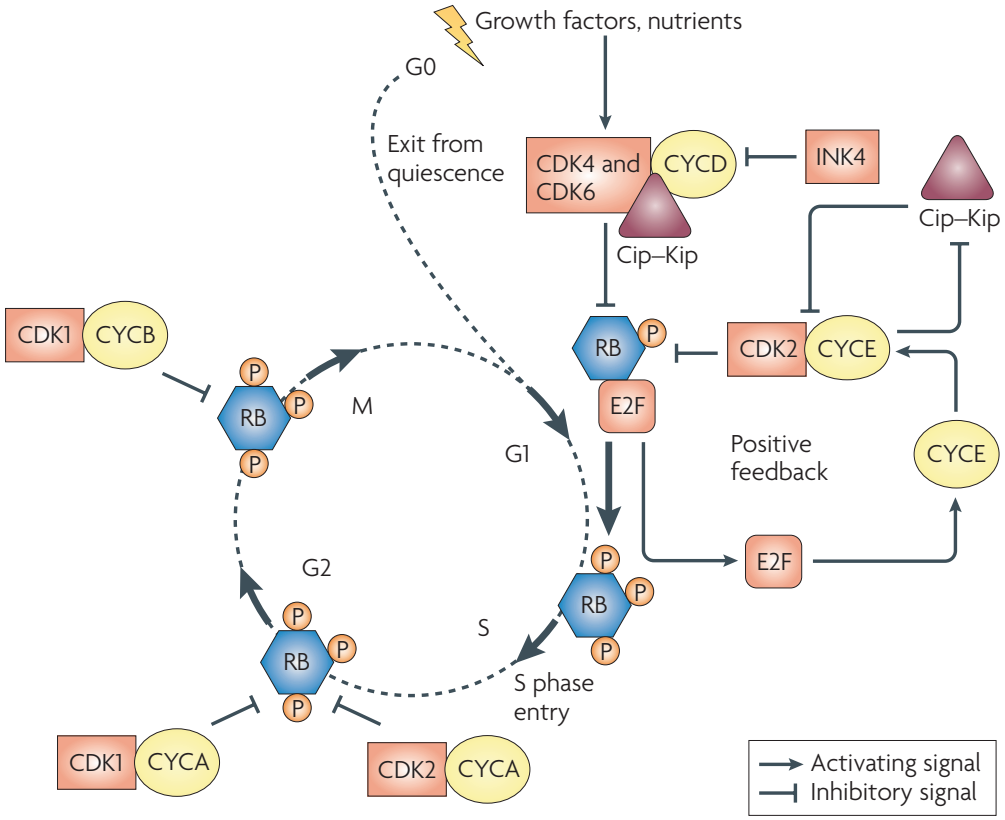

Fig. 32 The cell cycle control [105]

Unlike CDK4- and CDK6-mediated phosphorylation of pRb, CDK2 is less affected by external stimuli. CDK2 also intervenes throughout S phase and in G2/M transition to regulate cell growth and division. In general, CDK2 works as part of a complex, which involves cyclin A or E and cell cycle regulatory proteins, such as p21, PCNA, p27, $p45^{SKP2}$, $p19^{SKP1}$ and cks1/cks2. Inhibition of CDK2 activity may be critical for pRb-mediated cell cycle arrest. CDK2/Cyclin E and CDK2/Cyclin A complexes have different functions in the regulation of pRb-mediated repression of E2F. [105]

In particular, CDK2/cyclin A binds directly to E2F-1 and inhibits the DNA-binding activity of E2F-1/DP-1 complex. The activity of this complex is inhibited following phosphorylation by CDK2/Cyclin A. Overexpressed E2F, in the absence of CDK2 expression, can initiate entry into S phase. Likewise, overexpression of CDK2 can replace E2F activity in the transition to S phase. [105] Concerning the physiological inhibition of CDK2 activity, natural CDK inhibitors, such as members of the Cip/Kip and INK4 families, participate during cell cycle progression. [144] Not surprisingly, novel compounds able to replace altered tumour suppressor genes are prime targets in current cancer research. Moreover, restoring the functions of natural CDK2 inhibitors or perturbing CDK2 functions may reveal novel effective anticancer strategies through antiproliferative, cytostatic or pro-apoptotic mechanisms.

1.3.3.1. CDK2 activation mechanism

CDKs are activated in a two-step process: 1) binding to a cyclin and 2) phosphorylation of the complex formed (Fig. 33). In particular, CDK2 presents a relatively highly conserved N-terminal lobe (β-sheet), a C-terminal lobe (α-helix) and an ATP binding-site. [145,146]

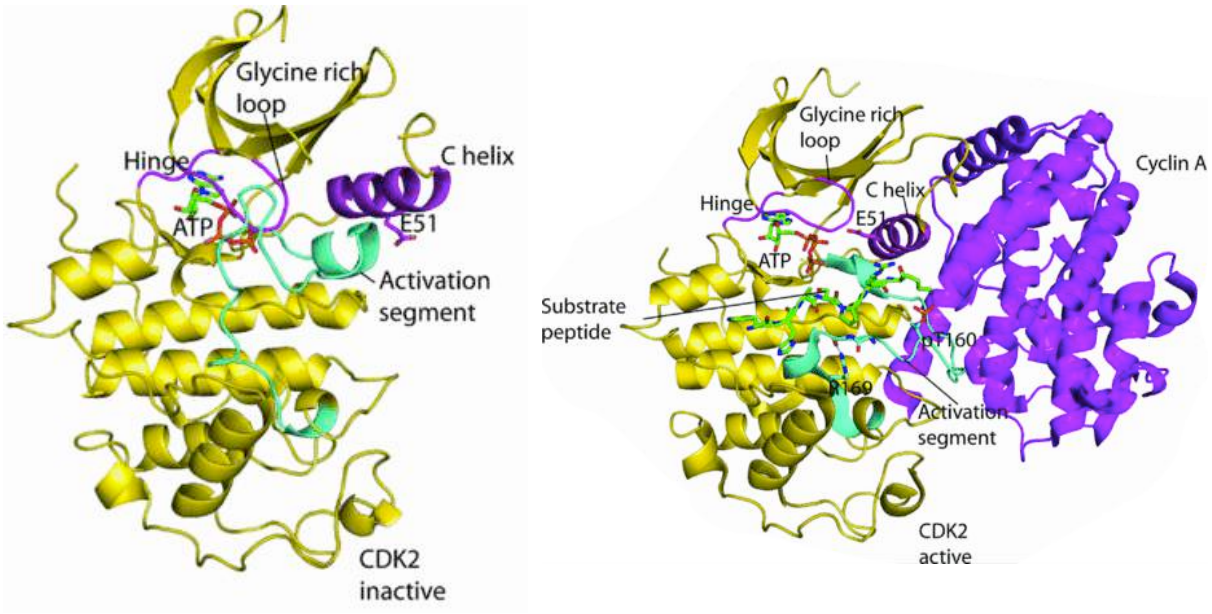

Fig. 33 ATP/CDK2/Cyclin A complex (pdb code: 1HCK) [145]

Although monomeric CDK2 will bind ATP, the residues within the ATP-binding site are incorrectly positioned to align the triphosphate moiety of ATP for catalysis, conferring a poor catalytic ability to the monomeric unit, which is regarded as almost completely inactive. Kinetic studies revealed that cyclin-binding increases the affinity of CDK2 for ATP by 3-fold and decreases its release from the active site by up to 5-fold. [147] In its inactive conformation, the T-loop blocks the access to the substrate-binding site and the conformation of the ATP pocket limits the interactions with the phosphate group of the ATP. Cyclin binding to the PSTAIRE sequence induces conformational changes freeing the entry of the ATP pocket, which is the first step for the activation of the multiprotein complex. In this step, Asp145, Glu51 and Lys33 participate altering their positions and thereby orienting the ATP for catalysis. The second step consists in the phosphorylation of the T-loop (Thr160) by CAK complex allowing CDK2 activation. [148]

1.3.3.2. CDK2 inhibitors

As previously mentioned, the ATP-binding domain is relatively highly conserved between the kinase family members, reflecting the difficulty of designing selective ATP-competitive kinase inhibitors, but despite different kinase inhibition approaches (outlined in Par. 1.1.), the majority of CDK2 inhibitors are ATP-competitive. [149-151]

The X-ray crystal structure of the ATP/CDK2/Cyclin A complex (Fig. 34) showed the presence of two key hydrogen bond interactions between ATP (**35**) and the CDK2-catalytic domain: 1) between purine N1 atom and Leu83 in the hinge region of CDK2; 2) between the amino group at the purine 6-position and the carbonyl group of Glu81 in the hinge region of CDK2. [145]

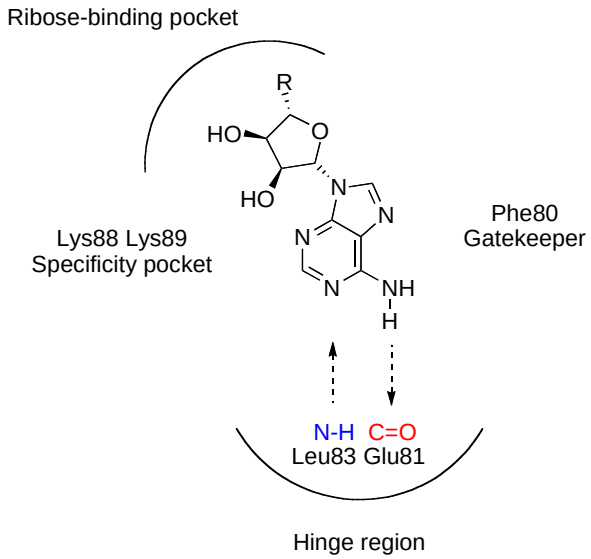

Fig. 34 Interactions of ATP (**35**) within CDK2

As highlighted in Fig. 34, there are then other hydrophobic and Van der Waals interactions between ATP and CDK2 active site, such as between the ATP ribose moiety and the hydrophobic pocket within the catalytic domain. All these interactions are peculiar for most of the ATP-competitive CDK2 inhibitors.

1.3.3.2.1. Purine-based CDK2 inhibitors

Previous work carried out at Newcastle University focused on the synthesis and evaluation of O^6-substituted guanine derivatives as potential CDK2 inhibitors. The CDK2 project at Newcastle University started with NU2058 (**36**, Fig. 35), an ATP-competitive purine-based inhibitor, which exhibited moderate inhibition of CDK1/Cyclin B and CDK2/Cyclin A, with IC_{50} values of 26 µM and 17 µM, respectively. NU2058 was shown to bind the CDK2/Cyclin-A complex *via* a triplet of hydrogen bonds between the purine and the CDK2 hinge region. The cyclohexylmethoxy moiety was shown to interact with the ribose-binding pocket, whilst the imidazole ring of the purine makes a π-π interaction with the Phe80 residue (Fig. 35). [152]

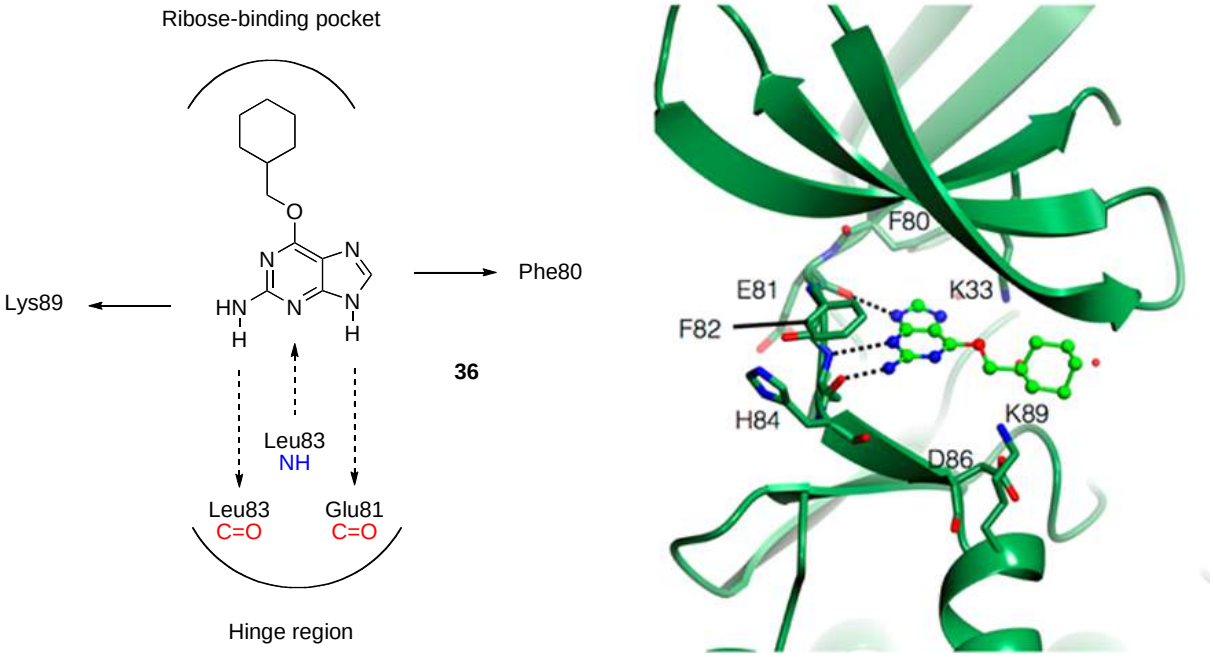

Fig. 35 CDK2-NU2058 (**36**) interactions (left) and CDK2-NU2058 (**36**) complex (right) [152]

Comparison of the binding mode of NU2058 (**36**) with other known purine-based inhibitors, such as olomoucine (**26**) bound to CDK2/Cyclin A, revealed a different binding orientation, indicating the formation of a triplet of hydrogen bonds with the CDK2 hinge region. Conversely, olomoucine (**26**) stretches out of the CDK2 ATP-binding domain and interacts with the specificity surface of the enzyme (Fig. 36). [153]

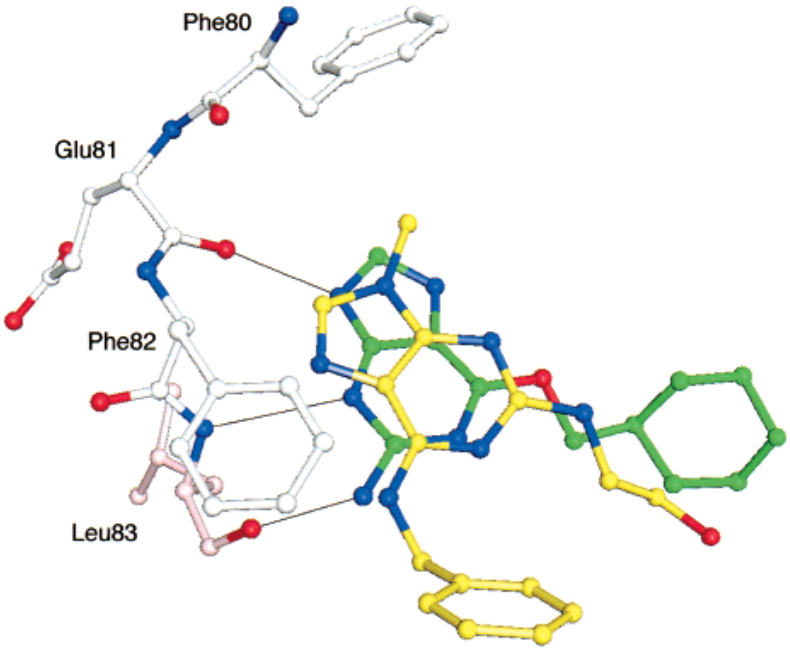

Fig. 36 NU2058 (**36**) and olomoucine (**26**) in complex with CDK2 (PDB code: 1E1V) [153]

SAR studies suggested that N^2-substitutions of NU2058 (**36**) would afford compounds with enhanced potency and selectivity and having a cyclic hydrophobic substituent for the O^6-position, such as the cyclohexylmethoxy moiety, seemed optimal for CDK2-inhibitory activity. [153]

In order to further probe the specificity pocket, a structure-based development was used to introduce different functionalities at the purine 2-position, whilst maintaining the cyclohexylmethoxy moiety. A series of novel interesting ATP-competitive CDK2 inhibitors were obtained.

A 2-anilino-6-cyclohexylmethoxy purine, NU6904 (**37**), was obtained. This compound showed an IC_{50} value of 1 μM on CDK2 and it also showed to be similarly active on CDK1. To confirm and rationalise this result, the crystal structure of NU6904/CDK2 complex was obtained. Within the CDK2 ATP-binding domain, NU6904 (**37**) showed the same H-bond interactions, as for NU2058 (**36**), with the CDK2 hinge region. The N^2-anilino group, as expected, stretched out towards the specificity pocket where Lys89 is and disclosing a π-π interaction with Asp86 (Fig. 37). [154]

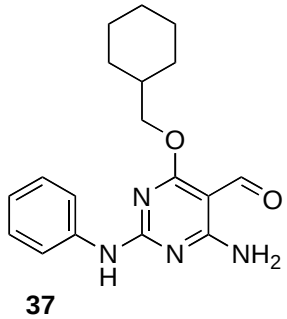

37

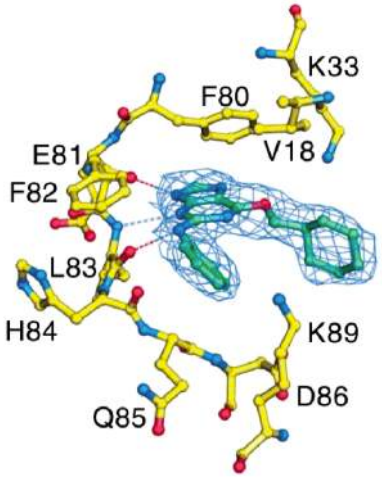

Fig. 37 NU6904 (**37**) and NU6904 (**37**) in complex with CDK2 (PDB code: 1H1Q) [154]

Another inhibitor was then explored having a chlorine substituent in meta-position on the N^2-anilino group (Fig. 38). However, the inhibitory activity of NU6086 (**38**) over CDK1 and CDK2 did not show any improvement compared to the parent compound NU2058 (**36**). [154]

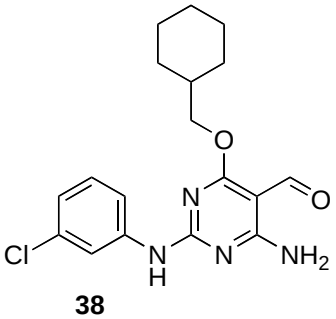

38

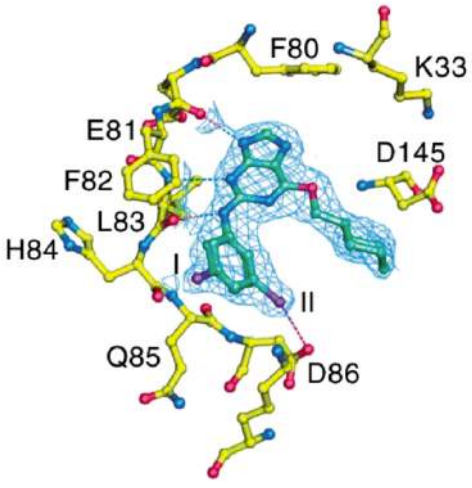

Fig. 38 NU6086 (**38**) and NU6086 (**38**) in complex with CDK2 (PDB code: 1H1R) [154]

In the attempt to increase the potency of CDK2 purine-based inhibitors, the introduction of a sulfonamide moiety, in para-position on the N^2-anilino substituent, allowed new interactions as for compound NU6102 (**39**, IC_{50} = 5 nM, for CDK2). A sulfonamide oxygen accepts an H-bond from the backbone NH of Asp-86, while the sulfonamide NH_2 group donates an H-bond to the side-chain carbonyl of Asp86 (Fig. 39). [154]

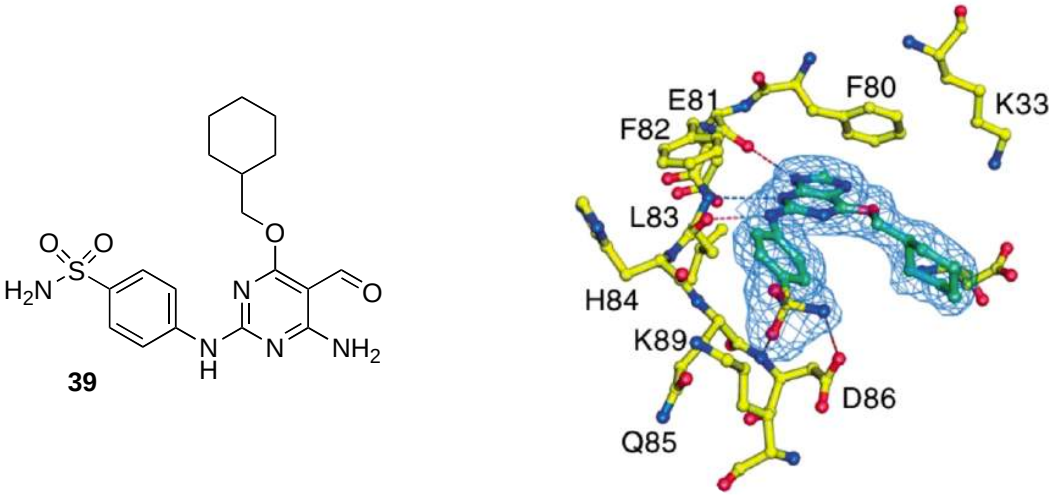

Fig. 39 NU6102 (**39**) and NU6102 (**39**) in complex with CDK2 (PDB code: 1H1S) [154]

Nevertheless, tumour cell growth inhibition for NU6102 (**39**) was only observed in the 1-10 µM concentration range, suggesting poor cellular uptake or failure to effectively compete with high intracellular levels of ATP. [154]

Sulfone derivatives led to NU6300 (**40**), the first irreversible CDK2 inhibitor, which showed an IC_{50} value of 63 nM on CDK2 (Fig. 40). Several studies revealed that NU6300 could be considered an irreversible inhibitor due to a covalent bond interaction between the electrophilic vinyl sulfone moiety and Lys89 within the CDK2 specificity pocket. This observation was confirmed by X-ray crystallography and supported by kinetic and molecular biology studies. [155]

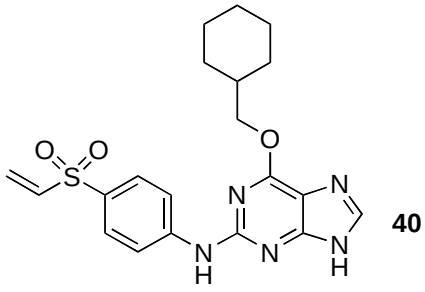

Fig. 40 NU6300 (**40**)

In particular, the vinyl sulfone moiety can be involved in a Michael addition reaction with nucleophilic residues, in our case NU6300 (**40**) showed to react with Lys89. [156] To demonstrate this irreversible behaviour several approaches were undertaken. Early biology studies showed compound NU6300 (**40**) displaying a time-dependent inhibition of CDK2, with enzyme activity decreasing as a function of the time of exposure to the inhibitor. [155]

The results showed the enzyme losing its activity proportionally to the inhibitor exposure time (Fig. 40), suggesting that a covalent modification was taking place. This was also confirmed by a parallel experiment, which engaged the inhibitor NU6310 (**41**), with an ethyl sulfone instead of a vinyl sulfone moiety (Fig. 41). [155]

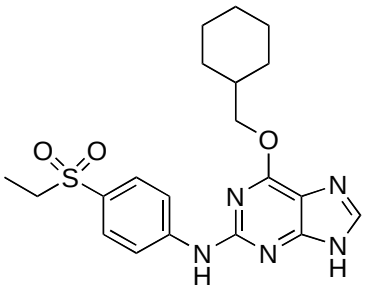

41

Fig. 41 NU6310 (**41**)

As expected, NU6310 (**41**) showed a reversible behaviour, as the CDK2/Cyclin A activity did not decrease in a time-dependent manner (Fig. 42).

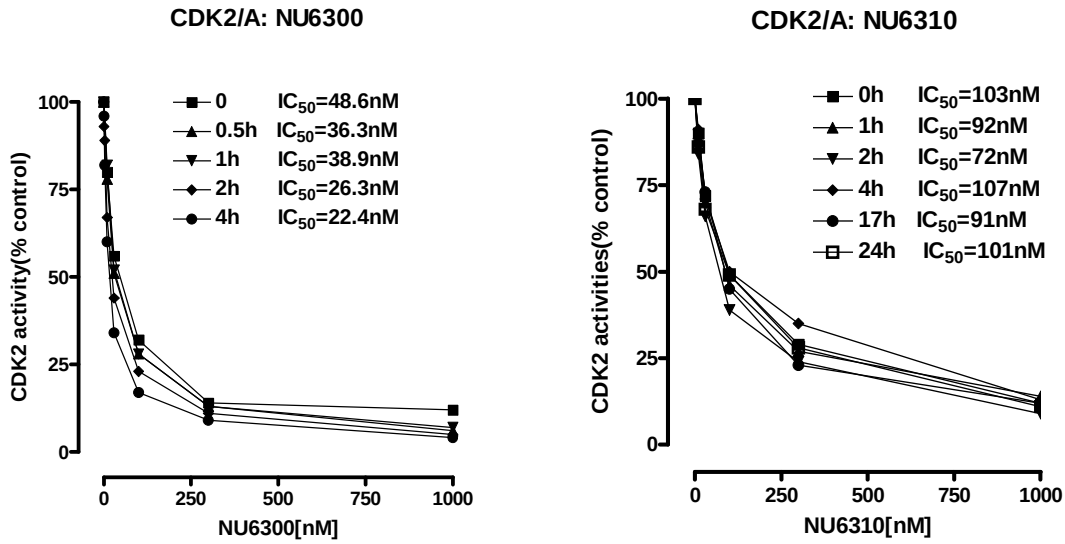

Fig. 42 Time-dependent inhibition assays with NU6300 (**40**, left) and NU6310 (**41**, right) [155]

A MS (MALDI-TOF) experiment, after incubation of the CDK2/Cyclin A complex with NU6300 (**40**), was also performed. As result NU6300 (**40**) was shown to label the enzyme.

Digestion studies with proteases were also carried out and showed that a lysine residue was labelled stoichiometrically with the inhibitor, even when the protein was treated with a large excess of NU6300 (**40**). A mutant CDK2 was also used, where Lys88 and Lys89 were mutated and no labelling of the enzyme by the inhibitor took place. Which lysine between the 88 and the 89 was labelled was confirmed by the X-ray crystal structure of the NU6300/CDK2/Cyclin A complex. [155]

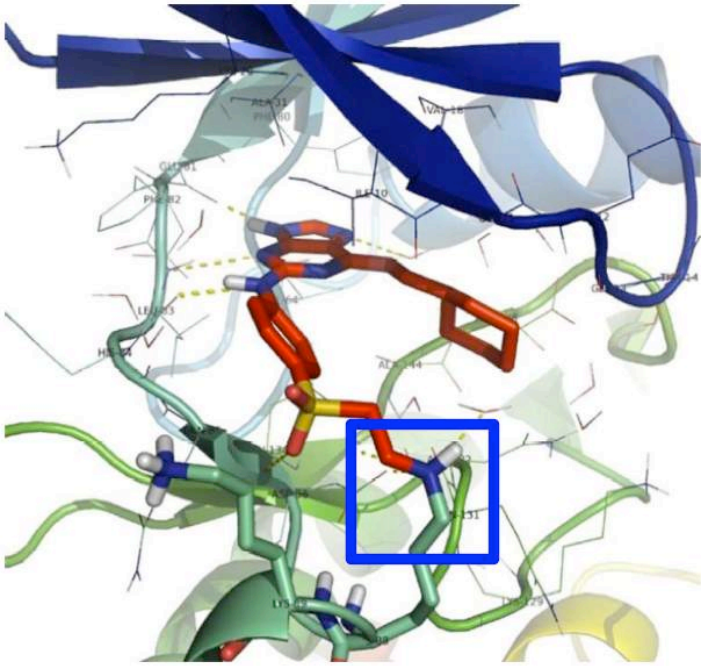

Fig. 43 NU6300/CDK2/Cyclin A complex [155]

The mechanism of the irreversible inhibition was proposed as follows:

- An initial reversible non-covalent interaction first takes place between the inhibitor (I) and CDK2 (E). In this way, the vinyl sulfone is oriented in close proximity to the nucleophilic residue within the catalytic domain to give a non-covalent complex.

- The covalent interaction then occurs resulting in an irreversible modification of CDK2 (Fig. 44).

$$E + I \underset{K_i}{\rightleftharpoons} E \bullet I \overset{k_2}{\underset{k_{-2}}{\dashrightarrow\!\!\!\dashleftarrow}} E - I$$

Initial non–covalent complex — Final covalent complex

Fig. 44 Mechanism for target-specific covalent inhibitors [157]

1.3.3.2.2. Safety of irreversible inhibitors

Compounds that cause irreversible inhibition of the activity of a biological target through covalent modification have, until recently, been unpopular as drug candidates because of the potential off-target toxicity. [157, 158]

There are two crucial differences, to consider, between covalent drugs and highly reactive compounds, which are able to generate electrophilic metabolites once administered. In particular, the latters typically exhibit much higher chemical reactivity than the weakly electrophilic warheads incorporated into covalent drugs. Consequently, chemically reactive drugs and reactive drug metabolites present a lower molecular selectivity in their covalent interactions than covalent drugs. Therefore, the risk of an adverse reaction should be lower with a covalent drug rather than with a reactive electrophile species, which indiscriminately modifies biological macromolecules. [157, 158]

Examples of irreversible drugs progress clinically demonstrate good efficacy and safety margins. The therapeutic applicability (Fig. 45) and success of irreversible binding kinase inhibitors is dependent on whether or not the covalent bond can be confined solely to the protein kinase of interest. [157, 158]
Moreover, irreversible inhibition has important and potential advantages concerning the drug pharmacodynamics.

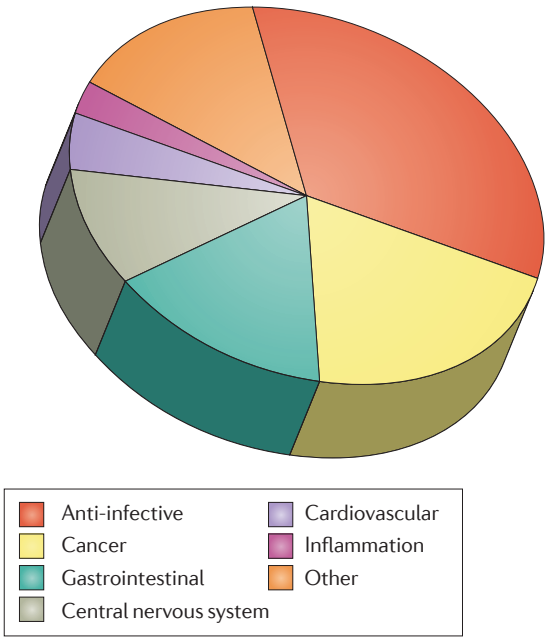

Fig. 45 Approved covalent drugs by therapeutic indication [157]

The dose level and frequency relates to the extent and duration of the resulting pharmacological effect. In particular, when covalent modification of a drug target is irreversible, the restoration of pharmacological activity requires re-synthesis of the biological target. Covalent kinase inhibitors with well-balanced recognition and reactivity should provide efficacy, selectivity and the safety margins, required for regulatory approval. [157, 158]

1.3.3.2.3. Pyrimidine-based CDK2 inhibitors

Structure-activity relationship (SAR) studies on the O^6-alkylguanine series revealed that the purine pharmacophore was not a prerequisite for CDK2-inhibitory activity. [153]

In an attempt to maintain the H-bond interactions observed for NU2058 (**36**), the pyrimidine NU6027 (**42**, IC_{50} = 1.3 µM, for CDK2) was first identified. The established SAR for this chemotype can be represented as in Fig. 46 (left). [153]

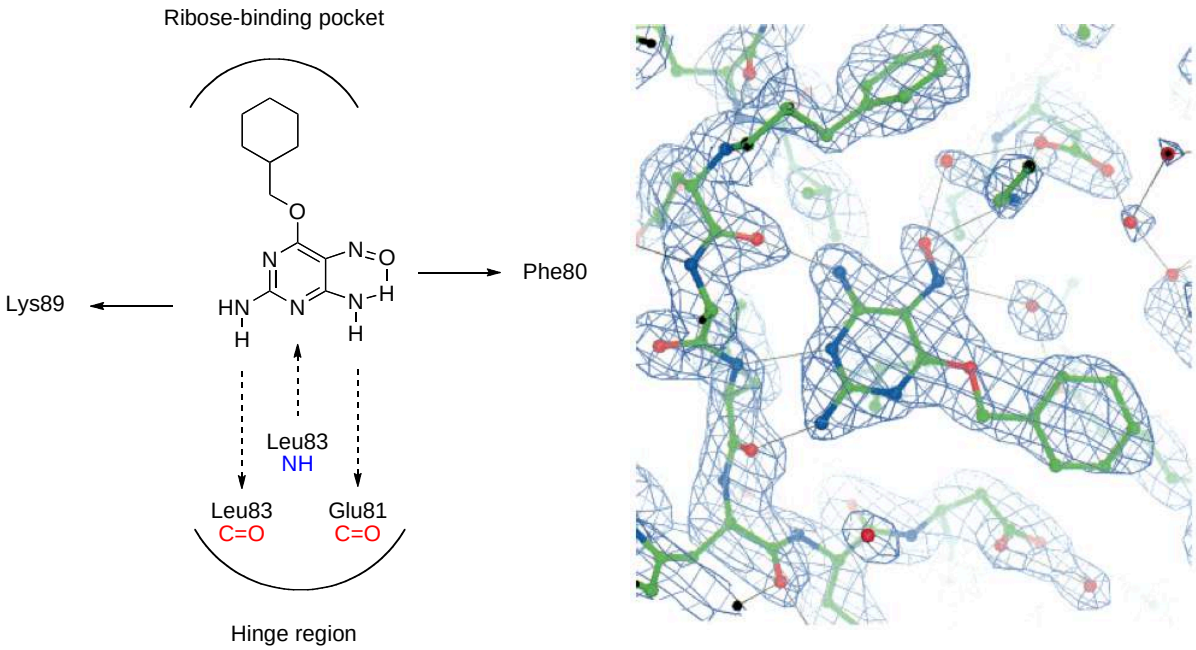

Fig. 46 NU6027 (**42**) - CDK2 Interactions [153]

The nitroso group at the pyrimidine 5-position forms an intramolecular hydrogen bond with the 6-amino group and constrains the molecule into the optimal binding orientation in a purine-mimetic manner. Removal of the nitroso group essentially showed to abolish CDK2-inhibitory activity. As for NU2058 (**36**), the pyrimidine NU6027 (**42**) displayed a competitive behaviour on CDK2 with respect to ATP. [153]

From NU6027 (**42**), a series of novel pyrimidine-based CDK2 inhibitors was synthesised in order to investigate structural variations at the pyrimidine 2-, 4- and 5- positions (Fig. 47). In particular, the substitution at the pyrimidine 2-position involved the 4-sulfonamide, 4-methoxy and 4-carboxylic acid functionalities. Smaller alkyl substituents, such as 4-ethoxy and sec-buthoxy were then introduced at the pyrimidine 4-position rather than the cyclohexylmethoxy moiety. Finally, nitroso and formyl substituents, at the pyrimidine 5-position, were also explored, with the aim of retaining the essential intramolecular H-bond with the pyrimidine 6-amino group. [159]

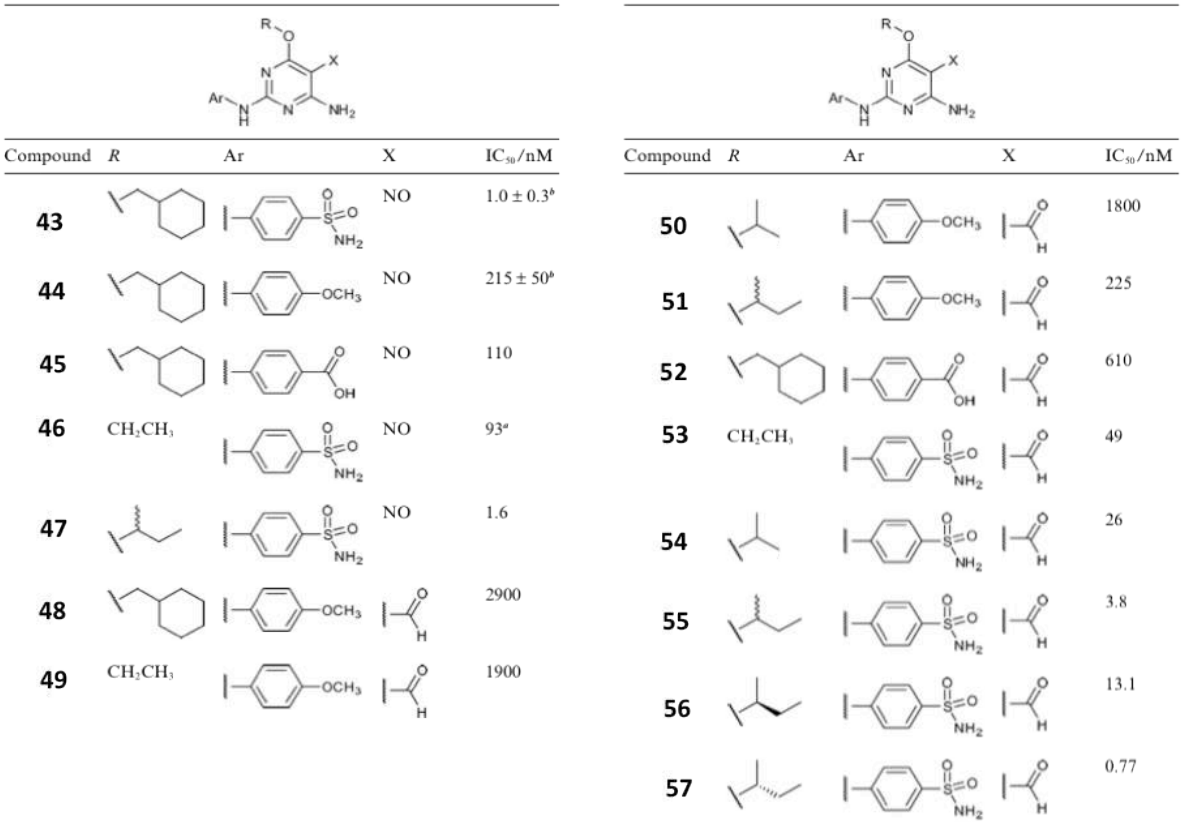

Fig. 47 Pyrimidine-based CDK2 inhibitors

The improvement of the inhibitory activity for this set of compounds, similar to the corresponding purine-based inhibitors, is consistent with the presence of the key hydrogen bond interactions made by the sulfonamide within the CDK2-catalytic domain. In particular, compounds **43**, **47**, **55** and **57** showed the best IC_{50} values against CDK2 and compound **57** can be considered one of the best CDK2 inhibitors known to date. Furthermore, it emerged that a small electron withdrawing group, at the pyrimidine 5-position, capable of making an intramolecular hydrogen bond with the 6-amino group was favoured and was crucial for the CDK2-inhibitory activity. [159]

2. AIMS

One part of the research, carried out at the University of Padua under the supervision of Prof. Giuseppe Zagotto, was aimed at the design and synthesis of bi-substrate CK2 inhibitors, while the second part, carried out at Newcastle University under the supervision of Prof. Roger J. Griffin† and Prof. Bernard T. Golding, concerned the design and synthesis of pyrimidine-based CDK2 inhibitors.

2.1. CK2 inhibitors

The purpose was to investigate the steric and the electronic space of the enzyme catalytic cavity, by synthesise potential bifunctional inhibitors. This term is to indicate the ability of the putative inhibitor to interact simultaneously with the ATP pocket and with the substrate-binding domain (Fig. 48).

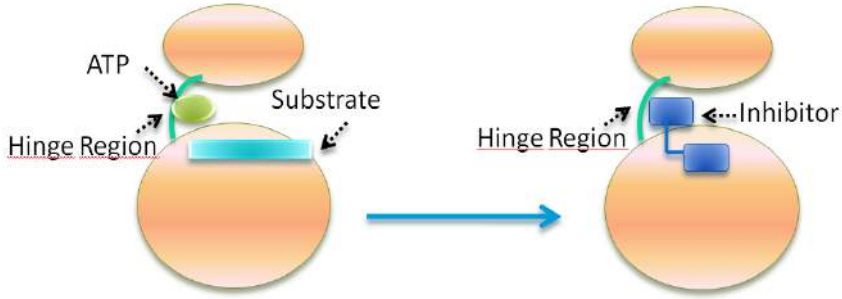

Fig. 48 Proposed binding mode for bifunctional CK2 inhibitors

The synthesis started from 2-mercaptobenzimidazole (**58**), to obtain a key intermediate, compound K137 (**12**, IC_{50} = 0.12 µM on CK2). [160]

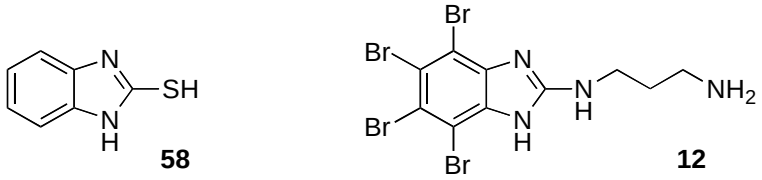

Fig. 49 2-mercaptobenzimidazole (**58**) and K137 (**12**)

K137 (**12**) was then linked, through an aliphatic spacer, to different acidic peptide chains. The peptidic chains, ending with free carboxyl groups, are thought to interact with basic residues adjacent to the substrate-binding domain, thus increasing the selectivity and the potency of the inhibitor. In order to understand the interaction of the inhibitors with the enzyme, the peptidic chains linked to the spacer without the benzimidazole scaffold were also synthesised.

2.2. CDK2 inhibitors

At Newcastle University, a series of pyrimidine-based CDK2 inhibitors was previously identified employing a crystal structure-based design approach. [159] The purpose of this research was the design and synthesis of novel irreversible pyrimidine-based CDK2 inhibitors. The first target investigated (**59**) is known to bind the hinge region of the kinase *via* a triplet of hydrogen bonds (Fig. 50).

The efficacy of the cyclohexylmethoxy substituent has been explained by examining the X-ray structure of NU6027 (**42**) bound to CDK2 (Fig. 46), which shows this moiety occupying the hydrophobic entrance to the ribose-binding pocket. [153] The 5-formyl group is important for CDK2-inhibitory activity, by forming an intramolecular H-bond with the 6-amino group, conferring a purine-mimetic structure to the inhibitor.

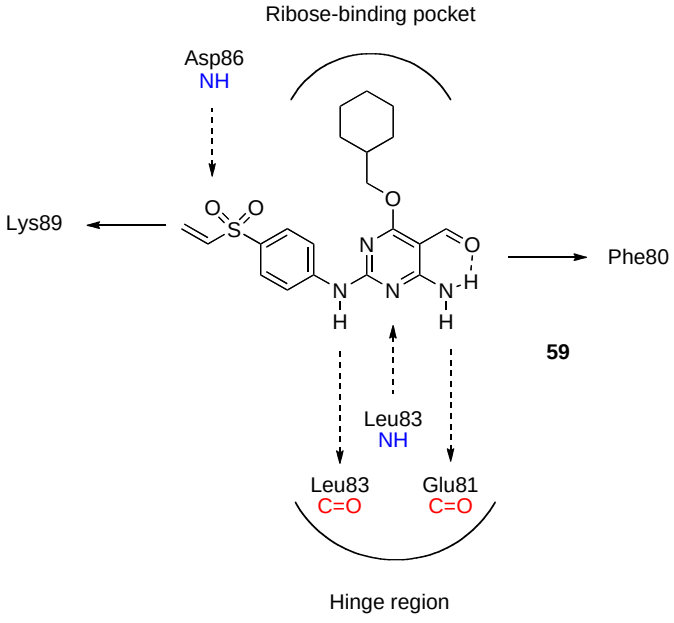

Fig. 50 CDK2-compound **59** interactions

The irreversible characteristics of the novel inhibitors were to be achieved by the presence of the vinyl sulfone moiety (Fig. 50), as explained in the previous sections (see Par. 1.3.3.2.1.). [155, 156]

Structural modifications at the pyrimidine 5-position, starting from compound **59**, were considered in order to investigate the binding affinity, potency and selectivity of the novel CDK2 irreversible inhibitors (Fig. 51).

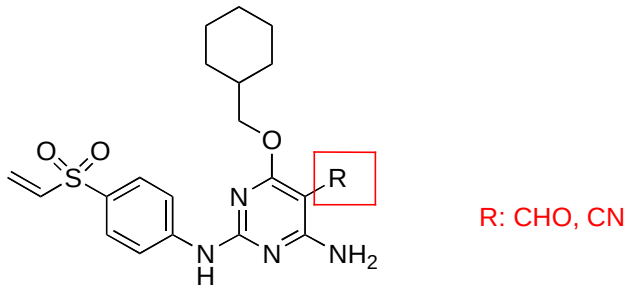

Fig. 51 Structural variations on the pyrimidine lead (I)

The effect, upon biological activity, of deletion of the cyclohexylmethoxy moiety at the pyrimidine 4-position from compound **59** was also investigated (Fig. 52).

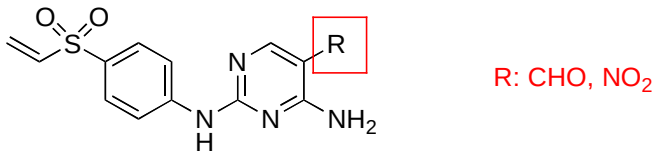

Fig. 52 Structural variations on the pyrimidine lead (II)

All new compounds were evaluated for CK2- and CDK2-inhibitory activity, as appropriate, with promising inhibitors being subjected to more comprehensive biological studies.

The CK2 and CDK2 projects have been carried out in collaboration with the Department of Biochemical Sciences and the Molecular Modeling Section (MMS - Department of Pharmaceutical Sciences) at the University of Padova and with the Paul O' Gorman (POG) Building at Newcastle University.

3. RESULTS AND DISCUSSION

3.1. CK2 inhibitors

The biochemistry and drug design experience gained through the study of polyhalogenated derivatives allowed using the benzimidazole scaffold as starting point to investigate new kinase inhibition strategies. [161-163]

K137 (**12**) was synthesised optimising a literature procedure (Scheme 1). [160] Starting from 2-mercaptobenzimidazole (**58**), intermediate **60** was obtained using Br_2 in a mixture of aqueous HBr and MeOH. The subsequent bromination, with Br_2 in water, gave rise to the mono-, di-, tri- and tetra-brominated intermediates, which were then separated by flash chromatography. It was not possible to take the bromination to completion, even modifying the reaction conditions. Finally, 1,3-diaminopropane was introduced into position 2 of the benzimidazole scaffold to give K137 (**12**)

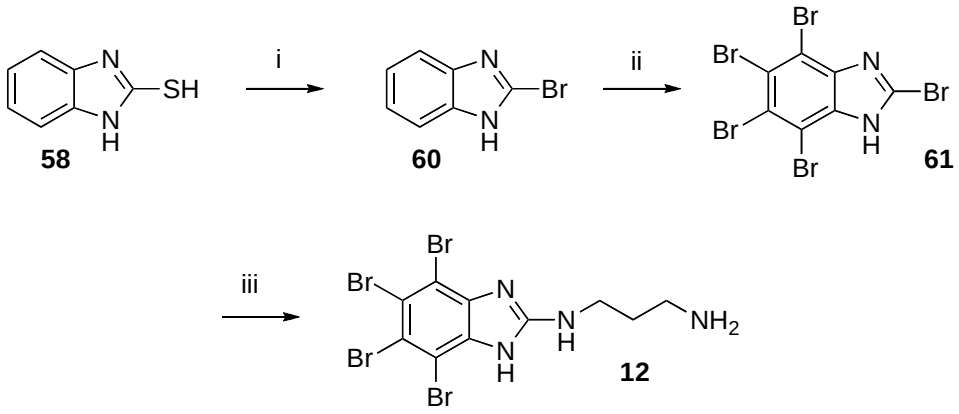

Scheme 1

Reagents and Conditions: i) Br_2, HBr, AcOH, rt, 4 h, 44%; ii) Br_2, H_2O, 50 °C - rt, 7 d, 45%; iii) 1,3-diaminopropane, 2-propanol, 80 °C, 2 d, 30%

Two strategies were then explored for the synthesis of the bi-substrate inhibitors:

- Stiffening the carbon chain.
- Insertion of polar atoms or groups.

In an attempt to exploit both characteristics it was decided to insert amide bonds in the side-chain of the novel inhibitors. The introduction of a hydrophilic aminoalkylamino residue might facilitate the transport of the inhibitors through the cell membrane.

Compound **12** was linked, through a spacer, to aspartic and glutamic peptidic chains of different length. As explained in the previous section, the peptidic chains linked to the spacer without compound **12** were synthesised, following the same procedure as for the synthesis of the bifunctional inhibitors. To introduce the spacer and synthesise intermediate **62** (Scheme 2), compound **12** was reacted with succinic anhydride.

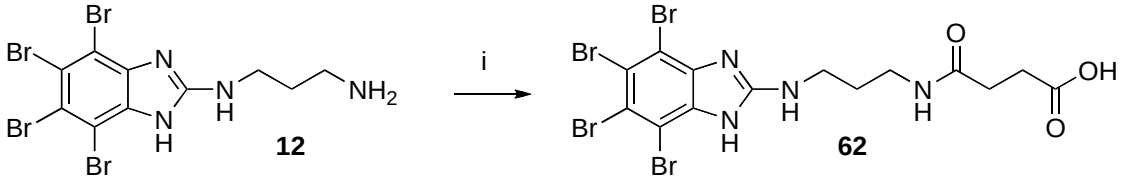

Scheme 2

Reagents and Conditions: i) Succinic anhydride, DMF, rt, 4 h, 63%.

The mechanism of this step involves nucleophilic attack by the amino group of K137 (**12**), which allows the ring opening of succinic anhydride (Fig. 53).

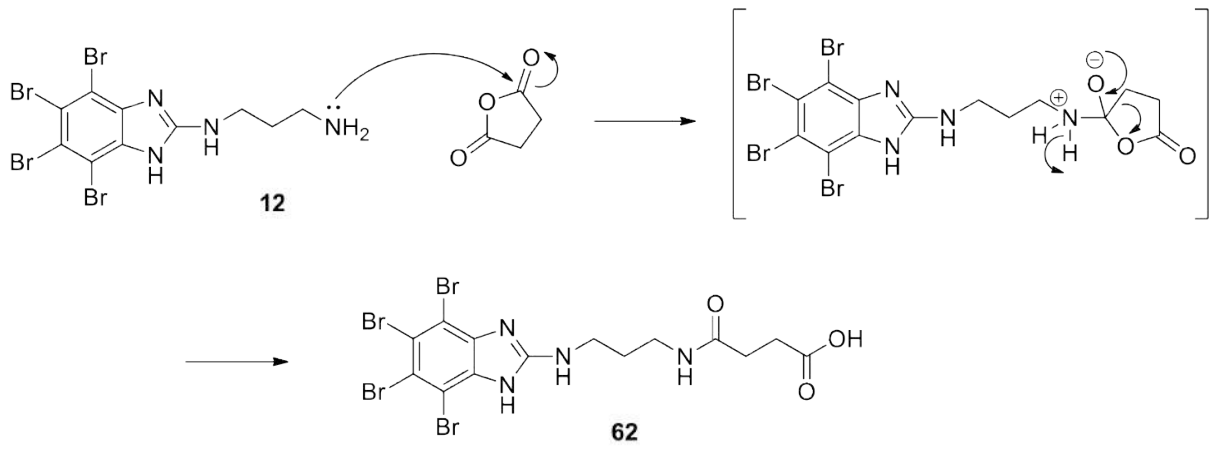

Fig. 53 Mechanism for the synthesis of intermediate **62**

The peptidic chains were then obtained with solid phase peptide synthesis (SPPS), a method pioneered by Merrifield R. B in the mid-twentieth century (Fig. 56). [164, 165] The peptide is built on a solid support, to which is covalently attached. Fmoc-Glu(OtBu)-Wang resin and Fmoc-Asp(OtBu)-Wang resin were used (Fig. 54).

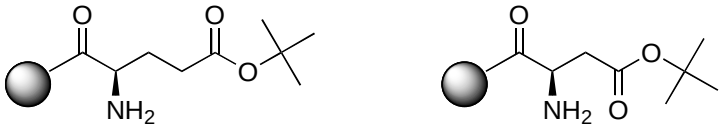

63 **64**

Fig. 54 Fmoc-Glu(OtBu)-Wang resin (**63**) and Fmoc-Asp(OtBu)-Wang resin (**64**)

Wang resin (**65**, Fig. 55) is the most commonly used resin for peptides. Wang resin is acid labile and finished peptides can be easily cleaved by treatment with TFA.

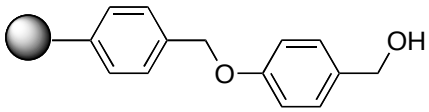

65

Fig. 55 Wang resin (**65**)

Manual SPPS involves (Fig. 56):

- Functionalisation of the resin,
- Coupling and deprotection reactions,
- Resin tests,
- Peptide cleavage from the resin,
- Precipitation protocols.

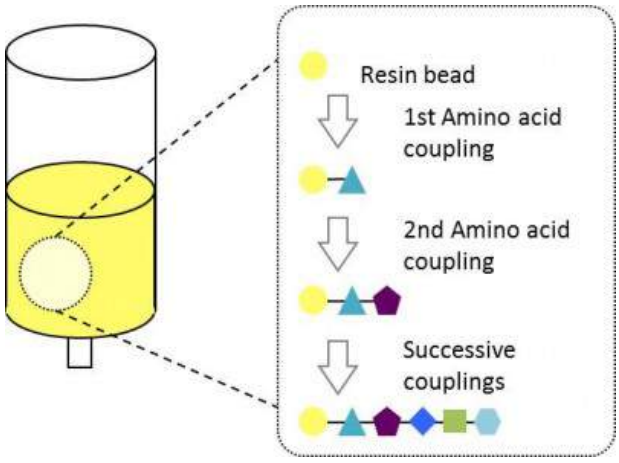

Fig. 56 SPPS protocol [166]

SPPS proceeded from C-terminal to N-terminal. The free N-terminal amine of a solid-phase attached peptide was coupled to a single N-protected amino acid unit. This unit was then deprotected, revealing a new N-terminal amine to which a further amino acid could be attached.

Three peptides were synthesised using SPPS protocol: a tri-glutamic peptide, a tetra-glutamic peptide and a tetra-aspartic peptide. The amino acids engaged in the synthesis belonged to the L-series and were Fmoc/OtBu protected. The Fmoc group is a widely used protective group, generally removed from the N-terminal of a peptide. The Fmoc group is stable in acidic conditions, while can be removed in basic conditions in the presence of secondary amines such as pyperidine (20% in DMF), through a β-elimination reaction (Fig. 57). As a result, dibenzofulvene and carbon dioxide are split off. [165, 167]

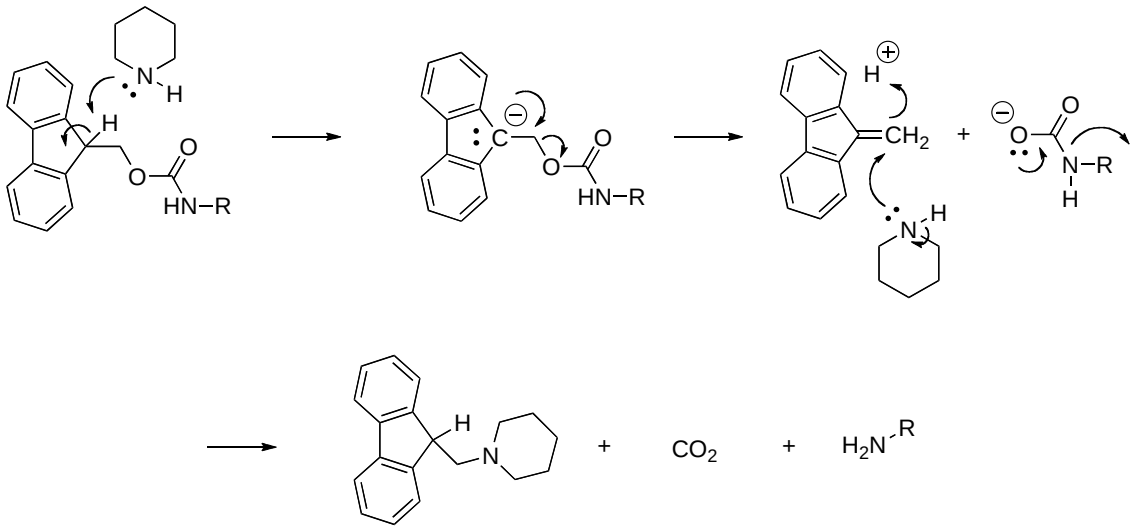

Fig. 57 Fmoc cleavage mechanism

After deprotection of the Fmoc group, phosphonium and uronium reagents, in the presence of DIPEA and HOBt (**66**), were used to activate the amino acids during the coupling reactions (Fig. 58).

The uronium salt reagent HBTU (**67**) was used for the synthesis of the peptidic chains, whereas the phosphonium reagent PyBOP (**68**) was used for the coupling of K137 (**12**) with the spacer to the peptides. PyBOP (**68**) reaction mechanism is similar to HBTU mechanism. [165]

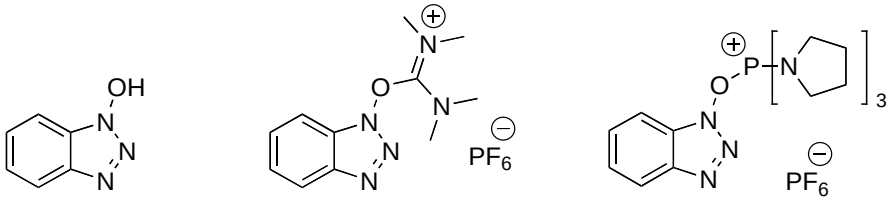

Fig. 58 HOBt (**66**), HBTU (**67**), PyBOP (**68**)

By nucleophilic attack, in basic conditions (DIPEA), on the HBTU (**67**) species, a highly reactive ester is formed, with the elimination of oxybenzotriazole, which subsequently attacks the activated carbon on the ester, with the elimination of tetramethylurea (Fig.59).

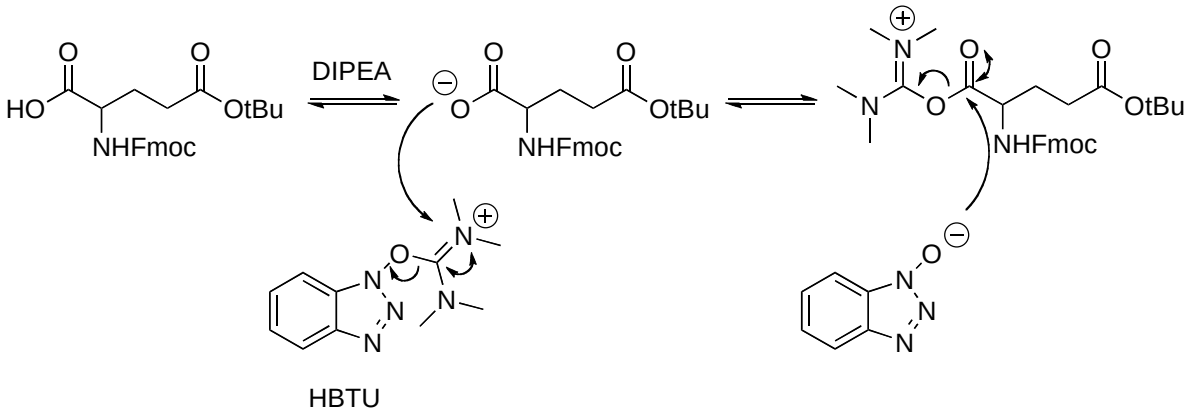

Fig. 59 Activation and coupling mechanism (I)

Finally, by nucleophilic attack the amino group of the N-terminal amino acid attacks the activated carbon on the ester forming the peptidic bond, with the elimination of hydroxybenzotriazole (Fig. 60).

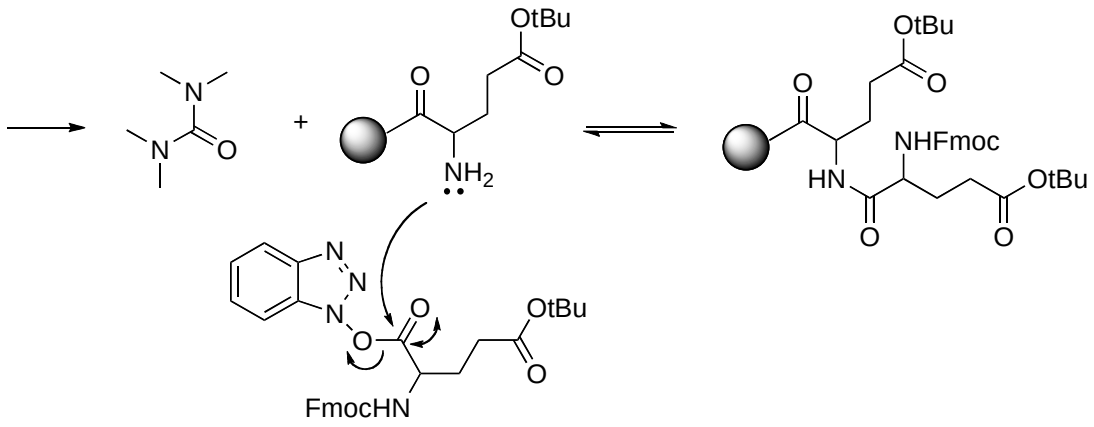

Fig. 60 Activation and coupling mechanism (II)

A coupling reaction on the resin was then carried out between the tetrabromobenzimidazole scaffold (**62**) and the peptides.

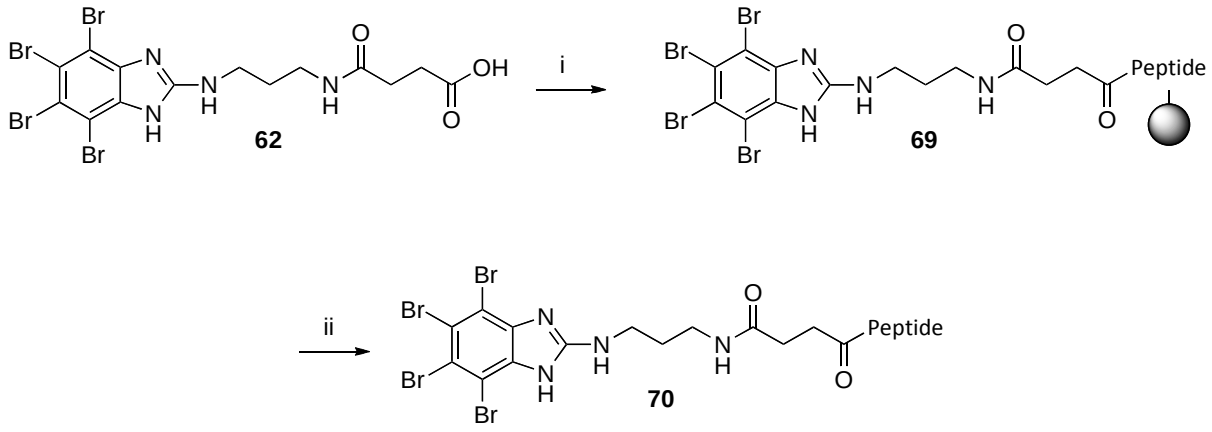

Scheme 3

Reagents and Conditions: i) HOBt, PyBOP, DIEA, MeOH, 1 h, rt; ii) TFA 95 %, TIS 3%, H_2O 2%, rt, 30 min, 8-56% over two steps.

Intermediate **62** was reacted with HOBt (**66**), PyBOP (**68**) and DIPEA in DMF, with a similar mechanism for the coupling reactions of the amino acids.

The carboxyl groups of the aspartic and glutamic acids were protected by tert-butyl ester groups (OtBu), easily removable in acidic conditions. A solution of TFA, TIS and H_2O (95:3:2 respectively) was used to remove these protecting groups from the solid support simultaneously with the removal of the final compound from the resin.. [165]

It is an elimination (E_1) reaction, a two-step reaction involving (Fig. 61):

- Protonation of the carbonyl oxygen.

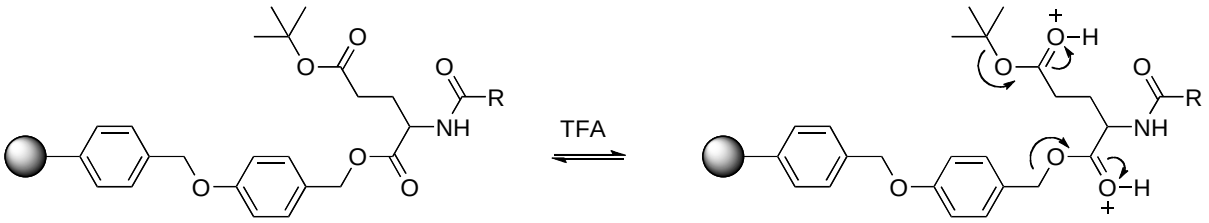

- Elimination of the tert-butyl ester group and cleavage of the peptide from the resin.

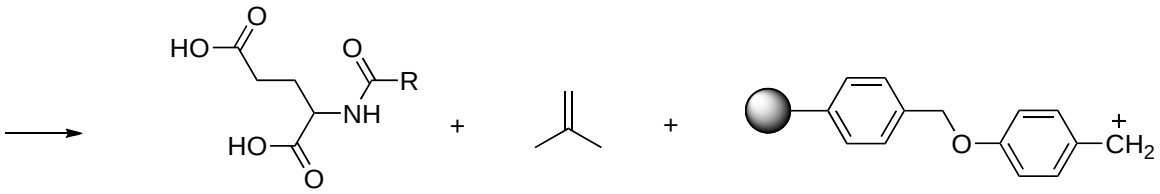

Fig. 61 OtBu deprotection mechanism and peptide cleavage

Polyhalogentaed benzimidazole derivatives (**71**, **72** and **75**) and the peptidic chains linked to the spacer (**73**, **74** and **76**) were obtained as follows (Fig. 62).

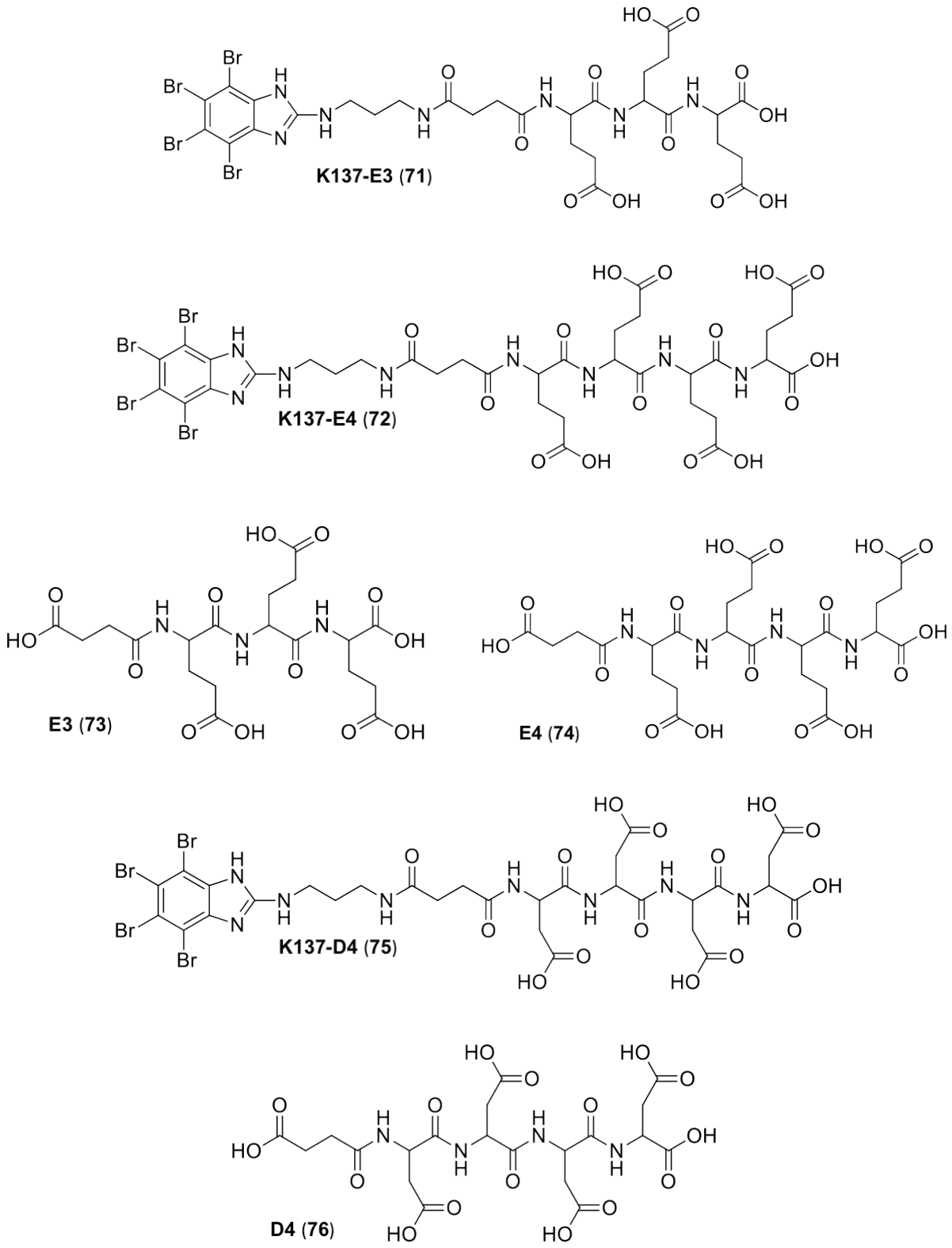

Fig. 62 Bi-substrate CK2 inhibitors

After biological evaluation of the bi-substrate inhibitors (see Par. 3.1.1.), all the carboxyl groups of compound **72** were esterified, in order to compare the CK2-inhibitory activity and the permeation through the cell-membrane.

K137-E4Me (**77**) was synthesised according to a literature procedure, using TMCS in MeOH (Scheme 4). [168]

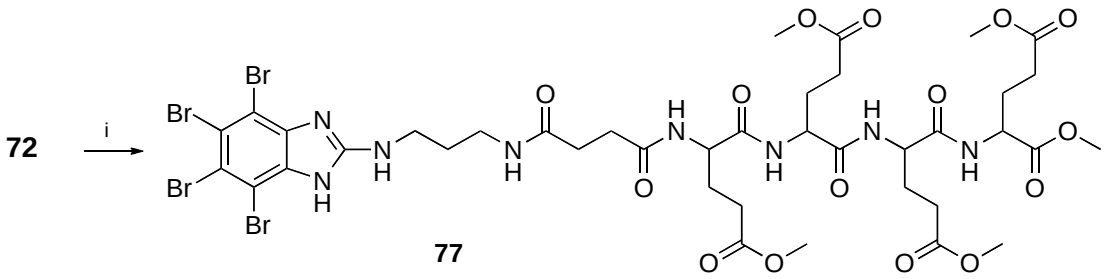

Scheme 4

Reagents and Conditions: i) TMCS, MeOH, rt, 10 min, 42%.

K137-E4Me (**77**) was also tested against recombinant CK2 to compare its inhibitory activity with K137-E4 (**72**), K137 (**12**) and CX-4945 (**1**).

3.1.1. Biological evaluation of CK2 inhibitors

Biological studies on novel CK2 inhibitors were carried out in the Department of Biochemical Sciences at the University of Padua (see Experimental Section).

In the *in vitro* assays, recombinant CK2 was reacted with radiolabelled [γ-^{33}P]-ATP and a peptide substrate (RRRADDSDDDDD) and the transfer of the radiolabelled γ-^{33}P-phosphate from ATP to the substrate was measured. The percentage of the phosphorylated substrate depending on the concentration of the inhibitor was recorded and the IC_{50} value was calculated for each inhibitor. The specificity of the inhibitors was evaluated testing them against a small panel of "in house" kinases and compared to the inhibitory activity of K137 (**12**, Chart 1).

Compounds	CK2	PLK2	CK1	HIPK2	PIM1	Aurora-A
K137 (**12**)	0.13	39	5.7	0.34	0.25	>40
K137-E3 (**71**)	0.033	2.34	34	>40	>40	>40
K137-E4 (**72**)	0.025	0.400	16	>40	>40	>40
K137-D4 (**75**)	0.035	3.76	21	>40	>40	>40
E3 (**73**)	>40	>40	>40	>40	>40	>40
E4 (**74**)	>40	>40	>40	>40	>40	>40
D4 (**76**)	>40	>40	>40	>40	>40	>40

Chart 1 IC_{50} values [μM]

Compound K137-E4 (**72**), containing four residues of glutamic acid in the peptidic chain, demonstrated the highest activity and was several fold more potent (25 nM vs 130 nM) than the purely competitive parent inhibitor K137 (**12**) against CK2.

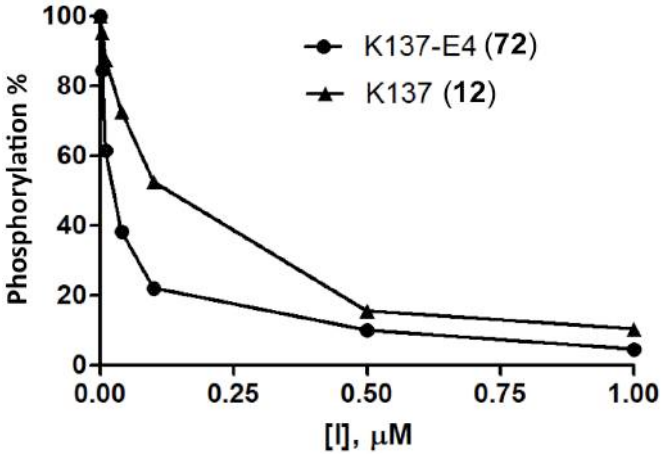

Fig. 63 CK2 inhibition curve of K137-E4 (**72**) compared to K137 (**12**)

Compound K137-E4 (**72**) was also more selective than K137 (**12**), failing to inhibit any other kinase as significantly as CK2 out of a panel of 140 enzymes, whereas K137 (**12**) inhibited 32 kinases more potently than CK2 (Fig. 64).

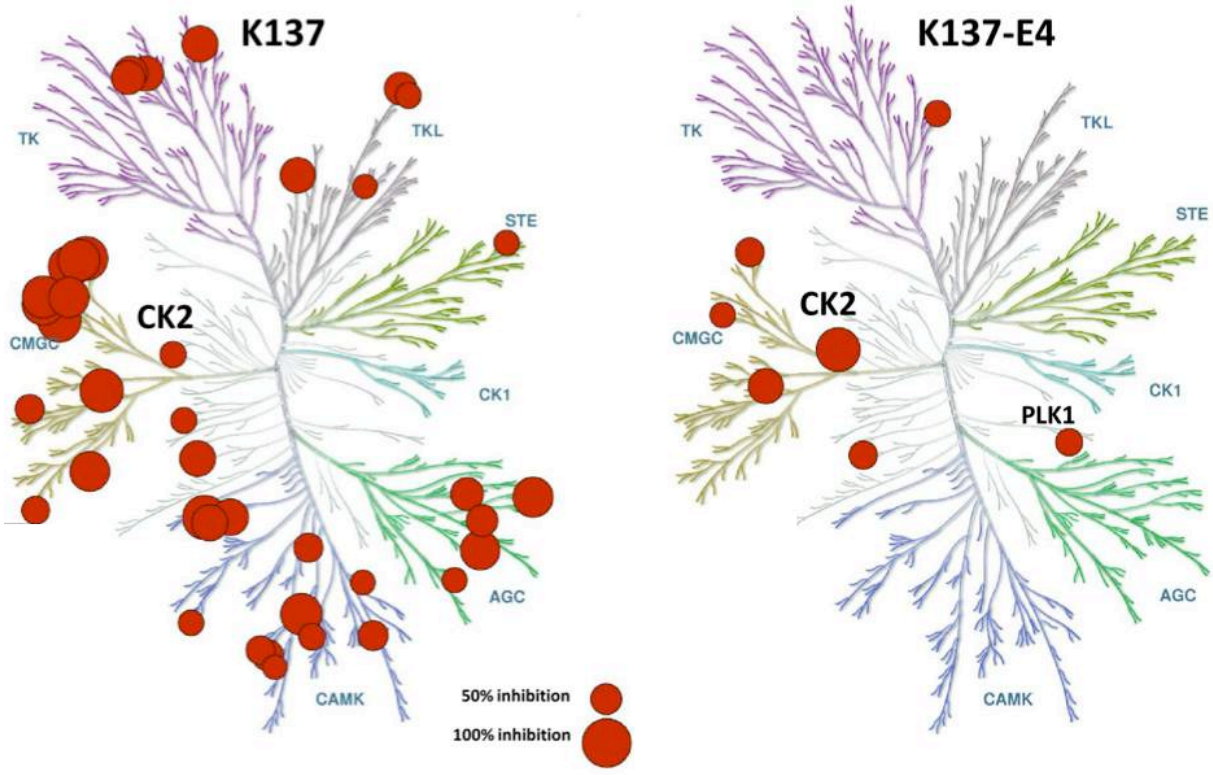

Fig. 64 Selectivity profiles of K137 (**12**, left) and K137-E4 (**72**, right)

Kinetics experiments were then performed using ATP or the peptide substrate (RRRADDSDDDDD) in the absence or presence of the indicated inhibitor (K137 or K137-E4) at varying concentrations (Fig. 65).

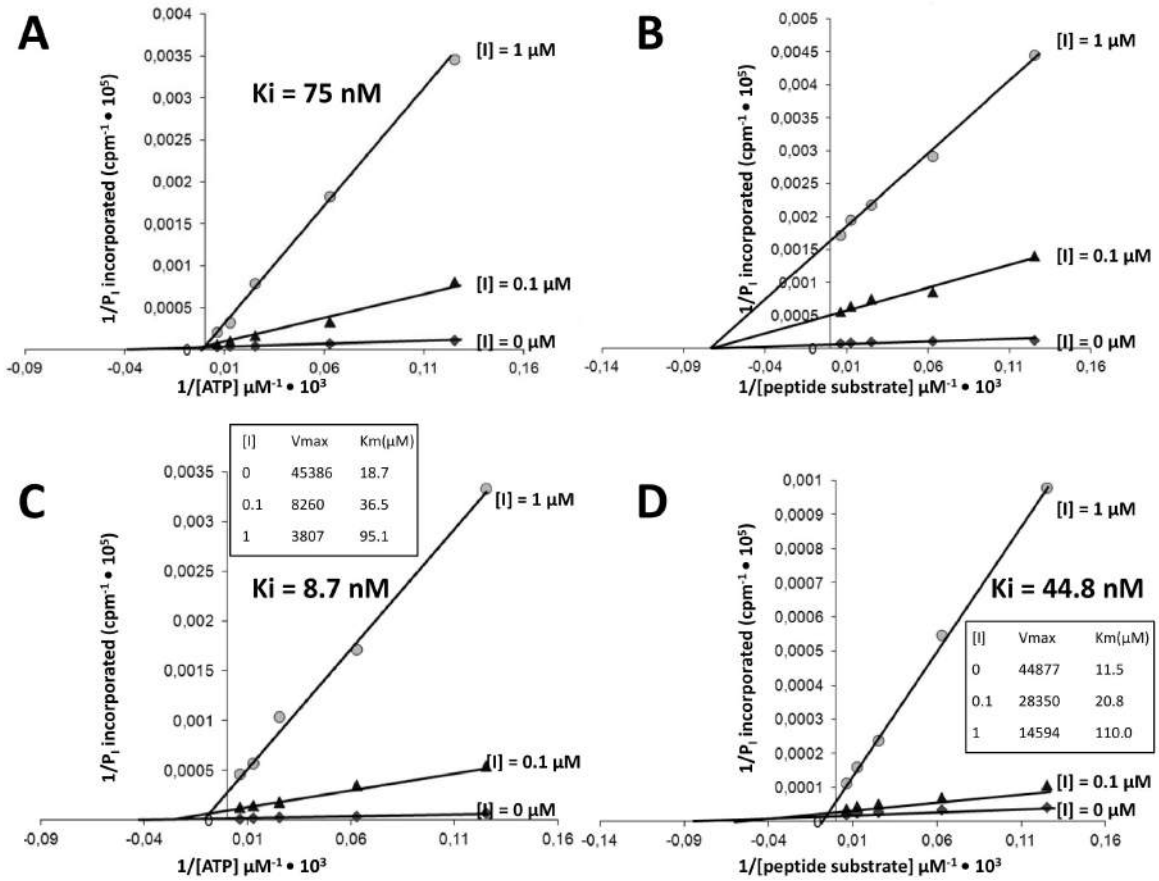

Fig. 65 Inhibition of CK2 by K137 (A, B) and K137-E4 (C, D) with respect to ATP (right) and to the peptide substrate RRRADDSDDDDD (left)

While the mode of inhibition of K137 (**12**) was purely competitive with respect to ATP and non competitive with respect to the peptide substrate (Fig. 65A and 65B), the kinetics experiments performed with K137-E4 (**72**, Fig. 65C and 65D) disclosed a mixed mode of inhibition with both the Vmax and the Km values (either for ATP or the peptide substrate) altered by increasing the inhibitor concentration. These results support the proposed dual mode of binding of the bifunctional inhibitors, which clearly compete with both ATP and the peptide substrate.

K137-E4 (**72**) was then subjected to more comprehensive biological studies to evaluate its inhibitory activity on endogenous CK2.

In the following assay HepG2 cell line (human liver hepatocellular carcinoma) was used, with CX-4945 (**1**) and K137 (**12**) serving as control compounds. The inhibitory activity of K137-E4 (**72**) on endogenous CK2 was confirmed conducting studies on HepG2 cell lysates. The autoradiography (Fig. 66), from the SDS-PAGE 11% assay, showed that K137-E4 (**72**) was active on endogenous CK2 by inhibiting phosphorylation of peptide substrates, especially at higher concentration (5 µM).

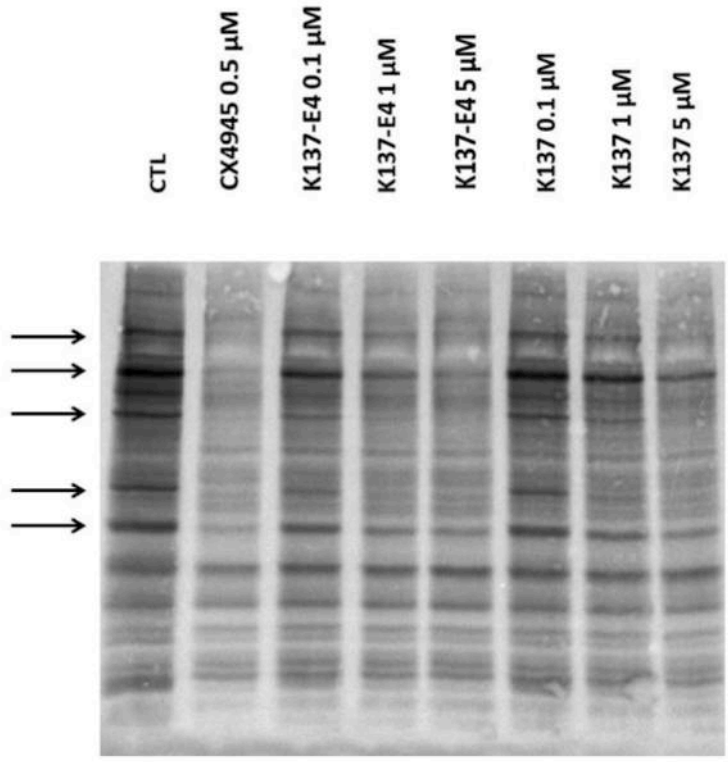

Fig. 66 *In vitro* assay on HepG2 cell lysates (CTL = control, peptide substrates of CK2 are indicated with arrows in the autoradiography).

Studies on cell viability were then performed in order to evaluate the permeation of the bifunctional inhibitor K137-E4 (**72**) through the cell membrane. A Jukrat cell line (human T lymphocyte cells from acute T cell leukaemia) was used, with CX-4945 (**1**) and K137 (**12**) serving as control compounds.

An MTT assay was carried out, which indicated that K137-E4 (**72**) was not able to cross the cell membrane, with cell viability maintained compared to CX-4945 (**1**) and K137 (**12**), as shown in Fig. 67. This is probably due to ionisation of the peptidic chains to carboxylates at physiological pH, which prevent permeation through the cell membrane.

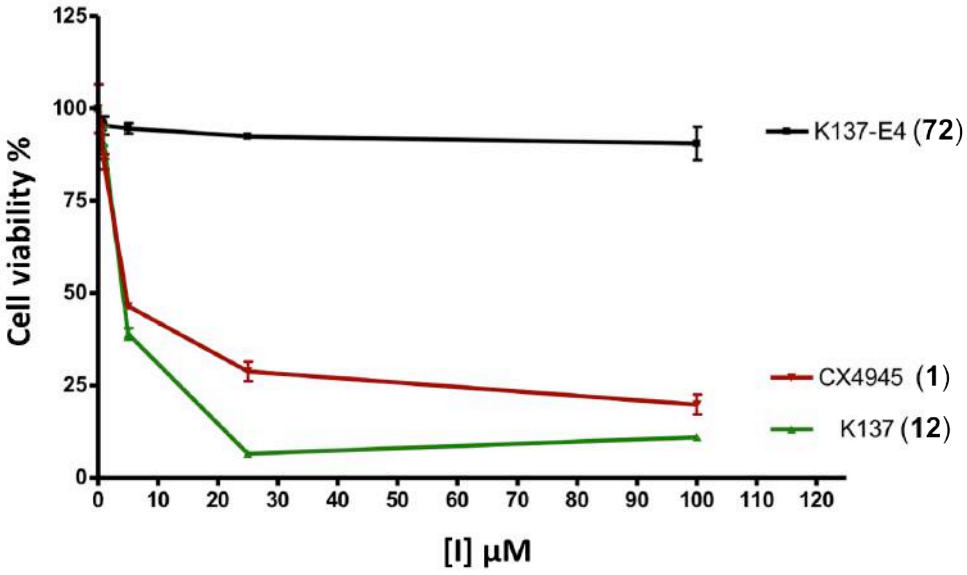

Fig. 67 Cell viability assay on Jukrat cells (I)

The esterified bifunctional inhibitor (K137-E4Me, **77**) was synthesised, in order to increase the hydrophobicity of K137-E4 (**72**) and thus facilitate the permeation through the cell membrane.

From the cell viability assay with Jukrat cells (Fig. 68), it emerged that compound K137-E4Me (**77**) was able to cross the cell membrane with respect to K137-E4 (**72**), but the inhibitory activity was still low compared to CX-4945 (**1**) and K137 (**12**). This was also confirmed by an assay on recombinant CK2, which showed an IC_{50} value of 10.32 µM for K137-E4Me (**77**).

The decrease in the CK2-inhibitory activity is probably due to the structural modification of compound K137-E4Me (**77**), with all the carboxyl groups esterified, which could results in the loss of the essential interactions between the peptide chain of the inhibitor and the basic residues adjacent to the CK2 substrate-binding domain.

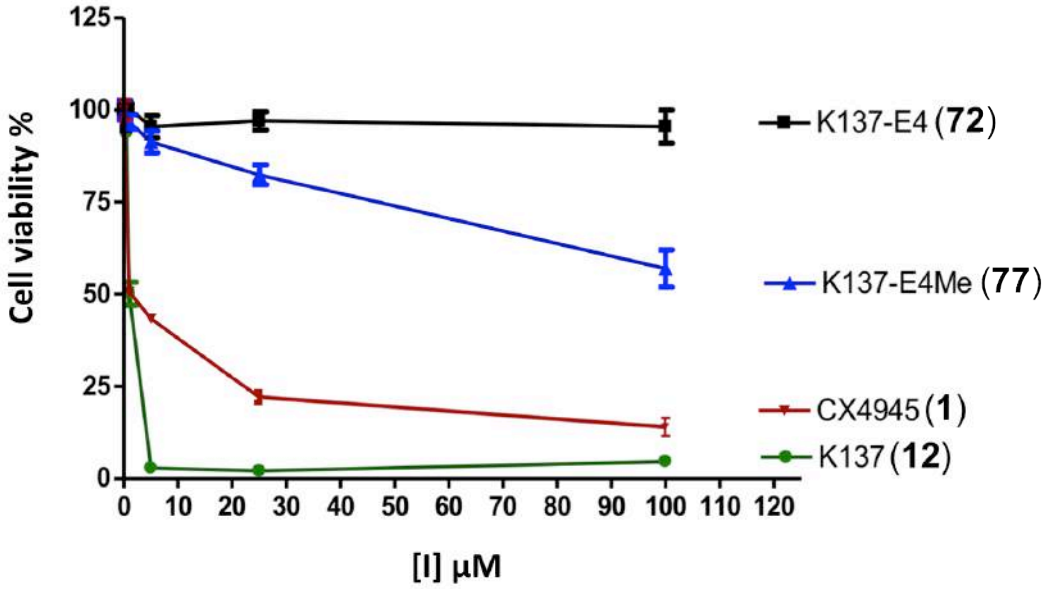

Fig. 68 Cell viability assay on Jukrat cells (II)

3.2. CDK2 inhibitors

The first target investigated for CDK2 irreversible inhibitors was compound **59**, having a formyl group at the pyrimidine 5-position, a cyclohexylmethoxy moiety at the pyrimidine 4-position and a vinyl sulfone moiety (side-chain) at the pyrimidine 2-position (Fig. 69).

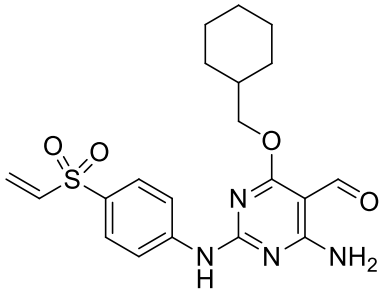

Fig. 69 Compound **59**

The side-chain with the sulfone moiety (**25**) was synthesised first. The following synthetic route (Scheme 5) was considered and proved to be straightforward.

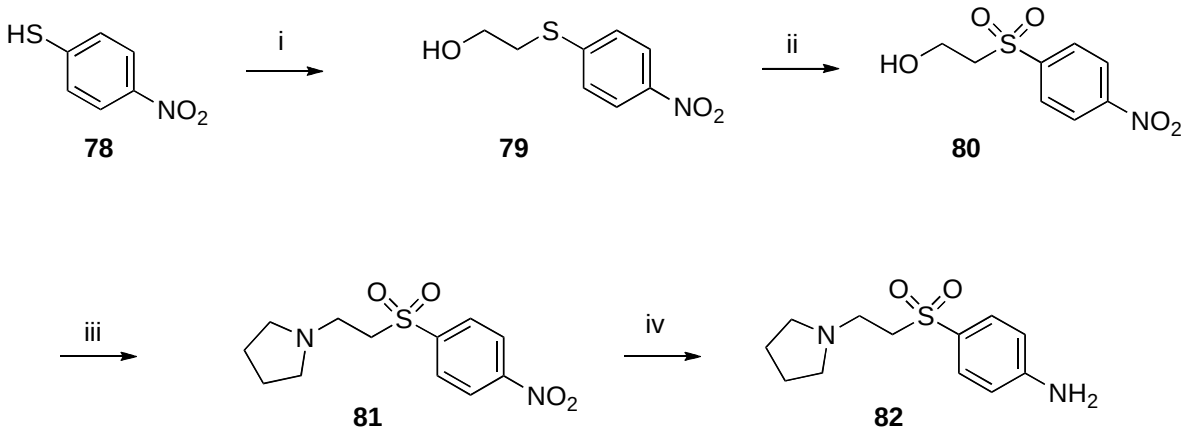

Scheme 5

Reagents and Conditions: i) 2-Chloroethanol, KOH, EtOH, reflux, 3 h, 100%; ii) mCPBA, DCM, 0 °C, 30 min, 100%; iii) Benzenesulfonyl chloride, pyrrolidine, NEt_3, DCM, rt, 2 h, 95%; iv) Zinc, AcOH, MeOH, 50 °C, 2 h, 99%.

Nucleophilic substitution of 2-chloroethanol was carried out with 4-nitrothiophenol (**78**), followed by an oxidation at the sulfur atom with mCPBA, to obtain the sulfone intermediate (**80**) in high yield. [169]

The hydroxyl group of **80** then reacted with benzenesulfonyl chloride to form a leaving group. Pyrrolidine acted as a base to deprotonate at the α-position of the sulfone, which triggered the elimination of the leaving group. The reactive vinyl sulfone, thus formed, reacted directly with pyrrolidine acting as a nucleophile, to give compound **81** (Fig. 70).

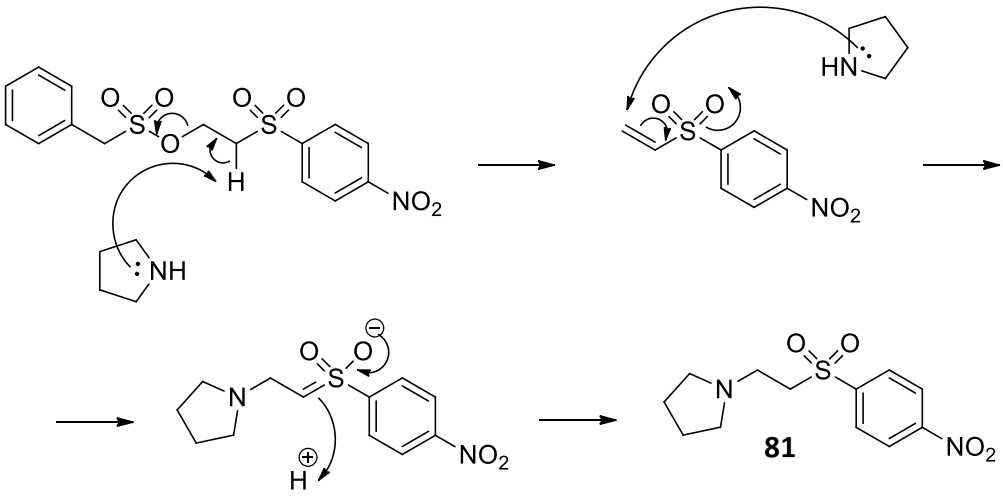

Fig. 70 Mechanism for pyrrolidine substitution

Finally, the nitro group was reduced to the corresponding amine in high yield, using zinc in acetic acid, giving intermediate **82**.

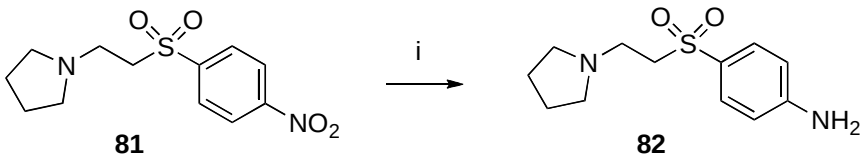

Scheme 6

Reagents and Conditions: i) Zinc powder, AcOH, MeOH, 50 °C, 2 h, 99%.

The synthetic route for the synthesis of compound **59** from 6-aminouracil (**83**) is shown in Scheme 7.

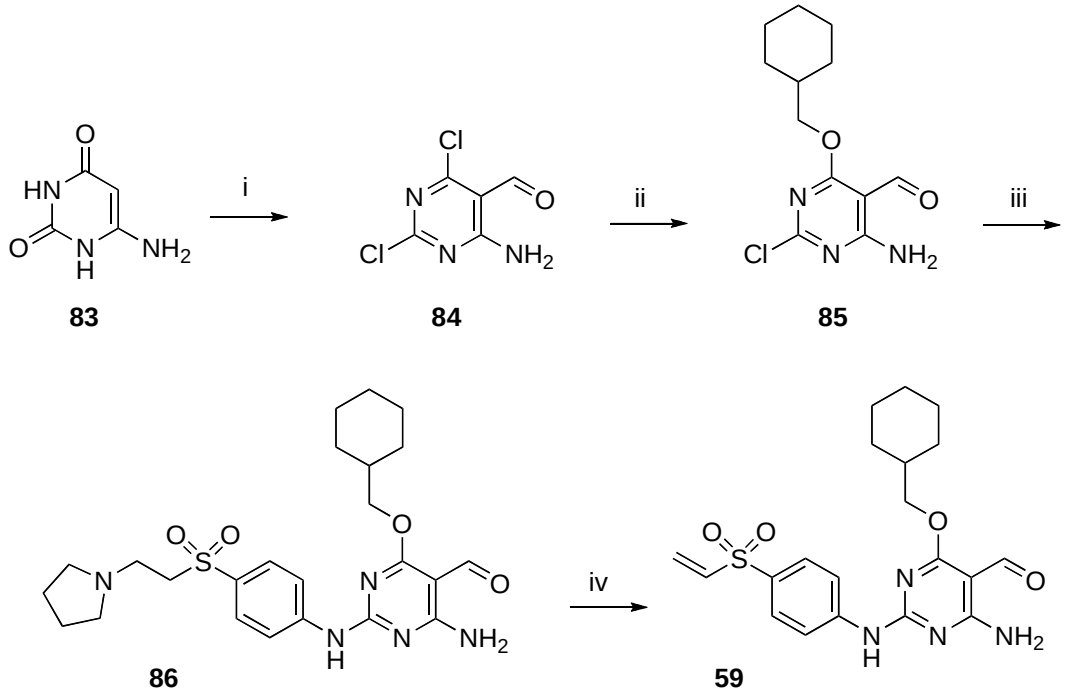

Scheme 7

Reagents and Conditions: i) $POCl_3$, DMF, reflux, on, 99%; ii) Cyclohexylmethanol, NaH, THF, rt, on, 17%; iii) **82**, TFE, TFA, 110 °C, 15 min (MW), 50%; iv) mCPBA, DCM, rt, 30 min, 53%.

A Vilsmeier-Haack reaction, using $POCl_3$ and DMF, was performed on 6-aminouracil (**83**). [170] The product (**84**) was obtained in high yield after optimisation of the reaction conditions. In particular, an excess of DMF (see Experimental Section) was added to the reaction mixture at 0 °C and the reaction was then allowed to stand at room temperature for 1 h before adding 6-aminouracil (**83**).

The Vilsmeier-Haack reaction mechanism proceeds as follows: DMF reacts with $POCl_3$, which eliminate the amide oxygen atom and replaces it with chloride (Fig. 68). The product is the Vilsmeier-Haack reagent, an iminium cation (Fig. 71). [171]

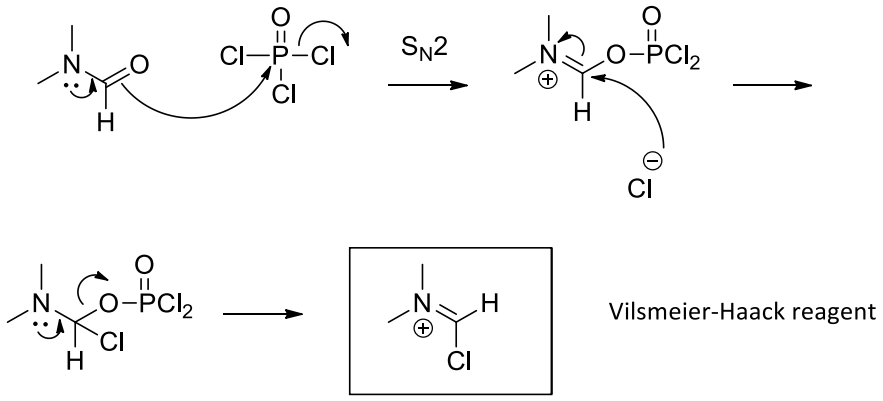

Fig. 71 Vilsmeier-Haack mechanism: formation of the iminium cation

The iminium cation then reacts with 6-aminouracil to give a more stable iminium salt. The aqueous work-up leads to the hydrolysis of the imine salt and removes any acids formed (Fig. 72). [171]

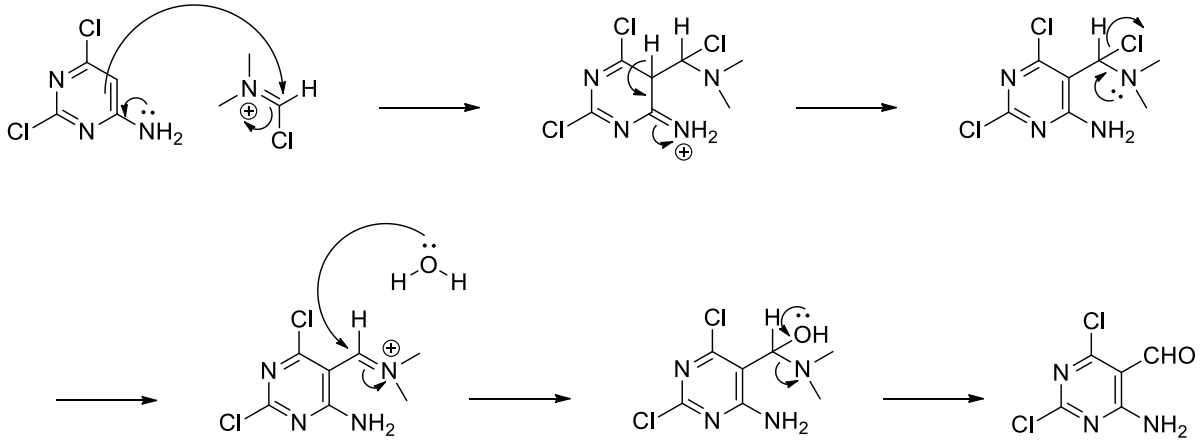

Fig. 72 Vilsmeier-Haack mechanism: formylation

Initially, the use of a lower amount of DMF (8 equiv. Vs 12 equiv.) negatively affected the yield (33-59% Vs 99%) of this step with isolation, after purification, of compound **84** and the reaction intermediate **84**^{i} (Fig. 73 and 74).

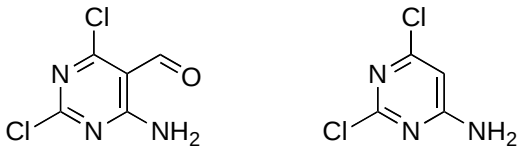

84 **84**^{i}

Fig. 73 Compounds **84** and **84**^{i}

The proposed mechanism for the formation of compound **84**^{i} might involve the following events: firstly, according to the Vilsmeier-Haack reaction, DMF reacts with $POCl_3$, giving the Vilsmeier-Haack reagent (Fig. 68). [171] Secondly, the iminium cation reacts with 6-aminouracil substituting the carbonyl groups with chlorine atoms (Fig. 74), giving compound **84**^{i} because there is insufficient DMF available to form sufficient Vilsmeier-Haack reagent to complete the reaction and give solely the desired final product (**84**).

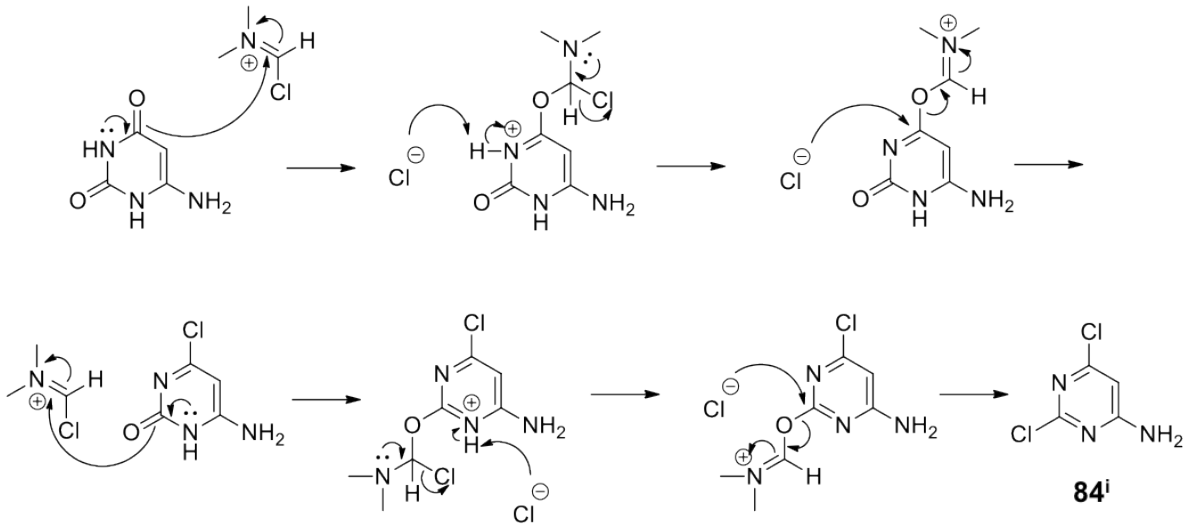

Fig. 74 Proposed mechanism for Vilsmeier-Haack reaction

NMR analysis (Fig. 75) supported the proposed mechanism (Fig. 74). In fact, the ^{1}H-NMR spectrum of compound **84**^{i}, where the formylation did not occur, showed two small peaks (δ 8.22, δ 7.02, 2H), correlated to the amino group at the pyrimidine 6-position and a sharp peak (δ 5.56, 1H) correlated to the proton at the pyrimidine 5-position (Fig.75A).

Sharp peaks between 2 and 4 ppm are due to the solvent (H_2O 3.3 ppm, s and DMSO 2.5 ppm, q).

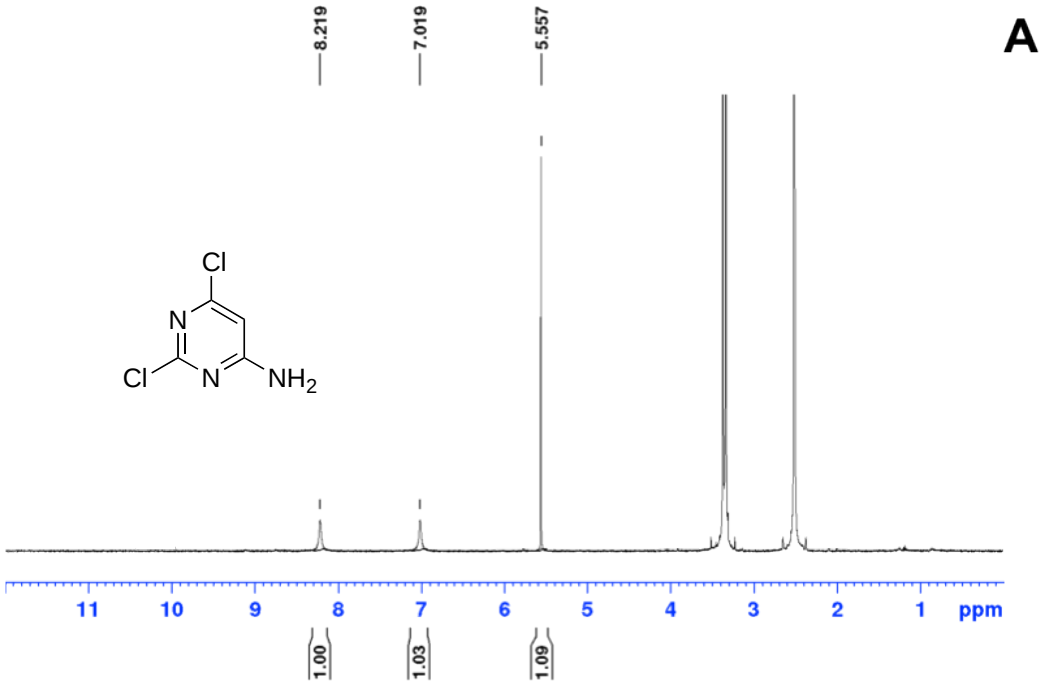

Whereas, the spectrum of compound **84** showed the proton of the formyl group (δ 10.20, 1H) and two small peaks (δ 9.12, δ 8.75, 2H) correlated to the amino group at the pyrimidine 6-position (Fig. 75B).

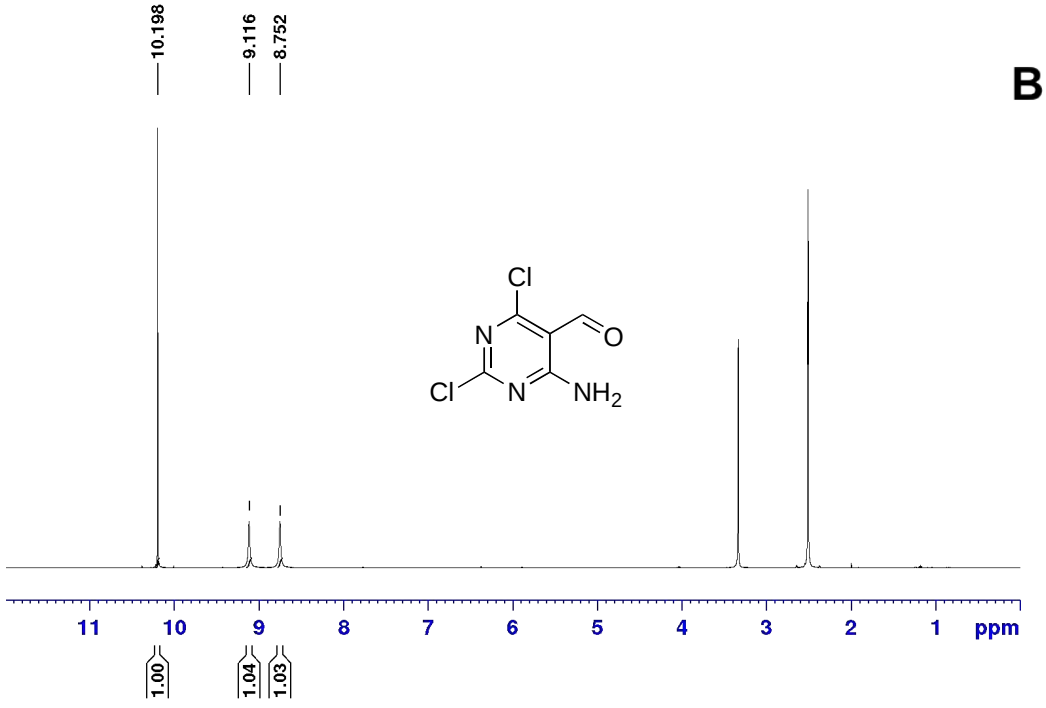

Fig. 75 ^{1}H-NMR spectra of compound **84**^{i} (**A**) and **84** (**B**)

The pyrimidine 2-, 4- and 6-position are activated for nucleophilic attack due to the presence of the adjacent electron-attracting nitrogen atoms. The second step of this synthetic route involved a nucleophilic substitution at the pyrimidine 4-position with cyclohexylmethanol.

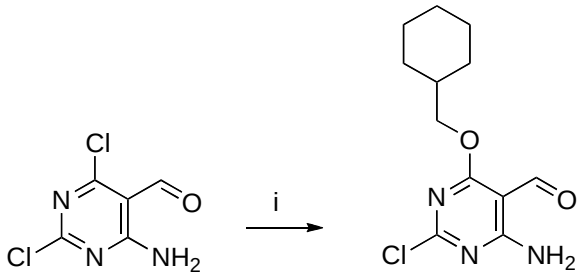

84 **85**

Scheme 8

Reagents and Conditions: i) Cyclohexylmethanol, NaH, THF, rt, on, **17%**.

From this step it was possible to isolate three different products after purification by chromatography on silica: two isomers with the cyclohexylmethoxy moiety at the pyrimidine 2- and 4-position (**85** and **85**^{i} respectively) and compound **85**^{ii}, where the substitution occurred both at the pyrimidine 2- and 4-position (Fig. 76).

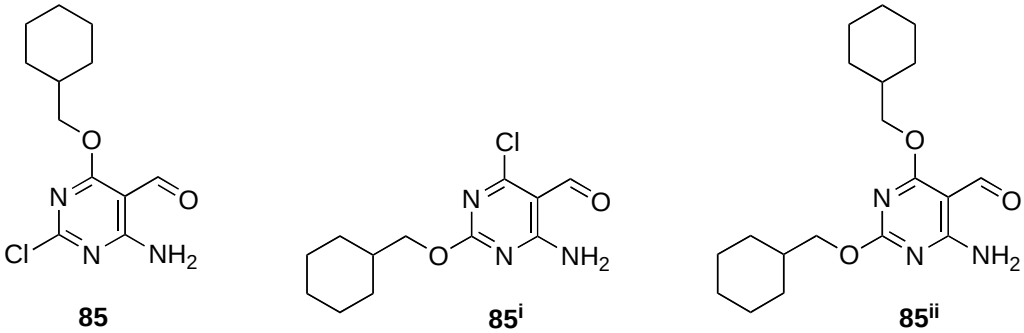

85 **85**^{i} **85**^{ii}

Fig. 76 Compounds **85**, **85**^{i} and **85**^{ii}

The desired final compound (**85**) was obtained in low yield (17%), although many attempts were undertaken in order to optimise the reaction conditions. In parallel, the equivalents of NaH and cyclohexylmethanol were progressively increased from 1 to 10 and variations of the reaction temperature and time were also explored.

The reactions were performed:

- At room temperature, which gave the desired product (**85**) with higher yield, performing the reaction in THF with 1.5 equivalents of NaH and cyclohexylmethanol.

- In an ice-bath (0-5 °C), which did not work, neither with 10 equivalents of NaH and cyclohexylmethanol.

- At reflux (65-67 °C), which gave solely the double substituted product, just performing the reaction with 1 equivalent of NaH and cyclohexylmethanol.

When the reactions worked, in all cases, the major product was the double substituted derivative (**85**^{ii}).

The two isomers (**85** and **85**^{i}) and the double substituted compound (**85**^{ii}) were then characterised by NMR spectroscopy (Fig. 77 for compounds **85** and **85**^{i} and Fig. 79 for compound **85**^{ii}).

Analysing the ^{1}H-NMR spectra (Fig. 77), the only difference between the two isomers (**85** and **85^{i}**) was the shape of the 6-amino group peak, which split into two small peaks (8.5-8.7 ppm) for both compounds (**85**) and (**85^{i}**), which had almost coalesced in the latter case.

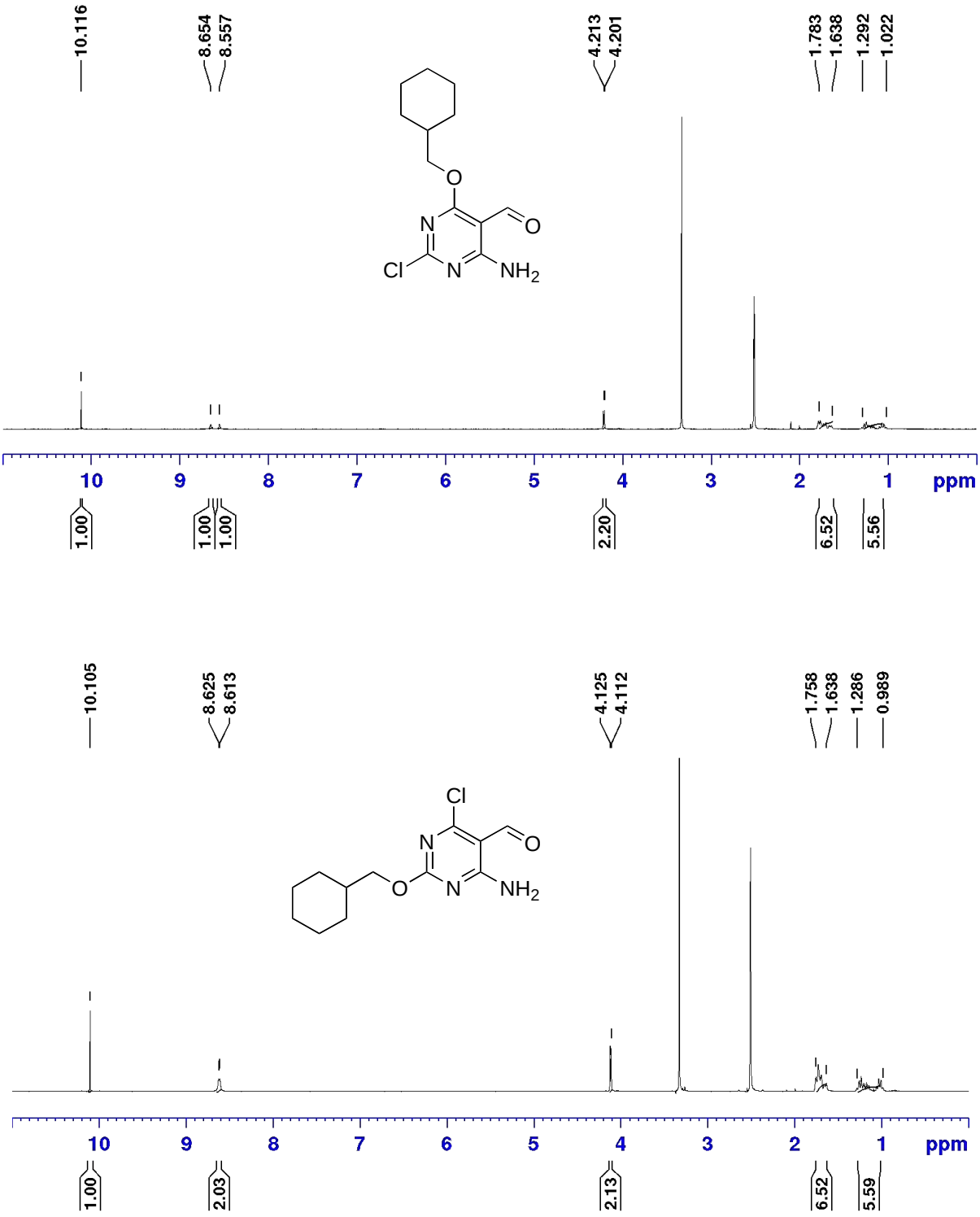

Fig. 77 ^{1}H-NMR spectra for compound **85** and **85^{i}**

Crystal structures of compounds **85** and **85**^{i} were also obtained, (Fig. 78, see Annex for crystal structure data).

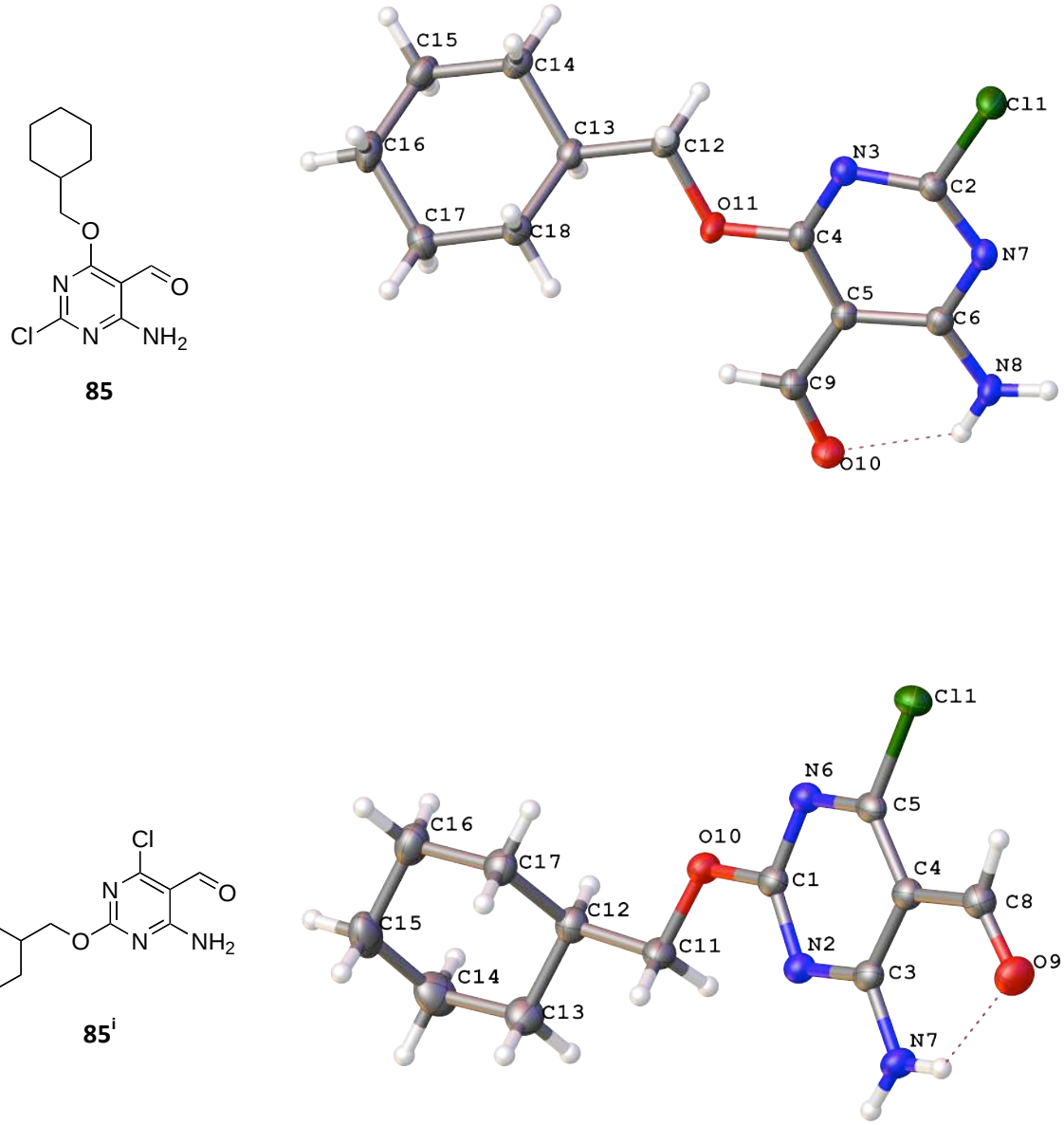

Fig. 78 Crystal structure of compounds **85** and **85**^{i}

The ^{1}H-NMR spectrum for the double substituted derivative (**85^{ii}**) shows two doublets (δ 4.18, 2H, δ 4.09, 2H), which can be correlated to the two linker -CH_2 groups of the cyclohexylmethoxy moieties at the pyrimidine 2- and 4-position and two multiplets (δ 1,72, 12H, δ 1.15, 10H), which integrate for two cyclohexylmethoxy moieties (22H).

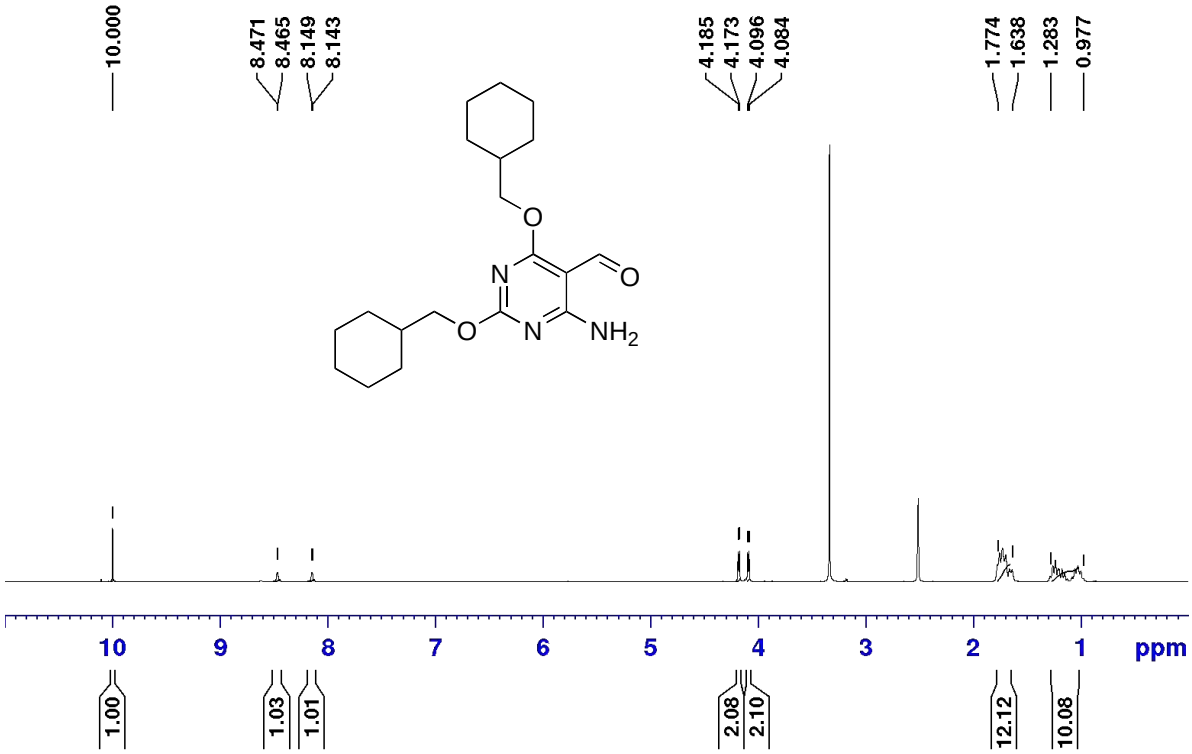

Fig. 79 ^{1}H-NMR spectrum for compound **85^{ii}**

The coupling reaction between intermediate **85** and the side-chain (**82**) was then carried out to give compound **86**. [172]

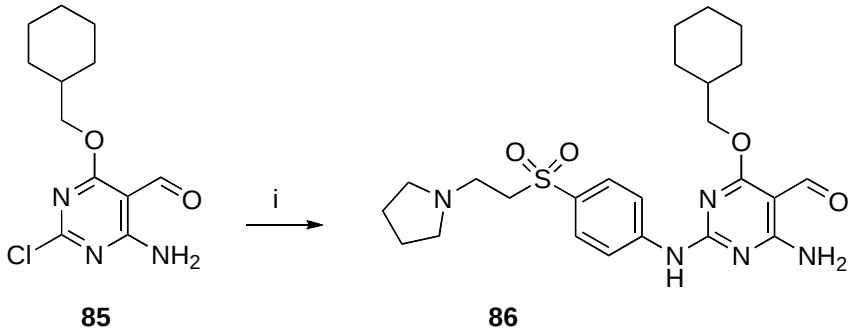

Scheme 9

Reagents and Conditions: i) **82**, TFA, TFE, MW 110 °C, 20 min, 50%.

The reaction involves the displacement of chloride at the pyrimidine 2-position. The reaction is catalysed under acidic conditions by addition of TFA, which activates the pyrimidine ring by protonation. Nucleophilic attack of the aniline is thereby promoted, accelerating the reaction rate. Upon formation of a tetrahedral intermediate, a proton is lost from the aniline nitrogen to give the desired product (**86**) by elimination of chloride (Fig. 80). [172]

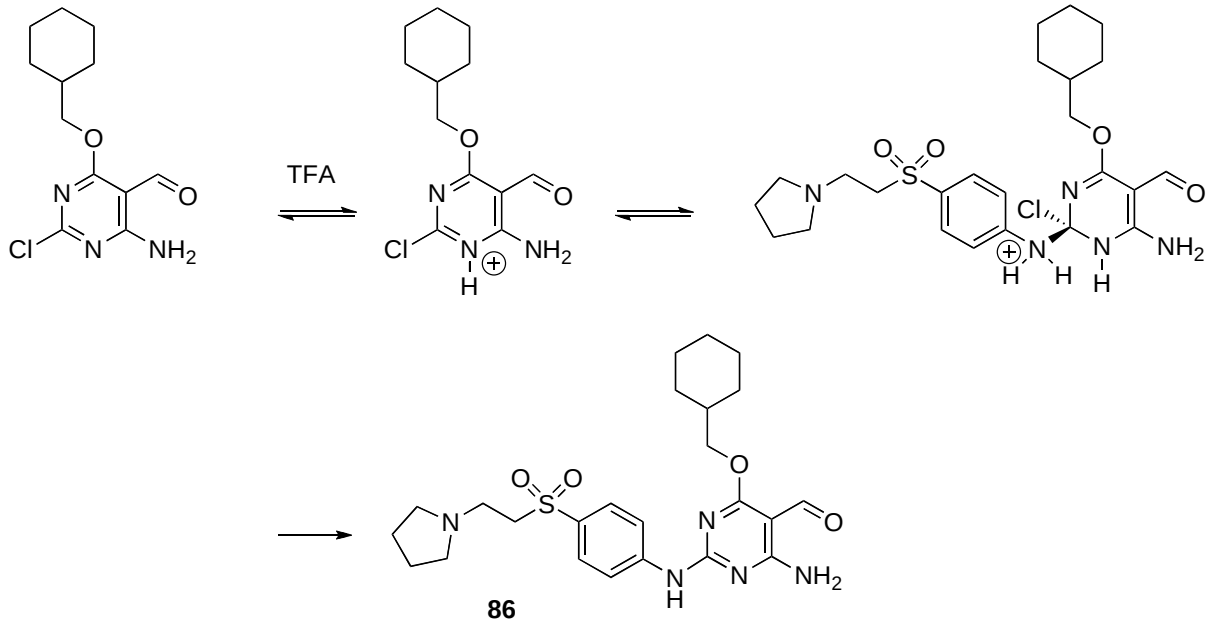

Fig. 80 TFA/TFE mechanism

The last step of this synthesis was performed to give the desired final product **59** *via* a Cope elimination. [156]

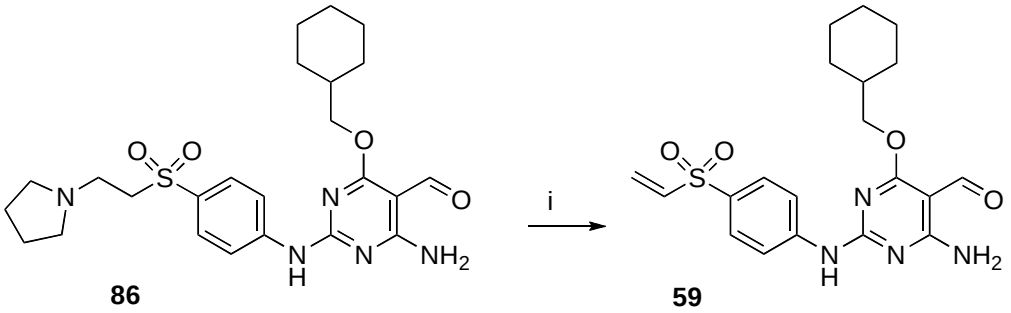

Scheme 10

Reagents and Conditions: i) mCPBA, DCM, 53%.

This process involves the formation of an N-oxide intermediate by oxidation of the tertiary amine on compound **86**. The N-oxide serves as a base to remove the α-hydrogen atom *via* a 5-membered cyclic transition state (Fig. 81). [156]

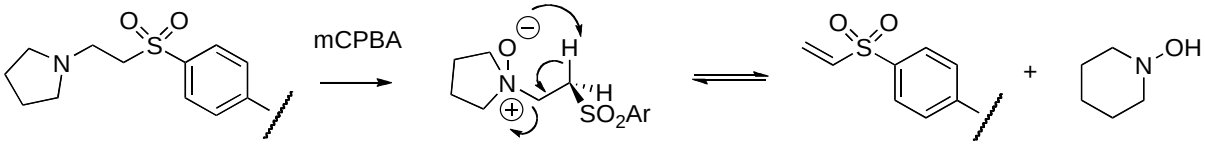

Fig. 81 Cope elimination mechanism

In parallel, several alternative synthetic routes, to obtain target compound **59** were considered in order to avoid, during the second step of the synthesis, the low yield owing to the formation of the two isomers (**85** and **85**^{i}) and the double substituted product (**85**^{ii}).

Sodium cyanoacetylcyanamide (**88**) was prepared starting from ethyl cyanoacetate and cyanamide (**87**), according to the procedure reported by Hirayama *et al* (Scheme 11). [173, 174]

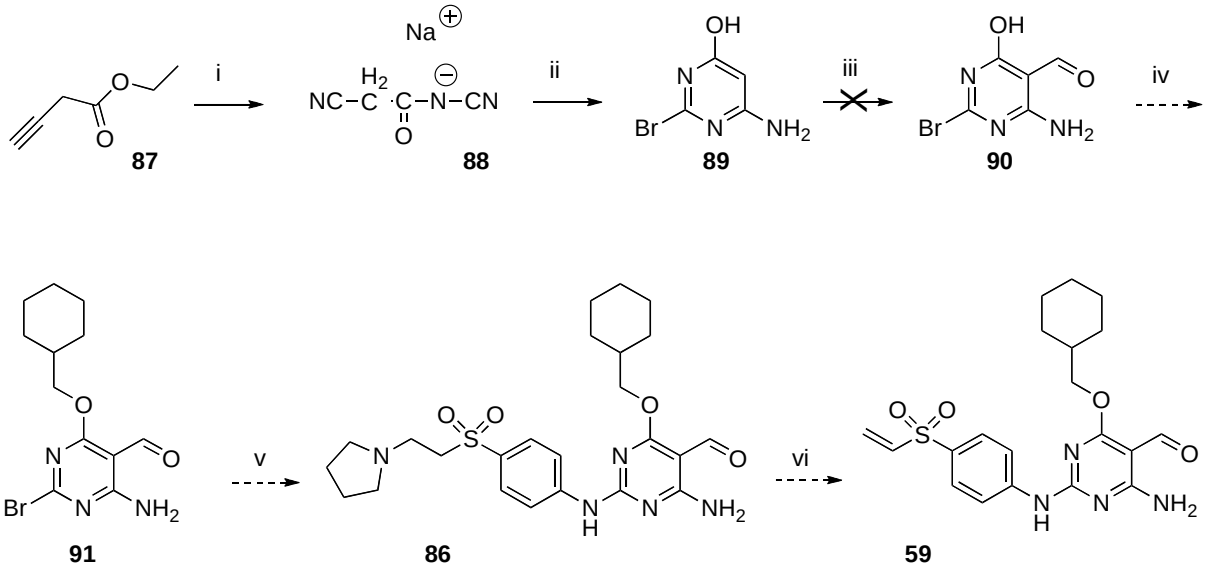

Scheme 11

Reagents and Conditions: i) Cyanamide, NaOMe, rt, 3-5 h, 91%; ii) HBr, AcOH, rt, 6 h, 76%; iii) $POCl_3$, DMF, 60 °C-reflux, 3 h, on.

Reaction of HBr with sodium cyanoacetylcyanamide (**88**) gave the 2-halogenopyrimidine (**89**). From intermediate **89** several attempts were made to give intermediate **90**, although they were not successful:

- A Vilsmeier-Haack reaction intended to give intermediate **90** was carried out, but did not work, even modifying the reaction conditions.

- A Mitsunobu reaction, which is a useful reaction for the conversion of primary and secondary alcohols into several functional groups, was performed with compound **89**, using PPh_3, DIAD and cyclohexylmethanol, to give substitution at the pyrimidine 4-position, but the reaction was not successful. After purification by chromatography on silica it was only possible to isolate triphenylphosphine oxide, a reaction by-product.

Another alternative route to obtain compound **59** was then proposed (Scheme 12). A convenient method, employing DABCO as leaving group, was investigated. [175] Reaction of intermediate **84** with DABCO in DMSO, to give intermediate **91**, was performed. As from the NMR spectrum it proved difficult to characterise the product of this step, it was engaged in the following step to give intermediate **85**, but the reaction was not successful (Scheme 12).

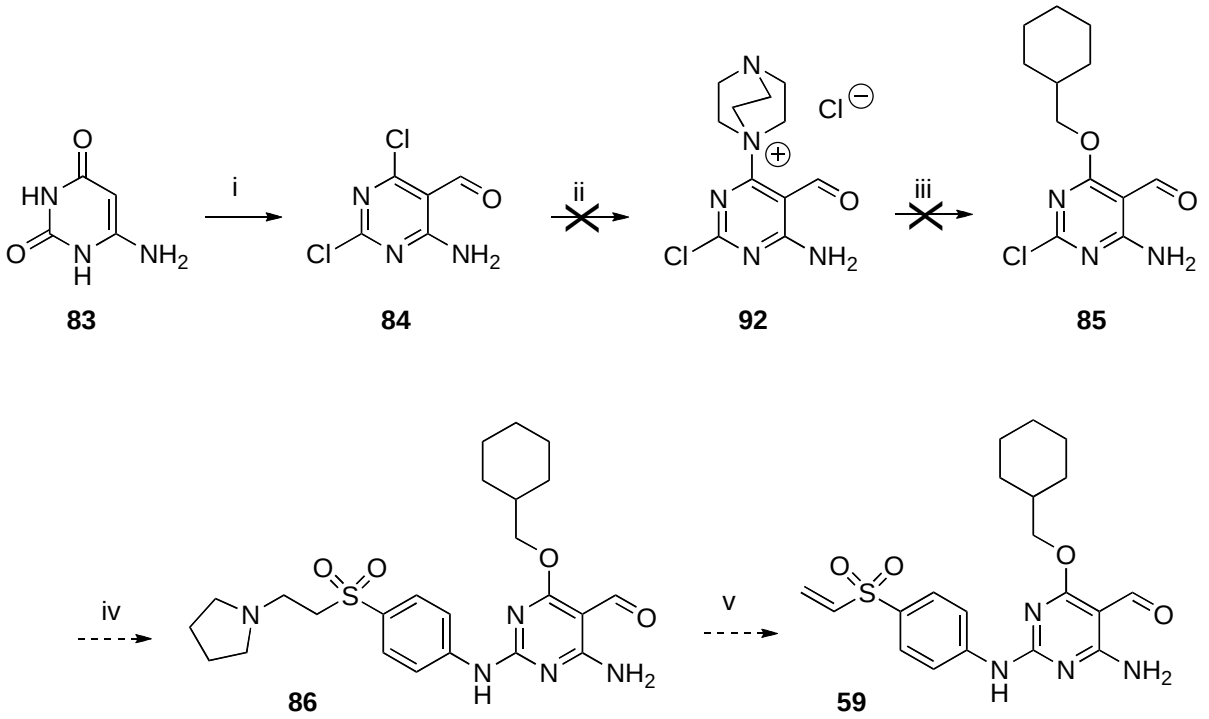

Scheme 12

Reagents and Conditions: i) $POCl_3$, DMF, 110 °C, 12 h, 99%; ii) DABCO, DMSO, rt, 12 h; iii) Cyclohexylmethanol, NaH, THF, rt, 12 h.

After the previous attempts, these synthetic routes were left aside.

The second target investigated for irreversible CDK2 inhibitors was compound **93**, having a nitrile group at the pyrimidine 5-position, a cyclohexylmethoxy moiety at the 4-position and a vinyl sulfone moiety (side-chain) at the pyrimidine 2-position. The oxime derivative (**94**) of compound **93** was also synthesised, in order to see whether the intramolecular hydrogen bond between the 6-amino group and the oxime functionality is retained (Fig. 82). Nevertheless, it should be noted that although -CN is electron-withdrawing like -CHO the nitrogen lone pair cannot form an intramolecular H-bond analogous to -CHO.

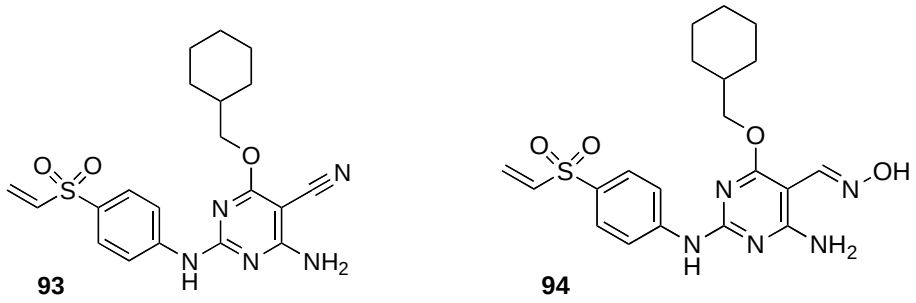

Fig. 82 Compounds **93** and **94**

The synthesis started from 6-aminouracil (Scheme 13). The first three steps of the synthesis followed the protocols as for compound **59**, with a Vilsmeier-Haack reaction on 6-aminouracil, a nucleophilic substitution at the pyrimidine 4-position with cyclohexylmethanol and the coupling reaction in TFA/TFE between the substituted pyrimidine (**85**) and the side-chain (**82**).

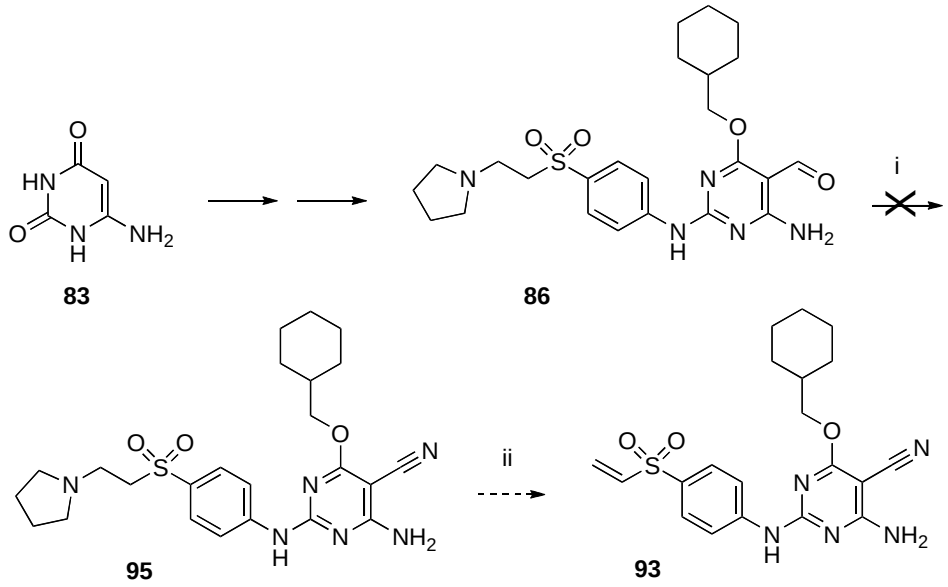

Scheme 13

To convert the formyl group at the pyrimidine 5-position into a nitrile group, different procedures were explored. Firstly, it was considered to convert the formyl group directly to the nitrile group, using the procedure of Chakraborti *et al*. [176] The proposed mechanism proceeds through an oxime intermediate which should give, after the aqueous workup, the final product with the nitrile group at the pyrimidine 5-position (Fig. 83).

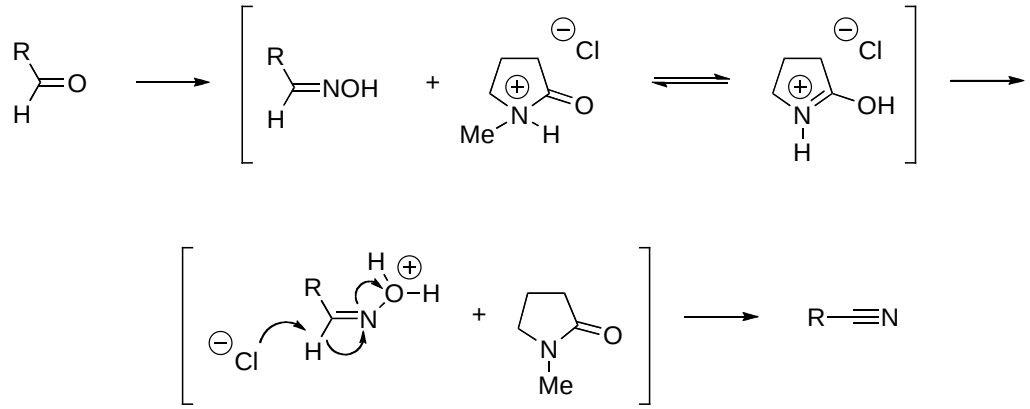

Fig. 83 Conversion of an aldehyde to a nitrile through an aldoxime intermediate

This reaction was carried out on intermediates **84** and **86** (Schemes 14 and 15). In both cases, the oxime intermediates (**96**^{i} and **96** represented in scheme 14 and 15 respectively) were isolated after purification, even if an aqueous work up was carried out.

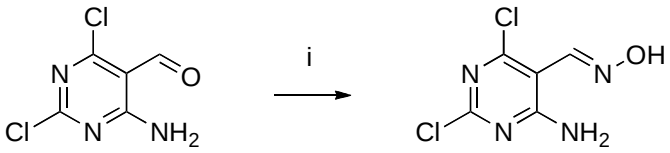

84 **96**^{i}

Scheme 14

Reagents and Conditions: i) H_2NOH, NMP, MW 110° C, 20 min, 22%.

Compound **96** was obtained as shown in Scheme 15.

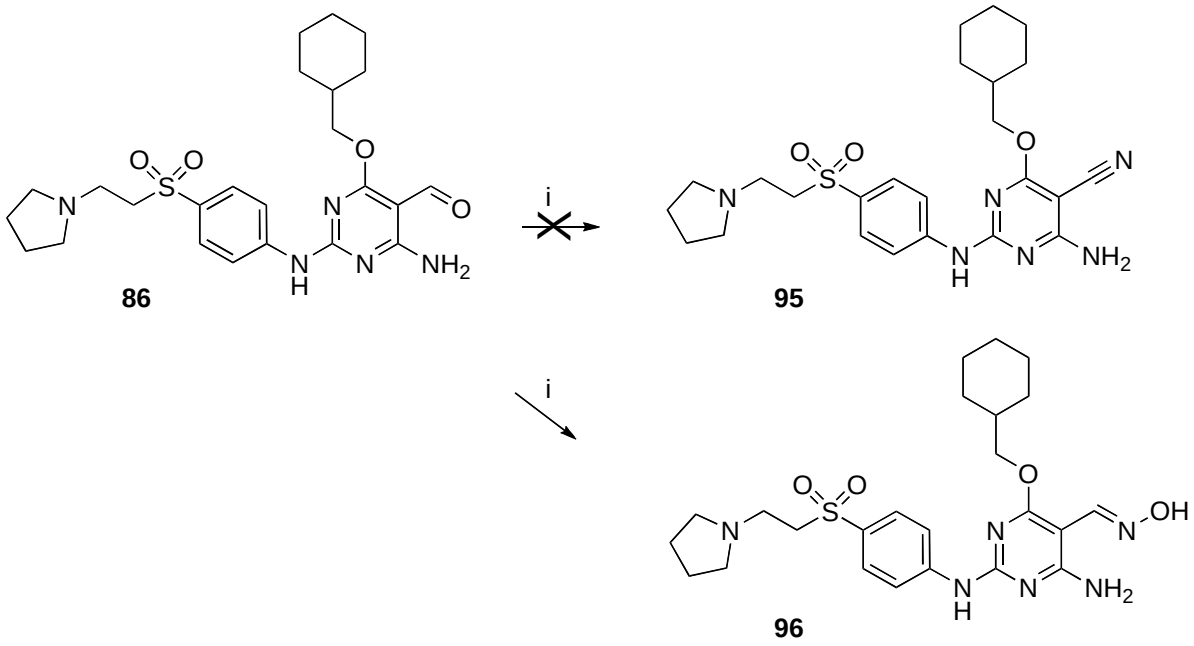

Scheme 15

Reagents and Conditions: i) H_2NOH, NMP, MW 110° C, 20 min, 17%.

The low yield obtained in this step is due to the presence of NMP, which proved difficult to remove from the crude product during the purification. To avoid the use of NMP as solvent, a different procedure was explored for the conversion of the formyl group to the oxime functionality.

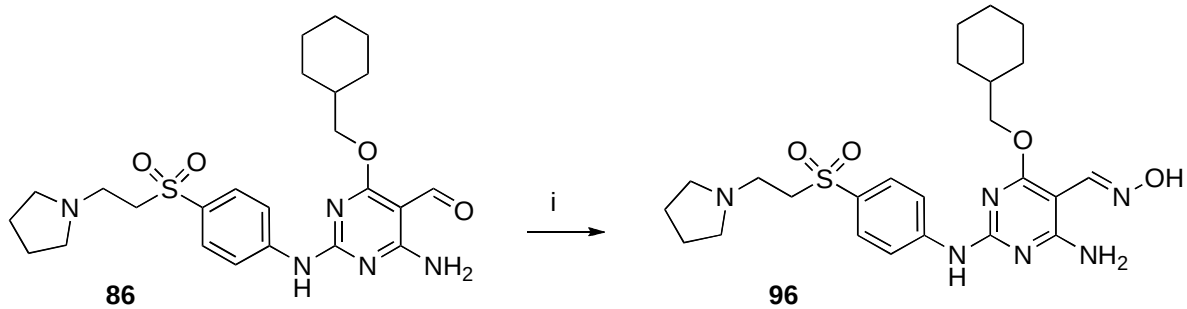

Scheme 16

Reagents and Conditions: i) H_2NOH, NaOH, H_2O, EtOH, rt, 5 h 36%.

After optimisation of this step, intermediate **96** was obtained in good yield and was then engaged in the next step, in which a procedure for the conversion of oximes to nitriles reported by Singh *et al* was used. [177]

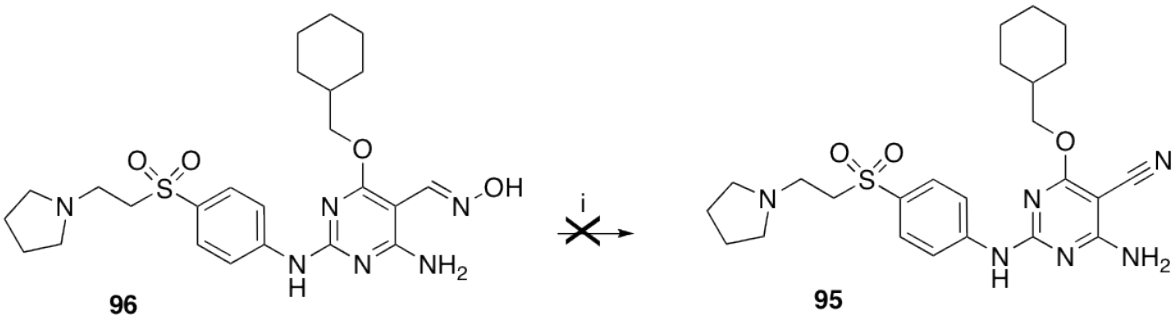

96 **95**

Scheme 17

Reagents and Conditions: i) DBU, PyBOP, DCM, rt, 5 h.

In the literature procedure DBU (**97**) and BOP (**98**) in DCM were used. BOP reagent is commonly used in the synthesis of peptides, but its use is discouraged because it liberates HMPA (**99**), which is carcinogenic.

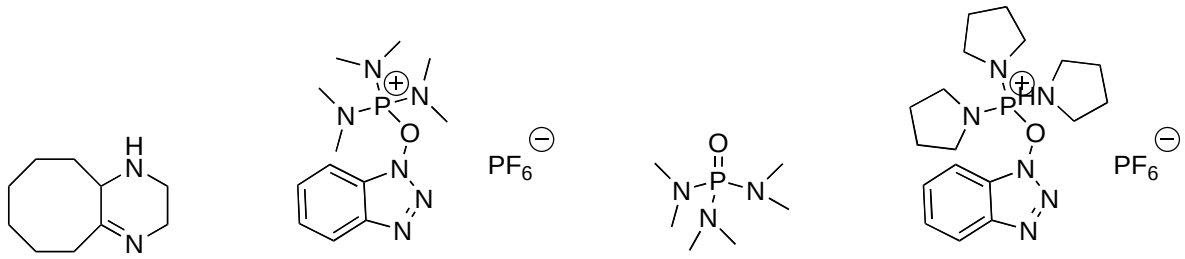

97 **98** **99** **100**

Fig. 84 DBU (**97**), BOP (**98**), HPMA (**99**) and PyBOP (**100**)

Hence, PyBOP (**100**) was firstly used instead of BOP (**98**). Our concern in this case was about the steric hindrance of PyBOP (**100**), because of the pyrrolidine rings.

The proposed mechanism for the formation of nitriles by dehydration of aldoximes with BOP (**98**) or PyBOP (**100**) is the same and was reported by Singh *et al.* [177]

Upon oxime deprotonation by DBU (**97**), initial reaction could occur by nucleophile substitution at the phosphorous atom of PyBOP (**100**), with the formation of a new phosphonium species, which reacts with DBU in order to eliminate phosphoryltripyrrolidine (Fig. 85).

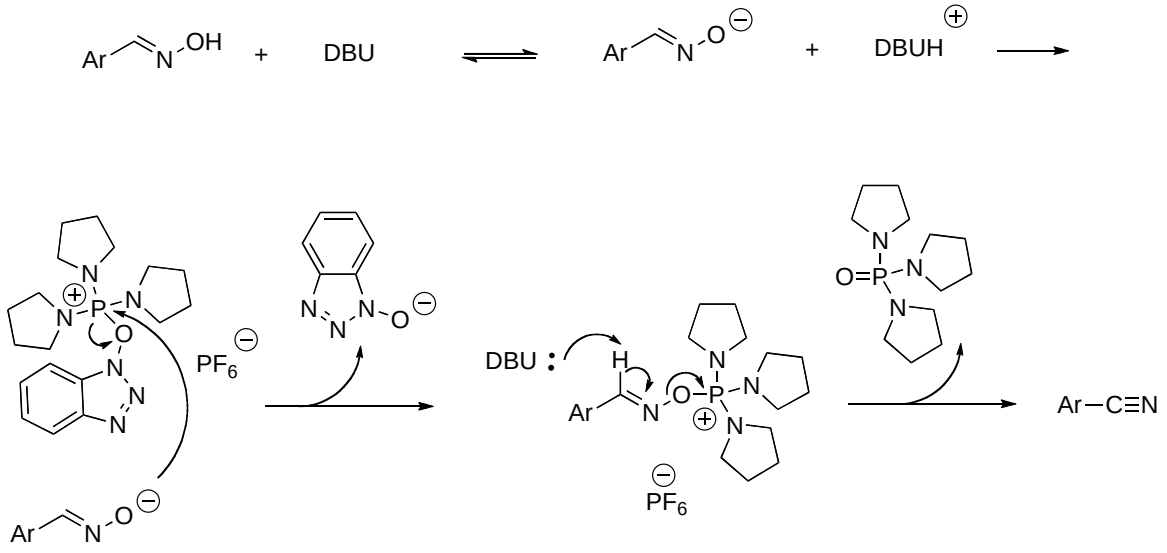

Fig. 85 Mechanism for the formation of nitriles

The reaction with PyBOP (**100**) was not successful. Hence, the reaction was carried out with BOP (**98**) and proved to work.

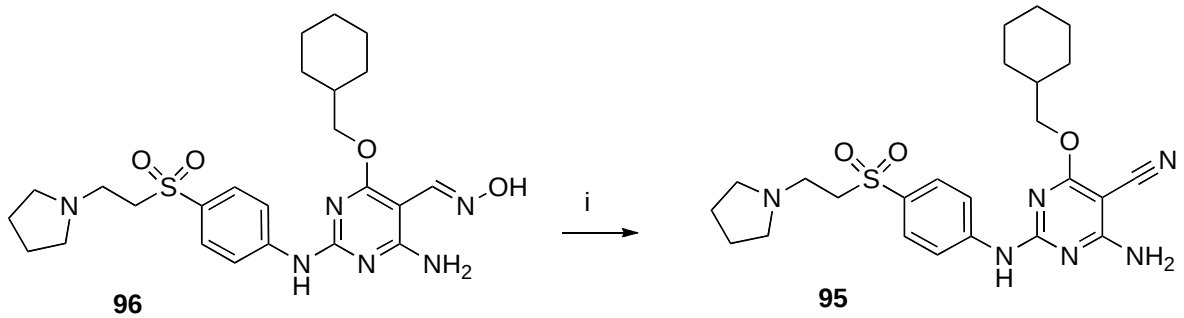

Scheme 18

Reagents and Conditions: i) DBU, BOP, DCM, rt, 5 h, 78%.

Finally, compound **95** was engaged in the oxidation step with mCPBA to obtain the final product **93** (Scheme 19).

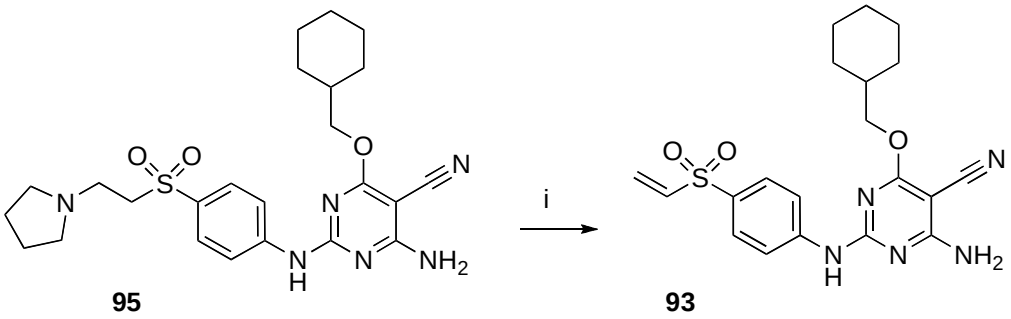

Scheme 19

Reagents and Conditions: i) mCPBA, DCM, 0 °C, 30 min, 37%.

Intermediate **96** was also enganged in the oxidation step with mCPBA to obtain the final product **94** (Scheme 20).

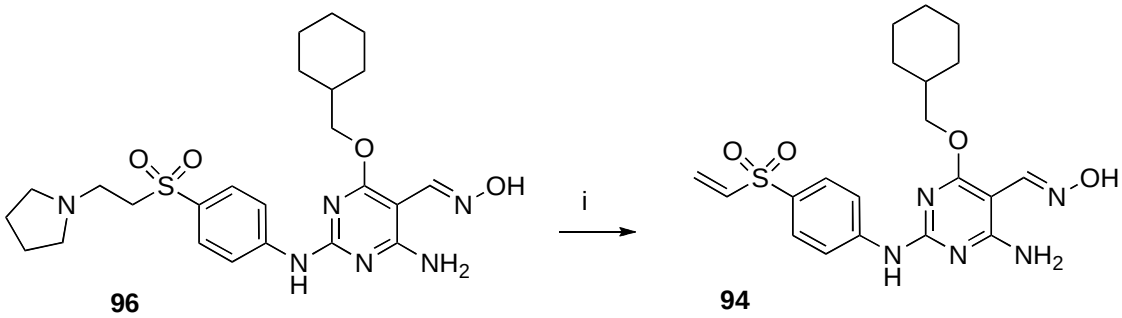

Scheme 20

Reagents and Conditions: i) mCPBA, DCM, 0 °C, 30 min, 49%.

After purification by flash chromatography on silica, the purity of compound **94** was checked by HPLC. The analysis showed compound **94** to be 68% pure (Fig. 86A) and so it was decided to proceed with a purification by preparative HPLC, but during the purification process compound **94** decomposed, as shown in Fig. 86B.

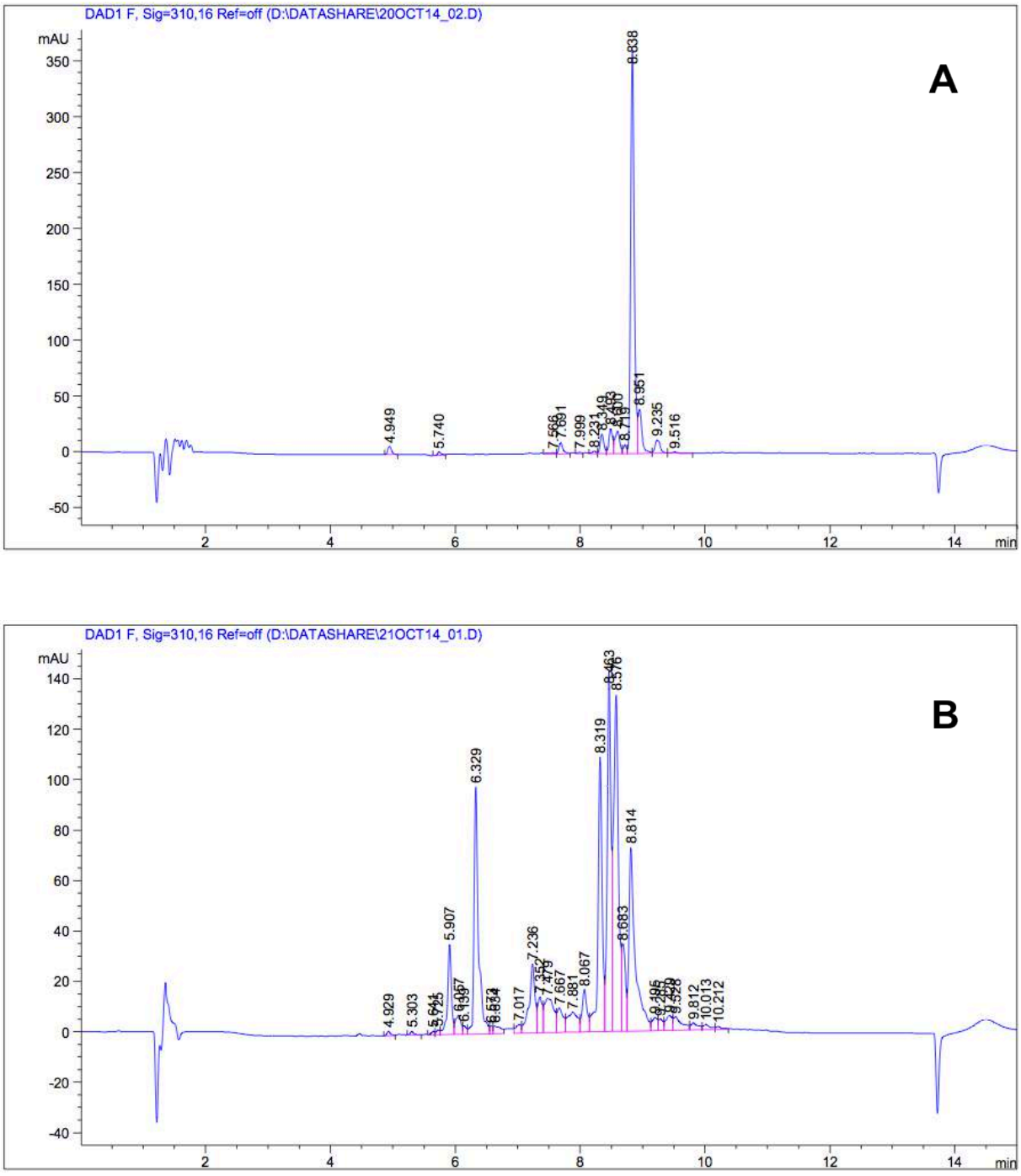

Fig. 86 Analytical HPLC spectra of **94** (A) and decomposition of **94** (B)

The decomposition of the final product **94** is probably due to the highly reactivity of the electrophilic vinyl sulfone moiety. For example, a reaction between the nucleophilic oxime functionality and the other extremity of the molecule could occur, as shown in the proposed mechanism in Fig. 87.

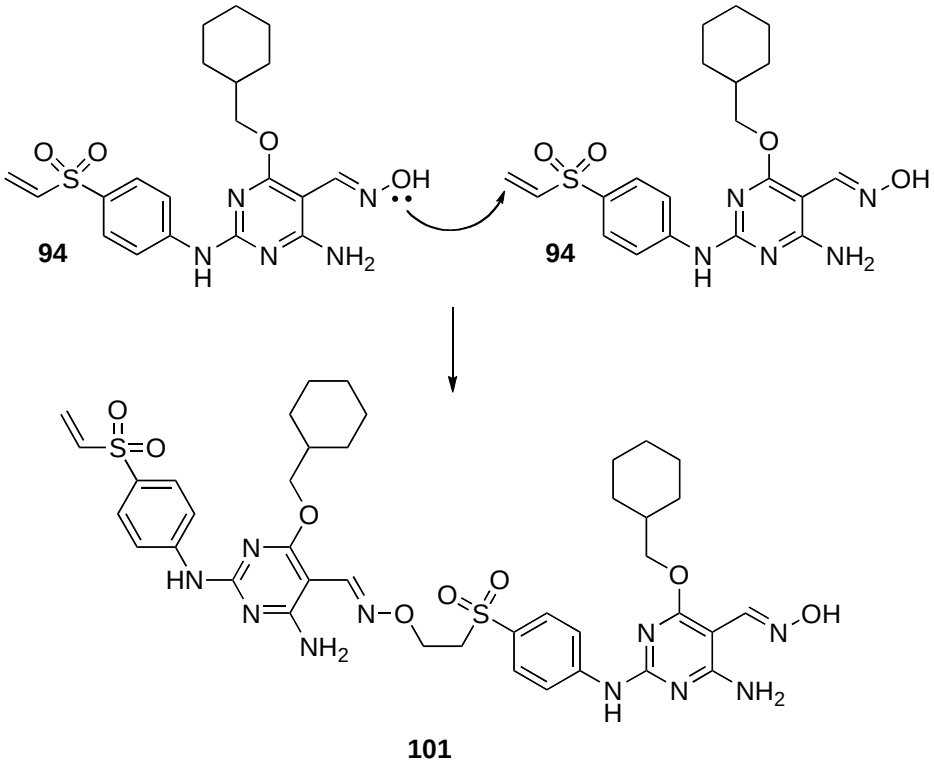

Fig. 87 Proposed mechanism for the decomposition of compound **94**

In parallel, synthetic routes for the pyrimidine-based CDK2 irreversible inhibitors having no substituents at the pyrimidine 4-position were proposed. This was to investigate the effect, upon biological activity (see Par. 3.2.1.), of removing the cyclohexylmethoxy moiety.

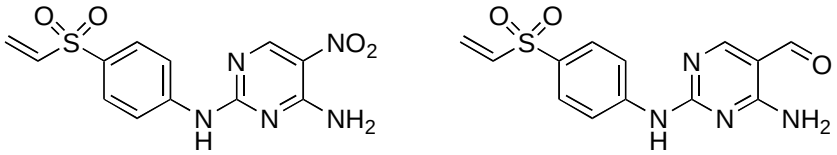

102 **103**

Fig. 88 Compounds **102** and **103**

The following scheme was performed for the synthesis of compound **102**, starting from 5-nitrouracil (**104**, Scheme 21).

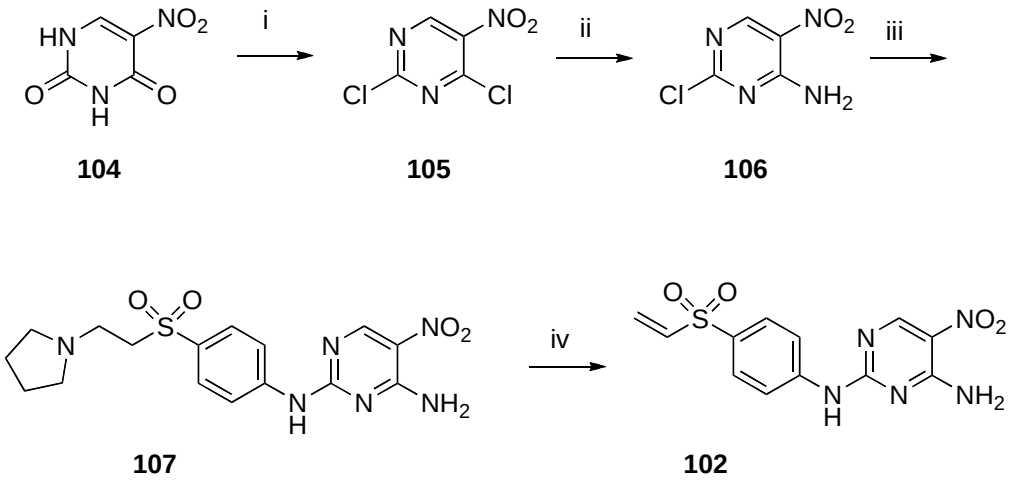

104 **105** **106** **107** **102**

Scheme 21

Reagents and Conditions: i) $POCl_3$, DMA, 190 °C, 1.5 h, 92%; ii) NH_3 aq, THF, 0 °C, 30 min 63%; iii) **82**, TFE, TFA, 110 °C, 15 min (MW), 56%; iv) mCPBA, DCM, 0 °C, 30 min, 31%.

The synthesis proved to be straightforward and the final product (**102**) was obtained in 31% yield.

The synthetic route involved: chlorination of compound **104**, followed by displacement of a chlorine atom by an amino group at the pyrimidine 6-position. The third step involved TFA/TFE coupling between the side-chain (**82**) and intermediate **106**, concluding with the N-oxidation with mCPBA and subsequent elimination of the pyrrolidine ring to give the final product **102**. Compound **107** was also evaluated on CDK2 to compare its inhibitory activity to that of the CDK2 irreversible inhibitors.

The following synthetic route was then proposed for the synthesis of compound **103**, starting from cytosine (**108**, Scheme 22).

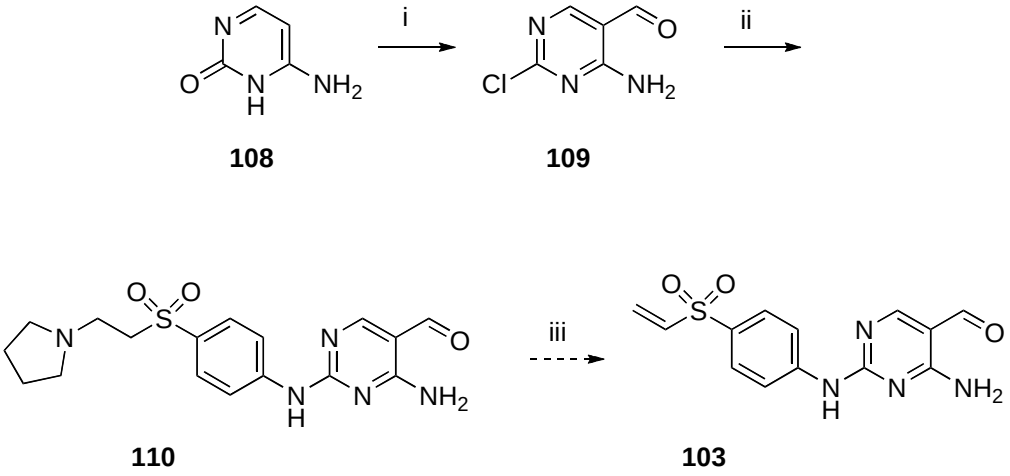

Scheme 22

Reagents and Conditions: i) $POCl_3$, DMF, 110 °C, 33%, 12 h. ii) **82**, TFE, TFA, 110 °C, 25 min (MW), 47%.

A Vilsmeier-Haack reaction on cytosine (**108**), using $POCl_3$ and DMF, was performed to give compound **109** in low yield. From the first step it was also possible to isolate a reaction intermediate (**109^{i}**) and a by-product (**109^{ii}**).

Fig. 89 Compounds **109^{i}** and **109^{ii}**

Compounds **109**^{i} and **109**^{ii} were characterised by NMR (^{1}H, ^{13}C) and HRMS. Compound **109**^{ii} was also characterised by obtaining its crystal structure (Fig. 90).

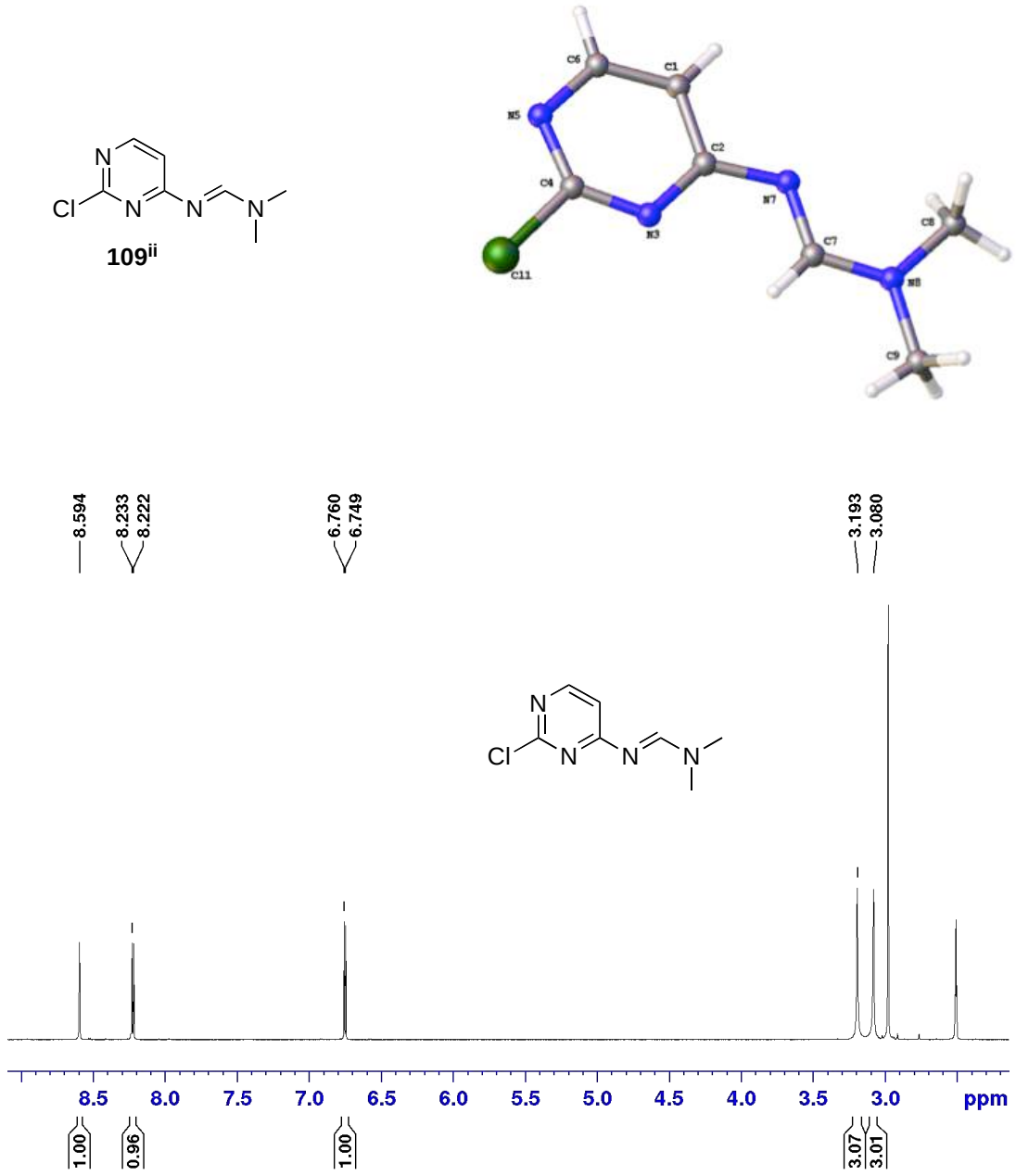

Fig. 90 Crystal structure and ^{1}H-NMR for compound **109**^{ii}

The reaction of intermediate **109** with the side-chain (**82**) to give compound **110** was then carried out. The side-chain (**82**) was introduced at the pyrimidine 2-position by displacement of the chlorine group. Oxidation of intermediate **110**, using mCPBA, will be performed to give the final product (**103**).

The by-product, compound **109**[ii], was also reacted first with $POCl_3$ in DMF (Scheme 23), to see whether a replacement with the formyl group at the pyrimidine 5-position could take place and then with the side-chain in TFA/TFE (Scheme 24), to see whether it was possible to obtain a potential and interesting irreverisble CDK2 inhibitor (**111**).

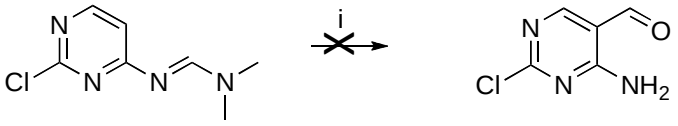

109[ii] **109**

Scheme 23

Reagents and Conditions: i) $POCl_3$, DMF, 110 °C, on.

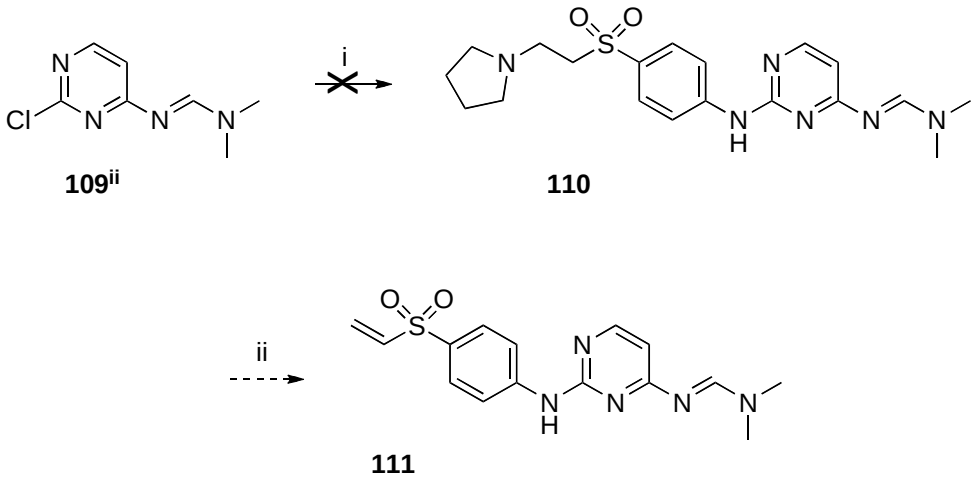

109[ii] **110** **111**

Scheme 24

Reagents and Conditions: i) **82**, TFE, TFA, 110-140 °C, 15-40 min (MW).

The reactions (Scheme 23 and 24) were not successful and, even changing the reaction conditions, in both cases the starting material (**109**[ii]) was recovered.

CDK2 irreversible inhibitors (**59**, **93**, **94**, **102**) and CDK2 reversible inhibitor (**107**) were obtained as follows (Fig. 91).

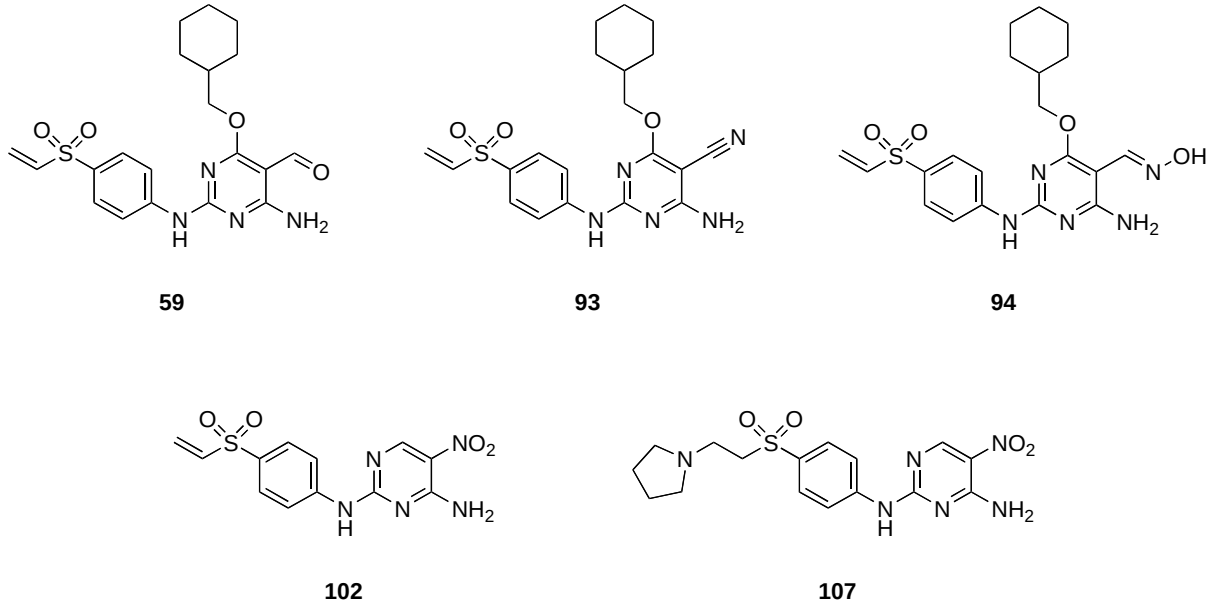

Fig. 91 CDK2 pyrimidine-based inhibitors

Concerning compound **94**, its CDK2-inhibitory activity was not evaluated as the inhibitor decomposed during the purification procedures, as previously explained.

3.2.1. Biological evaluation of CDK2 inhibitors

Biological assays were carried out in the Paul O'Gorman Building (POG), at Newcastle University.

The irreversible pyrimidine-based compounds, obtained as result of a Cope elimination reaction, can be involved in a Michael addition-type reaction with nucleophilic lysine residues within the CDK2-catalytic pocket. The proposed mechanism is shown in Fig. 92.

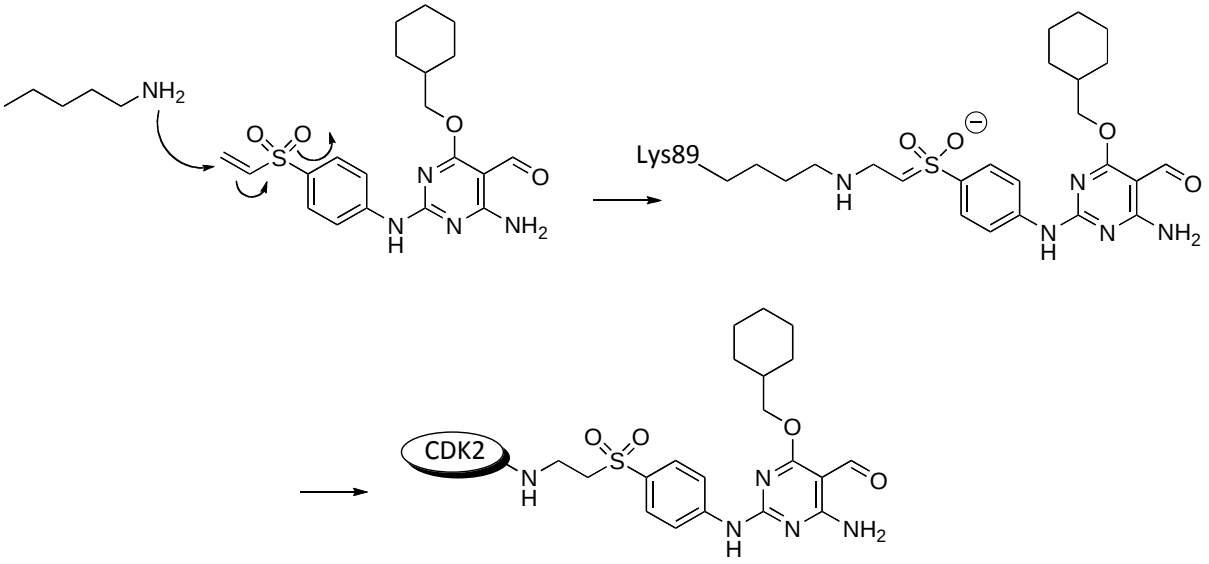

Fig. 92 Michael-addition reaction

Early studies to test vinyl sulfone compounds as CDK2 irreversible inhibitors were aimed at demonstrating that these compounds showed a time-dependent inhibition of the enzyme, with enzyme activity decreasing as a function of the time of exposure of the enzyme to the inhibitor. Hence, the catalytically active enzyme (pCDK2/cyclin A) was incubated with compounds **59** and **102**. Then, at different time periods, an aliquot of the incubation mixture was taken and tested to evaluate the enzymatic activity.

The results for the vinyl sulfone inhibitors (Fig. 93) showed that the kinase loses activity proportionally to the inhibitor exposure time, suggesting that a covalent modification is taking place.

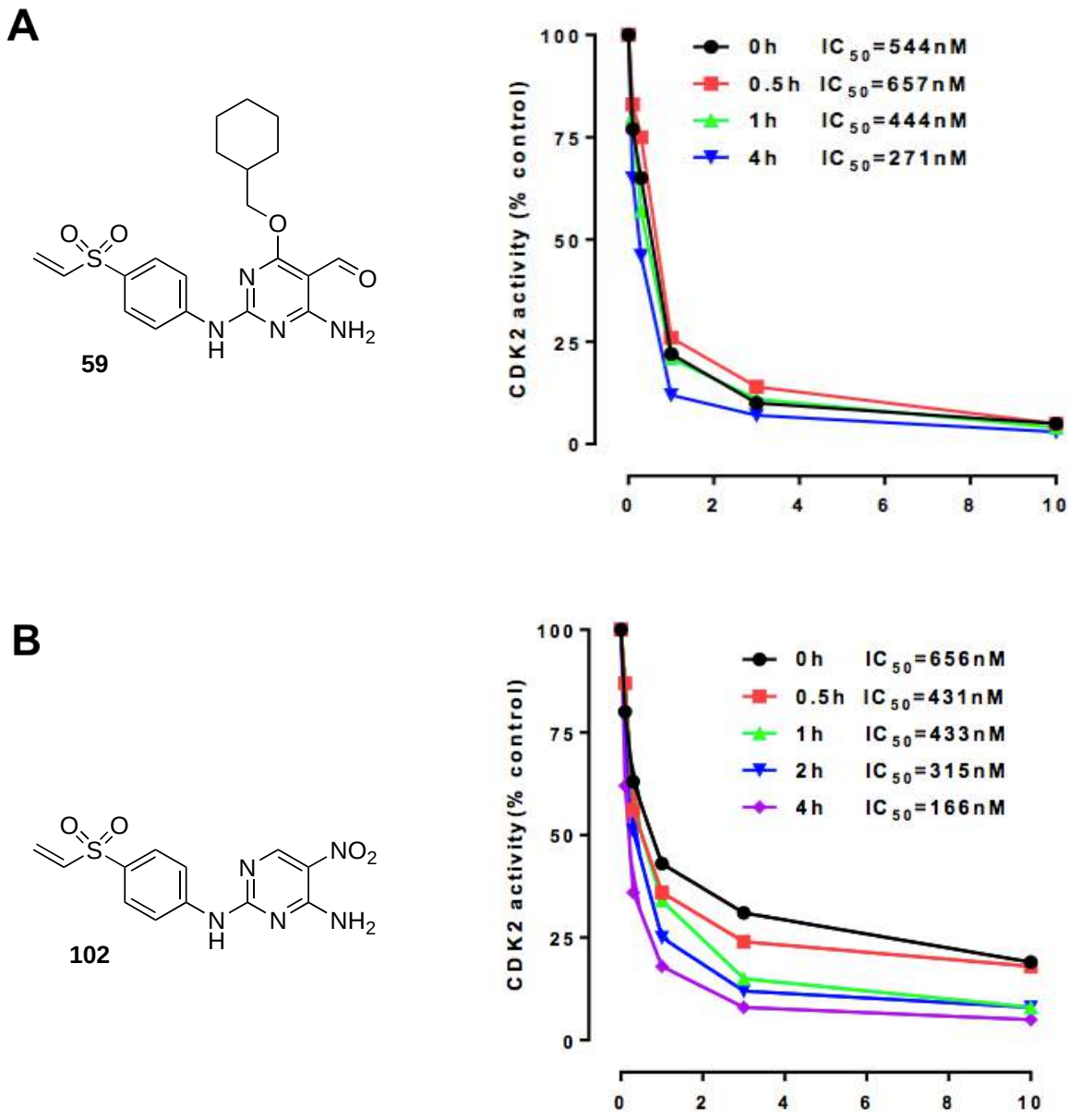

Fig. 93 Time-dependent CDK2 inhibition by compounds **59** (**A**) and **102** (**B**).

Furthemore, compound **107** was also tested in order to compare its activity with the vinyl sulfone inhibitors and further validate the hypothesis that the vinyl sulfone moiety covalently modifies a nucleophilic residue within CDK2-catalytic pocket (Fig. 94).

Hence, a parallel experiment was run on compound **107**, in which a pyrrolidine group replaces the vinyl moiety (Fig. 94). As expected for a reversible inhibitor, the activity of pCDK2/Cyclin A complex does not decrease in a time-dependent manner after incubation with the inhibitor (**107**).

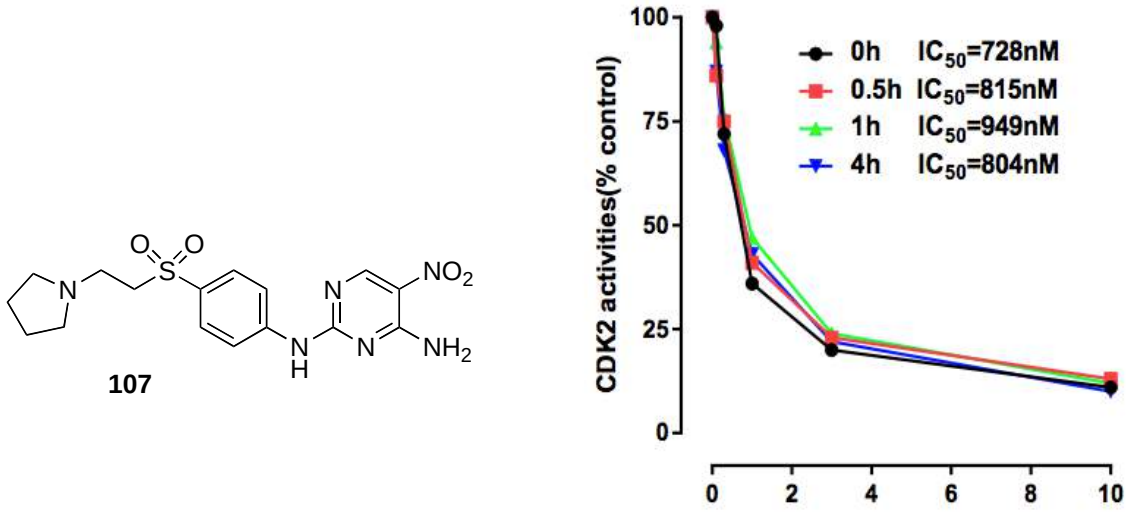

Fig. 94 Time-dependent CDK2 inhibition by compound **107**.

Biological assays for compound **93** are ongoing at Newcastle University.

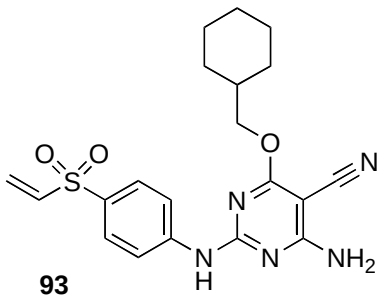

Fig. 95 Compound **93**

The biological results were also supported by docking studies, which are described in the following section and co-cristallography studies are in progress in the Paul O'Gorman Building (POG) at Newcastle University.

3.2.2. Docking studies

Docking studies were carried out in the Molecular Modeling Section (MMS) at the University of Padua.

Molecular docking is a useful tool to predict the 3D structure of an intramolecular complex between a ligand and a macromolecule. This approach is based on force fields, represented by a mathematical function, which describes the energy characteristics assumed by a molecule in a defined environment, when it adopts particular conformations or in comparison to other molecules. The aim of molecular docking is not only the prediction of binding poses, but it concerns also the qualitative analysis of macro-complexes according to scores, in which these complexes are ranked according to the extent of their interaction. For the docking studies the program GOLD (Genetic Optimised Ligand Docking) was used. During the docking protocol the protein remains rigid and the energy of the ligand is minimised at a minimum energy level. Once the binding site is selected it is possible to decide how many times the program must perform the ligand-protein interaction iteration and then the number of runs in order to generate all the possible conformations. The results are then organised in a database, in which all the conformations are listed based on the highest scoring function value. The CDK2 crystal structure was processed using MOE (Molecular Operating Environment).

The crystal structure of CDK2 was selected from the Protein Data Bank (PDB code: 1H1S, resolution 2.00 Å): CDK2/Cyclin A in complex with the inhibitor NU6102 (**5**, IC_{50} = 5.4 nM, Fig. 96). [154]

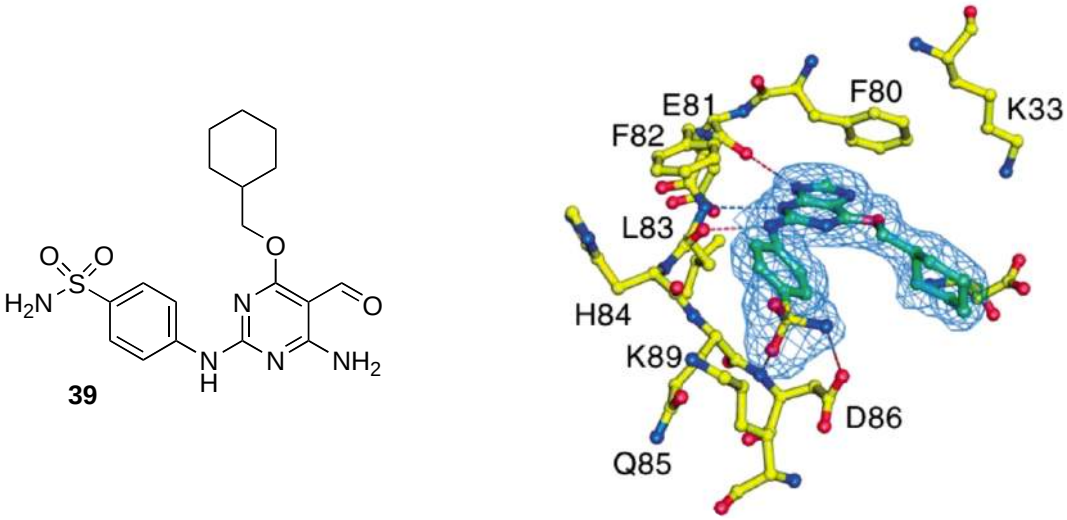

Fig. 96 NU6102 (**39**) co-crystallised within CDK2 ATP-pocket (PDB code: 1H1S) [154]

It was not possible to perform a covalent docking protocol to show the covalent bond between the Lys89 residue and the vinyl sulfone moiety of the side-chain, since it would have created bias. The existence of the covalent bond was confirmed by X-ray crystallography and supported by kinetic and molecular biology studies for compound NU6300 (**40**). NU6300 (**40**) was incubated with CDK2-Cyclin A complex. Then, a MS (MALDI-TOF) experiment was run and showed NU6300 (**40**) labelling the enzyme. Digestion experiments with proteases were also performed and showed that a lysine residue was labelled stoichiometrically with the inhibitor, even when the protein was treated with a large excess of NU6300 (**40**). A mutant CDK2 was also used, where Lys88 and Lys89 were mutated and no labelling of the enzyme by the inhibitor took place. Which lysine, between the 88 and the 89, was labelled during the previous experiments was confirmed by the X-ray crystal structure, which proved a specific reaction with Lys89.

The structures of the CDK2 inhibitors, engaged in the docking experiments, were designed using the interface "Builder" of MOE.

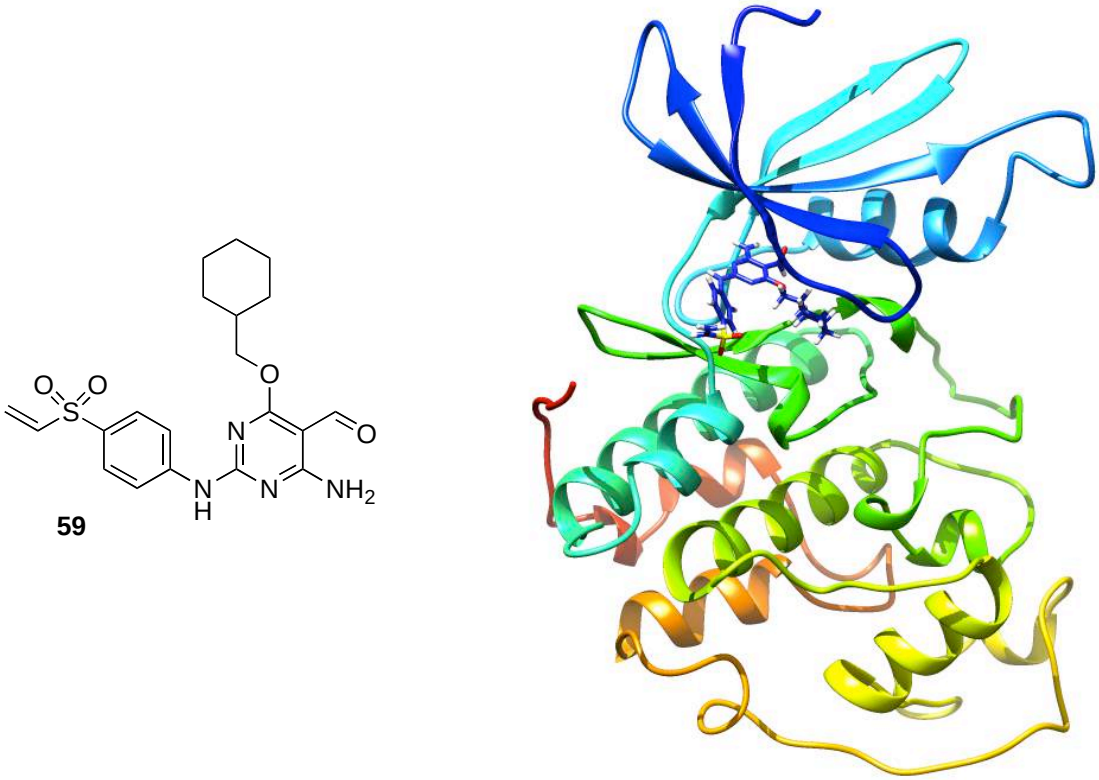

Fig. 97 Compound **59** docked within CDK2 (image implemented by CHIMERA Software)

Docking experiments engaging compound **59** (Fig. 98) revealed, as previously supposed, interactions of the inhibitor to the hinge region of the kinase via a triplet of hydrogen bonds:

- -N- group at the pyrimidine 1-position interacts with a residue of Leu83, as H-bond acceptor.
- -NH group at the pyrimidine 2-position interacts with a residue of Leu83, as H-bond donor.
- -NH_2 group at the pyrimidine 6-position interacts with a residue of Glu81, as H-bond donor.

The pyrimidine ring makes a hydrophobic interaction with a residue of Val18 and the 6-amino group with a residue of Phe80. The sulfone group in the side-chain makes an interaction, as H-bond acceptor, with a residue of Asp86. Finally, a cyclic hydrophobic substituent, in our case a cyclohexylmethoxy moiety, at the pyrimidine 4-position seems to be optimal for the occupancy of the hydrophobic channel within the CDK2 ribose-binding pocket.

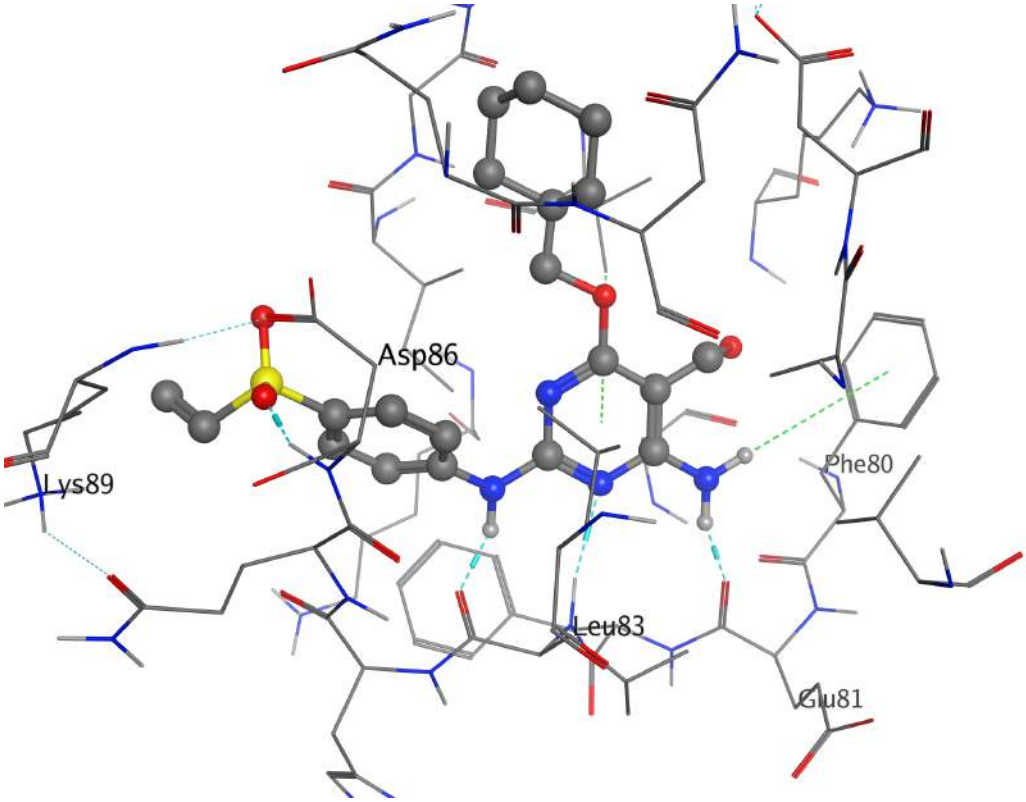

Fig. 98 In silico interactions between of the CDK2-compound **59** complex

It is then possible to see (Fig. 98) the proximity of the vinyl sulfone moiety to Lys89, which, due to a covalent bond interaction, is supposed to give, as for NU6300 (**40**), the irreversible behaviour to compound **59**.

A further detail which could also be helpful in understanding the conformation adopted by these irreversible inhibitors within the CDK2-catalytic domain is the conformational behaviour of substituted vinyl sulfone molecules (CH_3=$CHSO_2X$), exhaustively discussed in recent years. In particular, the experimental information was gained through electron diffraction and vibrational spectroscopy studies, which emphasised the existence of more than one conformer for this species (Fig. 99). [178, 179]

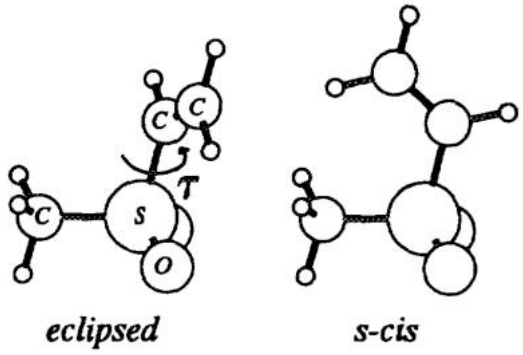

Fig. 99 Schematic representation of methyl vinyl sulfone

Theoretical calculations and vibrational spectra showed that the predominant conformation of methyl vinyl sulfone has the C=C bond eclipsed with one of the S=O bonds. The eclipsed conformation is also more stable, compared to the s-cis conformation and shows a dihedral angle τ between the C=C-S and C-S-C planes greater than 109° (Fig. 99). The high relative stability of the eclipsed conformation in vinyl sulfone molecules is a characteristic of the electronic distribution on the C=C-S=O chain. [178, 179]

As shown in Fig. 101, three CDK2 irreversible pyrimidine-based inhibitors (**59**, **93** and **102**, Fig. 100) were then superpositioned.

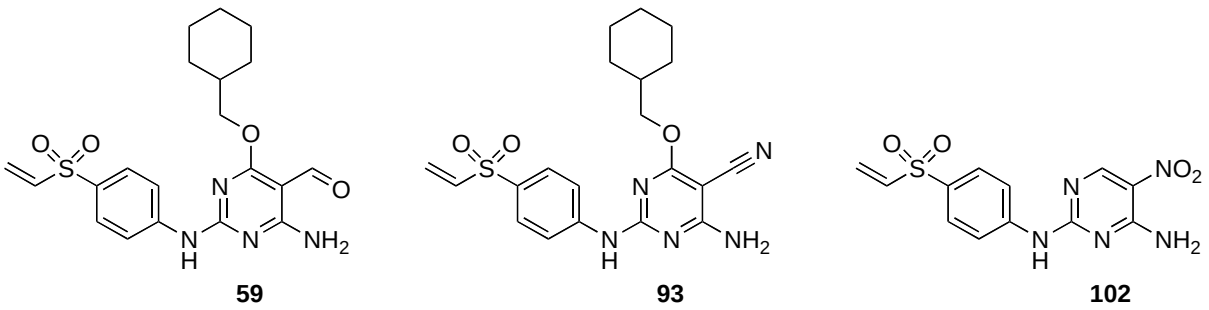

Fig. 100 CDK2 inhibitors: **59** (light blue), **93** (pink) and **102** (green)

The hydrophobic interactions with a residue of Val18 and a residue of Phe80 are maintained, as well as the H-bond interactions with Glu81, Leu83 and Asp86.

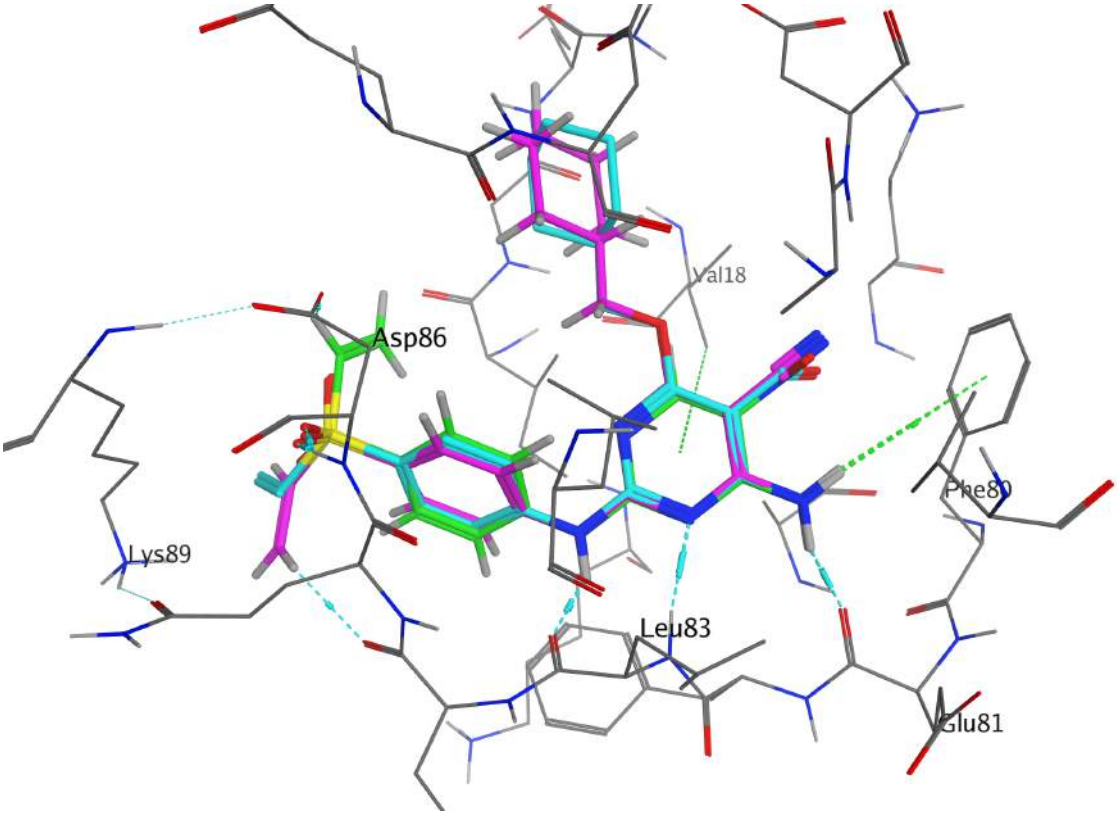

Fig. 101 Superposition of compounds **59**, **93** and **102** within the CDK2 ATP-binding domain

All these results will be then confirmed by co-crystallography studies, which are in progress in the POG at Newcastle University, Newcastle Upon Tyne, UK.

4. CONCLUSIONS

4.1. CK2 inhibitors

Novel bi-substrate CK2 inhibitors were obtained. Biological assays showed interesting results for the benzimidazole derivatives linked to the acidic peptide chains (compounds **71**, **72** and **75**), with IC_{50} values in the low nanomolar range. As expected, no significant results were obtained for the peptidic side-chains linked to the spacer (compounds **73**, **74** and **76**) without the benzimidazole scaffold, emphasising the importance of the polyhalogenated moiety in order to locate the molecule within the enzyme catalytic pocket.

In particular, compound K137-E4 (**72**) demonstrated the highest activity and was several fold more potent and selective than the parent inhibitor K137 (**12**). From the kinetic studies, compound **72** showed competitive activity toward both the ATP and the peptide substrate. In fact, the peptidic chains ending with carboxyl groups were supposed to interact with basic residues nearby the substrate-binding domain, while the benzimidazole moiety interacts with the ATP-binding domain.

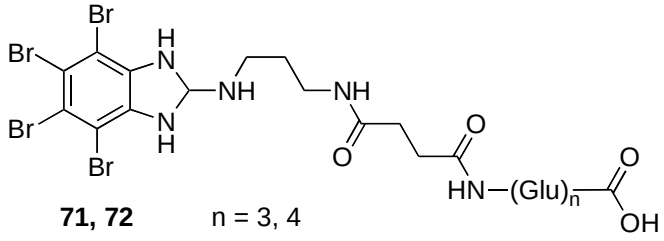

71, 72 n = 3, 4

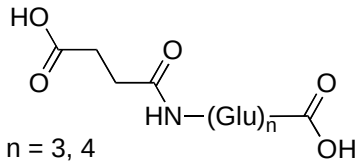

n = 3, 4

73, 74

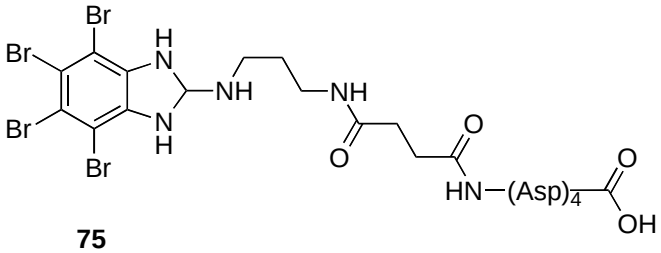

75

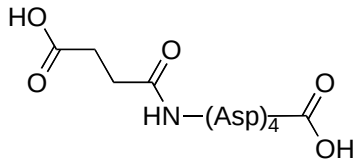

76

Compound **72** was then subjected to more comprehensive biological studies, in order to evaluate its inhibitory activity on endogenous CK2.

From studies on cell lysates it emerged that K137- E4 (**72**) was active on endogenous CK2, whereas, from subsequent studies on cell viability, it emerged that was not able to cross the cell membrane compared to CX-4945 (**1**) and K137 (**12**). This was probably due to ionisation, at physiological pH, of the peptidic chains to carboxylates, which prevent crossing the cell membrane. Compound K137-E4Me (**77**) was then synthesised and from the biological assays it emerged that was able to cross the cell membrane compared to K137- E4 (**72**), but the inhibitory activity was low compared to CX-4945 (**1**) and K137 (**12**). This was also confirmed by an assay on recombinant CK2, which showed an IC_{50} value of 10.32 µM for compound K137- E4Me (**77**).

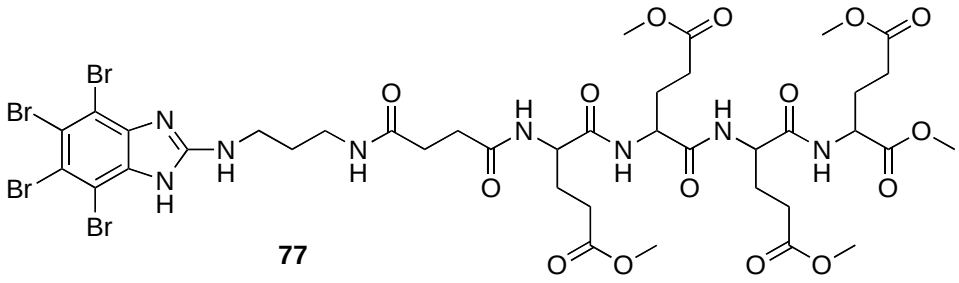

77

To conclude, the data presented provide an example of the potential and mode of action of bi-substrate kinase inhibitors, by showing that a moderately potent, purely ATP competitive CK2 inhibitor (**12**) can be converted into a much more effective and very selective CK2 antagonist. As the bifunctional inhibitors showed not to be active on cells, further work will consist in functionalising the benzimidazole scaffold with internalising peptides.

4.2. CDK2 inhibitors

Synthetic routes to obtain pyrimidine-based irreversible CDK2 inhibitors were proposed.

The first target investigated was compound **59**. Several attempts were made to synthesise it optimising the reaction conditions. Early biological data of compound **59** showed that the kinase loses activity proportionally to the inhibitor exposure time, suggesting that it acts as irreversible inhibitors.

Compound **93** was obtained and will be evaluated for CDK2-inhibitory activity. Compound **94** was also synthesised in order to see whether the intramolecular hydrogen bond between the 6-amino group and the oxime moiety was retained but, as explained in Par. 3.2., it decomposed during the purification procedures and will not be tested for CDK2-inhibitory activity.

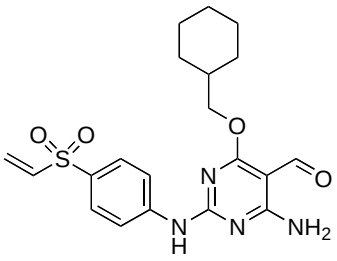

59

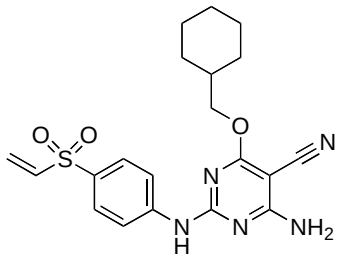

93

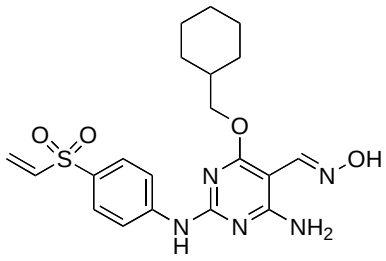

94

Future work on this scaffold, with the side-chain at the pyrimidine 2-position and the cyclohexylmethoxy moiety at the pyrimidine 4-position, will concern modifications at the pyrimidine 4-position with different alkyl groups.

Concerning the series of novel compounds having no substituents at the pyrimidine 4-position, compound **102** was obtained and the synthesis proved to be straightforward, while the synthesis of compound **103** still needs optimisation, in particular concerning the first step, which gave a reaction intermediate and a by-product. When tested on CDK2, compound **102** showed an irreversible behaviour with the kinase losing its activity proportionally to the inhibitor exposure time.

Moreover, compound **107** was also tested in order to compare its activity with the vinyl sulfone inhibitors and, as expected for a reversible inhibitor, the activity of CDK2/Cyclin A did not decrease in a time-dependent manner.

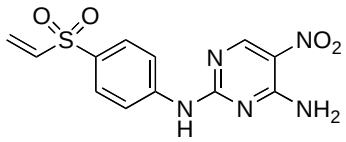

102

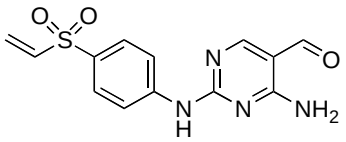

103

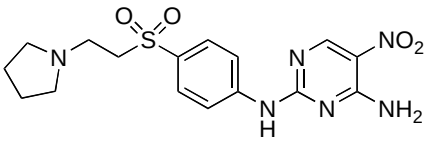

107

The biological results were supported by docking studies, as described in Par. 3.2.2. Concluding, co-crystallisation studies of compounds **59**, **93**, **102** and **107** within CDK2/Cyclin A complex are in progress in the POG at Newcastle University.

5. EXPERIMENTAL DATA

5.1. Materials and methods (CK2)

5.1.1. Reagents and solvents

All reagents used were purchased from Sigma-Aldrich, Fluka, Novabiochem and Iris Biotech GMBH. Solvents were purchased from Sigma-Aldrich, Carlo Erba, AnalaR Normapur and VWR Prolabo. Deuterated solvents for NMR analysis were purchased from Sigma-Aldrich. All reagents and solvents were used as received from commercial sources, with no further purification, unless otherwise stated.

5.1.2. Analytical techniques

^{1}H- and ^{13}C-NMR spectra were obtained from samples dissolved in deuterated dimethylsulfoxide (DMSO-d_6), using a Bruker Avance III Spectrometer (400 MHz for ^{1}H, 100 MHz for ^{13}C). Chemical shift values (δ) are reported in parts per million (ppm) and are referenced against TMS (tetramethylsilane), with splitting patterns abbreviated to: s (singlet), d (doublet), dd (doublet doublet), t (triplet) and m (multiplet). The coupling constant (J) is given in Hz and was calculated using the software package Topspin™ developed by Bruker Biospin. When ^{13}C values have not been quoted it is due to inability to visualise quaternary carbons.

Mass spectra were obtained using a Mariner Applied Biosystems spectrometer.

Ultraviolet (UV) analysis was performed using Heλios α UV-vis spectrophotometer (UNICAM, Thermo Electron Corporation) with an analysis range of 800-200 nm.

Melting points were determined using a Buchi Melting Point m-560 apparatus and were observed manually.

5.1.3. Chromatography

Medium pressure automated flash chromatography (MPLC) was performed using a Biotage flash chromatography system (Isolera One) with a solvent gradient calculated from TLC R_f values.

Thin layer chromatography (TLC) was performed using Merck TLC silica gel 60 F_{254}, with visualisation by UV light at 245 nm.

Analytical HPLC analysis was performed using a Shimadzu HPLC system with LC-10AD pumps, an SCL-10A controller, an SPD-10A detector and a Gastorr 154 degasser (Tokyo, Japan); all the data were processed by Starlet ChromStar software (Bruker, Bremen, Germany). Jupiter columns (C-18, 10 µ, 250 x 4.6 mm) were used.

Preparative HPLC analysis was performed using a Shimadzu HPLC system with LC-8A pumps, an SCL-10A controller, an SPD-6 detector and a ERC-3562 degasser. Vydac preparative columns (C-18, 10 µ 250 x 22 mm) were used.

5.1.4. Phosphorylation assays

Recombinant CK2 and all other protein kinases engaged in the biological assays were purified as described in reference [180]. The source of CK2 and of all other kinases is described in reference [181]. Recombinant CK2 (1 nM) was incubated for 10 min at 37 °C in a final volume of 25 µl containing 50 mM Tris/HCl (pH 7.5), 100 mM NaCl, 12 mM $MgCl_2$, 100 µM synthetic peptide substrate RRRADDSDDDDD and 20 µM [γ -^{33}P-ATP] (500–1000 cpm/pmol), unless indicated otherwise. The reaction was stopped by the addition of 5 µl of 0.5 M orthophosphoric acid before spotting aliquots onto phosphocellulose filters. Assays were stopped by spotting 25 µl onto phosphocellulose filters. Filters were washed four times in 75 mM phosphoric acid (5–10 ml each) and once in methanol and dried before counting. Conditions for the activity assays of all other protein kinases tested in experiments are as described or referenced in [180].

5.1.5. Kinetic determinations

Initial velocities were determined at each of the substrate concentration tested. Km values were calculated either in the absence or in the presence of increasing concentrations of inhibitor, from Lineweaver–Burk double-reciprocal plots of the data. The inhibition constant for K137 was then calculated by linear regression analysis of Km/Vmax against inhibitor concentration plots. Inhibition constants for K137-E4 were calculated using the equation 3.2 for mixed-model inhibition present in [182].

5.1.6. Selectivity profiles

Promiscuity Score (expressing the average inhibition of all of the kinases of the whole panel, by a given concentration of the inhibitor) and Hit Rates (expressing the percent of kinases inhibited >50% by a given compound) were calculated from the selectivity data as described in [77, 183].

5.1.7. Cell culture and treatments

Cells were cultured in an atmosphere containing 5% CO_2; HepG2 cells (liver hepatocellular carcinoma) were maintained adherent to DMEM medium (Sigma), Jurkat cells (immortalised line of human T lymphocyte cells) were maintained in suspension in RPMI 1640 medium (Sigma). Both media were then supplemented with 10% (v/v) fetal calf serum (FCS), 2 mM L-glutamine, 100 U/ml penicillin, and 100 µg/ml streptomycin. Cell treatments were performed in the culture medium at $1x10^6$ cells/ml for cells that grow in suspension, and about 70% of confluence for adherent cells, but with 1% FCS. Cell treatments with inhibitors were performed in the culture medium, but with 1 % (v/v) FCS. Control cells were treated with equal amounts of the inhibitor solvent (DMSO). The total amount of DMSO never exceeded 1 % (v/v) during cell treatment.

5.1.8. Cell lysis and western blot analysis

Cells were harvested by centrifugation, washed, and lysed as described in [184]. Protein concentration was determined by the Bradford method. Equal amounts of proteins were loaded on 11% SDS-PAGE, blotted on Immobilon-P membranes (Millipore), and processed in western blot (WB) with the indicated antibody, detected by chemiluminescence on a Kodak Image Station 440MM PRO.

5.1.9. Cell viability

For cell viability experiments, cell treatments were performed in 96-well plates at a density of 10^5 cells/100 µl for cells in suspension; $2x10^4$ adherent cells were seeded in 96-well plates in 100 µl medium, and left to adhere for one night before treatment. 1 h before the end of the incubation, 10 µl of MTT solution (5 mg/ml in PBS (Sigma)) was added to each well. Incubations were stopped by addition of 20 µl of lysis solution at pH 4.7, containing 20% (w/v) SDS, 50% (v/v) N,N-dimethylformamide, 2% (v/v) acetic acid and 25 mM HCl. Plates were read for OD at λ590 nm, in a Titertek Multiskan Plus plate reader (Flow Laboratories).

5.2. Index of synthesised compounds (CK2)

2-Bromo-1*H*-benzo[*d*]imidazole (**60**)

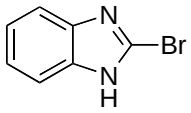

Compound	Mol. Weight	m/V	d (g/mL)	mmol	Equiv.
2-mercapto-benzimidazole (**58**)	150.20	200 mg	/	1.3	1
HBr	80.91	0.1 mL	1.490	1.8	1.35
AcOH	60.05	3 mL	0.791	/	/
Br_2	159.81	0.25 mL	3.119	4.8	3.6

2-Mercaptobenzimidazole (**58**, 200 mg) was dissolved in a pre-cooled (0-5 °C) mixture of HBr (0.1 mL) and AcOH (3 mL), with stirring. The reaction mixture was warmed up to 40-45 °C and Br_2 (0.25 mL, CARE!) was added portionwise. AcOH (1 mL) was added in order to dissolve the orange precipitate. The reaction mixture was stirred at room temperature overnight. The progress of the reaction was monitored by TLC and mass spectrometry. Crushed ice was added and the reaction mixture was left stirring overnight. The aqueous solution was extracted with EtOAc (3x30 mL). The combined extracts were dried ($MgSO_4$) and the solvent was removed in vacuo. The title compound (**60**) was obtained as a yellow solid with no further purification required (Yield: 44%).

Rf: 0.62 (DCM/MeOH, 90:10).

M.p.: 192 °C.

UV λ_{max} (EtOH): 249 nm.

^{1}H-NMR (400Mhz, DMSO-d_6) δ: 7.18 (m, Ar H, 2H), 7.50 (m, Ar H, 2H).

^{13}C-NMR (400MHz, DMSO-d_6) δ: 109.9, 122.7, 132.7, 168.6.

HRMS: Calcd for m/z = 196.9723 [M+H]+, Found m/z = 196.9723 [M+H]+.

2,4,5,6,7-Pentabromo-1*H*-benzo[*d*]imidazole (**61**)

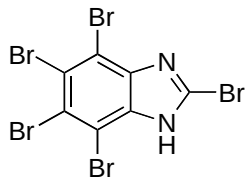

Compound	Mol. Weight	m/V	d (g/mL)	mmol	Equiv.
60	197.03	200 mg	/	1.01	1.00
H_2O	18.01	2.5 mL	/	/	/
Br_2	159.81	1.1 mL	3.119	21.4	21.05

To a stirred and refluxed suspension of compound **60** (200 mg) in water (2.5 mL), Br_2 (1.1 mL, CARE!) was added portionwise. After 6 h the temperature was decreased to 50 °C and the reaction mixture was stirred overnight. The progress of the reaction was monitored by TLC and HRMS. Br_2 (4 equiv.) was added and the mixture was stirred for 7 days, monitoring by TLC and HRMS. Crushed ice was added and the mixture was stirred overnight. The precipitate was filtered off and the aqueous solution was extracted with EtOAc (3x30 mL). The combined extracts were dried ($MgSO_4$) and the solvent was removed in vacuo. The precipitate and the extracted product were combined and purified by flash chromatography on silica (Hexane/EtOAc, 90:10). The title compound (**61**) was obtained as a yellow solid (Yield: 45%).

Rf: 0.66 (DCM/MeOH, 90:10).

M.p.: 268 °C.

UV λ_{max} (EtOH): 236, 267, 303 nm.

^{13}C-NMR (400MHz, DMSO-d_6) δ: 106.0, 122.2, 143.8, 165.7.

HRMS: Calcd for m/z = 508.6144 [M+H]+, Found m/z = 508.5525 [M+H]+.

N^1-(4,5,6,7-Tetrabromo-1*H*-benzo[*d*]imidazol-2-yl)propane-1,3-diamine (**12**)

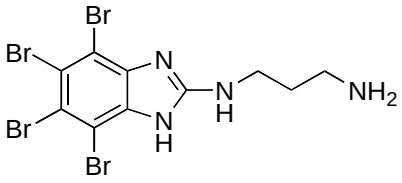

Compound	Mol. Weight	m/V	d (g/mL)	mmol	Equiv.
61	512.62	170 mg	/	0.3	1
1,3-diaminopropane	74.12	0.6 mL	0.888	6.9	21
propan-2-ol	60.10	15 mL	0.786	/	/

Compound (170 mg) was dissolved in propan-2-ol (15 mL) and 1,3-diaminopropane (0.6 mL) was added. The reaction mixture was stirred at reflux overnight. The progress of the reaction was monitored by TLC and 1,3-diaminopropane (1 equiv.) was added to the reaction mixture, which was stirred overnight. The solvent was removed in vacuo giving a yellow oil. The crude product was purified by chromatography on silica (DCM/MeOH/TEA, 89:10:1) giving the title compound (**12**) as a white solid (Yield: 30%).

Rf: 0.59 (DCM/MeOH, 90:10).

M.p.: 314°C.

UV λ_{max} (EtOH): 234, 310 nm.

^{1}H-NMR (400mhz, DMSO-d_6) δ: 1.74 (m, CH_2, 2H), 2.68 (t, CH_2, 2H), 3.18 (t, CH_2, 2H), 4.05 (s, NH, 1H), 6.76 (s, NH_2, 2H).

^{13}C-NMR (300MHz, DMSO-d_6) δ: 23.9, 29.9, 36.3, 105.9, 111.7, 144.4, 166.4.

HRMS: Calcd for m/z = 502.6144 [M+H]+, Found m/z = 502.7867 [M+H]+.

4-oxo-4-(3-(4,5,6,7-Tetrabromo-1*H*-benzo[*d*]imidazol-2-ylamino)propylamino)butanoic acid (**62**)

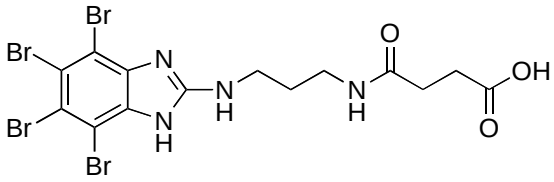

Compound	Mol. Weight	m/V	d (g/mL)	mmol	Equiv.
12	505.83	50 mg	/	0.1	1
Succinic Anhydride	100.07	10 mg	/	0.1	1
DIEA	129.25	0.017 mL	0.742	0.1	1
DMF	73.09	3 mL	0.944	/	/

Compound **12** (50 mg) was solubilised in DMF (3 mL). Succinic anhydride (10 mg) and DIEA (0.017 mL) were added to the reaction mixture, which was stirred at room temperature for 4 h. Water was added and a white precipitate was obtained. The reaction mixture was allowed to stand at 4 °C overnight. The precipitate was filtered off and dried overnight. The title compound was obtained as a white solid with no further purification required (Yield: 63%).

Rf: 0.53 (DCM/MeOH, 90:10).

M.p.: 213 °C.

UV λ_{max} (EtOH): 214 nm.

^{1}H-NMR (400 MHz, DMSO-d_6) δ: 1.67 (m, CH_2, 2H), 2.35 (t, CH_2, 2H), 2.45 (t, CH_2, 2H), 3.12 (t, CH_2, 2H), 3.36 (t, CH_2, 2H), 6.79 (s, NH, 1H), 7.95 (s, NH, 1H), 11.72 (s, OH, 1H).

^{13}C NMR [100 MHz, DMSO-d_6] δ: 27.1, 28.7, 30.9, 36.2, 36.9, 114.5, 126.3, 142.3, 145.4, 172.9, 177.3.

HMRS: Calcd for m/z = 602.7887 [M+H]+, Found m/z = 602.7999 [M+H]+.

2-(4-Carboxy-2-(4-carboxy-2-(4-oxo-4-(3-(4,5,6,7-tetrabromo-1*H*-benzo[*d*]imidazol-2-ylamino) propylamino)butanamido)butanamido)butanamido)pentanedioic acid (**71**)

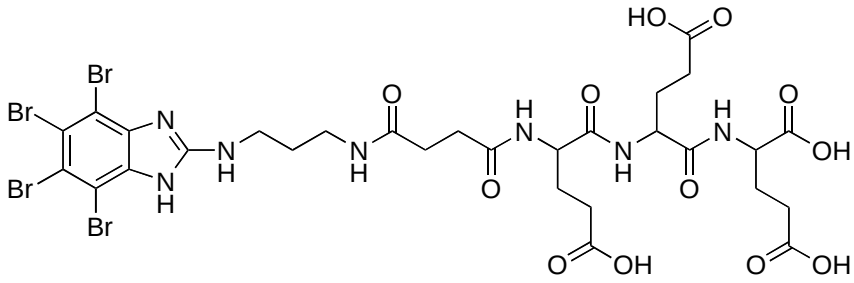

Compound	Mol. Weight	m/V	d (g/mL)	mmol	Equiv.
Fmoc-L-Glu(OtBu)-Wang Resin	/	50 mg	/	0.03	1.03
Fmoc-L-Glu(OtBu)-OH	425.50	38 mg	/	0.09	3
62	605.90	18 mg	/	0.03	1
HOBt	135.12	12 mg	/	0.09	3
HBTU	379.24	34 mg	/	0.09	3
PyBOP	520.39	16 mg	/	0.03	1
DIEA	129.25	0.041 mL	0.742	0.24	8
TFA (95%), TIS (3%), H_2O (2%)	/	1 mL	/	/	/
DMF	73.09	/	0.944	/	/

The peptidic chain for compound **71** was obtained using SPPS (Solid Phase Peptide Synthesis), which was performed manually using a Supelco reactor.

The procedure involved:

1. Swelling of the resin (Fmoc-L-Glu(OtBu)-Wang Resin) in DMF for 45 min.
2. Cleavage of the Fmoc group with a solution of piperidine (20%) in DMF (in 10 min).
3. Washing the resin with DMF.
4. Activation of the amino acid with HOBt/HBTU/DIEA in DMF.

5. Coupling reaction (45 min) repeated twice per amino acid.
6. Washing of the resin with DMF.

Steps 2 to 6 were repeated three times per amino acid, in order to obtain the tri-glutamic peptidic chain. Intermediate **62** (18 mg) was solubilised in DMF (3 mL) and HOBt (4 mg), PyBOP (16 mg) and DIEA (0.008 mL) were added. The solution was stirred at room temperature for 5 min and was then added to the resin for the coupling reaction. The resin was stirred at room temperature (1 h) and after 30 min PyBOP (16 mg) and DIEA (0.016 mL) were added again. The coupling reaction with intermediate **62** was repeated three times. The resin was finally washed thoroughly with DMF and DCM and dried in vacuo. To verify the formation of compound **71**, a small portion of the resin was treated with TFA (142.5 µL), TIS (4.5 µL) and H_2O (3 µL). The mixture was stirred for 45 min at room temperature and water was added to precipitate the products. The mixture was allowed to stand at 4 °C overnight. The resin was removed by filtration and the solvent was removed by spin-drying. The final products were characterised by HRMS. This procedure was repeated on the remaining resin, in order to deprotect the functional groups and to remove the products from the resin. A solution (1 mL) of TFA 95 %, TIS 3%, H_2O 2% was used. The final products were solubilised in aqueous NH_4OAc and freeze-dried. The crude product was purified by preparative HPLC: C-18 Jupiter column (10 µ, 250 x 22 mm). Solvents: phase A (TFA 0.05% in H_2O); phase B (TFA O.05% in CH_3CN/H_2O 90:10). Flow: 1 mL/min. λ= 216 nm and 280 nm. Gradient: 5 min (5% phase B), 20 min (30%-50% phase B), 1 min (90% phase B), 1 min (90%-30% phase B). Retention time: 14.38 min. The title compound (**71**) was obtained as a white solid (Yield: 8%).

^{1}H NMR [400 MHz, DMSO-d_6] δ: 1.83 - 2.31 (m, 9 x CH_2, 18H), 2.74 - 3.12 (m, 2 x CH_2, 4H), 3.82 - 4.03 (m, 3 x CH, 3H), 4.96 (s, NH, 1H), 5.75 (s, NH, 1H), 8.11 (s br, 3 x NH, 3H), 8.40 (s, NH, 1H), 10.54 (s, COOH, 1H), 10.89 (s, COOH, 1H), 11.01 (s, COOH, 1H), 11.20 (s, COOH, 1H).
^{13}C NMR [100 MHz, DMSO-d_6] δ: 20.1, 26.5, 26.6, 26.8, 27.2, 29.0, 30.2, 30.6, 30.9, 35.5, 35.9, 53.6, 53.9, 54.2, 113.3, 125.3, 146.7, 150.4, 173.6, 173.7, 173.8, 174.2, 174.7, 174.9, 175.2, 176.8.
HMRS: Calcd for m/z = 993.2439 [M+H]+, Found m/z = 993.9470 [M+H]+.

2-(2,5,8-Tris(2-carboxyethyl)-4,7,10,13-tetraoxo-17-(4,5,6,7-tetrabromo-1*H*-benzo[*d*]imidazol-2-ylamino)-3,6,9,14-tetraazaheptadecanamido)pentanedioic acid (**72**)

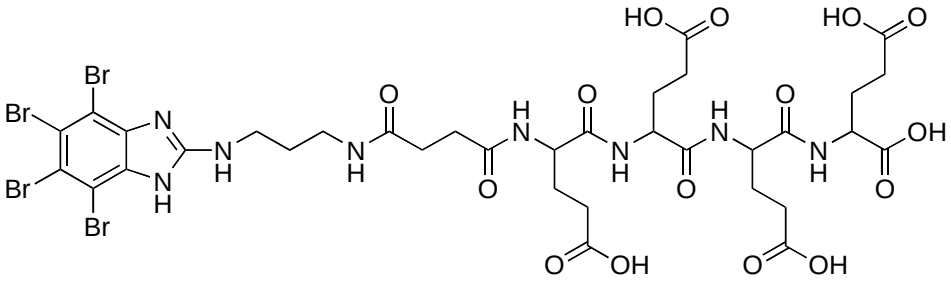

Compound	Mol. Weight	m/V	d (g/mL)	mmol	Equiv.
Fmoc-L-Glu(OtBu)-Wang Resin	/	50 mg	/	0.03	1.03
Fmoc-L-Glu(OtBu)-OH	425.50	38 mg	/	0.09	3
62	605.90	18 mg	/	0.03	1
HOBt	135.12	12 mg	/	0.09	3
HBTU	379.24	34 mg	/	0.09	3
PyBOP	520.39	16 mg	/	0.03	1
DIEA	129.25	0.041 mL	0.742	0.24	8
TFA (95%), TIS (3%), H_2O (2%)	/	1 mL	/	/	/
DMF	73.09	/	0.944	/	/

The peptidic chain for compound **72** was obtained using SPPS (Solid Phase Peptide Synthesis), which was performed manually using a Supelco reactor.

The procedure involved:

1. Swelling of the resin (Fmoc-L-Glu(OtBu)-Wang Resin) in DMF for 45 min.
2. Cleavage of the Fmoc group with a solution of piperidine (20%) in DMF (in 10 min).
3. Washing the resin with DMF.
4. Activation of the amino acid with HOBt/HBTU/DIEA in DMF.

5. Coupling reaction (45 min) repeated twice per amino acid.
6. Washing of the resin with DMF.

Steps 2 to 6 were repeated three times per amino acid, in order to obtain the tetra-glutamic peptidic chain. Intermediate **62** (18 mg) was solubilised in DMF (3 mL) and HOBt (4 mg), PyBOP (16 mg) and DIEA (0.008 mL) were added. The solution was stirred at room temperature for 5 min and was added to the resin for the coupling reaction. The resin was stirred at room temperature (1 h) and after 30 min PyBOP (16 mg) and DIEA (0.016 mL) were added again. The coupling reaction with intermediate **62** was repeated three times. The resin was finally washed thoroughly with DMF and DCM and dried in vacuo. To verify the formation of compound **72**, a small portion of the resin was treated with TFA (142.5 µL), TIS (4.5 µL) and H_2O (3 µL). The mixture was stirred for 45 min at room temperature and water was added to precipitate the products. The mixture was allowed to stand at 4 °C overnight. The resin was removed by filtration and the solvent was removed by spin-drying. The final products were characterised by HRMS. This procedure was repeated on the remaining resin, in order to deprotect the functional groups and to remove the products from the resin. A solution (1 mL) of TFA 95 %, TIS 3%, H_2O 2% was used. The final products were solubilised in aqueous NH_4OAc and freeze-dried. The crude product was purified by preparative HPLC: C-18 Jupiter column (10 µ, 250 x 22 mm). Solvents: phase A (TFA 0.05% in H_2O); phase B (TFA O.05% in CH_3CN/H_2O 90:10). Flow: 1 mL/min. λ= 216 nm and 280 nm. Gradient: 5 min (5% phase B), 30 min (30%-60% phase B), 1 min (90% phase B), 1 min (90%-30% phase B). Retention time: 14.33 min. The title compound (**72**) was obtained as a white solid (Yield: 44%).

^{1}H NMR [400 MHz, DMSO-d_6] δ: 1.82 - 2.31 (m, 11 x CH_2, 22H), 2.74 - 3.18 (m, 2 x CH_2, 4H), 3.83 - 4.01 (m, 4 x CH, 4H), 5.01 (s, NH, 1H), 5.69 (s, NH, 1H), 8.12 (s br, 4 x NH, 4H), 8.43 (s, NH, 1H), 10.45 (s, COOH, 1H), 10.77 (s, COOH, 1H), 11.00 (s, COOH, 1H), 11.12 (s, COOH, 1H), 11.18 (s, COOH, 1H).

^{13}C NMR [100 MHz, DMSO-d_6] δ: 20.7, 26.2, 26.5, 26.9, 27.2, 27.5, 29.6, 30.0, 30.6, 30.8, 31.3, 35.4, 35.6, 51.4, 53.7, 54.7, 55.5, 114.8, 124.2, 146.1, 151.9, 173.2, 173.3, 173.6, 174.0, 174.4, 174.6, 174.8, 175.0, 176.8, 178.1.

HMRS: Calcd for m/z = 1123.3579 [M+H]+, Found m/z = 1123.0224 [M+H]+.

2-(4-Carboxy-2-(4-carboxy-2-(3-carboxypropanamido)butanamido)butanamido)pentanedioic acid (**73**)

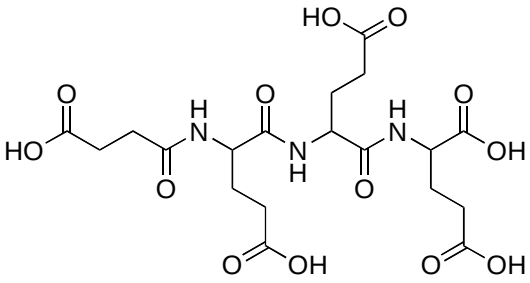

Compound	Mol. Weight	m/V	d (g/mL)	mmol	Equiv.
Fmoc-L-Glu(OtBu) Wang Resin	/	50 mg	/	0.03	1.03
Fmoc-L-Glu(OtBu)-OH	425.50	38 mg	/	0.09	3
Succinic anhydride	100.07	9 mg	/	0.03	1
HOBt	135.12	12 mg	/	0.09	3
HBTU	379.24	34 mg	/	0.09	3
DIEA	129.25	0.041 mL	0.742	0.24	8
TFA (95%), TIS (3%), H_2O (2%)	/	1 mL	/	/	/
DMF	73.09	/	0.944	/	/

Compound **73** was obtained using SPPS. The procedure was the same as for the peptidic chain of compound **71**. Once the peptides were ready, succinic anhydride was coupled to them. The coupling reaction was repeated three times, in order to have a better yield. The crude product was purified by preparative HPLC: C-18 Jupiter column (10 µ, 250 x 22 mm). Solvents: phase A (TFA 0.05% in H_2O); phase B (TFA O.05% in CH_3CN/H_2O 90:10). Flow: 1 mL/min. λ= 216 nm. Gradient: 3 min (5% phase B), 85 min (30%-90% phase B), 1 min (90% phase B), 1 min (90%-5% phase B). Retention time: 8.27 min. The title compound (**73**) was obtained as a white solid (Yield: 18%).

^{1}H NMR [400 MHz, DMSO-d_6] δ: 1.83 - 2.36 (m, 8 x CH_2, 16H), 3.84 - 4.10 (m, 3 x CH, 3H), 8.15 (s br, 3 x NH, 3H), 10.55 (s, COOH, 1H), 10.85 (s, COOH, 1H), 11.09 (s, COOH, 1H), 11.21 (s, COOH, 1H), 11.40 (s, COOH, 1H).

^{13}C NMR [100 MHz, DMSO-d_6] δ: 26.4, 26.6, 28.1, 30.2, 30.5, 30.8, 35.3, 35.8, 53.0, 53.9, 54.7, 173.6, 173.7, 174.0, 174.3, 174.6, 174.8, 175.1, 177.2.

HMRS: Calcd for m/z = 506.4300 [M+H]+, Found m/z = 506.1622 [M+H]+.

6,9,12-Tris(2-carboxyethyl)-5,8,11,14-tetraoxo-4,7,10,13-tetraazahexadecane-1,3,16-tricarboxylic acid (**74**)

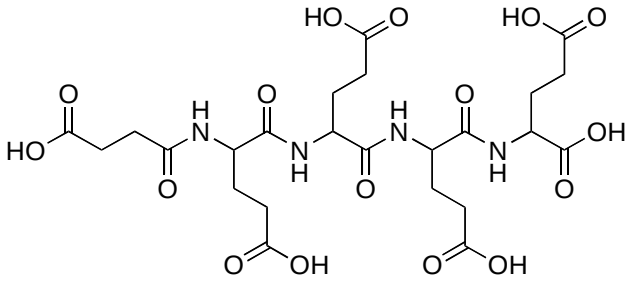

Compound	Mol. Weight	m/V	d (g/mL)	mmol	Equiv.
Fmoc-L-Glu(OtBu) Wang Resin	/	50 mg	/	0.03	1.03
Fmoc-L-Glu(OtBu)-OH	425.50	38 mg	/	0.09	3
Succinic anhydride	100.07	9 mg	/	0.03	1
HOBt	135.12	12 mg	/	0.09	3
HBTU	379.24	34 mg	/	0.09	3
DIEA	129.25	0.041 mL	0.742	0.24	8
TFA (95%), TIS (3%), H_2O (2%)	/	1 mL	/	/	/
DMF	73.09	/	0.944	/	/

Compound **74** was obtained using SPPS. The procedure was the same as for the peptidic chain of compounds **72**. Once the peptides were ready, succinic anhydride was coupled to them. The coupling reaction was repeated three times, in order to have a better yield. The crude product was purified by preparative HPLC: C-18 Jupiter column (10 µ, 250 x 22 mm). Solvents: phase A (TFA 0.05% in H_2O); phase B (TFA O.05% in CH_3CN/H_2O 90:10). Flow: 1 mL/min. λ= 216 nm. Gradient: 3 min (5% phase B), 85 min (30%-90% phase B), 1 min (90% phase B), 1 min (90%-5% phase B). Retention time: 11.82 min. The title compound (**74**) was obtained as a white solid (Yield: 53%).

^{1}H NMR [400 MHz, DMSO-d_6] δ: 1.81 - 2.34 (m, 10 x CH_2, 20H), 3.83 - 4.05 (m, 4 x CH, 4H), 8.12 (s br, 4 x NH, 4H), 10.10 (s, COOH, 1H), 10.78 (s, COOH, 1H), 11.01 (s, COOH, 1H), 11.15 (s, COOH, 1H), 11.20, (s, COOH, 1H), 11.35 (s, COOH, 1H).

^{13}C NMR [100 MHz, DMSO-d_6] δ: 25.9, 26.5, 26.8, 27.3, 30.3, 30.4, 31.0, 31.3, 35.3, 35.7, 53.1, 53.8, 54.8, 55.0, 173.1, 173.3, 173.6, 174.0, 174.1, 174.5, 174.8, 176.1, 178.0, 178.9.

HMRS: Calcd for m/z = 635.5439 [M+H]+, Found m/z = 635.2303 [M+H]+.

2-(2,5,8-Tris(carboxymethyl)-4,7,10,13-tetraoxo-17-(4,5,6,7-tetrabromo-1*H*-benzo[*d*]imidazol-2-ylamino)-3,6,9,14-tetraazaheptadecanamido)succinic acid (**75**)

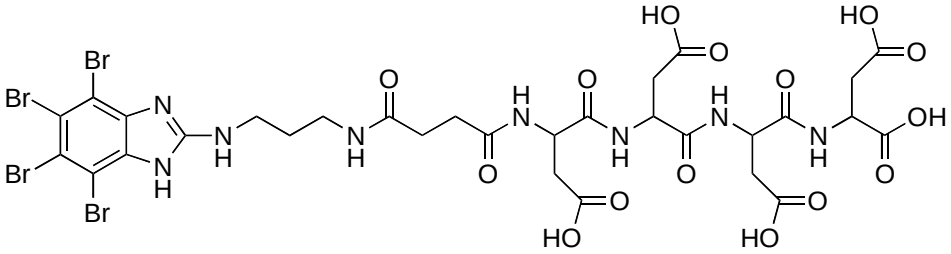

Compound	Mol. Weight	m/V	d (g/mL)	mmol	Equiv.
Fmoc-L-Asp(OtBu)-Wang Resin	/	50 mg	/	0.03	1.03
Fmoc-L-Asp(OtBu)-OH	441.45	40 mg	/	0.09	3
62	605.90	18 mg	/	0.03	1
HOBt	135.12	12 mg	/	0.09	3
HBTU	379.24	34 mg	/	0.09	3
PyBOP	520.39	16	/	0.03	1
DIEA	129.25	0.041 mL	0.742	0.24	8
TFA (95%), TIS (3%), H_2O (2%)	/	1 mL	/	/	/
DMF	73.09	/	0.944	/	/

Compound **75** was synthesised following the same procedure as for compounds **71** and **72**, but using Fmoc-L-Asp(OtBu)-Wang Resin. The peptidic chain (DDDD) was obtained using a Supelco reactor. Compound **62** was reacted with the peptidic chain to obtain the final product. The crude product was finally solubilised in aqueous NH_4OAc and freeze-dried.
It was solubilised again in aqueous TFA (0.1%). The title compound (**75**) was obtained as a white solid with no further purification required (Yield: 56%).

^{1}H NMR [400 MHz, DMSO-d_6] δ: 1.80 - 2.34 (m, 7 x CH_2, 14H) 2.73 - 3.16 (m, 2 x CH_2, 4H), 3.87 - 4.07 (m, 4 x CH, 4H), 5.05 (s, NH, 1H), 5.70 (s, NH, 1H), 8.13 (s br, 4 x NH, 4H), 8.45 (s, NH, 1H), 10.40 (s, COOH, 1H), 10.75 (s, COOH, 1H), 10.89 (s, COOH, 1H), 11.10 (s, COOH, 1H), 11.24 (s, COOH, 1H).

^{13}C NMR [100 MHz, DMSO-d_6] δ: 21.1, 27.6, 29.6, 30.0, 30.6, 30.9, 31.3, 35.4, 35.5, 52.7, 53.9, 54.1, 55.2, 114.0, 125.0, 146.2, 150.3, 173.1, 173.5, 173.8, 174.2, 174.5, 174.7, 174.9, 175.0, 176.8, 177.0.

HMRS: Calcd for m/z = 1067.2516 [M+H]+, Found m/z = 1066.8837 [M+H]+.

5,8,11-Tris(carboxymethyl)-4,7,10,13-tetraoxo-3,6,9,12-tetraazapentadecane-1,2,15-tricarboxylic acid (**76**)

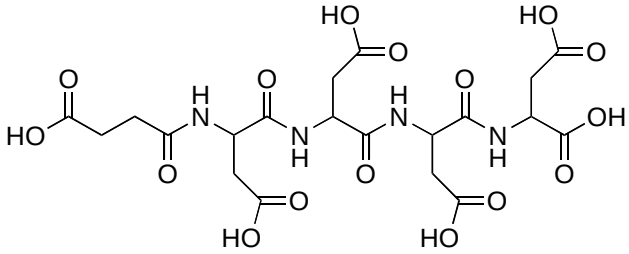

Compound	Mol. Weight	m/V	d (g/mL)	mmol	Equiv.
Fmoc-L-Asp(OtBu) Wang Resin	/	50 mg	/	0.03	1.03
Fmoc-L-Asp(OtBu)-OH	441.45	40 mg	/	0.09	3
Succinic anhydride	100.07	9 mg	/	0.03	1
HOBt	135.12	12 mg	/	0.09	3
HBTU	379.24	34 mg	/	0.09	3
DIEA	129.25	0.041 mL	0.742	0.24	8
TFA (95%), TIS (3%), H_2O (2%)	/	1 mL	/	/	/
DMF	73.09	/	0.944	/	/

The same procedure as for compounds **73** and **74** was used. The title compound **76** was obtained as a white solid with no further purification required (46%).

^{1}H NMR [400 MHz, DMSO-d_6] δ: 1.82 - 2.33 (m, 6 x CH_2, 12H), 3.85 - 4.04 (m, 4 x CH, 4H), 8.13 (s br, 4 x NH, 4H), 10.01 (s, COOH, 1H), 10.85 (s, COOH, 1H), 11.03 (s, COOH, 1H), 11.11 (s, COOH, 1H), 11.24, (s, COOH, 1H), 11.36 (s, COOH, 1H).

^{13}C NMR [100 MHz, DMSO-d_6] δ: 30.0, 30.3, 30.6, 31.2, 35.5, 35.9, 53.6, 53.9, 54.8, 55.2, 173.1, 173.3, 173.6, 173.8, 174.0, 174.5, 176.2, 177.0, 177.5.

HMRS: Calcd for m/z = 579.4376 [M+H]+, Found m/z = 579.1698 [M+H]+.

Dimethyl 2-(2,5,8-tris(3-methoxy-3-oxopropyl)-4,7,10,13-tetraoxo-17-(4,5,6,7-tetrabromo-1*H*-benzo[*d*]imidazol-2-ylamino)-3,6,9,14-tetraazaheptadecanamido)pentanedioate (**77**)

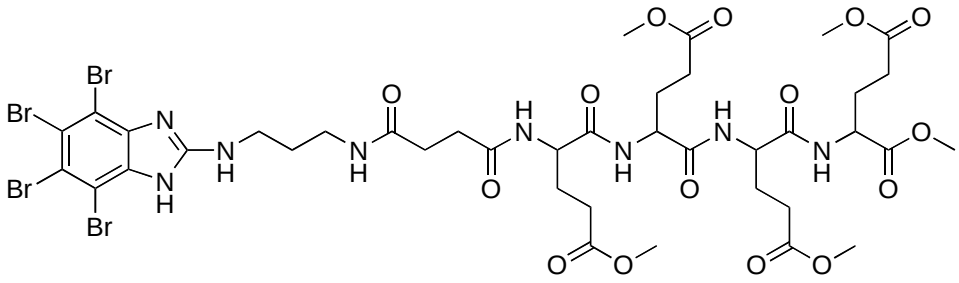

Compound	Mol. Weight	m/V	d (g/mL)	mmol	Equiv.
72	993.42	12 mg	/	0.01	1
TMCS	108.64	0.01 mL	0.856	0.09	8.4
MeOH	32.04	0.004 mL	0.791	0.09	8.4

To a suspension of compound **72** (12 mg) in dry methanol (0.004 mL) under nitrogen TMCS (0.01 mL) was added dropwise (0.01 mL) over 5 min. The clear solution obtained was stirred at room temperature for 10 min. The methanolic solution was dried in vacuo giving a white solid. The title compound (**77**) was obtained as a white solid (42%) with no further purification required.

^{1}H NMR [400 MHz, DMSO-d_6] δ: 1.91 (s br, 5 x CH_3, 15H), 2.03 - 2.36 (m, 11 x CH_2, 22H), 2.82 - 3.05 (m, 2 x CH_2, 4H), 3.73 - 4.01 (m, 4 x CH, 4H), 5.22 (s, NH, 1H), 5.87 (s, NH, 1H), 8.15 (s br, 4 x NH, 1H), 8.40 (s, NH, 1H), 10.42 (s, COOH, 1H), 10.90 (s, COOH, 1H), 11.04 (s, COOH, 1H), 11.10 (s, COOH, 1H), 11.22 (s, COOH, 1H).

^{13}C NMR [100 MHz, DMSO-d_6] δ: 21.3, 26.0, 26.3, 26.8, 27.3, 27.6, 29.5, 30.1, 30.5, 31.0, 31.4, 35.4, 35.9, 50.9, 54.1, 54.7, 55.0, 115.2, 123.6, 146.2, 152.1, 173.2, 173.3, 173.8, 174.0, 174.3, 174.7, 174.9, 175.5, 177.1, 178.0.

HRMS: calculated 1193.4557 (M+1), found 1193.6420.

5.3. Material and methods (CDK2)

5.3.1. Reagents and solvents

All reagents used were purchased from Sigma-Aldrich or Alfa-Aesar and were in excess of 95% purity unless otherwise stated. Solvents were purchased from Fisher-Scientific. Solvents stated as dry or anhydrous were stored in sealed glass bottles containing a SureSeal^{TM} or AcroSeal$^{(R)}$ septum. When required, solvent was removed from these bottles under dry nitrogen gas and used immediately. Deuterated solvents for NMR analysis were purchased from Sigma-Aldrich.

5.3.2. Analytical techniques

^{1}H- and ^{13}C-NMR spectra were obtained from samples dissolved in deuterated dimethylsulfoxide (DMSO-d_6) or acetonitrile (CD_3CN), using a Bruker, using a Bruker Avance III Spectrometer (500 MHz for ^{1}H, 125 MHz for ^{13}C). Chemical shift values (δ) are reported in parts per million (ppm) and are referenced against TMS (tetramethylsilane), with splitting patterns abbreviated to: s (singlet), d (doublet), t (triplet) and m (multiplet). The coupling constant (*J*) is given in Hz and was calculated using the software package Topspin^{TM} developed by Bruker Biospin and MNova. When ^{13}C values have not been quoted it is due to inability to visualise quaternary carbons. Attempts to observe such carbons were made using higher concentrations of analyte and increased scan times. However, in most cases signals for these carbons remained elusive. Fourier Transform Infrared (FTIR) spectra were obtained using a Bio-Rad FTS 3000mx diamond attenuated total reflectance spectrometer on purified samples with no further preparation.

LC-MS analysis was performed using a Micromass Platform LC electrospray mass spectrometer in positive ionisation mode (ES+) with a PDA 240-400 nm UV detector and a Waters Symmetry Shield RP18 3 µm, 4.6 x 20 mm column at a flow rate of 3 mL/min or a Waters Acquity UPLC system with PDA and ELSD employing both positive and negative ionisation modes and an Acquity UPLC BEH C18 1.7µm 2.1 x 50 mm column. The mobile phase consisted of 0.1% v/v formic $acid_{(aq)}$ / MeCN. Samples analysed by high-resolution mass spectrometry (HRMS) were submitted to the EPSRC national mass spectrometry service centre in Swansea.

Accurate mass analyses were measured using a Finnigan MAR 95 XP or a Finnigan MAR 900 XLT at Swansea EPSRC National Mass Spectrometry Service Centre (EPSRC, Chemistry Department, University of Wales Swansea, Wales, SA2 8PP).

Ultraviolet (UV) analysis were performed in EtOH using a Hitachi UV U2800A spectrophometer with an analysis range of 800-200 nm.

Infrared (IR) spectra were recorded as a neat sample on a Bio-Rad Excalibur FTS 3000MX diamond ATR spectrometer, equipped with a solid sampling device, in the range 4000-600 cm-1.

Melting points were determined using either a Stuart Scientific SMP3 or Stuart SMP40 automatic melting point apparatus and were observed manually.

5.3.3. Chromatography

Medium pressure automated flash chromatography (MPLC) was performed using a Biotage SP4 or a Varian IntelliFlash 310 flash chromatography system with a solvent gradient calculated from TLC *R*f values. MPLC performed on these systems used prepacked columns (KP-Sil, KP-NH or KP-C18).

Thin layer chromatography (TLC) was performed using Merck TLC silica gel 60 F_{254} or NH_2F_{254s} plates on aluminium and were visualised under UV light at 245 nm.

All compounds submitted for biological evaluation were in excess of 95% purity, which was determined using a Waters XTerra RP18, 5 µm (4.6 x 150 mm) column at 1 mL/min in both basic (0.1% aqueous ammonia and acetonitrile) and acidic (0.1% formic acid and acetonitrile) conditions with a gradient of 5-100% over 15 min.

5.3.4. Microwave-assisted reactions

Microwave assisted synthesis was performed in sealed Biotage microwave vials, using the Biotage Initiator Sixty microwave system.

5.3.5. Small-molecule X-ray crystallography

X-ray crystal structures were obtained by Dr. Ulrich Baisch in the X-ray Crystallography Unit, School of Chemistry, Bedson Building, Newcastle University, Newcastle upon Tyne, NE1 7RU.

5.3.6. Elemental analysis

Elemental analysis was carried out by Stephen Boyer in the Science Centre, London Metropolitan University, London, N7 7DD (http://www.londonmet.ac.uk/companyinfo).

5.3.7. Biological Evaluation of CDK2 inhibitors and structural biology

Evaluation of inhibitors for CDK2/cyclin A3 inhibitory activity and structural biology studies were conducted in the POG, Newcastle University, Newcastle upon Tyne.

5.3.8. CDK2/Cyclin A3 Biochemical Assay

Inhibition of human CDK2/Cyclin A3 was assayed using recombinant CDK2/cyclin A3 (10 µL) with 1 mg/mL histone H1 (150 µL, Sigma type III-S), in the presence of [γ-^{32}P] ATP (1-5 µL, 3000 Ci/mmol, Cat number NEG002A Perkin Elmer) and cold ATP (13.13 µL, 1 mM) in a final volume of 30 µl. The assay buffer (500 µL total volume) contained Tris-HCl pH 7.5 (50 mM) and MgCl2 (5 mM). The final DMSO concentration in the assay was 1% (V/V), after inhibitors stocks in 100% DMSO were diluted 1:10 in the appropriate assay buffer (3 µl + 27 µl buffer), followed by addition of 3 µl of 10% inhibitor solution to a total assay volume of 30 µl. Therefore, the final DMSO concentration was 1%, final inhibitor concentration was 1/100 of the original stock solution and the final ATP concentration in the assay was 12.5 µM. After incubation for 10 min at 30 °C, 25 µl aliquots were spotted onto 2.5 cm × 3 cm pieces of Whatman P81 phosphocellulose paper, and after 20 s, the filters were washed five times (> 5 min each time) in 1% phosphoric acid. The dry filters were transferred into 6 ml plastic scintillation vials, 5ml scintillation fluid (Amersham) was added, and the radioactivity was measured using a scintillation counter.

5.3.9. Bacterial expression and purification of T160pCDK2/Cyclin A

To ensure that the CDK2 was saturated with Cyclin A, a ratio of 0.5L: 1.5L of CDK2/Cyclin A was used. CDK2 phosphorylated at T160 was produced in E. coli by co-expression of human GST-CDK2 and S. cerevisiae GST–Cak1 (also called Civ1). E. coli strain B834 (DE3) pLysS, transformed with the coexpression plasmid, were grown in LB (lysogeny broth) medium supplemented with 50 µg/mL of ampicillin to an optical density of 0.9 at 37 °C and then at 20 °C for 1 h, before induction with 80 µM isopropyl-β-D-thiogalactoside (IPTG) and further incubation for 20–24 h at 20 °C. This incubation ensures complete phosphorylation of CDK2 by Civ 1.

Harvested cells were resuspended in HEPES-buffered saline (HBS, 20 mL) containing protease inhibitors (10 mM HEPES, pH 7.4, 135 mM NaCl, 3 mM EDTA, 0.01% (v/v) monothioglycerol and 0.01 % (w/v) sodium azide containing 0.1 mM phenylmethylsulphonyl fluoride (PMSF), 0.7 µg ml-1 pepstatin A and 0.5 µg ml-1 leupeptin), freeze-dried and stored at -20 °C.

Human cyclin A3 complementary DNA was generated by the polymerase chain reaction (PCR) using a Δ47 cyclin A expression plasmid as a template. Transformed B834 (DE3) pLysS cells, at an optical density of 0.6, were induced with 100 mM of IPTG at 37 °C for 30 min and further incubated at 20 °C for 3-4 h. Cells were stored as above. After standing at -20° overnight, as thawing was apparent 400 µL (25 mg/mL) lysozyme, 200 µL (10 mg/mL) RNAse A, 200 µL (2 mg/mL) DNAse I and 200 µL (1 M) $MgCl_2$ were added to the CDK2 and Cyclin A samples. Cells coexpressing GST-CDK2 and GST-Cak1 were then sonicated (till fluid) on ice in precooled tubes. Once sonication was finished the cells were transferred to an ice cold ultracentrifugation tube, which was filled with ice cold mHBS and balanced by weighing (to within 0.1 g). This step takes the volume up, which is beneficial for loading onto the affinity column (spin circa 25,000 x g at 4 °C). All the following steps were carried out at 4 °C with pre-cooled buffers (4 °C).

The clarified lysate was applied to a glutathione-Sepharose column equilibrated in HBS and washed with the same buffer. CDK2 was first loaded onto the column. GST-pCDK2/Cyclin A complex was eluted with freshly prepared 20 mM glutathione in HBS. A clarified lysate from thawed and sonicated cyclin A-expressing cells was then eluted and subjected to GST–3C-protease digestion (1/30 w/w, 16 h, 4 °C). The phosphorylated CDK2/Cyclin A complex eluted with the GST dimer. T160pCDK2/Cyclin A was further purified from GST and from GST-Cak1 by gel filtration (Superdex 75 HR 26/ 60) and a second glutathione-Sepharose column. Typical yields of pCDK2/Cyclin A were 10-15 mg from 1 L and 1.5 L of CDK2 and cyclin A cultures, respectively. The protein complex was finally concentrated to 10-12 mg/mL in 25 µL aliquots, rapidly freeze dried in liquid nitrogen and stored at -20 °C.

5.3.10. Crystallisation of T160pCDK2/Cyclin A-inhibitor complexes

Crystals will be obtained by the hanging drop method, using protein at a concentration of 10 mg ml^{-1}, 5% (v/v), DMSO and circa 5 mM inhibitor. Co-crystallisation of compounds **59**, **93**, **102** and **107** within CDK2/Cyclin A complex is ongoing in the POG at Newcastle University.

5.3.11. Molecular docking

The crystal structure of human CK2 was retrieved from the Protein Data Bank (PDB code: 1H1S) and processed in order to remove the ligands and water molecules. We used the Protonate 3D methodology, part of the MOE suite, for protonation state assignment by selecting a protonation state for each chemical group that minimizes the total free energy of the system. To estimate the electrostatic contributions, atomic partial charges for the ligands were calculated using PM3/ESP methodology. To minimise contacts between hydrogens, the structures were subjected to Amber99 force-field minimisation until the rms (root mean square) of conjugate gradient was <0.1 kcal • mol^{-1} •$Å^{-1}$ (1 Å = 0.1 nm) keeping the heavy atoms fixed at their crystallographic positions. For each selected compound, 25 independent docking runs were performed and searching was conducted within a user-specified docking sphere (20 Å radius and centered on the barycenter of the N253-4 (6.55) residue) with the Genetic Algorithm protocol and the GoldScore scoring function.

5.4. Index of synthesised compounds (CDK2)

2-((4-Nitrophenyl)thio)ethanol (**79**)

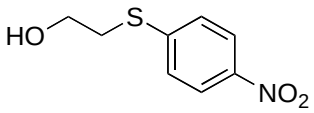

Compound	Mol. Weight	m/V	d (g/mL)	mmol	Equiv.
4-nitrothiophenol (**78**)	155.17	1 g	/	6	1
2-chloroethanol	80.51	1 mL	1.201	15	2.3
EtOH	46.07	2 mL	0.879	/	/
KOH	56.11	400 mg	/	7	1.1
H_2O	18.02	2.6 mL	1.00	/	/

4-Nitrothiophenol (**78**, 1 g) was suspended in EtOH (2 mL). A solution of KOH (400 mg) in water (2.6 mL) and 2-chloroethanol (1 mL) were added dropwise. The reaction mixture was heated at reflux for 3 h and cooled to room temperature. The progress of the reaction was monitored by LCMS. After standing the reaction mixture overnight at 4 °C the product had crystallised out. The sulfide was filtered off, washed thoroughly with water and dried. The aqueous phase was extracted with DCM (3x30 mL). The combined extracts were dried ($MgSO_4$) and the solvent was removed in vacuo giving a oil, which was combined with the precipitate. The crude product was purified by chromatography on silica (DCM/MeOH, 97:3) and the title compound (**79**) was obtained as yellow solid (Yield: 100%).

Rf: 0.76 (DCM/MeOH, 97:3).

M.p.: 58-60 °C.

UV λ_{max} (EtOH): 337 nm.

IR: 739, 841, 1054, 1325, 1503, 1573, 2913, 3536.

^{1}H NMR (500 MHz, DMSO-d_6) δ: 3.22 (t, *J* = 6.5 Hz, 2H), 3.66 (dd, *J* = 6.6, 5.7 Hz, 2H), 5.08 (t, *J* = 5.5 Hz, 1H), 8.13 (d, 2H), 7.53 (d, 2H).

^{13}C NMR (125 MHz, DMSO-d_6) δ: 33.7, 59.3, 123.8, 126.1, 144.3, 147.8.

HRMS: Calcd for m/z = 199.0376 [M+H]+, Found m/z = 199.1690 [M+H]+.

2-((4-Nitrophenyl)sulfonyl)ethanol (**80**)

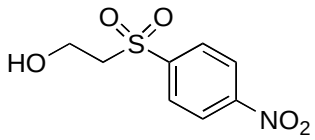

Compound	Mol. Weight	m/V	d (g/mL)	mmol	Equiv.
79	199.03	500 mg	/	2.5	1
mCPBA (77%)	172.57	900 mg	/	5.5	2.2
DCM	84.93	17 mL	1.33	/	/

Intermediate **79** (500 mg) was solubilised in dry DCM (17 mL). mCPBA (900 mg) was added at 0 °C. The resulting solution was stirred at 0 °C for 30 min. The progress of the reaction was monitored by LCMS. An additional equivalent of mCPBA in DCM (15 mL) was added and the reaction was stirred at 0 °C for 30 min. Basic water (Na_2CO_3) was added and the mixture was extracted with DCM (3x50 mL). The combined extracts were dried ($MgSO_4$) and the solvent was removed in vacuo. The crude product was purified by chromatography on silica (Petrol/EtOAc, 50:50) and the title compound (**80**) was obtained as a white solid (Yield: 100%).

Rf: 0.43 (Petrol/EtOAc, 50:50).

M.p.: 124-126 °C.

UV λ_{max} (EtOH): 251 nm.

IR: 734, 954, 1075, 1282, 1347, 1530, 3105, 3519.

^{1}H NMR (500 MHz, DMSO-d_6) δ: 3.61 (t, *J* = 5.9 Hz, 2H), 3.73 (t, *J* = 5.7 Hz, 2H), 4.91 (t, *J* = 5.2 Hz, 1H), 8.19 (d, *J* = 8.8 Hz, 2H), 8.44 (d, *J* = 8.8 Hz, 2H).

^{13}C NMR (125 MHz, DMSO-d_6) δ: 54.9, 57.4, 124.3, 129.5, 145.6, 150.3.

HRMS: Calcd for m/z = 232.0201 [M+H]+, Found m/z = 232.0275 [M+H]+.

1-(2-((4-Nitrophenyl)sulfonyl)ethyl)pyrrolidine (**81**)

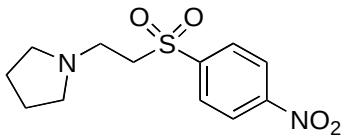

Compound	Mol. Weight	m/V	d (g/mL)	mmol	Equiv.
80	231.02	500 mg	/	2.2	1
Benzenesulfonyl chloride	176.62	0.42 mL	1.384	3.3	1.5
Et_3N	101.19	0.46 mL	0.726	3.3	1.5
Pyrrolidine	71.12	0.92 mL	0.852	11	5
DCM	84.93	25 mL	1.325	/	/

Intermediate **80** (500 mg, 2.2 mmol) was solubilised in dry DCM (25 mL). Et_3N (0.46 mL) and benzenesulfonyl chloride (0.42 mL) were added to the solution. The reaction was stirred at rt for 2 h. Pyrrolidine (0.92 mL) was added to the mixture and the reaction was stirred at rt for 30 min. The resulting mixture was washed with brine (3x50 mL) twice. The combined extracts were dried ($MgSO_4$) and the solvent was removed in vacuo. The crude product was purified by chromatography on silica (Petrol/EtOac, 60:40) and the title compound (**81**) was obtained as a yellow solid (Yield: 95%).

Rf: 0.36 (Petrol/EtOAc, 60:40).

M.p.: 130-132 °C.

UV λ_{max} (EtOH): 250 nm.

IR: 854, 1084, 1147, 1286, 1529, 2805, 3118.

^{1}H NMR (500 MHz, DMSO-d_6) δ: 1.46 (t, *J* = 3.6 Hz, 4H), 2.26 (m, 4H), 2.72 (t, *J* = 6.8 Hz, 2H), 3.66 (t, *J* = 6.8 Hz, 2H), 8.20 (d, *J* = 8.8 Hz, 2H), 8.43 (d, *J* = 8.8 Hz, 2H).

^{13}C NMR (125 MHz, DMSO-d_6) δ: 22.9, 23.1, 48.4, 48.5, 52.7, 53.4, 86.9, 124.1, 129.4.

HRMS: Calcd for m/z = 285.0831 [M+H]+, Found m/z = 285.0901 [M+H]+.

4-((2-(Pyrrolidin-1-yl)ethyl)sulfonyl)aniline (**82**)

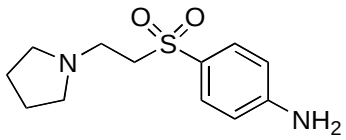

Compound	Mol. Weight	m/V	d (g/mL)	mmol	Equiv.
81	248.08	500 mg	/	1.8	1
Zinc	65.409	1.2 g	/	18	10
AcOH	60.05	8 mL	1.049	/	/
MeOH	32.042	8 mL	0.791	/	/

Intermediate **81** (500 mg) and zinc powder (1.2 g) were solubilised in MeOH (8 mL) and AcOH (8 mL). The reaction was stirred at 50 °C for 2 h. The reaction mixture was filtered through celite and the solvent was removed in vacuo. The crude product was purified by chromatography on silica (DCM/MeOH, 90:10) and the title compound (**82**) was obtained as a yellow oil (Yield: 99%).

Rf: 0.66 (DCM/MeOH, 90:10).

UV λ_{max} (EtOH): 270 nm.

IR: 1138, 1286, 2888, 2972, 3346.

^{1}H NMR (500 MHz, DMSO-d_6) δ: 1.57 - 1.64 (m, 4H), 2.28 - 2.37 (m, 4H), 2.56 - 2.65 (m, 2H), 3.23 - 3.30 (m, 2H), 6.13 (s, 2H), 6.64 (d, *J* = 8.7 Hz, 2H), 7.48 (d, *J* = 8.7 Hz, 2H).

^{13}C NMR (125 MHz, DMSO-d_6) δ: 21.0, 23.1, 48.6, 48.8, 53.1, 54.5, 112.6, 123.8, 129.6, 153.6, 172.0.

HRMS: Calcd for m/z = 255.1089 [M+H]+, Found m/z = 255.1159 [M+H]+.

4-Amino-2,6-dichloropyrimidine-5-carbaldehyde (**84**)

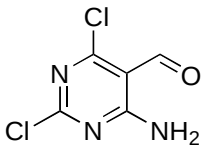

Compound	Mol. Weight	m/V	d (g/mL)	mmol	Equiv.
6-aminouracil (**83**)	127.10	1 g	/	8	1
$POCl_3$	153.33	4 mL	1.645	43	5.5
DMF	73.09	5 mL	0.944	64	8

DMF (2.5 mL) was added while stirring over 15 min to $POCl_3$ (4 mL) that was previously cooled in an ice bath at 5 °C. An excess of DMF (2.5 mL) was added until a white precipitate was obtained. The reaction mixture was warmed gently to dissolve the precipitate (rt, 1 h) and produce a clear solution, to which 6-aminouracil (**83**, 1 g) was added in small portions over 5 min. The mixture was heated at 110 °C overnight. The progress of the reaction was monitored by LCMS. The excess of $POCl_3$ was removed in vacuo leaving a red-brown oil, which was mixed with crushed ice and allow to stand at room temperature overnight. A yellow precipitate was obtained and collected by filtration through celite and dried in the oven overnight. The crude product was purified by chromatography on silica (Petrol/EtOAc, 80:20) and the title compound (**84**) was obtained as white solid (Yield: 99%).

Rf: 0.26 (Petrol/EtOAc, 80:20).

M.p.: 186-187.

UV λ_{max} (EtOH): 250, 316 nm.

IR: 1493, 1628, 1728, 2878, 3184, 3350.

^{1}H NMR (500 MHz, DMSO-d_6) δ: 8.75 (s, 1H), 9.12 (s, 1H), 10.20 (s, 1H).

^{13}C NMR (125 MHz, DMSO-d_6) δ: 106.5, 162.9, 165.1, 190.1.

HRMS: Calcd for m/z = 191.9659 [M+H]+, Found m/z = 191.9551 [M+H]+.

2-Amino-2-chloro-6-(cyclohexylmethoxy)pyrimidine-5-carbaldehyde (**85**)

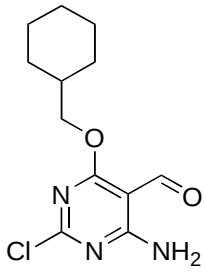

Compound	Mol.Weight	m/V	d (g/mL)	mmol	Equiv.
84	190.96	1 g	/	5	1
NaH (60%)	24.00	200 mg	/	8	1.5
THF	72.11	20 mL	0.889	/	/
Cyclohexylmethanol	108.14	0.8 mL	1.045	8	1.5

NaH (200 mg) and cyclohexylmethanol (0.8 mL) were stirred in anhydrous THF (20 mL) under nitrogen for 1 h at room temperature. Intermediate **84** (1 g, 5 mmol) was added and the reaction was stirred at room temperature overnight. The progress of the reaction was monitored by LCMS. The solvent was removed in vacuo and the residue was resuspended in DCM (20 mL) and washed with aqueous NH_4Cl (20 mL). The combined extracts were dried ($MgSO_4$) and the solvent was removed in vacuo. The crude product was purified by chromatography on silica (Petrol/EtOAc, 90:10) and the title compound (**85**) was obtained as white solid (Yield: 17%).

Rf: 0.63 (Petrol/EtOAc, 90:10).

M.p.: 130-131 °C.

UV λ_{max} (EtOH): 253, 303 nm.

IR: 789, 1311, 1439, 1542, 2850, 2920, 3129, 3347.

^{1}H NMR (500 MHz, DMSO-d_6): δ 0.98 - 1.33 (m, 5H), 1.57 - 1.83 (m, 4H), 4.21 (d, *J* = 6.0 Hz, 3H), 8.61 (d, *J* = 50.3 Hz, 2H), 10.12 (s, 1H).

^{13}C NMR (125 MHz, DMSO-d_6): 25.1, 25.8, 28.9, 38.7, 72.5, 95.3, 161.9, 163.4, 171.6, 187.9.

HRMS: Calcd for m/z = 268.0931 [M-H]-, Found m/z = 268.0856 [M-H]-.

4-Amino-6-(cyclohexylmethoxy)-2-((4-((2-(pyrrolidin-1-yl)ethyl)sulfonyl)phenyl) amino)pyrimidine-5-carbaldehyde (**86**)

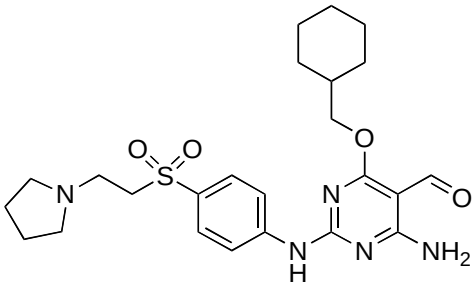

Compound	Mol. Weight	m/V	d (g/mL)	mmol	Equiv.
85	269.09	50 mg	/	0.19	1
82	254.11	100 mg	/	0.42	2.2
TFA	114.02	0.073 mL	1.489	/	/
TFE	100.04	0.73 mL	1.373	/	/

Intermediates **85** (50 mg) and **82** (100 mg) were added to TFE (0.73 mL) and the mixture was stirred at room temperature under a nitrogen atmosphere. TFA (0.073 mL) was added dropwise to the reaction mixture, which was subjected to microwave irradiation (20 min, 110 °C). Basic water ($NaHCO_3$) was added and the resulting solution was extracted with DCM (3x30 mL). The combined extracts were dried ($MgSO_4$) and the solvent was removed in vacuo. The crude product was purified by chromatography on silica (DCM/Et_3N, 99:1) to give the title compound (**86**) as a yellow oil (Yield: 50%).

Rf: 0.26 (DCM/Et_3N, 99:1).

UV λ_{max} (EtOH): 328 nm.

IR: 760, 822, 1023, 1410, 1657, 2823, 2940, 3401.

^{1}H NMR (500 MHz, DMSO-d_6): δ 1.18 (m, 5H), 1.57 (m, 4H), 1.73 (m, 6H), 2.31 (m, *J* = 5.9 Hz, 4H), 2.64 (t, *J* = 7.4 Hz, 2H), 3.44 (t, 2H), 4.25 (d, *J* = 6.0 Hz, 2H), 7.78 (d, *J* = 9.0 Hz, 2H), 7.99 (s, 1H), 8.09 (d, 2H), 8.49 (s, 1H), 9.98 (s, 1H), 10.17 (s, 1H).

^{13}C NMR (125 MHz, DMSO-d_6): 23.0, 25.2, 29.1, 36.7, 48.8, 53.0, 109.3, 119.2, 128.5, 146.7, 161.2, 198.1.

HRMS: Calcd for m/z = 488.2253 [M+H]+, Found m/z = 488.2314 [M+H]+.

4-Amino-6-(cyclohexylmethoxy)-2-((4-(vinylsulfonyl)phenyl)amino)pyrimidine-5-carbaldehyde (**59**)

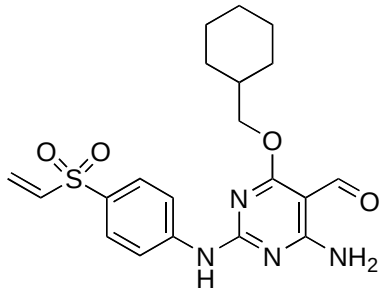

Compound	Mol. Weight	m/V	d (g/mL)	mmol	Equiv.
86	487.23	47 mg	/	0.1	1
mCPBA (77%)	172.57	28 mg	/	0.12	1.2
DCM	84.93	4 mL	1.325	/	/

Intermediate **86** (47 mg) was solubilised in DCM (4 mL). mCPBA (28 mg) was added to the reaction mixture, which was stirred at 0 °C for 30 min. The solvent was removed in vacuo. The crude product was purified by chromatography on silica (DCM), to give the title compound (**59**), which was obtained as an orange oil (Yield: 53%).

Rf: 0.2 (DCM/MeOH 90:10)

UV λ_{max} (EtOH): 230, 328 nm.

IR: 880, 1045, 1087, 1379, 2881, 2972, 3317.

^{1}H NMR (500 MHz, CD_3CN): δ 1.22 (m, 5H), 1.81 (m, 6H), 4.15 (d, *J* = 6.1 Hz, 2H), 6.09 (d, *J* = 9.9 Hz, 1H), 6.35 (d, *J* = 16.5 Hz, 1H), 6.81 (dd, *J* = 16.5, 9.9 Hz, 1H), 7.71 (d, *J* = 8.9 Hz, 1H), 7.94 (d, *J* = 8.5 Hz, 2H), 8.54 (s, 1H), 8.98 (s, 1H), 9.37 (s, 1H), 10.03 (s, 1H).

^{13}C NMR (125 MHz, CD_3CN): δ 21.0, 25.2, 25.8, 29.1, 36.8, 39.9, 45.5, 54.0, 67.7, 93.4, 119.1, 128.4, 145.0, 159.9, 163.9, 186.1.

HRMS: Calcd for m/z = 417.1518 [M+H]+, Found m/z = 417.1702 [M+H]+.

Sodium cyanoacetylcyanamide (**88**)

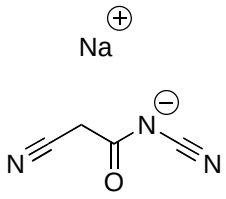

Compound	Mol. Weight	m/V	d (g/mL)	mmol	Equiv.
Cyanamide	42.04	1 g	/	24	1
Ethyl cyanoacetate (**87**)	113.11	2.55 mL	1.063	24	1
Sodium	23.00	550 mg	/	24	1
MeOH	32.04	24 mL	0.791	/	/

A solution of cyanamide (1 g) and ethyl cyanoacetate (**87**, 2.55 mL) in a methanolic solution of NaOMe (prepared with 550 mg of Na and 24 mL of MeOH) was allowed to stand at room temperature for 3-5 h. The solvent was removed in vacuo and the residue was treated with EtOH to give the title compound (**88**) as white solid with no further purification required (Yield: 91%).

M.p.: 122-123 °C.

UV λ_{max} (EtOH): 221 nm.

IR: 1620, 2175, 2959.

^{1}H NMR (500 MHz, DMSO-d_6): N.A.

^{13}C NMR (125 MHz, DMSO-d_6): N.A.

HRMS: Calcd for m/z = 132.0096 [M+H]+, Found m/z = 132.0112 [M+H]+.

6-Amino-2-bromopyrimidin-4-ol (**89**)

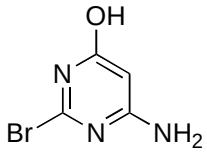

Compound	Mol. Weight	m/V	d (g/mL)	mmol	Equiv.
88	131.01	1 g	/	7.6	1
HBr	80.91	2.5 mL	1.49	45.6	6
AcOH	/	7.7 mL	1.049	/	/

To a solution of intermediate **88** (1 g) in AcOH (7.7 mL), HBr (2.5 mL, 45% in AcOH) was added over 5 min while stirring at room temperature. The reaction progress was monitored by LCMS. After 6 h the precipitate was collected by filtration and washed with AcOH and Et_2O, yielding the product (**89**) as a white solid with no further purification required (Yield: 76%).

Rf: 0.66 (Petrol/EtOAc, 80:20).

M.p.: 188-189 °C.

UV λ_{max} (EtOH): 215 nm.

IR: 3270, 3311, 3410.

^{1}H NMR (500 MHz, DMSO-d_6): δ 3.94 (s, 1H), 7.37 (s, 2H), 10.40(s, 1H).

^{13}C NMR (125 MHz, DMSO-d_6): δ 115.1, 152.9, 164.9, 187.1.

HRMS: Calcd for m/z = 189.9538 [M+H]+, Found m/z = 189.9647 [M+H]+.

4-Amino-2,6-dichloropyrimidine-5-carbaldehyde oxime (**96**^{i})

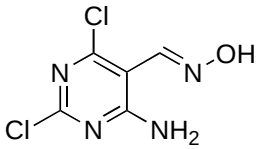

Compound	Mol. Weight	m/V	d (g/mL)	mmol	Equiv.
84	190.96	400 mg	/	2.1	1
H_2NOH HCl	69.49	292 mg	/	4.2	2
NMP	99.13	4 mL	1.03	/	/

Compound **84** (400 mg) and H_2NOH HCl (292 mg) were dissolved in NMP (2 mL) and the reaction mixture was subjected to microwave irradiation (110 °C, 20 min). Upon cooling to room temperature, H_2O (10 mL) was added and the mixture was extracted with DCM (3 x 30 mL) and washed with H_2O. The combined extracts were dried ($MgSO_4$) and the solvent was removed in vacuo. The crude product was purified by chromatography on silica (DCM/MeOH, 90:10) to give the title compound (**96**^{i}), which was obtained as a yellow oil (Yield: 22%).

Rf: 0.43 (DCM/MeOH, 90:10).

UV λ_{max} (EtOH): 215, 266, 309 nm.

IR: 1296, 1667, 2879, 2922.

^{1}H NMR (500 MHz, DMSO-d_6) δ: 8.07 (s, 2H), 8.62 (s, 1H), 9.23 (s, 1H).

^{13}C NMR (125 MHz, DMSO-d_6) δ: 106. 6, 150.3, 162.8, 164.1, 178.1.

HRMS: Calcd for m/z = 205.9762 [M+H]+, Found m/z = [M+H]+.

4-Amino-6-(cyclohexylmethoxy)-2-(4-(2-(pyrrolidin-1-yl)ethylsulfonyl)phenylamino) pyrimidine-5-carbaldehyde oxime (**96**)

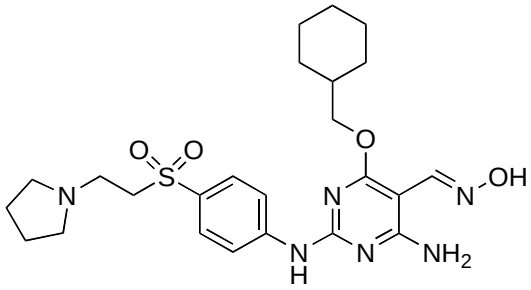

Compound	Mol. Weight	m/V	d (g/mL)	mmol	Equiv.
86	487.23	150 mg	/	0.31	1
H_2NOH HCl	69.49	44 mg	/	0.62	2
NMP	99.13	2 mL	1.03	/	/

Compound **86** (150 mg) and H_2NOH HCl (44 mg) were dissolved in NMP (2 mL) and the reaction mixture was subjected to microwave irradiation (110 °C, 20 min). Upon cooling to room temperature, H_2O (10 mL) was added and the mixture was extracted with DCM (3 x 30 mL). The combined extracts were dried ($MgSO_4$) and the solvent was removed in vacuo. The crude product was purified by chromatography on silica (DCM/MeOH, 90:10) to give the title compound (**96**), which was obtained as a pale yellow oil (Yield: 17%).

Rf: 0.49 (DCM/MeOH, 90:10).

UV λ_{max} (EtOH): 263, 326 nm.

IR: 879, 1045, 1087, 1379, 2882, 2972, 3322.

^{1}H NMR (500 MHz, DMSO-d_6) δ: 1.02 - 1.33 (m, 6H), 1.59 (t, *J* = 3.7 Hz, 4H), 1.65 - 1.86 (m, 7H), 2.30 - 2.36 (m, 3H), 2.59 - 2.70 (m, 2H), 3.39 - 3.44 (m, 2H), 4.17 (d, *J* = 6.1 Hz, 2H), 7.56 (s, 2H), 7.74 (d, *J* = 9.0 Hz, 2H), 8.06 (d, *J* = 8.9 Hz, 2H), 8.24 (s, 1H), 9.75 (s, 1H), 10.87 (s, 1H).

^{13}C NMR (125 MHz, DMSO-d_6) δ: 23.7, 25.9, 26.5, 29.7, 37.3, 49.1, 53.6, 54.6, 71.5, 85.7, 118.6, 129.0, 132.0, 144.1, 146.0, 158.0, 161.8, 167.2, 187.3.

HRMS: Calcd for m/z = 503.2362 [M+H]+, Found m/z = 503.2378 [M+H]+.

4-Amino-6-(cyclohexylmethoxy)-2-(4-(2-(pyrrolidin-1-yl)ethylsulfonyl)phenylamino) pyrimidine-5-carbaldehyde oxime (**96**)

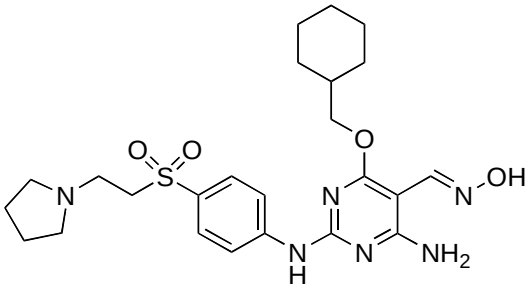

Compound	Mol. Weight	m/V	d (g/mL)	mmol	Equiv.
86	487.23	200 mg	/	0.41	1
H_2NOH HCl	69.49	43 mg	/	0.61	1.5
NaOH	40.00	33 mg	/	0.82	2
H_2O	18.01	3 mL	1	/	/
EtOH	46.07	3 mL	0.789	/	/

Compound **86** (200 mg) and H_2NOH HCl (43 mg) were dissolved in EtOH (3 mL). NaOH (33 mg) was solubilised in H_2O (3 mL) and the solution was added dropwise to the reaction mixture, which was stirred at room temperature for 4 h. The progress of the reaction was monitored by TLC and LCMS. Basic water (Na_2CO_3) was added and the mixture was extracted with DCM (3 x 30 mL). The combined extracts were dried ($MgSO_4$) and the solvent was removed in vacuo. The crude product was purified by chromatography on silica (DCM/MeOH, 90:10) to give the title compound (**96**), which was obtained as a yellow oil (Yield: 36%).

See pag. 182 for characterisation.

4-Amino-6-(cyclohexylmethoxy)-2-(4-(vinylsulfonyl)phenylamino)pyrimidine-5-carbaldehyde oxime (**94**)

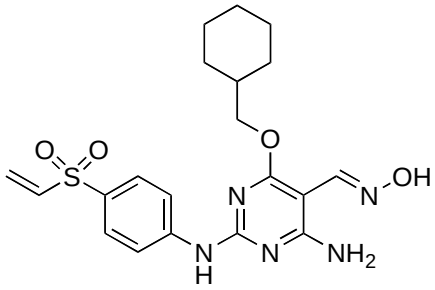

Compound	Mol. Weight	m/V	d (g/mL)	mmol	Equiv.
96	502.24	30 mg	/	0.06	1
mCPBA (77%)	172.57	16 mg	/	0.072	1.2
DCM	84.93	3 mL	1.33	/	/

Compound **96** (30 mg) was solubilised in DCM (3 mL). mCPBA (16 mg) was added to the reaction mixture, which was stirred at 0 °C for 30 min. The solvent was removed in vacuo. The crude product was purified by chromatography on silica (DCM) to give the title compound (**94**), which was obtained as a yellow oil (Yield: 49%).

Rf: 0.47 (DCM/MeOH, 90:10).

UV λ_{max} (EtOH): 263, 323 nm.

IR: 1017, 1410, 1449, 1640, 2833, 2945, 3306.

^{1}H NMR (500 MHz, DMSO-d_6) δ: 1.62 - 1.80 (m, 11H), 4.17 (d, *J* = 6.0 Hz, 12H), 6.10 (d, *J* = 9.8 Hz, 4H), 6.29 (d, *J* = 16.4 Hz, 1H), 7.60 (dd, *J* = 16.4, 9.9 Hz, 5H), 7.55 (s, 0H), 8.07 (d, *J* = 8.9 Hz, 1H), 8.25 (s, 1H), 9.80 (s, 4H), 10.88 (s, 1H).

^{13}C NMR (125 MHz, DMSO-d_6) δ: 25.3, 29.1, 29.3, 36.8, 40.6, 43.2, 54.0, 70.0, 93.4, 119.1, 128.4, 148.0, 159.9, 164.2, 190.0.

HRMS: Calcd for m/z = 432.1627 [M+H]+, Found m/z = 432.2117 [M+H]+.

4-Amino-6-(cyclohexylmethoxy)-2-(4-(2-(pyrrolidin-1-yl)ethylsulfonyl)phenylamino) pyrimidine-5-carbonitrile (**95**)

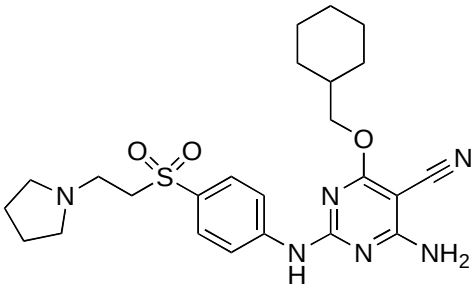

Compound	Mol. Weight	m/V	d (g/mL)	mmol	Equiv.
96	484.23	30 mg	/	0.06	1
DBU	152.24	0.021 mL	1.018	0.14	2.3
BOP	442.28	53 mg	/	0.12	2
DCM	84.93	3 mL	1.33	/	/

Compound **96** (30 mg) and BOP were dissolved in DCM. The reaction mixture was stirred at room temperature for 5 min before adding DBU dropwise. The progress of the reaction was monitored by TLC and LCMS and was stirred at room temperature for 4 h. H_2O was added and the mixture was extracted with EtOAc (3 x 30 mL) and washed with brine. The combined extracts were dried ($MgSO_4$) and the solvent was removed in vacuo. The crude product was purified by chromatography on silica (DCM/MeOH, 90:10) to give the title compound (**95**), which was obtained as a yellow oil (Yield: 78%).

Rf: 0.50 (DCM/MeOH, 90:10).

UV λ_{max} (EtOH): 314 nm.

IR: 1045, 1087, 1378, 2881, 2972.

^{1}H NMR (500 MHz, DMSO-d_6) δ: 1.13 - 1.33 (m, 5H), 1.53 - 1.60 (m, 4H), 1.68 - 1.86 (m, *J* = 28.1, 12.2 Hz, 6H), 2.28 - 2.36 (m, 4H), 2.64 (t, 2H), 3.42 (7, *J* = 7.4 Hz, 2H), 4.20 (d, *J* = 6.1 Hz, 2H), 7.48 (s, 2H), 7.75 (d, *J* = 9.0 Hz, 2H), 8.03 (d, 2H), 10.05 (s, 1H).

^{13}C NMR (125 MHz, DMSO-d_6) δ: 23.4, 25.6, 26.4, 29.3, 36.8, 49.2, 53.2, 54.3, 72.1, 119.4, 128.8, 132.3, 135.5, 142.2, 148.7, 159.2, 206.7.

HRMS: Calcd for m/z = 485.2257 [M+H]+, Found m/z = 485.2178 [M+H]+.

4-Amino-6-(cyclohexylmethoxy)-2-(4-(vinylsulfonyl)phenylamino)pyrimidine-5-carbonitrile (**93**)

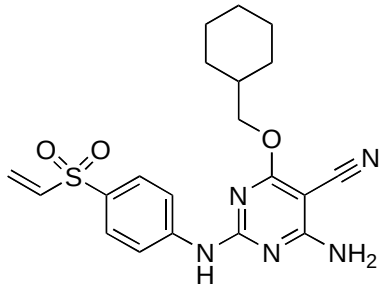

Compound	Mol. Weight	m/V	d (g/mL)	mmol	Equiv.
95	502.24	19 mg	/	0.04	1
mCPBA (77%)	172.57	12 mg	/	0.05	1.2
DCM	84.93	3 mL	1.33	/	/

Compound **95** (19 mg) was solubilised in DCM (3 mL). mCPBA (12 mg) was added to the reaction mixture, which was stirred at 0 °C for 30 min. The solvent was removed in vacuo. The crude product was purified by chromatography on silica (DCM) to give the title compound (**93**), which was obtained as an oil (Yield: 37%).

Rf: 0.48 (DCM/MeOH, 90:10).

UV λ_{max} (EtOH): 318 nm.

IR: 1087, 1380, 2879, 2972, 3308.

^{1}H NMR (500 MHz, DMSO-d_6) δ: 0.89 - 1.20 (m, 5H), 1.51 - 1.73 (m, 6H), 4.12 (d, J = 6.2 Hz, 2H), 6.02 (d, J = 9.8 Hz, 1H), 6.23 (d, J = 16.5 Hz, 1H), 6.97 (dd, J = 16.4, 9.9 Hz, 1H), 7.44 (s, 2H), 7.62 (d, J = 8.9 Hz, 2H), 7.96 (d, J = 8.7 Hz, 2H), 10.02 (s, 1H).

^{13}C NMR (125 MHz, DMSO-d_6) δ: 25.6, 26.4, 29.6, 37.1, 81.2, 119.9, 128.8, 139.8, 165.6, 193.0, 202.4.

HRMS: Calcd for m/z = 414.1522 [M+H]+, Found m/z = 414.1537 [M+H]+.

2,4-Dichloro-5-nitropyrimidine (**105**)

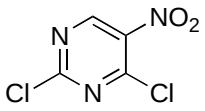

Compounds	Mol. Weight	m/V	d (g/mL)	mmol	Equiv.
5-nitrouracil (**104**)	157.01	50 mg	/	0.32	1
$POCl_3$	153.33	0.065 mL	1.645	0.64	2
DMA	121.18	1 mL	0.956	/	/

To a solution of 5-nitrouracil (**104**, 50 mg) in DMA (1 mL) $POCl_3$ (0.065 mL) was added and the mixture was heated gently to 190 °C for 1.5 h. the reaction mixture was cooled down to room temperature and the excess of $POCl_3$ was removed in vacuo. The residue was poured onto ice and the mixture was extracted with ether. The combined extracts were dried ($MgSO_4$) and the solvent was removed in vacuo. The crude product was purified by chromatography on silica (Petrol/EtOAc, 90:10), to give the title compound (**105**), which was obtained as a dark yellow solid (92%).

Rf: 0.42 (Petrol/EtOAc, 90:10)

M.p.: 28-32 °C.

UV λ_{max} (EtOH): 243 nm.

IR: 1073, 1746, 3047, 3093.

^{1}H NMR (500 MHz, DMSO-d_6): δ 9.18 (s, 1H).

^{13}C NMR (125 MHz, DMSO-d_6): δ 134.6, 140.8, 159.3, 166.5.

HRMS: Calcd for m/z =193.9446 [M+H]+, Found m/z = 193.9537 [M+H]+.

2-Chloro-5-nitropyrimidin-4-amine (**106**)

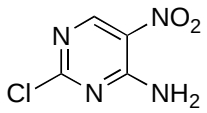

Compound	Mol. Weight	m/V	d (g/mL)	mmol	Equiv.
105	193.98	100 mg	/	0.5	1
NH_3 aq (1.5 M)	35.05	0.3 mL	0.779	0.4	0.8
THF	72.11	5 mL	0.889	/	/

NH_3 aq (0.3 mL) was added to a solution of intermediate (100 mg) in THF (5 mL) at 0 °C. The reaction mixture was stirred for 30 min and monitored by LCMS. The solvent was removed in vacuo. The crude product was purified by chromatography on silica (DCM/MeOH, 90:10), to give the title compound (**106**), which was obtained as a yellow solid (Yield: 63%).

Rf: 0.74 (DCM/MeOH, 90:10).

M.p.: 186-188 °C.

UV λ_{max} (EtOH): 216 nm.

IR: 3433, 3059.

^{1}H NMR (500 MHz, DMSO-d_6): δ 8.59 (s, 1H), 9.02 (s, 1H), 9.19 (s, 1H).

^{13}C NMR (125 MHz, DMSO-d_6): δ 126.6, 157.0, 157.6, 162.1.

HRMS: Calcd for m/z =174.9945 [M+H]+, Found m/z = 174.9823[M+H]+.

5-Nitro-N^2-(4-((2-(pyrrolidin-1-yl)ethyl)sulfonyl)phenyl)pyrimidine-2,4-diamine (**107**)

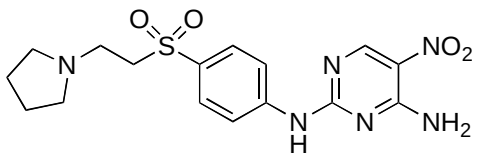

Compound	Mol. Weight	m/V	d (g/mL)	mmol	Equiv.
106	173.99	500 mg	/	3	1
82	254.11	1.6 g	/	6.3	2.2
TFA	114.02	0.55 mL	1.489	7	2.5
TFE	100.04	7.5 mL	1.373	/	/

Intermediates **106** (500 mg) and **82** (1.6 g) were added to TFE (5.5 mL) and the mixture was stirred at room temperature under a nitrogen atmosphere. TFA (0.55 mL, 7 mmol) was added dropwise to the reaction mixture, which was subjected to microwave irradiation (15 min at 160 °C). Basic water ($NaHCO_3$) was added and the solution was extracted with DCM (3x30 mL). The combined extracts were dried ($MgSO_4$) and the solvent was removed in vacuo. The crude product was purified by chromatography on silica (DCM/Et_3N, 99:1), to give the title compound, which was obtained as a yellow oil (Yield: 56%).

Rf: 0.33 (DCM/Et_3N, 99:1).

M.p.: 214-216 °C.

UV λ_{max} (EtOH): 261, 366 nm.

IR: 1129, 1229, 1535, 2797, 3279.

^{1}H NMR (500 MHz, DMSO-d_6) δ: 1.51 - 1.57 (m, 4H), 2.37 (s, 4H), 2.63 - 2.78 (m, 2H), 3.27 - 3.33 (m, 2H), 5.77 (s, 1H), 6.65 (d, *J* = 8.8 Hz, 2H), 7.45 (d, *J* = 8.7 Hz, 2H), 8.45 (s, 1H), 8.89 (s, 1H), 9.08 (s, 1H).

^{13}C NMR (125 MHz, DMSO-d_6) δ: 23.0, 48.6, 53.0, 54.0, 119.3, 128.6, 132.4, 144.1, 157.0, 157.4, 159.6.

HRMS: Calcd for m/z = 393.1267[M+H]+, Found m/z = 393.1322 [M+H]+.

5-Nitro-N^2-(4-(vinylsulfonyl)phenyl)pyrimidine-2,4-diamine (**102**)

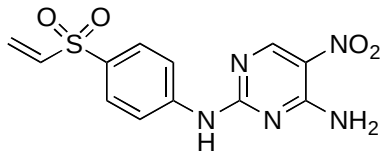

Compound	Mol. Weight	m/V	d (g/mL)	mmol	Equiv.
107	392.12	50 mg	/	0.13	1
mCPBA (77%)	172.57	36 mg	/	0.16	1.2
DCM	84.93	4 mL	1.33	/	/

Intermediate **107** (50 mg) was solubilised in DCM (4 mL) and mCPBA (36 mg) was added to the reaction mixture, which was stirred at 0 °C for 30 min. Basic water (Na_2CO_3) was added and the resulting solution was extracted with DCM (3x30 mL). The combined extracts were dried ($MgSO_4$) and the solvent was removed in vacuo. The crude product was purified by chromatography on silica (DCM), to give the title compound (**102**), which was obtained as a yellow solid (Yield: 31%).

Rf: 0.50 (DCM/MeOH, 90:10).

UV λ_{max} (EtOH): 365 nm.

IR: 1325, 1530, 1550, 2905, 3310.

^{1}H NMR (500 MHz, CD_3CN) δ: 6.04 - 6.14 (d, *J* = 9.9 Hz, 1H), 6.37 (d, *J* = 16.5 Hz, 1H), 6.78 - 6.88 (m, 1H), 7.80 - 7.90 (m, 2H), 8.08 (d, *J* = 8.5 Hz, 2H), 8.64 (s, 1H), 9.06 (s, 1H).

^{13}C NMR (125 MHz, DMSO-d_6) δ: 113.2, 119.6, 126.9, 128.4, 129.5, 132.8, 138.5, 143.7, 157.3, 157.4, 159.7.

HRMS: Calcd for m/z =322.0532 [M+H]+, Found m/z = 322.0603 [M+H]+.

4-Amino-2-chloropyrimidine-5-carbaldehyde (**109**)

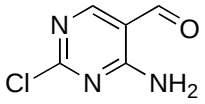

Compound	Mol. Weight	m/V	d (g/mL)	mmol	Equiv.
Cytosine (**108**)	111.04	250 mg	/	2	1
$POCl_3$	153.33	1 mL	1.645	/	/
DMF	73.09	1.5 mL	0.944	/	/

DMF (1 mL) was added while stirring over 15 min to $POCl_3$ (1 mL) that was previously cooled in an ice bath at 5 °C. DMF (0.5 mL) was added until a white precipitate was obtained. The reaction mixture was warmed gently to dissolve the precipitate (rt, 1 h) and produce a clear solution to which cytosine (**108**, 250 mg) was added in small portions. The mixture was heated at 110 °C overnight. The reaction progress was monitored by LCMS. The reaction mixture was mixed with crushed ice and stirred at room temperature for 15 min. Basic water ($NaHCO_3$) was added and the resulting solution was extracted with DCM (3x30 mL). The combined extracts were dried ($MgSO_4$) and the solvent was removed in vacuo. The crude product was purified by chromatography on silica (Petrol/EtOAc, 80:20) and the title compound (**109**) was obtained as a white solid (Yield: 33%).

Rf: 0.41 (Petrol/EtOAc, 80:20)

M.p.: 202-204 °C.

UV λ_{max} (EtOH): 270, 233 nm.

IR: 823, 1519, 1558, 1720, 2895, 2952, 3123.

^{1}H NMR (500 MHz, DMSO-d_6) δ: 7.19 (s, 1H), 8.56 (d, *J* = 6.4 Hz, 1H), 9.14 (s, 1H), 11.31 (s, 1H).

^{13}C NMR (125 MHz, DMSO-d_6) δ: 95.6, 159.2, 161.9, 163.4, 190.6.

HRMS: Calcd for m/z =158.0043 [M+H]+, Found m/z = 158.0012 [M+H]+.

4-Amino-2-((4-((2-(pyrrolidin-1-yl)ethyl)sulfonyl)phenyl)amino)pyrimidine-5-carbaldehyde (**110**)

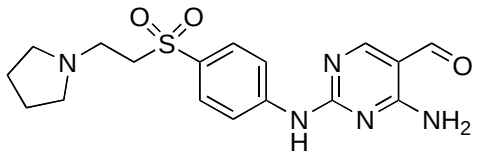

Compound	Mol. Weight	m/V	d (g/mL)	mmol	Equiv.
109	157.00	160 mg	/	1	1
82	254.11	560 mg	/	2.2	2.2
TFA	114.02	0.2 mL	1.489	2.5	2.5
TFE	100.04	2.3 mL	1.373	/	/

Intermediates **109** (160 mg) and **82** (560 mg) were added to TFE (2.3 mL) and the mixture was stirred at room temperature under a nitrogen atmosphere. TFA (0.2 mL) was added dropwise to the reaction mixture, which was subjected to microwave irradiation (25 min, 110 °C). Basic water ($NaHCO_3$) was added and the resulting solution was extracted with DCM (3x30 mL). The combined extracts were dried ($MgSO_4$) and the solvent was removed in vacuo. The crude product was purified by chromatography on silica (DCM/Et_3N, 99:1), to give the title compound, which was obtained as a yellow oil (Yield: 47%).

Rf: 0.23 (DCM/Et_3N, 99:1).

UV λ_{max} (EtOH): 262 nm.

IR: 880, 1046, 1087, 1379, 2881, 2972, 3253.

^{1}H NMR (500 MHz, DMSO-d_6) δ: 1.60 (q, *J* = 3.3 Hz, 4H), 2.29 - 2.38 (m, 4H), 2.69 (m, 2H), 3.41 - 3.58 (m, 2H), 7.76 - 7.91 (m, 4H), 8.39 (s, *J* = 1.8 Hz, 1H), 10.71 (s, 1H).

^{13}C NMR (125 MHz, DMSO-d_6) δ: 23.0, 45.6, 48.5, 53.0, 54.9, 89.0, 116.6, 118.8, 129.1, 142.7, 160.4.

HRMS: Calcd for m/z = 376.1375 [M+H]+, Found m/z = 376.1248 [M+H]+.

6. ANNEX

6.1. Crystal Structures

6.1.1. 4-amino-2-chloro-6-(cyclohexylmethoxy)pyrimidine-5-carbaldehyde (**85**)

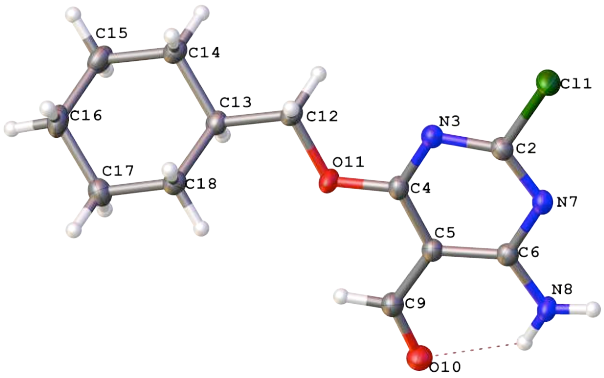

Table 1 Crystal data and structure refinement for compound 85

Identification code	EC-453-043t5
Empirical formula	$C_{12}H_{16}N_3O_2Cl$
Formula weight	269.73
Temperature/K	150.01(10)
Crystal system	monoclinic
Space group	$P2_1/c$
a/Å	4.74960(9)
b/Å	12.4692(2)
c/Å	21.6418(4)
α/°	90.00
β/°	96.2741(18)
γ/°	90.00
Volume/Å^3	1274.03(4)
Z	4
ρ_{calc}mg/mm^3	1.406

m/mm^{-1}	2.655
F(000)	568.0
Crystal size/mm^3	0.182 × 0.1485 × 0.04
2Θ range for data collection	8.2 to 132.6°
Index ranges	-5 ≤ h ≤ 5, -14 ≤ k ≤ 14, -25 ≤ l ≤ 25
Reflections collected	16865
Independent reflections	2228[R(int) = 0.0318]
Data/restraints/parameters	2228/0/228
Goodness-of-fit on F^2	1.063
Final R indexes [I>=2σ (I)]	R_1 = 0.0275, wR_2 = 0.0718
Final R indexes [all data]	R_1 = 0.0305, wR_2 = 0.0741
Largest diff. peak/hole / e Å^{-3}	0.24/-0.18

Table 2 Fractional Atomic Coordinates (×10^4) and Equivalent Isotropic Displacement Parameters (Å^2×10^3) for compound 85. U_{eq} is defined as 1/3 of of the trace of the orthogonalised U_{IJ} tensor.

Atom	*x*	*y*	*z*	U(eq)
Cl1	1570.4(7)	10053.8(2)	1205.47(16)	29.88(13)
O10	-6967(2)	6369.9(8)	-175.4(5)	31.0(2)
O11	-406(2)	6204.0(7)	1127.0(4)	28.4(2)
N3	525(2)	8012.8(9)	1147.3(5)	22.6(3)
N7	-2479(2)	9184.3(8)	488.8(5)	22.1(2)
N8	-6209(2)	8541(1)	-170.1(5)	24.6(3)
C2	-368(3)	8947(1)	908.4(6)	21.6(3)
C4	-1005(3)	7185.3(10)	911.6(6)	21.5(3)
C5	-3309(3)	7274.5(10)	447.5(6)	21.5(3)
C6	-4026(3)	8330.9(10)	248.4(6)	20.6(3)

C9	-4858(3)	6337.7(11)	204.0(6)	25.5(3)
C12	1729(3)	6053.2(11)	1655.1(6)	24.8(3)
C13	1661(3)	4874.1(10)	1807.7(6)	21.8(3)
C14	3438(3)	4631.3(11)	2425.1(6)	25.4(3)
C15	3271(3)	3441.4(12)	2588.0(7)	30.4(3)
C16	4121(3)	2725.9(12)	2066.3(7)	33.5(3)
C17	2434(3)	2986.5(11)	1442.2(7)	29.9(3)
C18	2623(3)	4177.5(11)	1289.1(6)	25.2(3)

Table 3 Anisotropic Displacement Parameters ($Å^2×10^3$) for RJG13004. The Anisotropic displacement factor exponent takes the form: $-2π^2[h^2a^{*2}U_{11}+...+2hka×b×U_{12}]$

Atom	U_{11}	U_{22}	U_{33}	U_{23}	U_{13}	U_{12}
Cl1	33.9(2)	19.32(19)	34.1(2)	- 0.84(12)	-7.02(15)	-3.82(12)
O10	34.2(5)	24.2(5)	31.8(5)	-1.1(4)	-8.1(4)	-2.0(4)
O11	35.5(5)	17.3(5)	29.2(5)	3.1(4)	-11.5(4)	2.0(4)
N3	25.6(6)	19.4(6)	22.2(5)	-0.1(4)	-0.2(4)	1.4(4)
N7	24.1(6)	17.4(5)	24.2(5)	1.1(4)	0.4(4)	1.7(4)
N8	27.3(6)	16.6(6)	28.0(6)	3.0(5)	-5.5(5)	2.0(5)
C2	24.5(6)	18.8(6)	21.5(6)	-1.0(5)	2.0(5)	-0.3(5)
C4	25.9(6)	17.8(6)	20.8(6)	1.5(5)	2.9(5)	3.1(5)
C5	24.8(6)	18.9(6)	20.4(6)	0.0(5)	0.9(5)	2.3(5)
C6	22.8(6)	20.1(6)	19.2(6)	0.0(5)	3.2(5)	1.9(5)
C9	31.6(7)	20.0(7)	24.3(7)	0.5(5)	-0.8(6)	1.6(5)
C12	27.6(7)	21.4(7)	23.2(7)	1.4(5)	-6.5(6)	1.7(5)
C13	21.4(7)	19.8(7)	23.5(7)	2.3(5)	-1.0(5)	1.0(5)
C14	28.8(7)	24.1(7)	22.4(7)	2.9(5)	-1.8(5)	1.0(6)
C15	34.7(8)	27.7(8)	27.4(7)	9.8(6)	-3.1(6)	0.1(6)

C16	36.8(8)	21.4(8)	41.1(9)	8.0(6)	-0.8(7)	4.7(6)
C17	36.9(8)	20.8(7)	31.7(8)	-1.6(6)	2.2(6)	1.9(6)
C18	29.7(7)	21.8(7)	23.2(7)	1.8(5)	-0.7(6)	0.6(5)

Table 4 Bond Lengths for compound 85.

Atom	Atom	Length/Å	Atom	Atom	Length/Å
Cl1	C2	1.7425(13)	C5	C6	1.4158(18)
O10	C9	1.2244(16)	C5	C9	1.4486(18)
O11	C4	1.3291(16)	C12	C13	1.5080(18)
O11	C12	1.4550(15)	C13	C14	1.5307(17)
N3	C2	1.3254(17)	C13	C18	1.5280(19)
N3	C4	1.3313(17)	C14	C15	1.5291(19)
N7	C2	1.3106(17)	C15	C16	1.527(2)
N7	C6	1.3637(17)	C16	C17	1.528(2)
N8	C6	1.3264(17)	C17	C18	1.5264(19)
C4	C5	1.4066(18)			

Table 5 Bond Angles for compound 85.

Atom	Atom	Atom	Angle/˚	Atom	Atom	Atom	Angle/˚
C4	O11	C12	119.91(10)	N8	C6	N7	117.07(11)
C2	N3	C4	113.18(10)	N8	C6	C5	122.38(12)
C2	N7	C6	115.32(11)	O10	C9	C5	124.28(12)
N3	C2	Cl1	114.73(9)	O11	C12	C13	105.55(10)
N7	C2	Cl1	114.21(10)	C12	C13	C14	111.16(11)
N7	C2	N3	131.05(12)	C12	C13	C18	112.22(11)
O11	C4	N3	119.48(11)	C18	C13	C14	110.38(11)

O11	C4	C5	116.32(11)	C15	C14	C13	110.84(11)
N3	C4	C5	124.20(12)	C16	C15	C14	111.83(12)
C4	C5	C6	115.67(11)	C15	C16	C17	111.93(12)
C4	C5	C9	121.37(11)	C18	C17	C16	111.17(12)
C6	C5	C9	122.95(11)	C17	C18	C13	111.35(12)
N7	C6	C5	120.55(11)				

Table 6 Hydrogen Bonds for compound 85.

D	H	A	d(D-H)/Å	d(H-A)/Å	d(D-A)/Å	D-H-A/°
N8	H8A	O10	0.884(19)	2.047(19)	2.7309(16)	133.4(15)

Table 7 Hydrogen Atom Coordinates (Å×10^4) and Isotropic Displacement Parameters (Å^2×10^3) for compound 85.

Atom	*x*	*y*	*z*	U(eq)
H8A	-7250(40)	7991(16)	-318(8)	35(4)
H8B	-6640(30)	9194(15)	-270(8)	29(4)
H9	-4090(30)	5663(14)	362(7)	29(4)
H12A	3600(40)	6269(13)	1542(8)	29(4)
H12B	1230(30)	6519(13)	1995(8)	27(4)
H13	-320(40)	4711(12)	1858(7)	21(4)
H14A	2800(40)	5068(13)	2761(8)	30(4)
H14B	5440(40)	4848(13)	2396(8)	29(4)
H15A	4450(40)	3284(13)	2974(8)	31(4)
H15B	1350(40)	3284(15)	2653(8)	36(4)
H16A	6190(40)	2833(14)	2026(8)	36(4)
H16B	3860(40)	1968(16)	2155(8)	37(4)

H17A	3110(40)	2559(14)	1106(8)	35(4)
H17B	380(40)	2780(14)	1457(7)	31(4)
H18A	1470(30)	4332(13)	895(8)	27(4)
H18B	4610(40)	4359(13)	1242(7)	27(4)

Experimental

Single crystals of $C_{12}H_{16}N_3O_2Cl$ **[compound 85]** were obtained. A suitable crystal was selected and **Xcalibur, Atlas, Gemini ultra** diffractometer was used. The crystal was kept at 150.01(10) K during data collection. Using Olex2 [1], the structure was solved with the XS [2] structure solution program using Direct Methods and refined with the XL [3] refinement package using Least Squares minimisation.

1. O. V. Dolomanov, L. J. Bourhis, R. J. Gildea, J. A. K. Howard and H. Puschmann, OLEX2: a complete structure solution, refinement and analysis program. J. Appl. Cryst. (2009). 42, 339-341.
2. XS, G.M. Sheldrick, Acta Cryst. (2008). A64, 112-122
3. XL, G.M. Sheldrick, Acta Cryst. (2008). A64, 112-122

Crystal structure determination of [EC-453-043t5]

Crystal Data for $C_{12}H_{16}N_3O_2Cl$ (M =269.73): monoclinic, space group $P2_1/c$ (no. 14), a = 4.74960(9) Å, b = 12.4692(2) Å, c = 21.6418(4) Å, β = 96.2741(18)°, V = 1274.03(4) Å^3, Z = 4, T = 150.01(10) K, μ(Cu Kα) = 2.655 mm^{-1}, *Dcalc* = 1.406 g/mm^3, 16865 reflections measured (8.2 ≤ 2Θ ≤ 132.6), 2228 unique (R_{int} = 0.0318) which were used in all calculations. The final R_1 was 0.0275 (>2sigma(I)) and wR_2 was 0.0741 (all data).

6.1.2. 4-amino-6-chloro-2-(cyclohexylmethoxy)pyrimidine-5-carbaldehyde (**85**^{i})

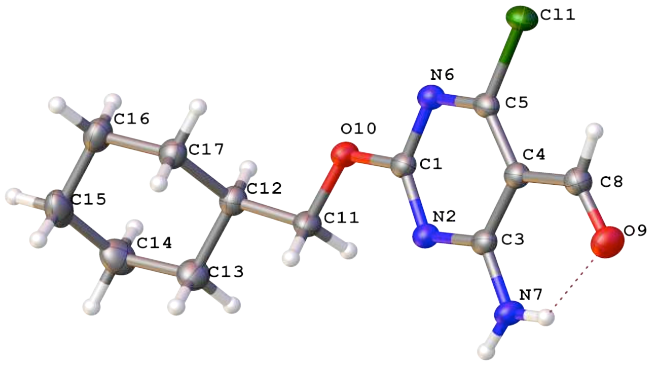

Table 1 Crystal data and structure refinement for compound 85^{i}

Identification code	EC-453-043t7
Empirical formula	$C_{12}H_{16}N_3O_2Cl$
Formula weight	269.73
Temperature/K	157(13)
Crystal system	monoclinic
Space group	$P2_1/c$
a/Å	13.1707(6)
b/Å	12.5444(5)
c/Å	8.1240(3)
α/°	90
β/°	107.015(5)
γ/°	90
Volume/Å^3	1283.48(10)
Z	4
ρ_{calc}mg/mm^3	1.396
m/mm^{-1}	2.635
Crystal size/mm^3	0.7322 × 0.5682 × 0.0344

2Θ range for data collection	7.018 to 132.622°
Index ranges	-15 ≤ h ≤ 15, -13 ≤ k ≤ 14, -7 ≤ l ≤ 9
Reflections collected	7615
Independent reflections	2235[R(int) = 0.0263]
Data/restraints/parameters	2235/0/227
Goodness-of-fit on F^2	1.051
Final R indexes [I>=2σ (I)]	R_1 = 0.0345, wR_2 = 0.0922
Final R indexes [all data]	R_1 = 0.0381, wR_2 = 0.0961
Largest diff. peak/hole / e $Å^{-3}$	0.22/-0.27

Table 2 Fractional Atomic Coordinates (×10^4) and Equivalent Isotropic Displacement Parameters ($Å^2$×10^3) for compound 85[i]. U_{eq} is defined as 1/3 of of the trace of the orthogonalised U_{IJ} tensor.

Atom	*x*	*y*	*z*	U(eq)
Cl1	6867.6(3)	9503.5(3)	1429.2(5)	29.10(16)
N	5845.0(12)	13426.1(11)	1668.4(18)	26.5(3)
O	3895.8(8)	10787.0(9)	3139.6(14)	26.1(3)
O1	7499.1(9)	12780.7(10)	536.6(17)	35.8(3)
N4	4848.9(10)	12129.7(10)	2399.4(16)	23.1(3)
N5	5311.1(10)	10281.6(11)	2367.5(17)	24.0(3)
C6	6102.7(12)	10565.5(12)	1778(2)	22.7(3)
C7	3167.0(12)	11608.2(14)	3348(2)	27.6(4)
C8	5685.0(12)	12394.7(12)	1831.7(19)	22.9(3)
C9	6358.6(12)	11602.8(13)	1444.4(19)	22.9(3)
C10	7240.7(13)	11873.5(14)	790(2)	27.7(4)
C11	4716.8(12)	11108.7(12)	2612.5(19)	22.6(3)
C12	2193.0(12)	11081.8(14)	3608(2)	26.4(4)

C13	1640.7(13)	10322.5(14)	2151(2)	28.2(4)
C14	1421.7(14)	11958.6(15)	3781(3)	33.8(4)
C15	412.9(15)	11498.3(17)	4059(3)	40.7(5)
C16	639.2(14)	9852.2(16)	2446(3)	35.7(4)
C17	-121.0(14)	10723.8(17)	2633(3)	40.1(4)

Table 3 Anisotropic Displacement Parameters ($Å^2×10^3$) for EC-453-043t7. The Anisotropic displacement factor exponent takes the form: $-2π^2[h^2a^{*2}U_{11}+...+2hka×b×U_{12}]$

Atom	U_{11}	U_{22}	U_{33}	U_{23}	U_{13}	U_{12}
Cl1	31.2(2)	22.2(2)	34.8(3)	-1.41(14)	11.21(17)	5.06(14)
N	28.7(7)	18.4(7)	34.5(7)	-0.8(6)	12.5(6)	-2.2(6)
O	25.1(5)	20.4(6)	34.7(6)	-0.5(5)	11.9(5)	-1.6(4)
O1	35.3(7)	30.9(7)	45.3(7)	2.4(5)	18.0(6)	-4.9(5)
N4	23.8(6)	19.2(6)	26.8(7)	-1.9(5)	7.9(5)	-1.0(5)
N5	24.8(6)	20.2(6)	26.8(7)	-0.4(5)	7.2(5)	-0.3(5)
C6	23.5(7)	20.4(8)	21.7(7)	-2.1(6)	2.7(6)	1.9(6)
C7	24.9(8)	23.0(8)	36.2(9)	-4.4(7)	10.8(7)	0.9(6)
C8	24.2(7)	21.2(8)	21.1(7)	-0.8(6)	3.3(6)	-1.5(6)
C9	23.5(7)	21.9(8)	22.0(7)	-1.0(6)	4.4(6)	-0.7(6)
C10	25.8(8)	27.0(9)	29.9(9)	-0.2(6)	7.7(7)	0.2(7)
C11	23.3(7)	20.3(7)	22.8(7)	-1.5(6)	4.4(6)	-0.9(6)
C12	25.8(8)	28.4(8)	25.9(8)	0.1(7)	9.3(6)	-2.0(6)
C13	27.3(8)	28.9(9)	28.1(9)	-1.8(7)	7.6(7)	-2.2(7)
C14	33.2(9)	32.9(10)	39.2(10)	-4.8(8)	16.6(8)	0.2(7)
C15	35.5(10)	45.4(11)	48.4(11)	3.3(9)	23.8(9)	5.7(9)
C16	30.2(9)	35.8(10)	40.8(10)	2.1(8)	9.6(8)	-7.8(8)
C17	25.0(9)	47.2(11)	48.5(11)	10.2(9)	11.4(8)	-2.0(8)

Table 4 Bond Lengths for compound 85[i].

Atom	Atom	Length/Å	Atom	Atom	Length/Å
Cl1	C6	1.7428(15)	C7	C12	1.512(2)
N	C8	1.324(2)	C8	C9	1.427(2)
O	C7	1.4513(19)	C9	C10	1.452(2)
O	C11	1.3365(19)	C12	C13	1.528(2)
O1	C10	1.222(2)	C12	C14	1.531(2)
N4	C8	1.354(2)	C13	C16	1.527(2)
N4	C11	1.311(2)	C14	C15	1.525(3)
N5	C6	1.317(2)	C15	C17	1.518(3)
N5	C11	1.349(2)	C16	C17	1.520(3)
C6	C9	1.391(2)			

Table 5 Bond Angles for compound 85[i].

Atom	Atom	Atom	Angle/˚	Atom	Atom	Atom	Angle/˚
C11	O	C7	116.60(12)	O1	C10	C9	124.84(16)
C11	N4	C8	115.95(14)	O	C11	N5	111.95(13)
C6	N5	C11	113.63(13)	N4	C11	O	119.24(14)
N5	C6	Cl1	114.15(11)	N4	C11	N5	128.81(14)
N5	C6	C9	125.92(14)	C7	C12	C13	113.27(13)
C9	C6	Cl1	119.92(12)	C7	C12	C14	108.18(14)
O	C7	C12	108.88(13)	C13	C12	C14	109.92(14)
N	C8	N4	116.32(14)	C16	C13	C12	110.89(14)
N	C8	C9	122.06(14)	C15	C14	C12	111.82(16)
N4	C8	C9	121.62(14)	C17	C15	C14	111.03(16)

C6	C9	C8	113.99(14)	C17	C16	C13	111.25(16)
C6	C9	C10	123.76(15)	C15	C17	C16	111.41(15)
C8	C9	C10	122.24(14)				

Table 6 Hydrogen Bonds for compound 85[i].

D	H	A	d(D-H)/Å	d(H-A)/Å	d(D-A)/Å	D-H-A/°
N	HA	O1	0.85(2)	2.06(2)	2.724(2)	134.7(19)

Table 7 Hydrogen Atom Coordinates (Å×10^4) and Isotropic Displacement Parameters (Å^2×10^3) for compound 85[i].

Atom	*x*	*y*	*z*	U(eq)
H7A	3559(16)	12063(18)	4340(30)	41(6)
H12	2383(14)	10661(16)	4690(30)	29(5)
H7B	2959(15)	12049(17)	2270(30)	32(5)
H14A	1769(17)	12440(20)	4720(30)	47(6)
H14B	1203(16)	12375(19)	2730(30)	42(6)
H13A	1479(17)	10710(18)	1050(30)	43(6)
H15A	620(17)	11123(19)	5190(30)	45(6)
H16A	827(17)	9417(18)	3490(30)	45(6)
H13B	2121(16)	9781(18)	2060(30)	33(5)
H17A	-740(20)	10420(19)	2870(30)	51(6)
H10	7633(15)	11259(16)	510(20)	28(5)
H15B	-88(18)	12087(19)	4110(30)	47(6)
H16B	266(17)	9367(18)	1470(30)	43(6)
H17B	-376(16)	11115(18)	1570(30)	39(5)
HA	6370(17)	13604(17)	1320(30)	35(5)

HB	5408(16)	13875(19)	1920(30)	34(5)

Experimental

Single crystals of $C_{12}H_{16}N_3O_2Cl$ **[compound 85^i]** were obtained. **Xcalibur, Atlas, Gemini ultra** diffractometer was used. The crystal was kept at 157(13) K during data collection. Using Olex2 [1], the structure was solved with the ShelXS [2] structure solution program using Direct Methods and refined with the ShelXL [3] refinement package using Least Squares minimisation.

1. O. V. Dolomanov, L. J. Bourhis, R. J. Gildea, J. A. K. Howard and H. Puschmann, OLEX2: a complete structure solution, refinement and analysis program. J. Appl. Cryst. (2009). 42, 339-341.
2. SHELXS, G.M. Sheldrick, Acta Cryst. (2008). A64, 112-122
3. SHELXL, G.M. Sheldrick, Acta Cryst. (2008). A64, 112-122

Crystal structure determination of [compound 85^i]

Crystal Data for $C_{12}H_{16}N_3O_2Cl$ (M =269.73): monoclinic, space group $P2_1/c$ (no. 14), a = 13.1707(6) Å, b = 12.5444(5) Å, c = 8.1240(3) Å, β = 107.015(5)°, V = 1283.48(10) Å^3, Z = 4, T = 157(13) K, μ(Cu Kα) = 2.635 mm^{-1}, *Dcalc* = 1.396 g/mm^3, 7615 reflections measured (7.018 ≤ 2Θ ≤ 132.622), 2235 unique (R_{int} = 0.0263) which were used in all calculations. The final R_1 was 0.0345 (I > 2σ(I)) and wR_2 was 0.0961 (all data).

6.1.3. (*E*)-*N*'-(2-chloropyrimidin-4-yl)-*N*,*N*-dimethylformimidamide (**109**[ii])

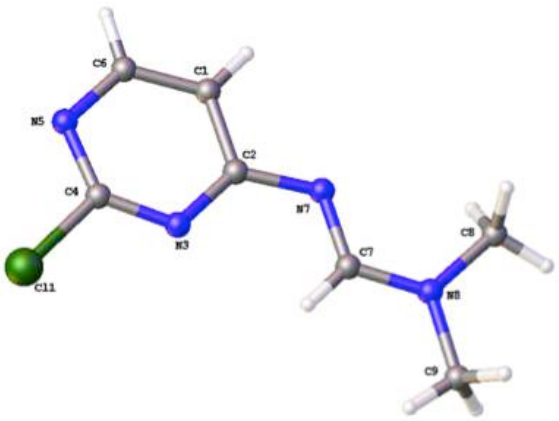

Table 1 Crystal data and structure refinement for compound 109[ii].

Identification code	rjg140001lr_fa
Empirical formula	C14H18N8Cl2
Formula weight	369.26
Temperature/K	290.00(10)
Crystal system	triclinic
Space group	P-1
a/Å	4.0647(4)
b/Å	11.6022(8)
c/Å	18.7182(19)
α/°	82.146(7)
β/°	87.135(8)
γ/°	88.027(7)
Volume/Å3	873.03(14)
Z	2
ρcalcg/cm3	1.405
μ/mm-1	3.467
F(000)	384.0
Crystal size/mm3	0.22 × 0.08 × 0.02
Radiation	CuKα (λ = 1.54184)

2Θ range for data collection/°	4.77 to 81.79
Index ranges	-3 ≤ h ≤ 3, -9 ≤ k ≤ 9, -15 ≤ l ≤ 15
Reflections collected	4189
Independent reflections	1112 [Rint = 0.0304, Rsigma = 0.0285]
Data/restraints/parameters	1112/0/221
Goodness-of-fit on F2	1.069
Final R indexes [I>=2σ (I)]	R1 = 0.0427, wR2 = 0.1038
Final R indexes [all data]	R1 = 0.0572, wR2 = 0.1147
Largest diff. peak/hole / e Å-3	0.18/-0.18

Table 2 Fractional Atomic Coordinates (×104) and Equivalent Isotropic Displacement

Parameters (Å2×103) for rjg140001lr_fa. Ueq is defined as 1/3 of of the trace of the orthogonalised UIJ tensor.

Atom	x	y	z	U(eq)
Cl1	7397(4)	8631.9(12)	8626.3(8)	80.4(7)
Cl2	-571(4)	3773.7(12)	6488.4(9)	87.4(8)
N3	5162(12)	8961(4)	7344(4)	57.5(14)
N5	4497(14)	10524(6)	8049(3)	71.1(16)
N7	3107(11)	9197(6)	6152(4)	61.3(14)
N8	3755(11)	7674(5)	5481(4)	62.3(14)
N13	2101(13)	4112(4)	7672(4)	60.6(14)
N15	-562(12)	5742(6)	6986(3)	66.4(15)
N17	4622(14)	4369(6)	8757(3)	59.3(15)
N18	7292(13)	2790(4)	9385(3)	61.6(14)
C1	2447(15)	10712(7)	6875(4)	73(2)
C2	3623(16)	9588(7)	6796(5)	56.7(17)
C4	5446(14)	9473(7)	7919(4)	58.4(17)
C6	2966(17)	11138(5)	7493(5)	76(2)
C7	4104(14)	8138(8)	6080(4)	61.8(18)

C8	2216(16)	8348(5)	4872(4)	80(2)
C9	4693(15)	6471(5)	5425(3)	80(2)
C11	2004(17)	5968(7)	8067(4)	64.5(18)
C12	2941(16)	4799(8)	8158(4)	54.8(17)
C14	458(17)	4659(8)	7125(4)	61.8(17)
C16	297(17)	6401(5)	7482(5)	66.6(18)
C17	5727(17)	3296(8)	8817(4)	62.3(18)
C18	7972(15)	3439(5)	9969(3)	79(2)
C19	8444(15)	1578(5)	9455(3)	79(2)

Table 3 Anisotropic Displacement Parameters (Å2×103) for rjg140001lr_fa. The Anisotropic displacement factor exponent takes the form: -2π2[h2a*2U11+2hka*b*U12+…].

Atom	U11	U22	U33	U23	U13	U12
Cl1	107.0(14)	62.6(11)	73.7(13)	-12.9(9)	-26.4(10)	13.3(9)
Cl2	120.4(15)	60.3(12)	88.0(14)	-26.2(10)	-38.6(11)	16.6(10)
N3	70(4)	49(4)	54(4)	-6(4)	-15(3)	2(3)
N5	92(4)	39(4)	85(5)	-18(4)	-17(4)	11(3)
N7	80(4)	39(4)	66(5)	-11(3)	-13(3)	6(3)
N8	80(4)	51(4)	58(4)	-12(4)	-17(3)	5(3)
N13	71(4)	53(4)	62(4)	-17(4)	-18(3)	3(3)
N15	88(4)	39(4)	75(4)	-16(4)	-11(3)	13(3)
N17	73(4)	37(4)	69(5)	-11(3)	-11(3)	4(3)
N18	82(4)	42(4)	63(4)	-11(3)	-15(3)	3(3)
C1	97(5)	54(6)	73(6)	-22(5)	-24(4)	9(4)
C2	64(4)	48(6)	63(6)	-20(6)	-6(4)	-8(4)
C4	71(5)	49(6)	54(5)	4(4)	-15(4)	-1(4)
C6	102(6)	35(4)	90(6)	-9(6)	-24(5)	19(4)
C7	66(4)	60(6)	59(6)	-6(5)	-7(4)	-1(4)
C8	107(5)	63(4)	73(5)	-15(4)	-23(4)	1(4)
C9	102(5)	52(5)	90(5)	-23(4)	-12(4)	13(4)

C11	82(5)	39(6)	74(6)	-12(4)	-10(4)	11(4)
C12	50(4)	58(7)	54(6)	2(5)	-8(4)	4(4)
C14	65(5)	57(6)	69(6)	-25(4)	-5(4)	-5(4)
C16	84(5)	35(4)	80(5)	-8(6)	-4(5)	9(4)
C17	69(5)	64(6)	54(6)	-7(4)	-8(4)	-8(4)
C18	92(5)	73(4)	75(5)	-20(4)	-20(4)	1(4)
C19	89(5)	63(5)	89(5)	-18(4)	-23(4)	6(4)

Table 4 Bond Lengths for rjg140001lr_fa.

Atom	Atom	Length/Å	Atom	Atom	Length/Å
Cl1	C4	1.742(6)	N13	C14	1.326(8)
Cl2	C14	1.751(6)	N15	C14	1.305(7)
N3	C2	1.342(7)	N15	C16	1.347(7)
N3	C4	1.310(7)	N17	C12	1.369(7)
N5	C4	1.317(7)	N17	C17	1.301(7)
N5	C6	1.346(7)	N18	C17	1.323(7)
N7	C2	1.373(7)	N18	C18	1.453(6)
N7	C7	1.303(7)	N18	C19	1.458(6)
N8	C7	1.325(7)	C1	C2	1.397(7)
N8	C8	1.447(7)	C1	C6	1.348(7)
N8	C9	1.450(6)	C11	C12	1.385(7)
N13	C12	1.352(7)	C11	C16	1.354(7)

Table 5 Bond Angles for rjg140001lr_fa.

Atom	Atom	Atom	Angle/˚	Atom	Atom	Atom	Angle/˚
C4	N3	C2	115.9(5)	N7	C2	C1	116.9(8)
C4	N5	C6	112.6(5)	N3	C4	Cl1	115.0(7)
C7	N7	C2	117.5(6)	N3	C4	N5	130.5(5)
C7	N8	C8	120.1(5)	N5	C4	Cl1	114.6(7)

C7	N8	C9	121.8(6)	N5	C6	C1	123.2(5)
C8	N8	C9	117.9(6)	N7	C7	N8	122.6(6)
C14	N13	C12	114.4(5)	C16	C11	C12	118.8(6)
C14	N15	C16	112.9(5)	N13	C12	N17	121.9(7)
C17	N17	C12	118.4(6)	N13	C12	C11	119.9(6)
C17	N18	C18	120.6(5)	N17	C12	C11	118.2(8)
C17	N18	C19	122.6(6)	N13	C14	Cl2	114.5(7)
C18	N18	C19	116.8(6)	N15	C14	Cl2	114.5(7)
C6	C1	C2	118.7(6)	N15	C14	N13	131.0(5)
N3	C2	N7	124.1(7)	N15	C16	C11	122.8(5)
N3	C2	C1	119.1(6)	N17	C17	N18	123.0(6)

Table 6 Torsion Angles for rjg140001lr_fa.

A	B	C	D	Angle/˚	A	B	C	D	Angle/˚
C2	N3	C4	Cl1	179.1(4)	C12	N13	C14	Cl2	179.0(4)
C2	N3	C4	N5	-1.0(9)	C12	N13	C14	N15	-2.1(9)
C2	N7	C7	N8	-179.5(5)	C12	N17	C17	N18	-177.9(5)
C2	C1	C6	N5	-1.7(10)	C12	C11	C16	N15	0.6(9)
C4	N3	C2	N7	179.8(5)	C14	N13	C12	N17	179.5(5)
C4	N3	C2	C1	-0.3(8)	C14	N13	C12	C11	1.6(8)
C4	N5	C6	C1	0.6(9)	C14	N15	C16	C11	-0.8(8)
C6	N5	C4	Cl1	-179.2(4)	C16	N15	C14	Cl2	-179.4(4)
C6	N5	C4	N3	0.9(9)	C16	N15	C14	N13	1.7(9)
C6	C1	C2	N3	1.5(9)	C16	C11	C12	N13	-1.0(8)
C6	C1	C2	N7	-178.6(5)	C16	C11	C12	N17	-179.0(5)
C7	N7	C2	N3	1.9(8)	C17	N17	C12	N13	7.2(8)
C7	N7	C2	C1	-178.0(5)	C17	N17	C12	C11	-174.8(5)
C8	N8	C7	N7	0.0(8)	C18	N18	C17	N17	-2.3(8)
C9	N8	C7	N7	-176.1(5)	C19	N18	C17	N17	178.4(5)

Table 7 Hydrogen Atom Coordinates (Å×104) and Isotropic Displacement Parameters (Å2×103) for rjg140001lr_fa.

Atom	x	y	z	U(eq)
H1	1327	11157	6507	88
H6	2230	11894	7537	91
H7	5100	7689	6465	74
H8A	227	8719	5036	120
H8B	1702	7842	4530	120
H8C	3699	8929	4646	120
H9A	5805	6142	5849	120
H9B	6139	6437	5007	120
H9C	2757	6039	5383	120
H11	2539	6446	8402	77
H16	-308	7187	7421	80
H17	5401	2865	8444	75
H18A	9888	3896	9838	118
H18B	8358	2906	10398	118
H18C	6118	3944	10057	118
H19A	7549	1203	9084	119
H19B	7736	1187	9920	119
H19C	10807	1544	9407	119

Experimental

Single crystals of C14H18N8Cl2 [rjg140001lr_fa] were obtained. A suitable crystal was selected and a Xcalibur, Atlas, Gemini ultra diffractometer was used. The crystal was kept at 290.00(10) K during data collection. Using Olex2 [1], the structure was solved with the XT [2] structure solution program using Direct Methods and refined with the XL [3] refinement package using Least Squares minimisation.

1. Dolomanov, O.V., Bourhis, L.J., Gildea, R.J, Howard, J.A.K. & Puschmann, H. (2009), J. Appl. Cryst. 42, 339-341.
2. Sheldrick, G.M. (2008). Acta Cryst. A64, 112-122.
3. Sheldrick, G.M. (2008). Acta Cryst. A64, 112-122.

Crystal structure determination of [rjg140001lr_fa]

Crystal Data for C14H18N8Cl2 (M =369.26 g/mol): triclinic, space group P-1 (no. 2), a = 4.0647(4) Å, b = 11.6022(8) Å, c = 18.7182(19) Å, α = 82.146(7)°, β = 87.135(8)°, γ = 88.027(7)°, V = 873.03(14) Å3, Z = 2, T = 290.00(10) K, μ(CuKα) = 3.467 mm-1, Dcalc = 1.405 g/cm3, 4189 reflections measured (4.77° ≤ 2Θ ≤ 81.79°), 1112 unique (Rint = 0.0304, Rsigma = 0.0285) which were used in all calculations. The final R1 was 0.0427 (I > 2σ(I)) and wR2 was 0.1147 (all data).

6.2. Elemental Analysis

6.2.1. 4-amino-2,6-bis(cyclohexylmethoxy)pyrimidine-5-carbaldehyde (**85**[ii])

Empirical formula = $C_{19}H_{29}N_3O_3$

Molecular Mass = 347.22 gmol-1

SAMPLE	%C	%H	%N
EC-453-133	65.49	8.50	12.13

Stephen Boyer

Science Centre

London Metropolitan University

29 Hornsey Road

London N7 7DD

Companies Act 2006 : http://www.londonmet.ac.uk/companyinfo

7. REFERENCES

1. Pinna, L. A., Meggio, F. Protein kinase CK2 ("casein kinase-2") and its implication in cell division and proliferation. *Prog. Cell Cycle Res*., **1997**, 3, 77-97.
2. Hardcastle, I. R., Golding B. T., Griffin, R. J. Designing inhibitors of cyclin-dependent kinases. *Ann. Rev. Pharmacol. Toxicol.*, **2002**, 42, 325-348.
3. Jans, D. A., Hubner, S. Regulation of protein transport to the nucleus: central role of phosphorylation. *Physiol. Rev.*, **1996**, 76 (3), 651-685.
4. www.scq.ubc.ca/protein-phosphorylation-a-global-regulator-of-cellular-activity
5. Bononi, A., Agnoletto, C., De Marchi, E., Marchi, S., Patergnani, S., Bonora, M., Giorgi, C., Missiroli, S., Poletti, F., Rimessi, A., Pinton, P. Protein Kinases and Phosphatases in the Control of Cell Fate. *Enzyme Res.*, **2011**, 1-26.
6. Ubersax, J. A., Ferrell, Jr. J. E. Mechanism of specificity in protein phosphorylation. *Nat. Rev. Mol. Cell Biol.*, **2007**, 8, 530-541.
7. Venter J. C., *et al*. The sequence of the human genome. *Science*, **2001**, 291, 1304-1351.
8. www.cellsignal.com/common/content/content.jsp?id=kinases-human-protein
9. Hunter, T. Protein kinases classification. Methods Enzymol., **1991**, 200, 3-37.
10. Hanks, S. K., Hunter, T. The eukaryotic protein kinase superfamily: kinase (catalytic) domain structure and classification. *FASEB J.*, **1995**, 9, 576-596
11. Gyungsoon Park, Servin, J. A., Turner, G. E., Altamirano, L., Colot, H. V., Collopy, P., Litvinkova, L., Li, L., Jones, C. A., Diala, F. G., Dunlap, J. C., Borkovich K. A. Global analysis of serine-threonine protein kinase genes in neurospora crassa. *Eukaryot Cell*, **2011**, 1553-1564.
12. Scheeff, E. D., Bourne, P. E. Structural evolution of the protein kinase-like superfamily. *PLoS Comput. Biol.*, **2005**, 1, 359-381.
13. Taylor, S. S., Kornev, A. P. Protein kinases: evolution of dynamic regulatory proteins. *Trends Biochem. Sci.*, **2011**, 65-77.
14. http://users.ox.ac.uk/~wolf3196/
15. Barr, F. A., Elliott, P. R., Gruneberg, U. Protein phosphatases and the regulation of mitosis. *J. Cell Sci.*, 124, **2011**, 2323-2334
16. Cohen, P. Protein kinases - The major drug targets of the twenty-first century? *Nat. rev. Drug Discov.*, **2002**, 1, 309-315.

17. Dancey, J.; Sausville, E. A., Issues and progress with protein kinase inhibitors for cancer treatment. *Nat. Rev. Drug Disc.* **2003,** 2, 296-313.
18. Tsatsanis, C.; Spandidos, D. A. The role of oncogenic kinases in human cancer (Review). *Int. J. Mol. Med.* **2000,** *5*, 583-590.
19. Davies, S. P., Reddy, H., Caivano, M., Cohen, P. Specificity and mechanism of action of some commonly used protein kinase inhibitors. *Biochem. J.*, **2000**, 351, 95–105.
20. Johnson, L. N. Protein kinase inhibitors: contributions from structure to clinical compounds. *Q. Rev. Biophys.*, **2009**, 42, 1-40.
21. Mah, R., Thomas, J. R., Shafer, C. M. Drug discovery considerations in the development of covalent inhibitors. *Bioorg. Med. Chem. Lett.*, **2014**, 24, 33–39.
22. Venerando, A., Ruzzene, M., Pinna, L. A. Casein kinase: the triple meaning of misnomer *Biochem. J.,* **2014**, 460, 141–156.
23. Bibby, A. C., Litchfield, D. W. The multiple personalities of the regulatory subunit of protein kinase CK2: CK2 dependent and CK2 independent roles reveal a secret identity for CK2β. *Int. J. Biol. Sci.,* **2005**, 1, 67-79.
24. Meggio, F., Pinna, L. A., One-thousand-and-one substrates of protein kinase CK2? *FASEB J.,* **2003**, 17, 349-368.
25. Cheong, J. K., VirshupInt. D. M. Casein family: complexity in the family. *J. Biochem. Cell B.*, **2011**, 43, 465–469
26. Niefind, K., Pütter, M., Guerra, B., Issinger, O. G., Schomburg. D. GTP plus water mimic ATP in the active site of protein kinase CK2. *Nat. Struct. Mol. Biol.*, **1999**, 6, 1100 – 1103.
27. Litchfield, D. W. Protein kinase CK2: structure, regulation and role in cellular decisions of life and death. *Biochem. J.,* **2003**, 369, 1-15.
28. Cozza, G. The dark side of protein kinase CK2 inhibition. *Curr. Med. Chem.,* **2011**, 18, 2867-2884.
29. Cozza, G., Bortolato, A., Moro, S. How druggable is protein kinase 2? *Med. Res. Rev.,* **2010**, 30, 419-462.
30. Turowec, J. P., St. Denis, N. A., Litchfield, D. W. Casein kinase II. *Encyclopedia of Signaling Molecules*, **2012**, 234-242.
31. Battistutta, R. Structural bases of protein kinase CK2 inhibition. *Cell Mol. Life Sci.*, **2009**, 66, 1868-1889.

32. Sajnaga, E., Szyszka, R., Kubiński, K. Site-directed mutagenesis in the research of protein kinases - the case of protein kinase CK2. *Genet. Mol. Biol.*, **2013**, 7, 133-166.
33. Mazzorana, M., Pinna, L. A., Battistutta, R. A structural insight into CK2 inhibition. *Mol. Cell Biochem.,* **2008**, 316, 57-62.
34. Sarno, S., Ghisellini, P., Pinna, L. A. Unique activation mechanism of protein kinase CK2: the n-terminal segment is essential for constitutive activity of the catalytic subunit but not of the holoenzyme. *J. Biol. Chem.,* **2002**, 277, 22509-22514.
35. Battistutta, R., De Moliner, E., Sarno, S., Zanotti, G., Pinna, L. A. Structural features underlying selective inhibition of protein kinase CK2 by ATP site-directed tetrabromo-2-benzotriazole. *Protein Sci.*, **2001**, 10, 2200–2206.
36. Pinna, L. A., Cohen, P. T. W. Inhibitors of protein kinases and protein phosphates. **2006**, 131.
37. Lebrin, F., Chambaz, E. M., Bianchini, L. A role for protein kinase CK2 in cell proliferation: evidence using a kinase-inactive mutant of CK2 catalytic subunit α. *Oncogene*, **2001**, 20, 2010-2022.
38. Montenarh, M. Cellular regulators of protein kinase CK2. *Cell Tissue Res.*, **2010**, 342, 139-146.
39. Zhang, C., Vilk, G., Canton, D. A., Litchfield, D. W. Phosphorylation regulates the stability of the regulatory CK2beta subunit. *Oncogene*, **2002**, 23, 3754-64.
40. Palen, E., Traugh, J.A. Phosphorylation of casein kinase II. Biochemistry, **1991**, 22, 5586-90.
41. Agostinis,P., Goris, J., Pinna, L. A., Merlevede, W. Regulation of Casein Kinase 2 by Phosphorylation/Dephosphorylation. *Biochem. J.,* **1987**, 248, 785-789
42. Tuazon, P. T., Traugh, J.A. Casein kinase I and II - multipotential serine protein kinases: structure, function and regulation. *Adv. Second Messenger Phosphoprotein Res.*, **1991**, 23, 123-164.
43. Hanif, I. M., Hanifa, I. M., Shazibd, M. A., Ahmade, K. A., Pervaiz, S. Casein Kinase II: An attractive target for anti-cancer drug design *Int. J. Biochem. Cell B.,* **2010**, 1602–1605.
44. Benitez, M. J., Mier, G., Briones, F., Moreno, F. J., Jimenez, J. S. A surface-plasmon-resonance analysis of polylysine interactions with a peptide substrate of protein kinase CK2 and with the enzyme. *Biochem. J.,* **1997**, 324, 987-994.

45. Raaf, J., Kloppfleisch, K., Issinger, O. G., Niefind, K. The catalytic subunit of human protein kinase CK2 structurally deviates from its maize homologue in complex with the nucleotide competitive inhibitor emodin. *J Mol Biol.*, **2008**, 377, 1-8.
46. Dowling,J. E., Chuaqui, C., Pontz, T. W., Lyne, P. D., Larsen, N. A., Block, M. H., Chen, H., Su, N., Wu, A., Russell, D., Pollard, H., Lee, J. W., Peng, B., Thakur, K., Ye, Q., Zhang, T., Brassil, P., Racicot, V., Bao, L., Denz, C. R., Cooke, E. Potent and Selective Inhibitors of CK2 Kinase Identified through Structure-Guided Hybridization. *ACS Med. Chem. Lett.,* **2012**, 4, 278-283.
47. Bosc, D. G., Graham, K. C., Saulnier, R. B., Zhangi, C., Prober, D., Gietz, R. D., Litchfield, D. W. Identification and Characterization of CKIP-1, a Novel Pleckstrin Homology Domain-containing Protein That Interacts with Protein Kinase CK2. *J. Biol. Chem.,* **2000**, 275, 14295-14306.
48. Glover, C.V., 3rd. On the physiological role of casein kinase II in Saccharomyces cerevisiae. *Prog Nucleic Acid Res Mol Biol.*, **1998**, 59, 95-133.
49. Pinna, L. A. Protein kinase CK2: a challenge to canons. *J. Cell Sci.*, **2002**, 115, 3873-3878.
50. St-Denis, N. A., Litchfield, D. W. Protein kinase CK2 in health and disease: From birth to death: the role of protein kinase CK2 in the regulation of cell proliferation and survival. *Cell Mol. Life Sci.*, **2009**, 66, 1817-1829.
51. http://www.pha.jhu.edu/~ghzheng/old/webct/note7_3.htm.
52. Lorenz, P., Pepperkok, R., Pyerin, W. Requirement of casein kinase 2 for entry into and progression through early phases of the cell cycle. *Cell Mol. Biol. Res*., **1994**, 40, 519-527.
53. Pepperkok, R., Lorenz, P., Ansorge, W., Pyerin, W. Casein kinase II is required for transition of G0/G1, early G1, and G1/S phases of the cell cycle. *J. Biol. Chem.*, **1994**, 269, 6986-6991.
54. Schneider, E., Kartarius, S., Schuster, N., Montenarh, M. The cyclin H/cdk7/Mat1 kinase activity is regulated by CK2 phosphorylation of cyclin H. *Oncogene,* **2002**, 21, 5031-5037.
55. Panova, T. B., Panov, K. I., Russell, J., Zomerdijk, J. C. Casein kinase 2 associates with initiation-competent RNA polymerase I and has multiple roles in ribosomal DNA transcription. *Mol. Cell Biol.,* **2006**, 26, 5957- 5968.

56. Lin, C. Y., Navarro, S., Reddy, S., Comai, L. CK2-mediated stimulation of Pol I transcription by stabilization of UBF-SL1 interaction. *Nucleic Acids Res.,* **2006**, 34, 4752-4766.
57. Sarrouilhe, D.; Filhol, O.; Leroy, D.; Bonello, G.; Baudry, M.; Chambaz, E.M.; Cochet, C., The tight association of protein kinase CK2 with plasma membranes is mediated by a specific domain of its regulatory beta-subunit. *Biochim. Biophys. Acta,* **1998**, 1403, 199-210.
58. Iimoto, D. S., Masliah, E., DeTeresa, R., Terry, R. D., Saitoh, T. Aberrant casein kinase II in Alzheimer's disease. *Brain research,* **1990**, *507*, 273-280.
59. Greenwood, J. A., Scott, C. W., Spreen, R. C., Caputo, C. B., Johnson, G. V. Casein kinase II preferentially phosphorylates human tau isoforms containing an amino-terminal insert. Identification of threonine 39 as the primary phosphate acceptor. *J. Biol. Chem.,* **1994**, 269, 4373-4380.
60. Okochi, M., Walter, J., Koyama, A., Nakajo, S., Baba, M., Iwatsubo, T., Meijer, L., Kahle, P. J., Haass, C. Constitutive phosphorylation of the Parkinson's disease associated alpha-synuclein. *J. Biol. Chem.,* **2000**, 275, 390-397.
61. Lee, G., Tanaka, M., Park, K., Lee, S. S., Kim, Y. M., Junn, E., Lee, S. H., Mouradian, M. M. Casein kinase II-mediated phosphorylation regulates alpha-synuclein/synphilin-1 interaction and inclusion body formation. *J.Biol. Chem.,* **2004**, 279, 6834-6839.
62. Ishii, A., Nonaka, T., Taniguchi, S., Saito, T., Arai, T., Mann, D., Iwatsubo, T., Hisanaga, S., Goedert, M., Hasegawa, M. Casein kinase 2 is the major enzyme in brain that phosphorylates Ser129 of human alpha-synuclein: Implication for alpha-synucleinopathies. *FEBS Lett.,* **2007**, 581, 4711- 4717.
63. Jones, S., Yakel, J. L. Casein kinase ii (protein kinase ck2) regulates serotonin 5-ht(3) receptor channel function in ng108-15 cells. *Neuroscience*, **2003**, 119, 629-634.
64. Kohlstedt, K., Shoghi, F., Muller-Esterl, W., Busse, R., Fleming, I. CK2 phosphorylates the angiotensin-converting enzyme and regulates its retention in the endothelial cell plasma membrane. *Circulation research*, **2002**, 91, 749-756.
65. Alvisi, G., Jans, D. A., Guo, J., Pinna, L. A., Ripalti, A. A protein kinase CK2 site flanking the nuclear targeting signal enhances nuclear transport of human cytomegalovirus ppUL44. *Traffic,* **2005**, 6, 1002-1013.

66. Kaushik, R., Shaila, M. S. Cellular casein kinase II-mediated phosphorylation of rinderpest virus P protein is a prerequisite for its role in replication/transcription of the genome. *J. Gen. Virol.,* **2004**, 85, 687-691.
67. El-Guindy, A. S., Miller, G. Phosphorylation of Epstein-Barr virus ZEBRA protein at its casein kinase 2 sites mediates its ability to repress activation of a viral lytic cycle late gene by Rta. *J. Virol.,* **2004**, *78*, 7634-7644.
68. Meggio, F., D'Agostino, D. M., Ciminale, V., Chieco-Bianchi, L., Pinna, L. A. Phosphorylation of HIV-1 Rev protein: implication of protein kinase CK2 and pro-directed kinases. *Biochem. Biophys. Res. Commun.,* **1996**, 226, 547-554.
69. Seitz, G., Munstermann, U., Schneider, H. R., Issinger, O. G. Characterization of casein kinase II in human colonic carcinomas after heterotransplantation into nude mice. *Biochem. Biophys. Res. Commun.,* **1989**, 163, 635-641.
70. Munstermann, U., Fritz, G., Seitz, G., Lu, Y. P., Schneider, H. R., Issinger, O. G. Casein kinase II is elevated in solid human tumours and rapidly proliferating non-neoplastic tissue. *Eur. J. Biochem.,* **1990**, 189, 251-257.
71. Wang, G., Unger, G., Ahmad, K. A., Slaton, J. W., Ahmed, K. Downregulation of CK2 induces apoptosis in cancer cells--a potential approach to cancer therapy. *Mol. Cell Biochem.,* **2005**, 274, 77-84.
72. Cozza, G., Bortolato, A., Menta, E., Cavalletti, E., Spinelli, S., Moro, S. ATP non-competitive Ser/Thr kinase inhibitors as potential anticancer agents. *Anticancer Agents Med Chem,* **2009**, 9, 778-786.
73. Ferguson, A. D., Sheth, P. R., Basso, A. D., Paliwal, S., Gray, K., Fischmann, T. O., Hung, V. L. Structural basis of CX-4945 binding to human protein kinase CK2. *FEBS Lett.,* **2011**, 585, 104-110.
74. Zandomeni, R., Zandomeni, M. C., Shugar, D., Weinmann, R. Casein kinase type II is involved in the inhibition by 5,6-dichloro-1-beta-D- ribofuranosylbenzimidazole of specific RNA polymerase II transcription. *J. Biol. Chem.,* **1986**, 261, 3414-3419.
75. Ruzzene, M., Penzo, D., Pinna, L.A., Protein kinase CK2 inhibitor 4,5,6,7-tetrabromobenzotriazole (TBB) induces apoptosis and caspase-dependent degradation of haematopoietic lineage cell-specific protein 1 (HS1) in Jurkat cells. *Biochem. J.,* **2002**, 364, 41-47.

76. Bortolato, A. Rational Design of New Protein Kinases Inhibitors of Pharmaceutical Interest. PhD thesis, **2008**, 49.
77. Pagano, M. A., Bain, J., Kazimierczuk, Z., Sarno, S., Ruzzene, M., Di Maira, G., Elliott, M., Orzeszko, A., Cozza, G., Meggio, F., Pinna, L. A. The selectivity of inhibitors of protein kinase CK2 : An update. *Biochem. J.*, **2008**, 415, 353-365.
78. Battistutta, R., Mazzorana, M., Cendron, L., Bortolato, A., Sarno, S., Kazimierczuk, Z., Zanotti, G., Moro, S., Pinna, L. A. The ATP-binding site of protein kinase CK2 holds a positive electrostatic area and conserved water molecules. *Chembiochem.*, **2007**, 8, 1804-1809.
79. Politzer, P., Lane, P., Concha, M. C., Ma, Y., Murray, J. S. An overview of halogen bonding. *J. Mol. Model*., **2007**, 13, 305 – 311.
80. Battistutta, R., Mazzorana, M., Sarno, S., Kazimierczuk, Z., Zanotti, G., Pinna, L. A. Inspecting the structure- activity relationship of protein kinase CK2 inhibitors derived from tetrabromo-benzimidazole. *Chem. Biol*., **2005**, 12, 1211-1219.
81. Zien, P., Duncan, J. S., Skierski, J., Bretner, M., Litchfield, D. W., Shugar, D. Tetrabromobenzotriazole (TBBt) and tetrabromobenzimidazole (TBBz) as selective inhibitors of protein kinase CK2: Evaluation of their effects on cells and different molecular forms of human CK2. *Biochim. Biophys. Acta*, **2005**, 1754, 271-280.
82. Lavogina, D., Enkvist, E., Uri, A. Bisubstrate inhibitors of protein kinases: from principle to practical applications. *Chem. Med. Chem.*, **2010**, 1, 23-34.
83. Enkvist, E., Viht, K., Bischoff, N., Vahter, J., Saaver, S., Raidaru, G., Issinger, O. G., Niefind, K., Uri, A. A subnanomolar fluorescent probe for protein kinase CK2 interaction studies *Org. Biomol. Chem.*, **2012**, 43, 8645-8653.
84. Schneider, C. C., Kartarius, S., Montenarh, M., Orzeszko, A., Kazimierczuk, Z. Modified tetrahalogenated benzimidazoles with CK2 inhibitory activity are active against human prostate cancer cells LNCaP in vitro. *Bioorg. Med. Chem*., **2012**, 20, 4390-4396.
85. Middleton, E. Effect of plant flavonoids on immune and inflammatory cell function. *Adv. Exp. Med. Biol.*, **1998**, 439, 175-182.
86. Lolli, G. Inhibition of protein kinase CK2 by flavonoids and tyrphostins. A structural insight. *Biochem*., **2012**, 51, (31), 6097-107.

87. Sekiguchi, Y., Nakaniwa, T., Kinoshita, T., Nakanishi, I., Kitaura, K., Hirasawa, A., Tsujimoto, G., Tada, T. Structural insight into human CK2a in complex with the potent inhibitor ellagic acid. *Bioorg. Med. Chem. Lett.*, **2009**, 19, 2920-2923.
88. Cozza, G., Bonvini, P., Zorzi, E., Poletto, G., Pagano, M. A., Sarno, S., Donella-Deana, A., Zagotto, G., Rosolen, A., Pinna, L. A., Meggio, F., Moro, S. Identification of ellagic acid as potent inhibitor of protein kinase CK2: a successful example of a virtual screening application. *J. Med. Chem.*, **2006**, 49, 2363-2366.
89. Chilin, A., Battistutta, R., Bortolato, A., Cozza, G., Zanatta, S., Poletto, G., Mazzorana, M., Zagotto, G., Uriarte, E., Guiotto, A. Coumarin as attractive casein kinase 2 (CK2) inhibitor scaffold: An integrated approach to elucidate the putative binding motif and explain structure- activity relationships. *J. Med. Chem.*, 2008, 51, 752-759.
90. Raaf, J., Klopffleisch, K., Issinger, O. G., Niefind, K. The Catalytic Subunit of Human Protein Kinase CK2 Structurally Deviates from Its Maize Homologue in Complex with the Nucleotide Competitive Inhibitor Emodin. *J. Mol. Biol.*, **2008**, 377, 1-8.
91. Yim, H., Lee, Y. H., Lee, C. H., Lee, S. K. Emodin, an anthraquinone derivative isolated from the rhizomes of Rheum palmatum, selectively inhibits the activity of casein kinase II as a competitive inhibitor. *Planta Med.*, **1999**, 65, 9-13.
92. Sarno, S., Moro, S., Meggio, F., Zagotto, G., Dal Ben, D., Ghisellini, P., Battistutta, R., Zanotti, G. and Pinna, L. A. Toward the rational design of protein kinase casein kinase-2 inhibitors. *Pharmacol. Ther.*, **2002**, 93, 159-168.
93. Scapin, G. Structural biology in drug design: selective protein kinase inhibitors. *Drug Discov. Today*, **2002**, 601-611.
94. De Moliner, E., Moro, S., Sarno, S., Zagotto, G., Zanotti, G., Pinna, L. A., Battistutta, R. Inhibition of protein kinase CK2 by anthraquinone-related compounds. A structural insight. *J. Biol. Chem.*, **2003**, 278, 1831-1836.
95. Pagano, M. A., Bain, J., Kazimierczuk, Z., Sarno, S., Ruzzene, M., Di Maira, G., Elliott, M., Orzeszko, A., Cozza, G., Meggio, F., Pinna, L. A. The selectivity of inhibitors of protein kinase CK2 : An update. *Biochem. J.*, **2008**, 415, 353-365.
96. Nie, Z., Perretta, C., Erickson, P., Margosiak, S., Almassy, R., Lu, J., Averill, A., Yager, K. M., Chu, S. Structure- based design, synthesis, and study of pyrazolo[1,5-a][1,3,5]tri- azine derivatives as potent inhibitors of protein kinase CK2. *Bioorg. Med. Chem. Lett.*, **2007**, 17, 4191-4195.

97. Nie, Z., Perretta, C., Erickson, P., Margosiak, S., Lu, J., Averill, A., Almassy, R., Chu, S. Structure-based design and synthesis of novel macrocyclic pyrazolo[1,5-a] [1,3,5]triazine compounds as potent inhibitors of protein kinase CK2 and their anticancer activities. *Bioorg. Med. Chem. Lett.*, **2008**, 18, 619-623.
98. Vangrevelinghe, E., Zimmermann, K., Schoepfer, J., Portmann, R., Fabbro, D., Furet, P. Discovery of a potent and selective protein kinase CK2 inhibitor by high-throughput docking. *J. Med. Chem.,* **2003**, 46, 2656-2662.
99. Sarno, S., de Moliner, E., Ruzzene, M., Pagano, M. A., Battistutta, R., Bain, J., Fabbro, D., Schoepfer, J., Elliott, M., Furet, P., Meggio, F., Zanotti, G., Pinna, L. A. Biochemical and three-dimensional-structural study of the specific inhibition of protein kinase CK2 by [5-oxo-5,6- dihydroindolo-(1,2-a)quinazolin-7-yl]acetic acid (IQA). *Biochem. J.*, **2003**, 374, 639-646.
100. Pargellis, C., Tong, L., Churchill, L., Cirillo, P. F., Gilmore, T., Graham, A. G., Grob, P. M., Hickey, E. R., Moss, N., Pav, S., Regan, J. Inhibition of p38 MAP kinase by utilizing a novel allosteric binding site. *Nat Struct Biol,* **2002**, *9*, 268-272.
101. Harper, J. W., Adams, P. D. Cyclin-Dependent Kinases. *Chem. Rev.,* **2001**, 101, 2511-2526.
102. Jackson, P. The Hunt for Cyclin. *Cell*, **2008**, 134, 199-202.
103. Collins, I., Garrett, M. D. Targeting the cell division cycle in cancer: CDK and cell cycle checkpoint kinase inhibitors. *Curr. Opin. Pharmacol.*, **2005**, 5, 366-373.
104. Malumbres, M., Barbacid, M. Cell cycle, CDKs and cancer: a changing paradigm. *Nat. Rev.,* **2009**, 9, 153-166.
105. Lapenna, S., Giordano, A. Cell cycle kinases as therapeutic targets for cancer. *Nat. Rev.,* **2009**, 8, 547-566.
106. http://www.pha.jhu.edu/~ghzheng/old/webct/note7_3.htm.
107. Malumbres, M., Barbacid, M. Mammalian Cyclin-Dependent Kinases. *Trends Biochem. Sci.*, **2005**, 30, 630-641.
108. Vermeulen, K., Van Bockstaele, D. R., Berneman, Z. N. The cell cycle: a review of regulation, deregulation and therapeutic targets in cancer. *Cell Prolif.*, **2003**, 36, 131-49.
109. Malumbres, M. & Barbacid, M. To cycle or not to cycle: a critical decision in cancer. *Nat. Rev. Cancer*, **2001**, 1, 222-231.

110. Abbas, T.; Dutta, A., CDK2-activating kinase (CAK) - More questions than answers. *Cell Cycle* **2006,** *5* (10), 1123-1124.
111. Larochelle, S.; Pandur, J.; Fisher, R. P.; Salz, H. K.; Suter, B., Cdk7 is essential for mitosis and for in vivo Cdk-activating kinase activity. *Genes & Development* **1998,** *12* (3), 370-381.
112. Harper, J. W.; Elledge, S. J., The role of Cdk7 in CAK function, a retrospective. *Gen. Dev.* **1998,** *12* (3), 285-289.
113. Maestre, C., Delgado-Esteban, M., Gomez-Sanchez, J. C., Bolanos, J. P., Almeida, A. Cdk5 phosphorylates Cdh1 and modulates cyclin B1 stability in excitotoxicity. *EMBO J.,* **2008**, 27, 2736-2745.
114. Rickert, P., Seghezzi, W., Shanahan, F., Cho, H., Lees, E. Cyclin C/CDK8 is a novel CTD kinase associated with RNA polymerase II. *Oncogene*, **1996**, 12, 2631-2640.
115. Lim, S., Kaldis, P. Cdks, cyclins and CKIs: roles beyond cell cycle regulation. *Development* **2013**, 140, 3079-3093.
116. Pavletich, N. P. Mechanisms of Cyclin-dependent Kinase Regulation: Structures of Cdks, their Cyclin Activators, and Cip and INK4 Inhibitors. *J. Mol. Biol.,* **1999,** *287*, 821-828.
117. Galons, H., Oumata, N., Meijer, L. Cyclin-dependent kinase inhibitors: a survey of recent patent literature. *Expert Opin. Ther. Patents*, **2010**, 20, 377-404.
118. Boye, E., Grallert, B. The 2001 Nobel Prize in Physiology or Medicine. Tidsskr. Nor. Laegeforen., **2001**, 121, 3500.
119. Weinberg, R. A. The Retinoblastoma Protein and Cell-Cycle Control. *Cell,* **1995,** 81, 323-330.
120. Zhu, Y., Alvarez, C., Doll, R., Kurata, H., Schebye, X. M., Parry, D., Lees, E. Intra-S-phase checkpoint activation by direct CDK2 inhibition. *Mol. Cell. Biol.* **2004,** 24, 6268-6277.
121. Taylor, W. R., Stark, G. R. Regulation of the G2/M transition by p53. *Oncogene*, **2001**, 20, 1803.
122. Garrett, M. D., Fattaey, A. CDK inhibition and cancer therapy. *Curr. Opin. Genet. Dev.,* **1999,** *9*, 104-111.
123. Huwe, A., Mazitschek, R., Giannis, A. Small molecules as inhibitors of cyclin-dependent kinases. *Angew. Chem., Int. Ed.,* **2003,** 42, 2122-2138.

124. Knockaert, M., Greengard, P., Meijer, L. Pharmacological inhibitors of cyclin-dependent kinases. *Trends Pharmacol. Sci.,* **2002,** 23, 417-425.
125. Sielecki, T. M., Boylan, J. F., Benfield, P. A., Trainor, G. L. Cyclin-dependent kinase inhibitors: useful targets in cell cycle regulation. *J. Med. Chem.,* **2000,** 43, 1-18.
126. Senderowicz, A. M. Flavopiridol: the First Cyclin-Dependent Kinase Inhibitor in Human Clinical Trials. *Investigat. New Drugs*, **1999**,17, 313-320.
127. Havlicek, L., Hanus, J., Vesely, J., Leclerc, S., Meijer, L., Shaw, G., Strnad, M. Cytokinin-Derived Cyclin-Dependent Kinase Inhibitors: Synthesis and cdc2 Inhibitory Activity of Olomoucine and Related Compounds. *J. Med. Chem.,* **1997**, 40, 408-412.
128. Meijer, L., Raymond, E. Roscovitine and Other Purines as Kinase Inhibitors. From Starfish Oocytes to Clinical Trials. *Acc. Chem. Res.,* **2003**, *36*, 417- 425.
129. Squires, M. S., Cooke, L., Lock, V., Qi, W., Lewis, E. J., Thompson, N. T., Lyons, J. F., Mahadevan, D. Biological characterization of AT7519, a small-molecule inhibitor of cyclin-dependent kinases, in human tumor cell lines. *Mol. Cancer Ther.,* **2009**, 8, 324-332.
130. Pennati, M., Campbell, A. J., Curto, M., Binda, M., Cheng, Y., Wang, L. Z., Curtin, N., Golding, B. T., Griffin, R. J., Hardcastle, I. R., Henderson, A., Zaffaroni, N., Newell, D. R. Potentiation of paclitaxel-induced apoptosis by the novel cyclin-dependent kinase inhibitor NU6140: A possible role for survivin down- regulation. *Mol. Cancer Ther.*, **2005**, 4, 1328-1337.
131. Kodym, E., Kodym, R., Reis, A. E., Habib, A. A., Story, M. D., Saha, D. The small-molecule CDK inhibitor, SNS-032, enhances cellular radiosensitivity in quiescent and hypoxic non-small cell lung cancer cells. *Lung Cancer*, **2009**, 66, 37-47.
132. De Pinto, W., Chu, X. J., Yin, X., Smith, M., Packman, K., Goelzer, P., Lovey, A., Chen, Y., Qian, H., Hamid, R., Xiang, Q., Tovar, C., Blain, R., Nevins, T., Higgins, B., Luistro, L., Kolinsky, K., Felix, B., Hussain, S., Heimbrook, D. In vitro and in vivo activity of R547: a potent and selective cyclin-dependent kinase inhibitor currently in phase I clinical trials. *Mol. Cancer Ther.*, **2006**, 5, 2644-2658.
133. Diab, S., Eckhardt, S., Tan, A., Frenette, G., Gore, L., Depinto, W., Grippo, J., DeMario, M., Mikulski, S., Papadimitrakopoulou, S. A phase I study of R547, a novel, selective inhibitor of cell cycle and transcriptional cyclin dependent kinases (CDKs). *J. Clin. Oncol.*, **2007**, 25, 3528.

134. Joshi, K. S., Rathos, M. J.,Joshi, R. D., Sivakumar, M.,Mascarenhas, M.,Kamble, S.,Lal, B.,Sharma, S. In vitro antitumor properties of a novel cyclin-dependent kinase inhibitor, P276-00. *Mol. Cancer Ther.*, **2007**, 6, 918-925.
135. Joshi, K. S., Rathos, M. J., Mahajan, M., Wagh, V., Shenoy, S., Bhatia, D., Chile, S., Sivakumar, M., Maier, A., Fiebig, H. H., Sharma, S. P276-00, a novel cyclin-dependent inhibitor induces G1–G2 arrest, shows antitumor activity on cisplatin-resistant cells and significant in vivo efficacy in tumor models. *Mol. Cancer Ther.*, **2007**, 6, 926-934.
136. Siemeister, G., Luecking, U., Wagner, C., Detjen, K., Mc Coy, C., Bosslet, K. Molecular and pharmacodynamic characteristics of the novel multi-target tumor growth inhibitor ZK 304709. *Biomed. Pharmacother.*, **2006**, 60, 269-272.
137. Scholz, A., Wagner, K., Welzel, M., Remlinger, F., Wiedenmann, B.,Siemeister, G., Rosewicz, S., Detjen, K. M. The oral multitarget tumour growth inhibitor, ZK 304709, inhibits growth of pancreatic neuroendocrine tumours in an orthotopic mouse model. *Gut.*, **2009**, 58, 261-270.
138. Emanuel, S. Rugg, C. A., Gruninger, R. H., Lin, R., Fuentes-Pesquera, A., Connolly, P. J., Wetter, S. K., Hollister, B., Kruger, W. W., Napier, C., Jolliffe, L., Middleton, S. A. The in vitro and in vivo effects of jnj-7706621: a dual inhibitor of cyclin-dependent kinases and Aurora kinases. *Cancer Res.*, **2005**, 65, 9038-9046.
139. Akli, S., Van Pelt, C. S., Bui, T., Meijer, L., Keyomarsi, K. Cdk2 is required for breast cancer mediated by the low-molecular-weight isoform of cyclin E. *Cancer Res*., **2011**, 71, 3377-3386.
140. Tetsu, O., Mc Cormick, F. Proliferation of cancer cells despite CDK2 inhibition. *Cancer Cell*, **2003**, 3, 233-245.
141. Berthet, C., Aleem, E., Coppola, V, Tessarollo, L., Kaldis, P. CDK2 knockout mice are viable. *Curr. Biol.*, **2003**, 13, 1775-1785.
142. Horiuchi, D., Huskey, N. E., Kusdra, L., Wohlbol, L., Merrick, K. A., Zhang, C., Creasman, K. J., Shokat, K. M., Fisher, R. P., Goga, A. Chemical-genetic analysis of cyclin-dependent kinase 2 function reveals an important role in cellular transformation by multiple oncogenic pathways. *Proc. Natl. Acad. Sci.,* **2012**, 109, E1019-E1027.

143. Barriere, C., Santamaria, D., Cerqueira, A., Galan, J., Martin, A., Ortega, S., Malumbres, M, Dubus, P., Barbacid, M. Mice thrive without Cdk4 and Cdk2. *Mol. Oncol.,* **2007**, 1, 72-83.
144. Ortega, S., Malumbres, M., Barbacid, M. Cyclin D-dependent kinases, INK4 inhibitors and cancer. *Biochim. Biophys. Acta*, **2002**, 73-87.
145. Schulze-Gahmen, U., De Bondt, H. L., Kim, S. H. High-resolution crystal structures of human cyclin-dependent kinase 2 with and without ATP: bound waters and natural ligand as guides for inhibitor design. *J.Med.Chem.*, **1996**, 39, 4540-4546.
146. Endicott, J., Noble, M. Structural characterization of the cyclin-dependent protein kinase family. *Biochem. Soc. Trans.*, **2013**, 41, 1008-1016.
147. Heitz, F., Morris, M. C., Fesquet, D., Cavadore, J. C., Doree, M., Divita, G. Interactions of cyclins with cyclin-dependent kinases: A common interactive mechanism. *Biochemistry* **1997,** 36, 4995-5003.
148. Jeffrey, P. D., Russo, A. A., Polyak, K., Gibbs, E., Hurwitz, J., Massagué, J., Pavletich, N. P. Mechanism of CDK activation revealed by the structure of cyclinA-CDK2 complex. *Nature*, **1995**, 376, 313-320.
149. Dar, A. C., Shokat, K. M. The evolution of protein kinase inhibitors from antagonists to agonists of cellular signaling. *Annu. Rev. Biochem.*, **2011**, 80, 769-795.
150. Liu, Y., Gray, N. S. Rational design of inhibitors that bind to inactive kinase conformations. *Nat. Chem. Biol.*, **2006**, 2, 358-364.
151. Zhang, J., Yang, P. L., Gray, N. S. Targeting cancer with small molecule kinase inhibitors. *Nat. Rev. Cancer*, **2009**, 9, 28-39.
152. Carbain, B., Paterson, D. J., Anscombe, E., Campbell, A. J., Cano, C., Echalier, A., Endicott, J., Golding, B. T., Haggerty, K., Hardcastle, I. R., Jewsbury, P. J., Newell, D. R., Noble, M., Roche, C., Wang, L. Z., Griffin, R. J. 8-Substituted O^6-Cyclohexylmethylguanine CDK2 Inhibitors: Using Structure-Based Inhibitor Design to Optimize an Alternative Binding Mode. *J. Med. Chem.,* **2014**, 57, 56−70.

153. Arris C. E., Boyle, F. T., Calvert, A. H., Curtin, N. J., Endicott, J. A., Garman, E. F., Gibson, A. E., Golding, B. T., Grant, S., Griffin, R. J., Jewsbury, P., Johnson, L. N., Lawrie, A. M., Newell, D. R., Noble, M., Sausville, E. A., Schultz, R., Yu, W. Identification of Novel Purine and Pyrimidine Cyclin-Dependent Kinase Inhibitors with Distinct Molecular Interactions and Tumor Cell Growth Inhibition Profiles. *J. Med. Chem.*, **2000**, 43, 2797-2804.

154. Davies, T.G., Bentley, J. Arris, C. E., Boyle, F. T., Curtin, N. J., Endicott, J. A., Gibson, A. E., Golding, B. T., Griffin, R. J., Hardcastle, I. R., Jewsbury, P., Johnson, L. N., Mesguiche, V., Newell, D. R., Noble, M., Tucker, J. A., Wang, L., Whitfield, H. J. Structure-based design of a potent purine-based cyclin-dependent kinase inhibitor. *Nat. Struct. Biol.*, **2002**, 9, 745-749.

155. Meschini, E. Purine-Based Dual Inhibitors of CDK2 and CDK7. PhD Thesis, **2011**, 159-170.

156. Griffin, R. J., Henderson, A., Curtin, N. J., Echalier, A., Endicott, J. A., Hardcastle, I. R., Newell, D. R., Noble, M., Wang, L. Z., Golding, B. T. Searching for cyclin-dependent kinase inhibitors using a new variant of the Cope elimination. *J. Am. Chem. Soc.*, **2006**, 10, 6012-6013.

157. Singh, J., Petter, R. C., Baillie, T. A., Whitty, A. The resurgence of covalent drugs, *Nat. Rev.*, **2011**, 10, 307-317.

158. Barf, T., Kaptein, K. Irreversible Protein Kinase Inhibitors: Balancing the Benefits and Risks. *J. Med. Chem.*, **2012**, 55, 6243-6262.

159. Marchetti, F., Cano, C., Curtin, N. J., Golding, B. T., Griffin, R. J., Haggerty, K., Newell, D. R., Parsons, R. J., Payne, S. L., Wang, L. Z., Hardcastle, I. R. Synthesis and biological evaluation of 5-substituted O4-alkylpyrimidines as CDK2 inhibitors. *Org. Biomol. Chem.*, **2010**, 8, 2397–2407.

160. Andrzejewska, M., Pagano, M. A., Meggio, F., Brunati, A. M., Kazimierczuk, Z. Polyhalogenobenzimidazoles: synthesis and their inhibitory activity against casein kinases. *Bioorg. Med. Chem.*, **2003**, 11, 3997-4002.

161. Zawada, K., Wolniak, M., Kazimierczuck, Z., Wawer, I. Structural studies of 4,5,6,7-tetrabromobenzimidazole derivatives by means of solid-state ^{13}C, ^{15}N NMR spectroscopy and DFT calculations. *J. Mol. Strut.*, **2009**, 918, 174–182.

162. Pagano, M. A., Poletto, G., Di Maira, G., Cozza, G., Ruzzene, M., Sarno, S., Bain, J., Elliott, M., Moro, S., Zagotto, G., Meggio, F., Pinna, L. A. Tetrabromocinnamic Acid (TBCA) and Related Compounds Represent a New Class of Specific Protein Kinase CK2 Inhibitors. *ChemBioChem,* **2007**, 8, 129-139.
163. Pagano, M. A., Andrzejewska, M., Ruzzene, M., Sarno, S., Cesaro, L., Jenny Bain, J., Elliott, M., Meggio, F., Kazimierczuk, Z., Pinna, L. A. Optimization of Protein Kinase CK2 Inhibitors Derived from 4,5,6,7-Tetrabromobenzimidazole. *J. Med. Chem.,* **2004**, 47, 6239-6247.
164. Merrifield, R. B. Solid Phase Peptide Synthesis. I. The Synthesis of a Tetrapeptide. *J. Am. Chem. Soc.*, **1963**, *85*, 2149-2154.
165. Peptides: Synthesis, Structures and Applications. *Bernd Gutte Ed.*, **1995**, 3, 94-159.
166. http://www.iproteos.com/peptide-synthesis/.
167. Kociénski, P. J. Protecting groups. *Thieme Ed.,* **1994**, 403-408, 528-533.
168. More S.S., Vince, R. Inhibition of Glyoxalase I: The First Low-Nanomolar Tight-Binding Inhibitors. *J. Med. Chem*., **2009**, 52, 4650-4656.
169. Mag, M., Muth, J., Jahn, K., Peyman, A., Kretzschmar, G., Engels, J., W., Uhlmann, E. Synthesis and Binding Properties of Oligodeoxynucleotides Containing Phenylphosphon(othio)ate Linkages. *Bioorg. Med. Chem.*, **1997**, 5, 2213-2220.
170. Marchetti, F., et al. Structure-based design of 2-arylamino-4-cyclohexylmethoxy-5-nitroso-6-aminopyrimidine inhibitors of cyclin-dependent kinase 2. *Org. Biomol. Chem.*, **2007**, 5, 1577-1585.
171. Kürti, L., Czako, B. Strategic applications of named reactions in organic synthesis. *Elsevier Academic Press*, **2005**, 468-469.
172. Whitfield, H., Griffin, R. J., Hardcastle, I. R., Henderson, A., Meneyrol, J., Mesguiche, V., Sayle, K. L., Golding, B. T. Facilitation of addition-elimination reactions in pyrimidines and purines using trifluoroacetic acid in trifluoroethanol. *J. Chem. Soc. Chem. Comm.*, **2003**, 22, 2802-2803.
173. Hirayama, T., Kamada, M., Tsurumi, H., Minura, M. A novel synthesis of Pyrimidines. I. Cyclization of N-Cyano-cyanoaceto Derivatives. *Chem. Pharm. Bull.*, **1976**, 24, 26-36.
174. Dewar, J. H. Purines, pyrimidines and imidazoles. Part XXI. Some uracils and isocytosines. *J. Chem. Soc.*, **1965**, 1642-1648.

175. Lembicz, N. K., Grant, S., Clegg, W., Griffin, R. J., Heat, S. L., Golding, B. T. Facilitation of displacements at the 6-position of purines by the use of 1,4-diazobicyclo[2.2.2]octane as leaving group. *J. Chem. Soc.*, **1997**, 1, 185-186.
176. Chakraborti, A.K., Kaur, G. One-Pot Synthesis of Nitriles from Aldehydes Under Microwave Irradiation: Influence of Medium and mode of Microwave Irradiation on Product Formation. *Tetrahedron*, 55, 1999, 13265-13268.
177. Singh, M.,K., Lakshman, M. K. A Simple Synthesis of Nitriles from Aldoximes. *J. Org. Chem*., **2009**; 74(8) 3079-3084.
178. Fantoni, A. C., Corbelli, G. Microwave Spectrum, Dipole Moment and Conformation of Methyl Vinyl Sulfone. *J. Mol. Spec.*, **1994**, 164, 319-327.
179. Fantoni, A. C., Marañón, J. Conformational Properties of Methyl Vinyl Sulfone: Ab Initio Geometry Optimization and Vibrational Analysis. *Struct. Chem.*, **1996**, 7, 51-58.
180. Sarno, S., Mazzorana, M., Traynor, R., Ruzzene, M., Cozza, G., Pagano, M. A., Meggio, F., Zagotto, G., Battistutta, R., Pinna, L. A. Structural features underlying the selectivity of the kinase inhibitors NBC and dNBC: role of a nitro group that discriminates between CK2 and DYRK1A. *Cell Mol. Life Sci.,* **2012**, 69, 449-460.
181. Bain, J., Plater, L., Elliott, M., Shpiro, N., Hastie, J., McLauchlan, H., Klevernic, I., Arthur, J. S., Alessi, D. R., Cohen, P. The selectivity of protein kinase inhibitors: a further update. *Biochem. J.*, **2007**, 408, 297-315.
182. Copeland, R. A. Evaluation of Enzyme Inhibitors in Drug Discovery. *Wiley*, **2005**.
183. Graczyk, P. P. (2007) Gini coefficient: a new way to express selectivity of kinase inhibitors against a family of kinases. *J. Med. Chem.*, **2007**, 50, 5773-5779.
184. Di Maira, G., Brustolon, F., Bertacchini, J., Tosoni, K., Marmiroli, S., Pinna, L. A., Ruzzene, M. Pharmacological inhibition of protein kinase CK2 reverts the multidrug resistance phenotype of a CEM cell line characterized by high CK2 level. *Oncogene*, **2007**, 26, 6915-6926.